Investigation of Whiplash Associated Disorders using Finite Element Neck Models with Active Musculature in Frontal, Rear and Lateral Impact

by

David Shen

A thesis
presented to the University of Waterloo
in fulfillment of the
thesis requirement for the degree of
Master of Applied Science
in
Mechanical and Mechatronics Engineering

Waterloo, Ontario, Canada, 2020

AUTHOR'S DECLARATION

I hereby declare that I am the sole author of this thesis. This is a true copy of the thesis, including any required final revisions, as accepted by my examiners.

I understand that my thesis may be made electronically available to the public.

Abstract

Whiplash associated disorders (WAD) represent one of the most frequent injuries following a motor vehicle collision, with a significant economic cost of upwards of $29 billion in the United States and €10 billion in Europe. Although high severity neck injuries associated with high velocity impacts can be fatal, WADs can occur from low speed impact scenarios that can result in acute soft tissue injury, but can transition into chronic symptoms that can be detrimental to the quality of life for the victim. In addition, the female population has been identified to be twice as vulnerable to sustain WADs with twice the risk to develop chronic symptoms, compared to the male population. WADs originate from tissue lesions due to non-physiological motion or excess motion past the physiologic loading range of the cervical spine. Epidemiological data has associated WADs with frontal, rear, lateral impact scenarios, with the rear impact configuration having the largest injury risk. However, the total absolute incidence of WADs from frontal and lateral impacts are equal to or exceed those from rear impacts. Anatomical sites that are susceptible to injury and pain response include the cervical facet joint, spinal ligaments, intervertebral disc, nerve roots and dorsal root ganglia, muscles and vertebral arteries. Injuries that originate from these anatomical sites are difficult to diagnose due to challenges in identifying non-observable macroscopic tissue damage and limitations in current medical imaging techniques. Current methods to investigate WAD include volunteer, post mortem human subject (PHMS), anthropometric test device (ATD), and animal experiments; however, these methods do not include the combination of active muscles, tissue level injury and pain response that are applicable to a human. Detailed finite element (FE) human body models (HBMs) were developed to address some of these limitations, particularly incorporating the effect of active musculature and the ability to predict crash induced injuries (CIIs) at the local tissue level for multidirectional impacts. The objective of the study was to investigate the injury risk at the tissue level following frontal, rear and lateral impact conditions using two HBMs that represent a 50^{th} percentile male and 5^{th} percentile female. In addition, a new muscle activation scheme was developed and applied to the HBMs and the sensitivity of active muscle parameters was investigated for each impact scenario.

The head and neck models of the Global Human Body Models Consortium (GHBMC) 50^{th} percentile male (M50-O v.4-5) and 5^{th} percentile female (F05-O v.3-1) were used to investigate the kinematic and tissue level response in 8g frontal, 7g rear and 7g lateral impact conditions. A new open-loop muscle activation scheme was proposed to improve the reflex muscle activation response of both models under all loading conditions. The new activation scheme was applied to an upper and lower bound assessment of muscle activation, based on varying physiologic cross-sectional area (PCSA) and muscle activation onset time from reported literature values, and assessed using head kinematics. Lastly, the male and female

models were compared for the various impact conditions (frontal, rear, lateral), based on kinematic response, tissue level response, and the potential for injury risk at the tissue level.

The proposed open-loop muscle activation scheme improved the head kinematics outcome, compared to human volunteer tests relative to the baseline muscle activation, for both the M50 and F05 models for all impact directions. The effect of varying PCSA and muscle activation onset time on head kinematics was largest for the lateral impact, compared to frontal and rear impact conditions. The muscle activation strategy affected the neck position in the sagittal plane during the impact, which was sensitive to lateral impacts because increased neck flexion enabled increased lateral bending coupled with increased axial rotation. The kinematic and predicted tissue-level injury risk were similar between the M50 and F05 models for the frontal and rear impact directions, attributed to the confounding effects of both stature and local tissue dimensions. The lateral impact direction predicted the highest injury risk for the capsular ligament, and compression of the nerve root and dorsal root ganglia at the lower cervical vertebral levels for both the M50 and F05 models. No injury risk was predicted by both models in the rear impact condition, although the impact scenario considered was in the transitional region from non-injured to injured as reported in the literature. The low injury risk in rear impact was attributed to the non-physiological facet joint gap and the numerical implementation of the capsular ligament. In addition, the F05 model demonstrated consistently lower head rotational displacement compared to the M50, attributed to the non-physiological planar facet joint profile, which restricted axial rotation of the vertebrae.

An average stature male and a small stature female HBM were enhanced with a new open-loop muscle activation strategy resulting in improved head kinematics for frontal, lateral and rear impact scenarios. Assessment at the tissue level demonstrated the highest injury risk in the lateral impact condition for both M50 and F05 models. In general, the injury risk between the M50 and F05 models were similar in the frontal and rear impact conditions due to confounding effects of stature and local neck tissue dimensions, while the lateral impact condition resulted in different capsular ligament post-traumatic injury locations because of the reduced vertebral motion from the non-physiological facet joint cartilage of the F05 model. Application of the upper and lower bound activation scheme demonstrated the highest sensitivity in model response to the lateral impact condition, while the rear impact condition demonstrated the lowest sensitivity. Future research should investigate a range of impact severities to determine the injury tolerance for each impact direction.

Acknowledgements

I would like to express my sincere gratitude and thank my supervisor Dr. Duane Cronin for his exceptional guidance and patience during the duration of my Masters.

Thank you to all current and past members of the Impact Mechanics and Material Characterization (IMMC) research group for all the great memories.

Special thanks to the Global Human Body Model Consortium (GHBMC) and the Natural Sciences and Engineering Research Council of Canada (NSERC) for sponsoring this research.

Finally, I would like to thank my parents for always supporting me.

Table of Contents

List of Figures

List of Tables

CHAPTER 1: INTRODUCTION

Whiplash associated disorders (WAD) (commonly known as neck sprains and strains) are the most frequent injuries observed following a motor vehicle collision, accounting for 27.8% of all injuries treated in US hospital emergency departments (Quinlan et al., 2004; Gustafsson et al., 2015; Kullgren et al., 2013). The total annual cost as a consequence of whiplash is significant at an estimated $3.9 to $29 billion in the United States and €10 billion in Europe, representing a great social economic burden to society, and personal burden to the affected individuals (Lord et al., 1996; Freeman et al., 1999; Ritcher et al., 2000). It is estimated that the incidence of WAD has increased two to ten times over the past three decades, with a predicted incidence rate in North America and Europe of approximately 300 per 100,000 inhabitants (Versteegon et al., 1998; Ritcher et al., 2000; Holm et al., 2008). The occurrence of fatal and severe injuries that result from motor vehicle collisions have reduced due to advancements in vehicle safety, while the incidence of low severity soft tissue injuries and the risk of disability resulting from these low severity injuries have both increased since the early 1980s (Kullgren et al., 2002). Although high severity neck injuries can be life threatening or even fatal, low severity soft tissue neck injuries can be disabling and develop into chronic symptoms that can be detrimental to the quality of life for the injured victim (Cronin, 2014). This is problematic because soft tissue injury in the neck is the highest occurring injury in terms of frequency with an estimated half of all WAD victims still reporting symptoms one year after the initial incident (Carroll et al., 2008). Furthermore, the female population have exhibited twice the susceptibility to WAD compared to the male population. In addition, females are reported to have twice the risk for development of chronic symptoms (Carlsson et al., 2012; Carstensen et al., 2012). Epidemiological studies have identified that WAD can occur from frontal, rear, and side impacts, where the rear impact condition represented the highest risk of sustaining WAD (Kullgren et al., 2013; Watanabe et al., 2000; Hell et al., 2003; Martin et al., 2008; Cassidy et al., 2000; Berglund et al., 2002; Morris and Thomas, 1996; Kullgreen et al., 2000; Jakobsson et al., 2000). Despite rear end impacts having the highest injury risk, the absolute number of WAD incidents that result from frontal and side impact are often equal to or exceed the total number of occurrences from rear impact events, which signifies the importance of WAD that develops from frontal and side impacts (Berglund et al., 2003, Kullgren et al., 2013; Martin et al., 2008, Morris and Thomas, 1996).

WADs are thought to originate from tissue lesions due to non-physiological motions of the cervical spine segments or excess motion past the physiologic range (Curatolo et al., 2011). Several anatomical sites

with the potential for tissue injury and pain response have been proposed in the literature including the cervical facet joint, spinal ligaments, intervertebral disc, nerve root and ganglia, muscles, and vertebral arteries, with the cervical facet joint being the most developed in terms of research with the most evidence as the leading source of neck pain (Siegmund et al., 2009; Curatolo et al., 2011; Bogduk, 2011; Cronin, 2014). Furthermore, the cervical facet joint has been confirmed to contain nociceptors, which indicate the potential for pain development with further supporting evidence from animal models of pain from nociceptor signalling and behavioural sensitivity studies (Siegmund et al., 2009; Lu et al., 2005; Lee et al., 2004; Lee et al., 2008, Bogduk, 2002). A challenging aspect of WAD is the difficult diagnosis of the anatomical sources of pain for patients because the injured soft tissues do not undergo catastrophic failure that cause complete rupture, but are rather distracted beyond the physiologic loading range that can cause micro lesions to form (Yoganandan et al., 1988), where damage cannot be observed macroscopically (Nordin and Frankel, 2001). This presents challenges in the process of clinical diagnosis as these types of lesions are undetectable using current medical imaging techniques (Yoganandan et al., 2001, Dullerud et al., 2010; Vetti et al., 2011; Li et al., 2013). In addition to challenges in the diagnosis process, it is difficult to quantify the pain response with respect to the mechanical loading of a tissue due to ethical restrictions for in-vivo human testing. Several methods are currently used to investigate the injury mechanisms of WAD including anthropometric test devices (ATD), post mortem human subjects (PHMS), in-vivo volunteer testing, animal models, and finite element (FE) modelling approaches. ATDs such as the BioRID are mechanical human surrogates that are currently used to assess the safety of modern production vehicles but have low levels of biofidelity, are not frangible, can only predict injury for a global body region, and are limited to a single impact direction. Experiments that utilize PHMS provide increased biofidelity and allow the investigation of injury in high severity events, but lack muscle tone, cannot assess physiologic or pain response, and are often more representative of the aged population. Human volunteer testing is ideal as it offers the highest level of biofidelity that includes muscle tone and active musculature, but exposures to human volunteers are limited to non-injurious inputs due to strict ethical regulations. Animal models can provide insight on nociceptor activation and chronic pain development, but limitations in animal models include distinct biological and anatomical differences compared to a human (Winkelstein et al., 2011). Human body models (HBM) have been developed to address some of these limitations and are useful tools that incorporate the response of passive and active muscles that allow predictions of kinematic and kinetic response, which can be related to injury. One of the most valuable benefit of utilizing a HBM is the ability to predict local injury for any body region at the tissue level (Cronin, 2014; Yang et al., 2018; Schmitt et al., 2019). This is crucial in discerning detailed injury locations to understand complex injury mechanisms such as whiplash injury for a given impact scenario. Furthermore, HBM can be used to conduct detailed sensitivity analysis of input parameters and have the added benefit of removing the effects of subject and

biological variability by incorporating deterministic mechanical and failure tissue properties that result in a single answer for a given load case (Cronin, 2014). The objective of this study was to utilize two HBMs (Global Human Body Model Consortium, 50th percentile male and 5th percentile female) to investigate the response of soft tissue neck injury in frontal, rear, and lateral impact loading conditions through quantification of local tissue strains. Furthermore, the effect of active muscle parameters on global kinematics and injury potential and the development of an improved muscle activation strategy was implemented.

This thesis is organized in five chapters. Background information that is crucial for understanding the content of this thesis is provided in Chapter 2. Chapter 3 builds upon the knowledge described in Chapter 2 to highlight the methodology used to conduct the investigation. Chapter 4 presents the result of the study, and Chapter 5 provides discussion about the results in relation to the current literature, in addition to highlighting limitations of the study.

CHAPTER 2: BACKGROUND

2.1 Anatomy

2.1.1 Anatomic Planes and Directions

The anatomic position describes an individual in a baseline configuration that is standing upright with the head, feet and palms facing forward (Figure 2-1) (Standring, 2008). This baseline configuration is critical because it standardizes a consistent method to describe human anatomy regardless of the instantaneous position of the individual. These planes and directions allow the description of body parts relative to the body at a global scale, or at a local scale when describing one part relative to another.

Three imaginary orthogonal planes intersect the body in the anatomical position: frontal (coronal), transverse (axial), and sagittal (median) plane, and are primarily used to describe sections in the body (Figure 2-1) (Standring, 2008). The frontal plane is oriented vertically and divides the body into front and back sections. The median plane is oriented vertically and bisects the body into symmetric left and right halves. The transverse plane is oriented horizontally and divides the body into top and bottom parts. These planes are often used in conjunction with a reference point or landmark on the body to identify where the plane is situated.

The superior (above) direction points upwards towards the head while the inferior (below) direction points downward towards the feet (e.g. eyes are located superior to the nose while the mouth is located inferior to the nose). The posterior direction is directed rearward toward the back, while the anterior direction is directed toward the front of the body (belly). The medial direction defines parts that are close to the median plane (e.g. center of the body) while the lateral direction defines parts that are away from the median plane in the left or right direction. Ipsilateral can be defined as a part or occurrence that is located on the same side of the body, relative to a reference structure. Contralateral is defined as a part or occurrence that is located on the opposite side of the body, with respect to the reference structure. Superficial define structures that lie toward the outer surface of a body region and deep define structures that lie away from the surface of a body region (e.g. skin is superficial to muscle). Proximal describes structures that are situated towards the attachment or center of the body, while distal define structures that are situated away from the attachment or the center of the body (e.g. hands are distal relative to the elbow).

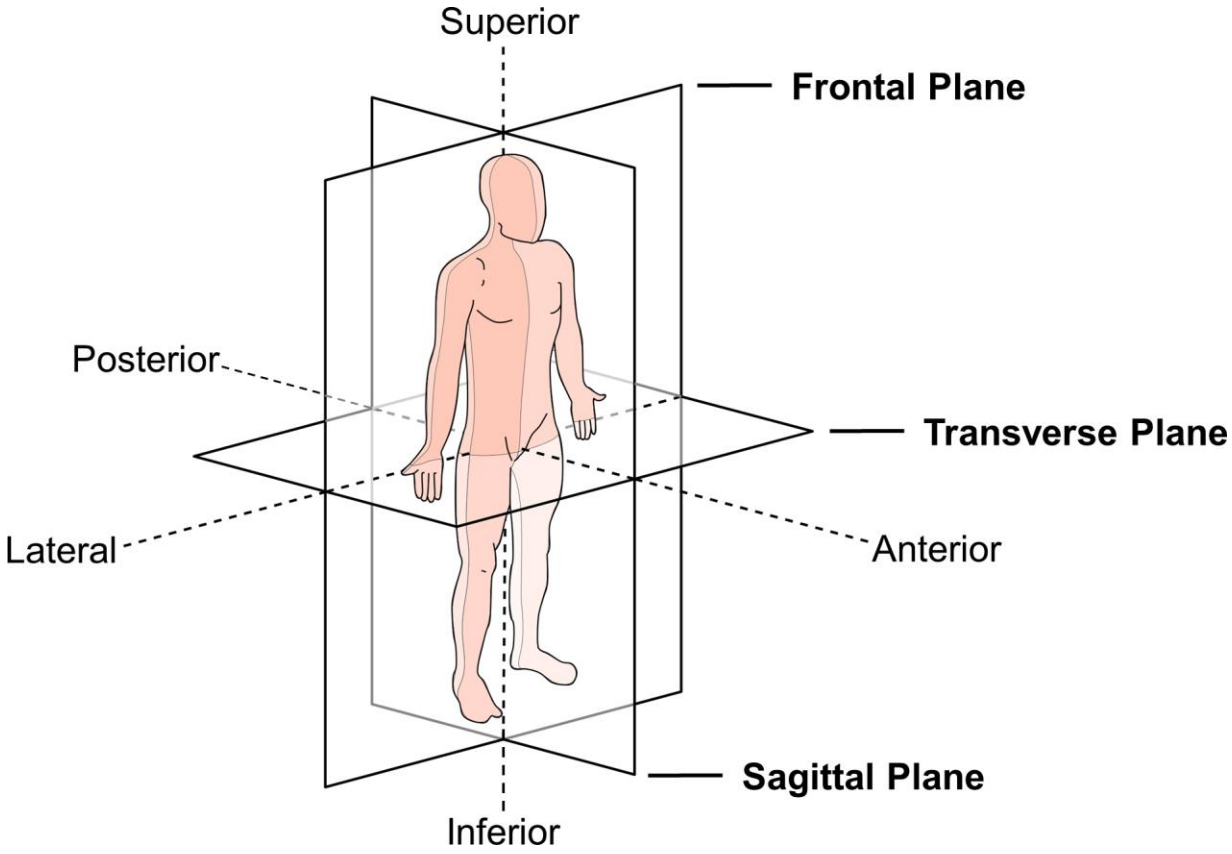

FIGURE 2-1: ANATOMICAL PLANES AND DIRECTIONS

[Adapted from "Anatomical Planes" by CFCF (CC BY-SA 3.0) https://commons.wikimedia.org/wiki/File:Anatomical_Planes.svg]

2.1.2 Neck Motion Terminology

The basic movement of the head-neck complex can be divided into four primary motions: flexion, extension, lateral bending, and axial rotation (Figure 2-2) (Standring, 2008). Flexion refers to anterior bending of the neck (e.g. looking down at the ground) and is the neck motion experienced during a frontal crash. Conversely, extension refers to posterior bending of the neck (e.g. looking up at the sky) and is the primary neck motion during a rear end impact. Lateral flexion or lateral bending refers to the motion of the head when tilted towards either side of the shoulder. Axial rotation refers to rotation of the head-neck complex along the longitudinal direction of the vertebrae alignment (e.g. looking left and right at a road intersection). Due to the high number of sensory systems located on the head (visual, auditory, olfactory, gustatory), the neck structure must have enough flexibility to enable large ranges of motion to provide interactions with the surrounding environment.

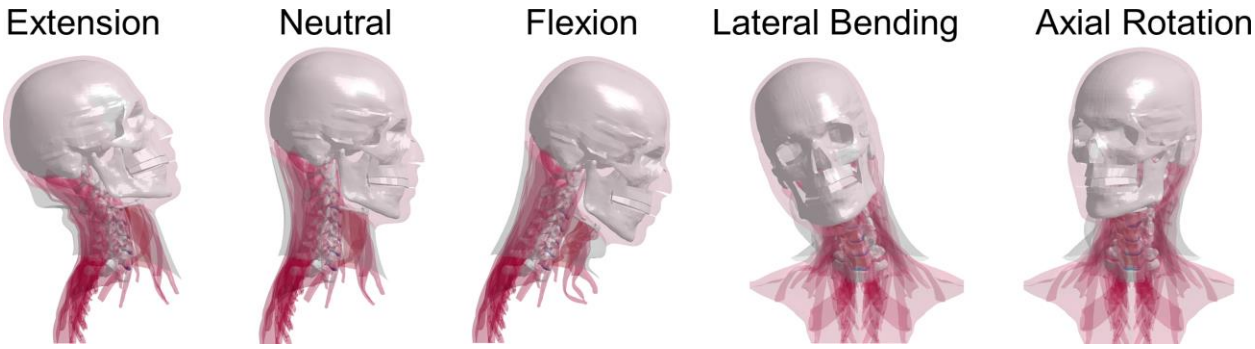

FIGURE 2-2: PRIMARY NECK MOTIONS

The vertebral column is composed of individual bones called vertebrae and are connected as a continuous column. It is a vital structural component in the human body as it forms a connection from the head, leading to the thoracic region and down to the sacrum. It is not only a load bearing structure that must support external forces but must contain and protect the central nervous system (i.e. spinal cord) and delicate vascular structures. Furthermore, it provides important musculature attachment points along the entire column to facilitate movement from the head, down to the lower back. In addition to providing these structural functions, the vertebral column must be flexible enough to accommodate normal day-to-day movements within physiologic ranges of motion.

The vertebral column can be broken down into five distinct sections: the cervical (C) spine, thoracic (T) spine, the lumbar (L) spine, the sacrum, and the coccyx (Figure 2-3) (Standring, 2008). The cervical, thoracic, and lumbar sections are where motion occurs. The cervical spine is composed of seven vertebrae, the thoracic spine is composed of twelve vertebrae, and the lumbar spine, five vertebrae. The cervical spine has the unique functionality to provide the largest range of motions in all directions while forming a connection between the head to the neck (Figure 2-4).

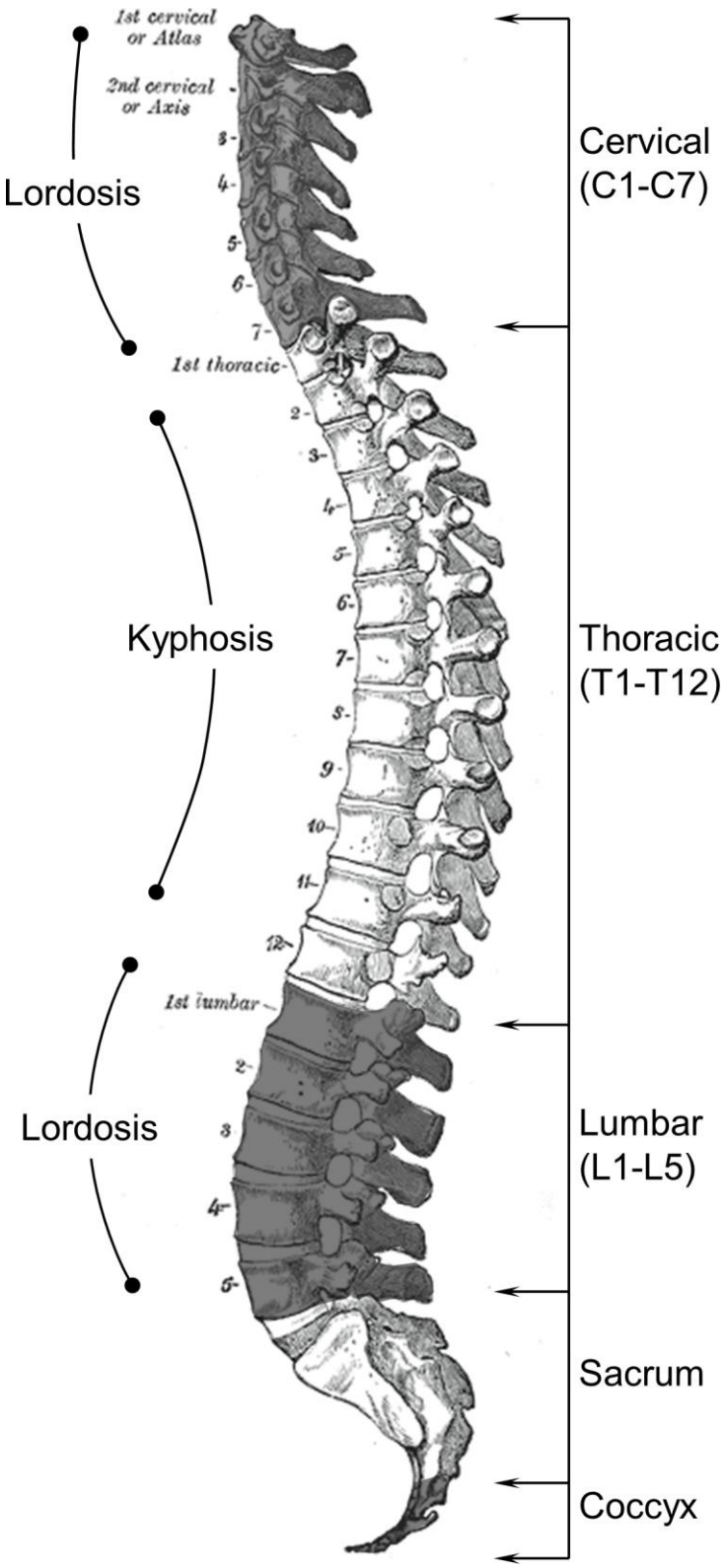

FIGURE 2-3: HUMAN VERTEBRAL COLUMN ILLUSTRATING DIFFERENT SECTIONS AND SPINAL CURVATURES *(Adapted from Gray, 1918)*

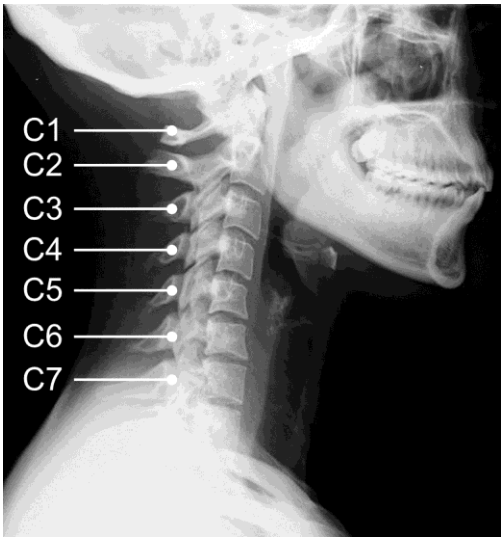

FIGURE 2-4: LATERAL RADIOGRAPHY OF THE CERVICAL SPINE
[Adapted from "Lateral neck X-ray of whiplash" by Jmarchn (CC BY-SA 3.0) https://commons.wikimedia.org/wiki/File:Lateral_neck_X-ray_of_whiplash.jpg]

The thoracic spine contains unique joints to allow attachment of individual ribs and connects the cervical spine to the lumbar spine. The lumbar spine connects the thoracic spine and the sacrum while featuring the largest vertebrae in the column to bear the weight of the head-neck complex and torso. When referring to a specific vertebra, the common terminology is to designate the spinal level followed by a number. Each section of the vertebral column is numbered starting from one, in descending order from the superior to inferior direction. For example, the seventh cervical vertebra can be denoted as "C7". A spinal segment or motion segment is a functional unit consisting of a pair of adjacent vertebrae and intermediate connective tissues and are denoted as the spinal level followed by the number of the superior vertebra, followed by the number of the inferior vertebra. For example, the motion segment that consists of the fourth and fifth cervical vertebra can be denoted as "C45".

Each vertebra exhibit common features and interconnectivity such as containing two synovial joints and a fibrocartilaginous intervertebral disc, with the exception of the first and second cervical vertebrae (Standring, 2008). The size of the vertebra increases in the inferior direction, with the lumbar spine containing the largest vertebrae. When viewed from the lateral aspect, the spinal column is not straight but exhibits a natural anatomic curvature in each spinal section (Figure 2-3). Lordotic curvature or lordosis is referred to as posterior concavity while kyphotic curvature or kyphosis is referred to as anterior concavity. Both the cervical and lumbar spine exhibits lordotic curvature, while the thoracic spine exhibits kyphotic curvature. The curvatures at each spinal section are often different between individuals and will change through life.

2.1.3 Cervical Spine Structures

Cervical Vertebrae

There are many structural similarities between vertebrae in the different regions of the cervical spine. The third to seventh cervical vertebra have very similar anatomic features and characteristics and are referred to as the lower cervical spine (LCS). There is a trend for the vertebrae to increase in dimension in the inferior direction due to the progressive addition of body weight from subsequent posterior structures (Standring, 2008). Each motion segment in the neck allow a limited quantity of movement, however when the summation of all motion segments are considered, it provides the greatest range of motion in the vertebral column (Standring, 2008). The cervical spine contains the smallest vertebrae and is unique with a transverse foramen in the transverse process through which the vertebral artery passes.

The first and second cervical vertebrae (upper cervical spine) contain unique anatomic features that are separate from the lower cervical spine vertebrae. This is the only vertebral segment in the neck that is not connected by an intervertebral disc and are held together only by a complex arrangement of ligaments and two facet joints (Standring, 2008).

The vertebrae are comprised of four main structures: the vertebral body, two articular pillars, and the spinous process (Standring, 2008). These structures are connected by the vertebral arch, which contains the pedicle and lamina. The vertebral body, pedicle and lamina form a triangular void in the center called the vertebral foramen, through which the spinal cord passes. There are seven processes in the cervical vertebra: two transverse processes, four articular processes, and one spinous process. Each process may contain a small protrusion of bone called a tubercle, which serves as additional attachment points for ligament and muscle. The vertebral body is located anteriorly, with a superior surface that is saddle-shaped and an inferior surface that is concave. This unique geometry limits anteroposterior and lateral movement between adjacent vertebrae in the neck. The transverse process and the lamina protrude bilaterally from the vertebral body and forms a circular opening called the transverse foramen, through which the vertebral artery passes into the brain (Figure 2-5).

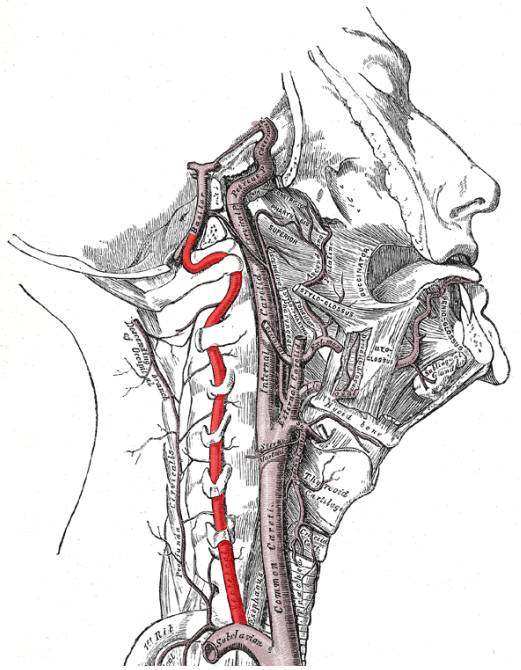

FIGURE 2-5: VERTEBRAL ARTERIES PASSING THROUGH THE VERTEBRAL FORAMEN *(Adapted from Gray, 1918)*

The two articular pillars feature both a superior and inferior oval surface called the articular facet surface and are located anterolateral to the vertebral body. The superior articular facet surface is directed in the posterosuperior direction while the inferior articular facet surface is facing the anteroinferior direction. The two lamina sections travel posteromedially and meet at a junction to form the spinous process. The spinous process is the primary component in the lower cervical spine that can be felt through palpation on the posterior surface of the neck. Indentations on both the superior and inferior surface of the pedicles form the superior and inferior vertebral notches. The vertebral notch from adjacent vertebrae creates a passageway called the intervertebral foramen, through which the spinal nerve root exits the spinal cord (Figure 2-6).

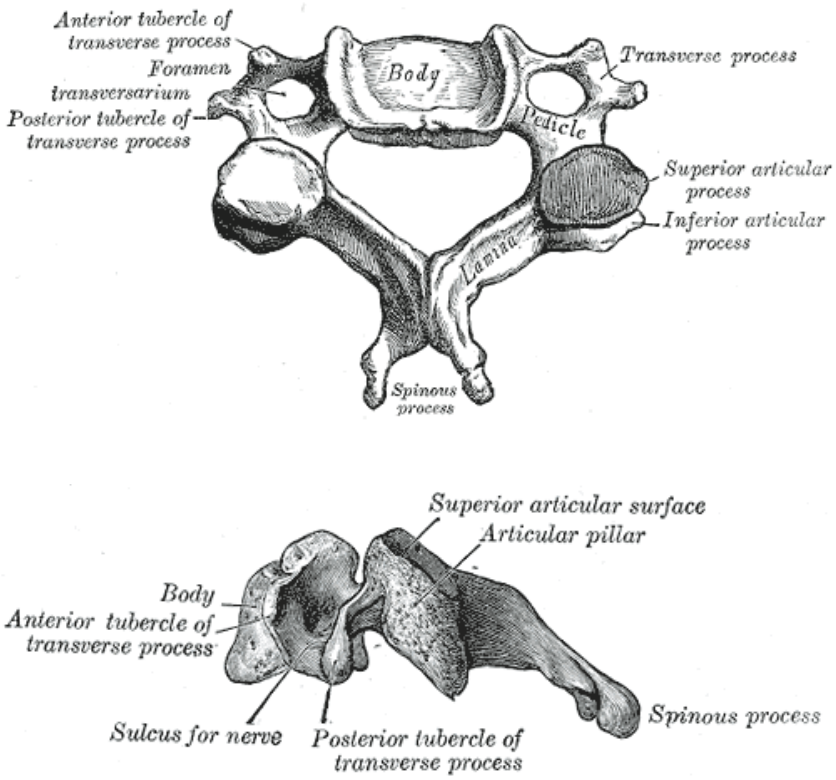

FIGURE 2-6: LOWER CERVICAL VERTEBRA *(Adapted from Gray, 1918)*

Bone tissues are complex biological materials possessing anisotropic, asymmetric (different tensile and compressive properties), viscoelasticity, and strain rate dependent material properties. The vertebra is constructed of two types of bone tissue called cortical and trabecular bone (Figure 2-7). Cortical (compact) bone surrounds the exterior walls of the vertebra with characteristics of high density and strength to withstand large compressive forces. Trabecular (spongy) bone is located within the outer cortical shell with characteristics of lower density (porous) and has a unique anisotropic lattice structure. The lattice structures of the bone tissue are called trabeculae and are oriented along the principal axis of stress to provide strength to the vertebra. Together, cortical and trabecular bone create a strong, lightweight structure to ensure each vertebra can endure the forces experienced during everyday life.

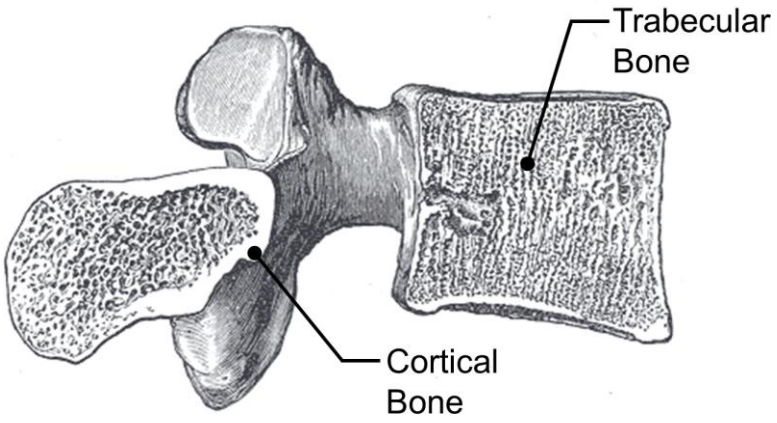

FIGURE 2-7: VERTEBRA BONE COMPOSITION *(Adapted from Gray, 1918)*

The first cervical vertebra (C1), also known as the atlas, is ring-shaped and responsible for supporting the base of the skull (Figure 2-8). There are no intervertebral discs between the skull and the atlas or with the second cervical vertebra (axis) due to the absence of a vertebral body. The main structure of the atlas is composed of two articular pillars connected by the anterior arch and the posterior arch. These two structures create a void in the center of the atlas that can be divided into two compartments. The first compartment occupies approximately one third of the anterior portion of the opening and encloses the odontoid process of the axis (Standring, 2008). The remaining portion (approximately two thirds) is occupied by the spinal cord. The transverse process extends bilaterally from the articular pillars and houses the transverse foramen. The superior articular facet surface is "kidney" shaped and acts as the base to accept the pair of occipital condyles on the skull (Standring, 2008). The atlas has a long transverse process, which provides large moment arms to help muscles make small adjustments to stabilize the head.

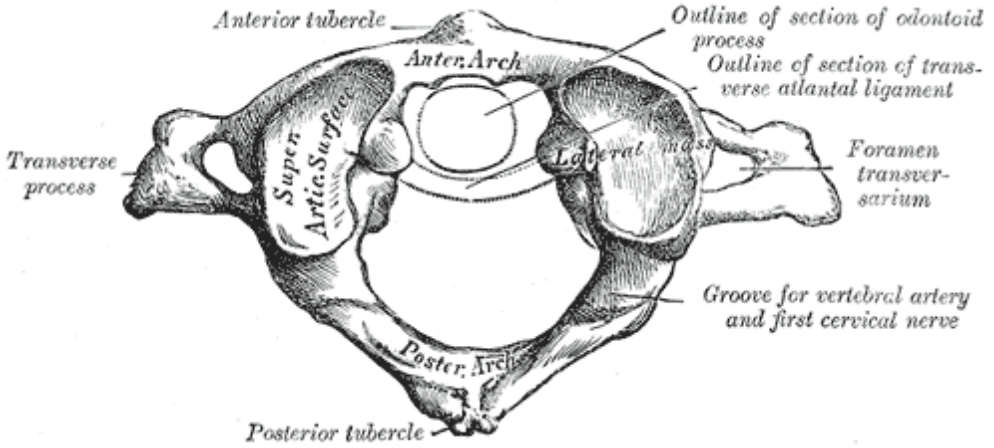

FIGURE 2-8: POSTERIOR VIEW OF THE ATLAS *(Adapted from Gray, 1918)*

The second cervical vertebra, commonly referred to as the axis, provides an axel to which the atlas and skull can rotate about (Figure 2-9). The most prominent feature of the axis is the odontoid process or dens, which protrudes superiorly from the vertebral body (Standring, 2008). The dens are positioned anterior to the spinal cord and held in position by the anterior arch and transverse ligament in the atlas. The transverse process is notably smaller, and the spinous process is thicker and stronger when compared to the inferior vertebrae (Standring, 2008). The two articular facet surface provides a platform to which the atlas and skull rotate.

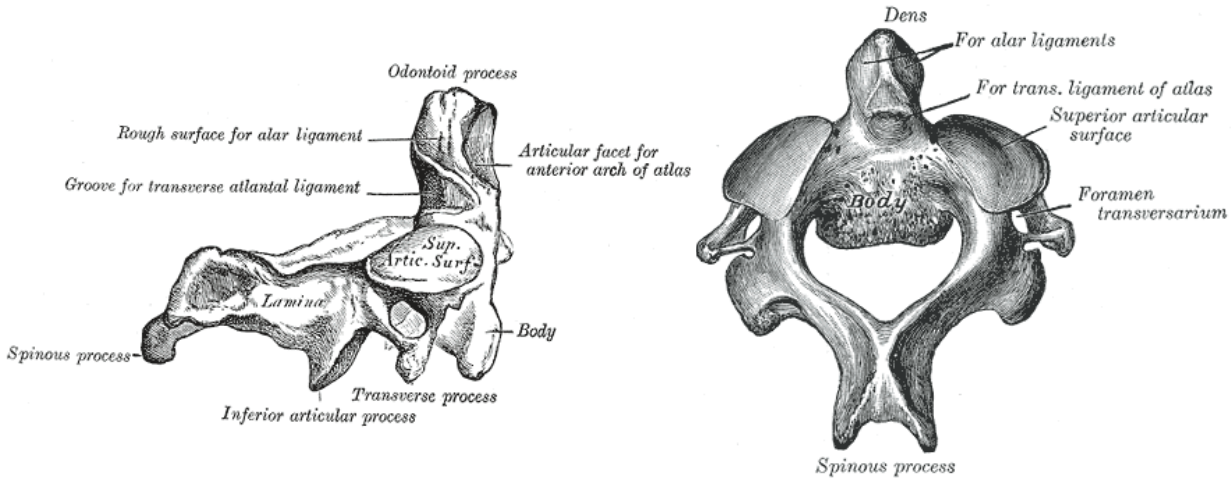

FIGURE 2-9: C2 VERTEBRA (AXIS) LATERAL AND SUPERIOR-OBLIQUE VIEW *(Adapted from Gray, 1918)*

Ligaments

Ligaments are the fibrous connective tissue that provides a connection between adjacent vertebrae to ensure stability and limit neck motions to within physiological limits. Ligaments are primarily composed of a compact collection of proteins called collagen and elastin (Standring, 2008). Collagen proteins are wrapped and linked together to create fibres that form the structural integrity of most tissues in the human body. Collagen is viscoelastic and responsible for the tensile strength of the ligament, while elastin is highly stretchable and exhibits a hyperelastic response. In general, these two proteins enable flexibility but provide substantial tensile strength when stretched. The ratio of collagen and elastin determine the mechanical response of the ligament (Yoganandan et al., 2001). Due to this composition, ligaments are tensile resistant structures with a negligible compression response. Like other biological tissues, ligaments are strain rate dependent, nonlinear viscoelastic materials that exhibit four distinct tensile loading regions: toe, linear, traumatic, post-traumatic, and rupture region (Mattucci and Cronin, 2015). When a ligament is distracted, there is an initial nonlinear region called the toe region, where collagen fibres begin to straighten from the

initial relaxed crimped state. The fibres transition into the linear response region (constant stiffness) when all collagen fibres have straightened and are fully engaged in resisting the tensile load. As distraction continues, microlesions may form in the ligament and stiffness will begin to decrease when stretched beyond the physiological limit as the ligament response enters the traumatic region (Yoganandan et al., 2001; Yoganandan et al., 1988). In this phase of loading, the ligament remains intact while damage cannot be observed macroscopically (Nordin and Frankel, 2001) and the ligament stiffness will continually decrease as microlesions increase, until macroscopic failure occurs at the ultimate load where the stiffness drops momentarily to zero and will enter the post-traumatic region. At this state, bundles of collagen fibres have ruptured, causing a steep decrease in the force response. In the post-traumatic region, the force response will continue to drop as bundles of collagen fibres progressively fail until the ligament is fully ruptured (i.e. no force response) (Dewit and Cronin, 2012).

Two bands of strong ligaments run longitudinally along the vertebral bodies and travel from the axis down to the sacrum (Standring, 2008). These ligaments are composed of individual fibres that are layered on top of each other and run continuously, spanning up to four vertebrae. The anterior longitudinal ligament (ALL) is located along the anterior surface of the vertebral bodies and travels from the skull down to the sacrum (Figure 2-10). The primary function of the ALL is to resist neck extension and provide stability to the cervical column.

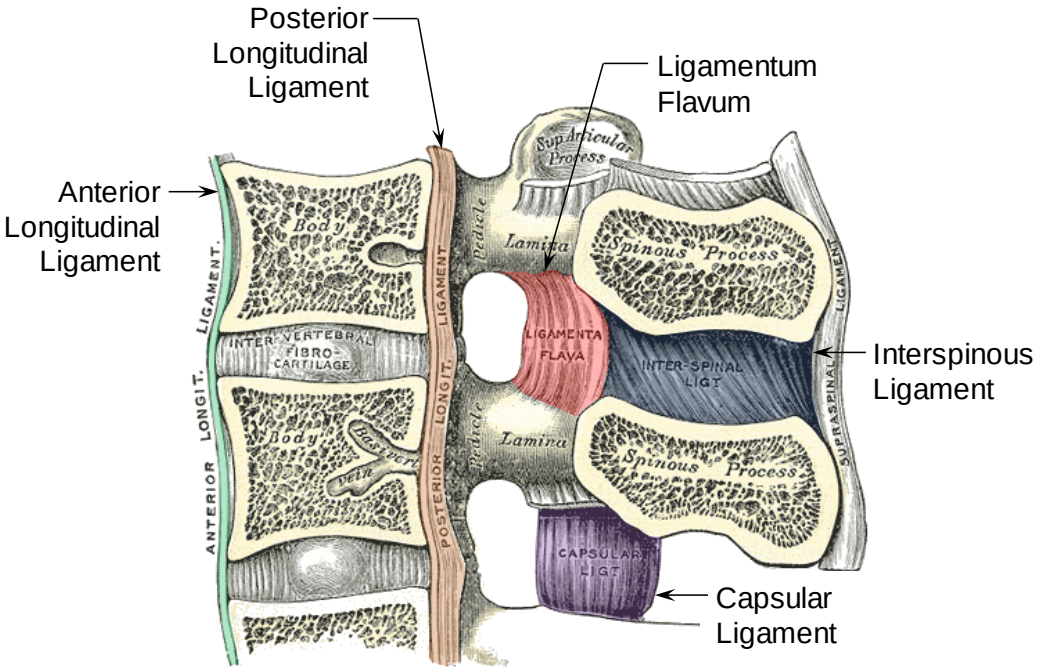

FIGURE 2-10: LOWER CERVICAL SPINE LIGAMENTS (SAGITTAL SECTION VIEW) *(Adapted from Gray, 1918)*

The posterior longitudinal ligament (PLL) is located along the posterior surface of the vertebral bodies, which is also the anterior surface of the spinal canal (Figure 2-10). The primary function of the PLL is to resist neck flexion and provide stability to the cervical spine. These two ligaments not only adhere to the anterior and posterior surface of the vertebral bodies but also to the surface of the intervertebral disc.

The capsular ligament (CL) surrounds the periphery of each articular process to form an enclosure for the facet joint (Figure 2-10). The two pairs of CL are located on every segment level in the cervical spine including the atlanto-axial and atlanto-occipital joints.

The ligamentum flavum (LF) runs through the posterior surface of the vertebral canal, connecting the laminae of adjacent vertebrae (Figure 2-10). Unlike the longitudinal ligaments, the LF is not continuous, but connect the inferior surface of the superior laminae to the superior surface of the inferior laminae. The LF resist neck flexion by reducing motion between adjacent laminae.

The interspinous ligaments (ISL) run vertically and connect adjacent spinous processes (Figure 2-10). This ligament covers the entire length of the spinous process and primarily limit neck flexion during movement.

The upper cervical spine (UCS) is connected by a complex arrangement of ligaments due to the absence of an intervertebral disc (Figure 2-11, Figure 2-12). The anterior atlanto-occipital membrane (AAOM) connects the superior surface of the anterior atlantal arch to the anterior margin of the foramen magnum (Standring, 2008). Running continuous from the AAOM, the anterior atlanto-axial membrane (AAAM) attaches onto the anterior surface of the C2 vertebral body. The AAAM is continuous with the ALL in the lower cervical segment levels. The posterior atlanto-occipital membrane (PAOM) connects the posterior atlantal arch to the posterior margin of the foramen magnum. The posterior atlantal-axial membrane (PAAM) is located directly below the PAOM and attach onto the posterior surface of the C2 vertebral body. The PAAM is a continuation of the LF in the lower cervical segment levels.

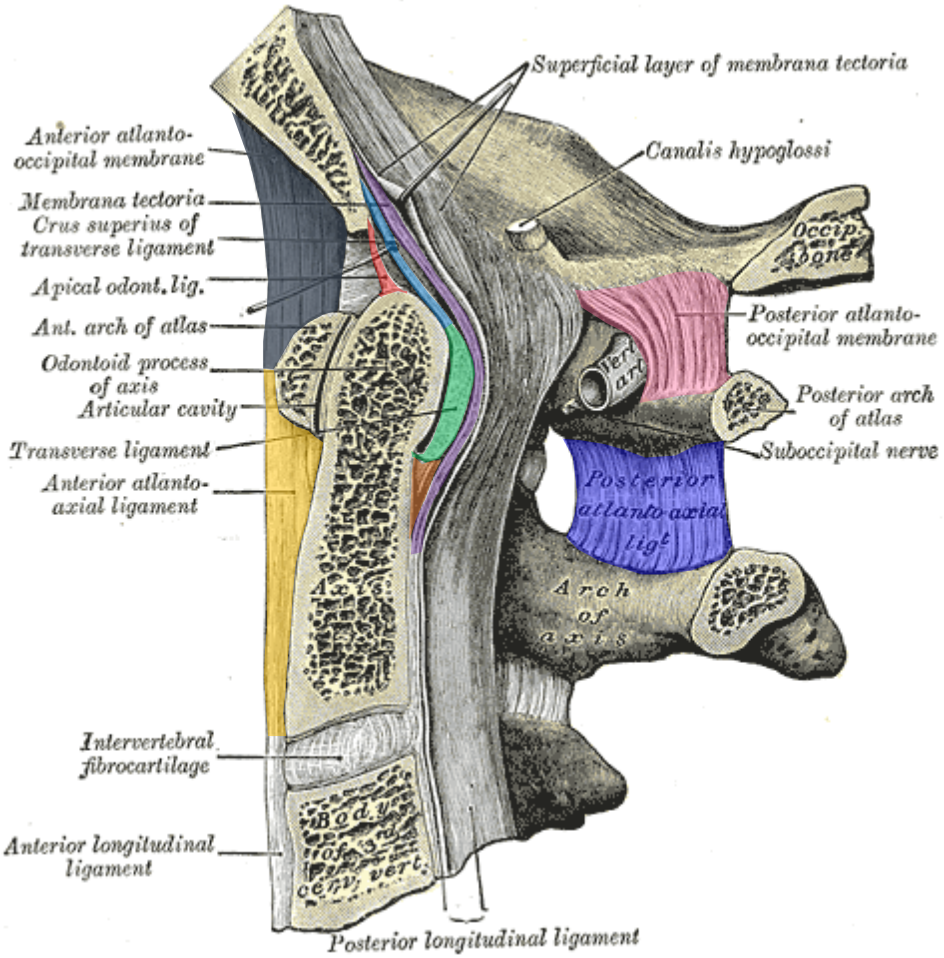

FIGURE 2-11: LEFT SAGITTAL SECTIONAL VIEW OF THE UCS *(Adapted from Gray, 1918)*

The tectorial membrane is a band of tissue that runs from the posterior surface of the C2 vertebral body and attach onto the basilar occipital bone. This ligament is continuous with the PLL from the lower segment levels.

The transverse ligament runs laterally from the lateral mass of the atlas and confines the odontoid process of the axis onto the anterior atlantal arch (Standring, 2008). The transverse ligament is located anterior to the tectorial membrane. From the medial aspect of the transverse ligament, additional fibers run longitudinally to connect the transverse ligament to the posterior surface of the C2 vertebral body (inferior cruciate ligament) and the occipital bone (superior cruciate ligament). Together, these three ligaments form the cruciate ligament of the atlas. The apical ligament run longitudinally from the apex of the odontoid process to connect onto the anterior margin of the foramen magnum and is located anterior to the superior cruciate ligament. The alar ligament consists of two bands of tissue that extends bilaterally from the

odontoid process and attach onto the lateral margins of the foramen magnum near the medial aspect of the occipital condyles.

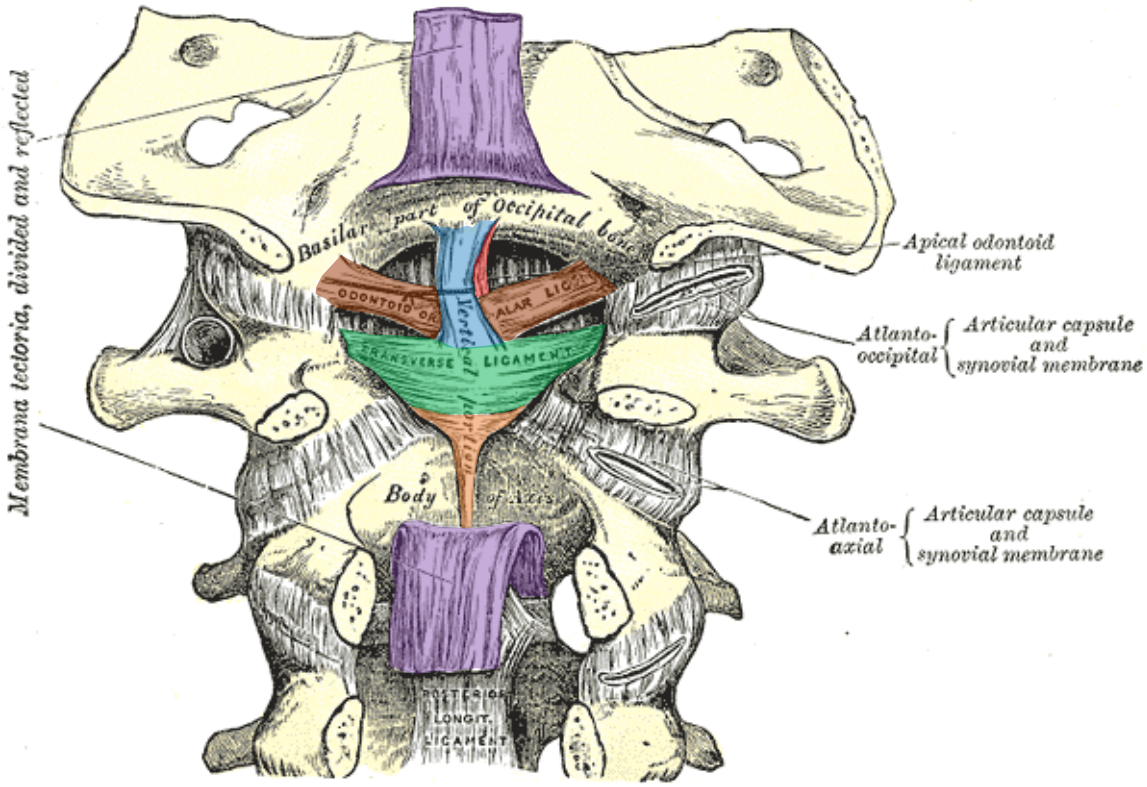

FIGURE 2-12: POSTERIOR VIEW OF UCS LIGAMENTS *(Adapted from Gray, 1918)*

Intervertebral Disc

The intervertebral disc is a fibrocartilaginous connection situated between each adjacent vertebral body in the cervical spine, with the exception of the atlantoaxial joint (C1-C2). The disc forms an amphiarthrodial (slightly movable) joint between adjacent vertebral bodies, reinforced by the anterior and posterior longitudinal ligaments (Standring, 2008). In the cervical vertebrae, the anterior region of the disc has a greater thickness when compared to the posterior region and is attributed to the lordotic curvature of the cervical spine (Standring, 2008). The inferior and superior ends of the disc adhere to the vertebral endplate that is consisted of a layer of cartilage found at the superior and inferior surface of the vertebral body. In addition, the anterior and posterior regions of the disc are adhered to the anterior and posterior longitudinal ligaments.

The disc has two primary components: a tough outer annulus fibrosus and the internal nucleus pulposus (Figure 2-13) (Standring, 2008). The annulus fibrosus is a composite structure that constitutes layers of

anisotropic lamellae arranged concentrically around each disc. Each lamella layer has collagen fibres that are arranged parallel to each other at an angle of approximately ±25 degrees to ±45 degrees from the transverse plane (Cassidy et al., 1989) and are surrounded by a matrix of water and proteoglycans called the ground substance. The angles of the collagen fibres alternate between each successive lamella layer to provide stability during any neck motion (particularly axial rotation).

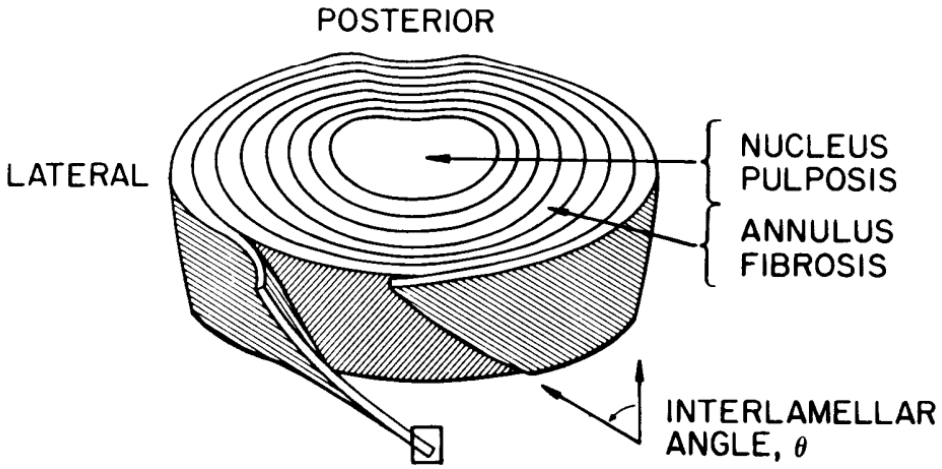

FIGURE 2-13: IVD ANNULUS FIBROSUS COLLAGEN FIBER ANGLE *(Adapted from Cassidy et al., 1989)*

The nucleus pulposus is an incompressible fluid-like gelatinous material located within the annulus fibrosus with the primary purpose of resisting and distributing compressive loads to the vertebral endplates. Together, this unique composition of the intervertebral disc allow for flexibility between vertebrae and provide shock absorption by deforming amid neck movements. During compression, the nuclear material expands outwards, causing radial expansion and increased bulging of the annulus fibrosus, loading the collagen fibres in tension (Figure 2-14). For example, during anterior bending, the posterior region of the disc is loaded in tension while the anterior region is in compression (Figure 2-14). This mechanism of loading can be applied for all other bending directions during neck movement.

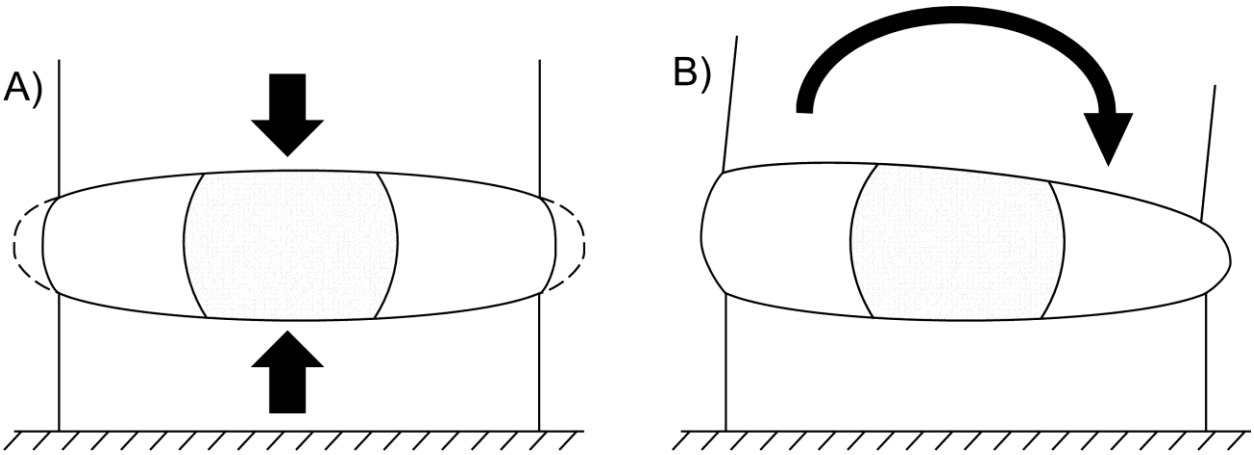

FIGURE 2-14: IVD RESPONSE: A) COMPRESSION, B) BENDING

Facet Joint

The facet (zygapophysial) joints are bilateral synovial joints, located at the posterolateral aspect of a motion segment, formed by the inferior articular surface of the superior vertebra, and the superior articular surface of the inferior vertebra (Standring, 2008). This joint is classified as a diarthrodial (freely movable) joint (Standring, 2008). The articular surface of the articular process is covered in a layer of articular cartilage, which has characteristically low friction and enables the contacting surfaces of the bone to glide smoothly to prevent damage to the subchondral bone (bone underneath the cartilage). The exterior of the facet joint is surrounded circumferentially by the articular capsule (capsular ligament), while the interior contains a separate lining called the synovial membrane. This membrane secretes synovial fluid to help lubricate and reduce friction between the cartilage surfaces during traction. The synovial fluid fills the joint cavity created between the two articular cartilage surfaces and surrounding membrane. Located subjacent to the synovial membrane exists intra-articular structures called the synovial fold (meniscoids), particularly in the anterior and posterior regions of the facet joint. The synovial fold surrounds the periphery of the joint and consists of adipose and fibrous connective tissues and functionally, have been hypothesized to help distribute compressive forces across the contacting joint surface (Jaumard et al., 2011).

The main function of the facet joint is to guide and limit movement between adjacent vertebrae, prevent potential damage to surrounding soft tissues, and transfer compressive forces throughout the cervical column. Therefore, the general movement of the neck is largely dictated by the shape and orientation of the facet joint. The surface of the joint is inclined at an angle of approximately 45° within the sagittal plane with the superior face of the articular process facing towards the posteromedial direction (Panjabi et al., 1993). This orientation limits mobility for adjacent cervical motion segments (excluding atlas and axis) in axial rotation, lateral bending, and lateral/anteroposterior translations, but allows for extensive ranges of

motion in flexion and extension. Additionally, the facet geometry results in axial and lateral motion of the cervical vertebra to be coupled, meaning during lateral bending, axial rotation will also occur, and vice versa (Bogduk and Mercer, 2001). Although motions such as axial rotation and lateral bending are limited, the summation of movements between all cervical segments is still substantial and enables a high degree of neck mobility.

Nerve Roots

The nerve roots and spinal nerves located within the vertebral column are part of the nervous system, which is considered to be the most complex system in the human body. The nervous system can be divided into two networks: the central nervous system and the peripheral nervous system (Standring, 2008). The central nervous system (CNS) consists of the brain and spinal cord, while the peripheral nervous system (PNS) refers to cranial and spinal nerves and associated branching nerve structures located throughout the body. Communication between the CNS and the body occurs via the PNS nerve fibres through the afferent (sensory) fibres and efferent (motor) fibres (Figure 2-15) (Standring, 2008). This network can be perceived as an input-output system where afferent fibres transmit information into the CNS via sensory receptors in the periphery, and efferent fibres relay information from the CNS to peripheral systems (e.g. skeletal muscle for contraction). These long nerve fibres that travel throughout the body are called axons and are extensions of nerve cells (neurones), which function to encode, relay and transmit information via nerve impulses (Standring, 2008).

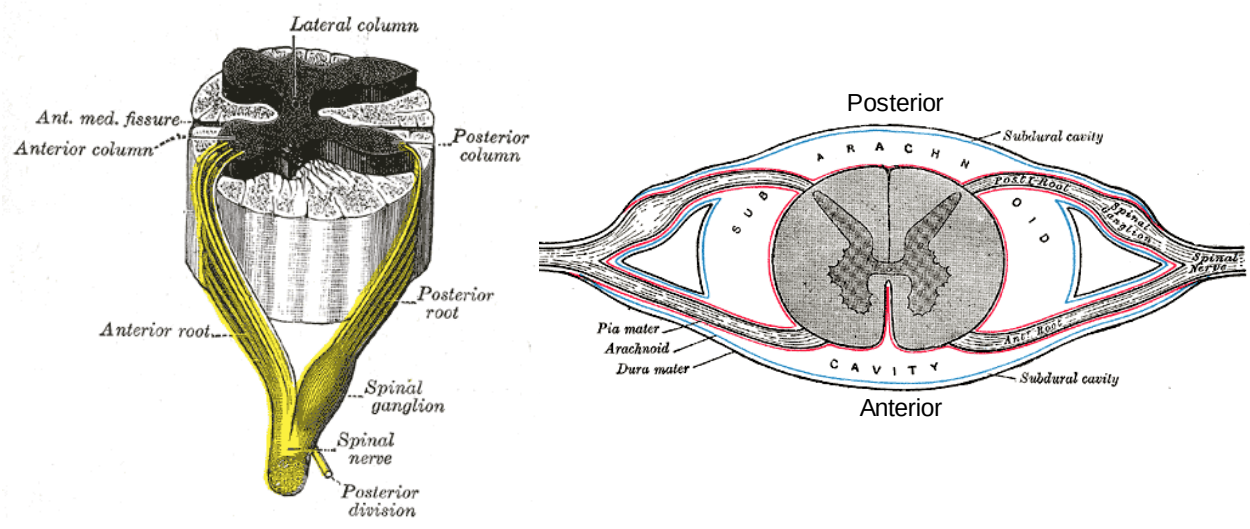

FIGURE 2-15: NERVE ROOTS, SPINAL NERVE, AND SPINAL CORD: LEFT LATERAL VIEW AND SUPERIOR VIEW *(Adapted from Gray, 1918)*

The spinal nerves and nerve roots form the transitional structures between the CNS and PNS (Standring, 2008). There are eight pairs of spinal nerves in the cervical spine (C1-C8), and are composed of both motor and sensory fibres. The nerve roots are designated by the vertebra inferior to the root (e.g. C3 spinal nerve is located between C2 and C3 and C8 is located between C7 and T1). Two pairs of spinal nerves exit bilaterally from the vertebral canal and run anterolaterally between adjacent vertebrae through the intervertebral foramen (Figure 2-16). Each pair of spinal nerves are formed from the union of the dorsal (sensory) and ventral (motor) root, while each dorsal and ventral root are comprised of multiple adjacent dorsal and ventral rootlets originating from the spinal cord (Standring, 2008). The dorsal root contains afferent nerve fibres and ventral roots contain efferent fibres. Along the dorsal root between the spinal cord and the spinal nerve constitutes a distinct section called the dorsal root ganglion (Standring, 2008). The ganglion contains a cluster of afferent neuronal cell bodies and is physically prominent by the enlarged diameter of the dorsal root, just before the junction that forms the spinal nerve.

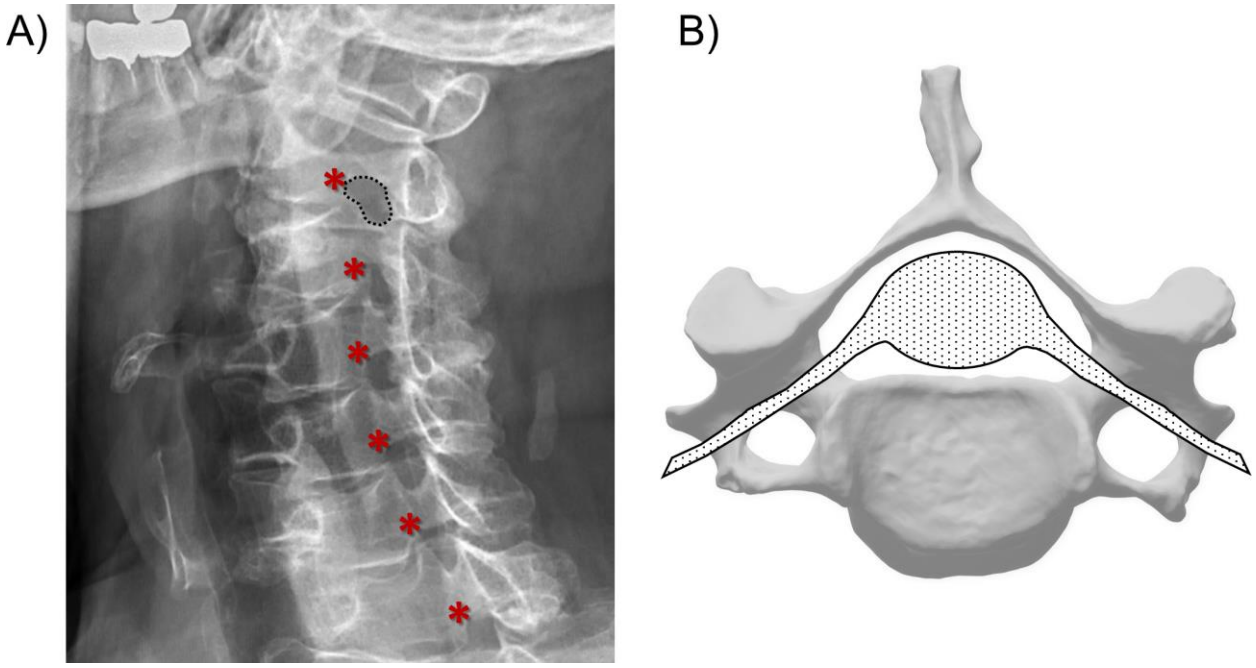

FIGURE 2-16: A) LATERAL VIEW OF THE CERVICAL SPINE, IVF MARKED BY ASTERISK (C23 FORAMEN OUTLINED), B) SPINAL NERVES EXITING IVF, SUPERIOR VIEW

[Adapted from "Projectional radiograph of cervical foraminal stenosis" by Mikael Häggström (CC0 1.0) https://commons.wikimedia.org/wiki/File:Projectional_radiograph_of_cervical_foraminal_stenosis.jpg; "Human cervical vertebra" by Eric Bauer (CC BY 4.0) https://commons.wikimedia.org/wiki/File:Human_cervical_vertebra.stl]

Muscles

The human body is comprised of three different types of muscle tissue: skeletal, cardiac, and smooth. Skeletal muscles are voluntary, reflexive, striated and are responsible for voluntary control to facilitate the movement of the body. Cardiac muscles are involuntary and striated and are only located in the walls of the heart and surrounding vascular structures. Smooth muscles are non-striated, involuntary and constitute the lining of vessels of the circulatory system and hollow organs (e.g. stomach, intestines, bladder, etc.).

Skeletal muscles are composed of hierarchical tissues ranging from the muscle as a whole, down to the individual contractile units of a single muscle cell (Figure 2-17) (Standring, 2008). A muscle is composed of bundles of fascicles, and each fascicle contains bundles of muscle fibres. Each muscle fibre is constructed from bundles of myofibrils that are composed of longitudinally aligned contractile units called a sarcomere (basic contractile units). Each hierarchical component of a muscle are enclosed by collagenous sheathes known as the epimysium (whole muscle), perimysium (fascicles), and endomysium (muscle fibres) (Standring, 2008). Within each muscle fibre, individual myofibrils are surrounded by a cellular membrane structure called the sarcoplasmic reticulum. This membrane carries calcium ions, which are critical in the role of initiating and terminating muscle contraction. Each sarcomere unit measures approximately 2.6 μm in length in a human skeletal muscle at a resting state (Kamibayashi and Richmond, 1998). The sarcomere is composed of actin (thin) and myosin (thick) filaments. The current understanding of skeletal muscle contractions is based on the sliding filament theory, and is briefly described at a high level below.

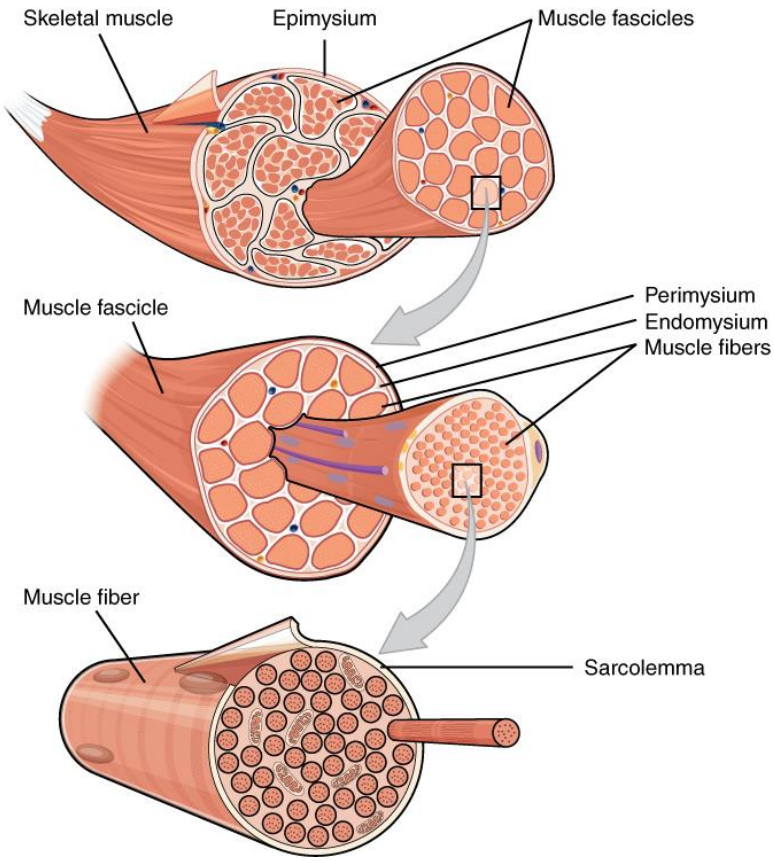

FIGURE 2-17: HIERARCHICAL STRUCTURE OF SKELETAL MUSCLE AND CONNECTIVE TISSUES
[Adapted from "10.2 Skeletal Muscle, Figure 1" by Rice University (CC BY 4.0) https://opentextbc.ca/anatomyandphysiology/chapter/10-2-skeletal-muscle/]

Stimulation from motor neurons causes an action potential that travels to the muscle fibre and arrives at the neuromuscular junction. This action potential causes depolarization of the sarcoplasmic reticulum and initiates a release of calcium ions into the muscle fibres through a series of electrochemical events. Actin-binding sites exist on the thin filament (actin) for the myosin heads to attach onto (Figure 2-18). These binding sites are covered by two regulatory proteins called tropomyosin and troponin. Calcium ions released by the sarcoplasmic reticulum bind with troponin and induce a modification in the shape of both proteins, which reveal the binding sites (Standring, 2008). The myosin heads can proceed to attach onto the active binding sites to form cross-bridges and pull the actin inward that result in contraction (Figure 2-19). Each stroke of the myosin head cause movement of 1 nm to 5 nm (Standring, 2008), with average total shortening of 1 μm for each sarcomere.

Muscle relaxation occurs in the opposite manner and begins when the nerve impulse from the motor neurons stops firing. The release of calcium ions into the muscle fibres is reversed and travel back into the sarcoplasmic reticulum as repolarization of the membrane occurs (Standring, 2008). This causes the

troponin to cover the actin-binding sites, preventing cross bridge formation, which results in the actin to slide outward. As the cross bridges decrease, muscle tension falls until the muscle fibres reaches a relaxed state.

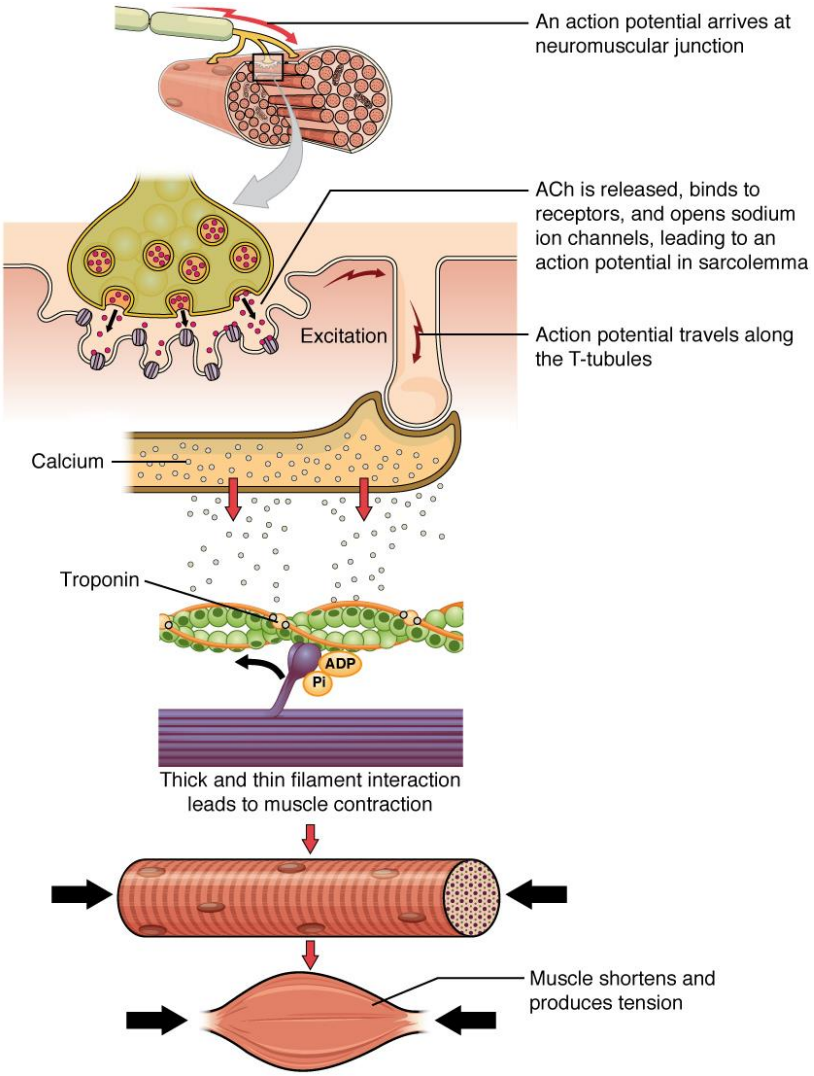

FIGURE 2-18: SLIDING FILAMENT MODEL OF MUSCLE CONTRACTION

[Adapted from "10.3 Muscle Fiber Contraction and Relaxation, Figure 1" by Rice University (CC BY 4.0) https://opentextbc.ca/anatomyandphysiology/chapter/10-3-muscle-fiber-contraction-and-relaxation/]

The force that a muscle can generate is a summation of the forces produced at each cross bridge at the molecular level (Standring, 2008). Therefore, the force produced by each skeletal muscle is directly proportional to the number of muscle fibres, hence is proportional to the cross-sectional area, known as the PCSA.

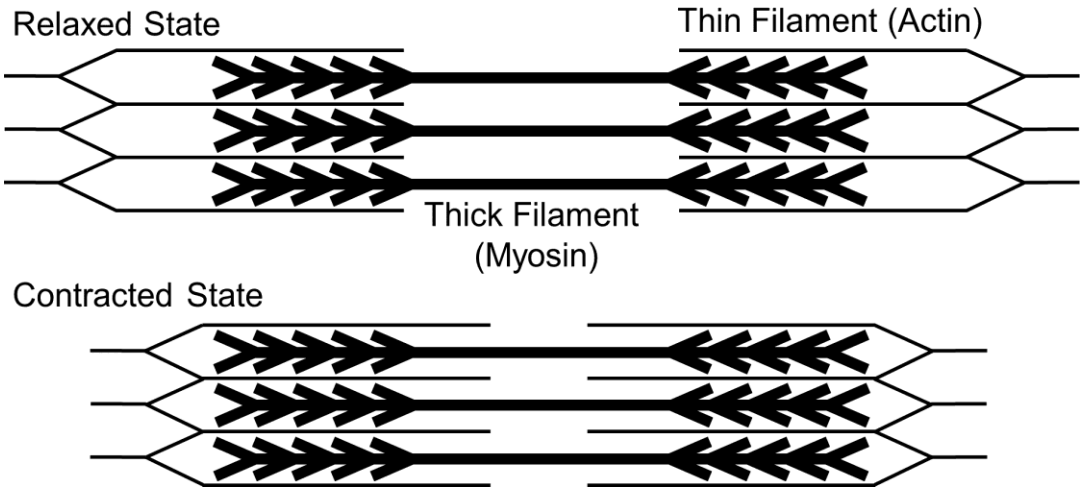

FIGURE 2-19: DEPICTION OF A SARCOMERE UNDERGOING CONTRACTION

There are three types of muscle contraction that a skeletal muscle can produce: concentric, eccentric and isometric contraction. Concentric contraction occurs when muscles are being contracted while shortening in length (e.g. bicep curl). Eccentric contraction is the opposite of concentric contraction where a muscle is activated but increasing in length (e.g. quadriceps when walking downhill). Isometric contraction refers to muscles that are activated but maintained at a static length during activation (e.g. plank exercise).

Skeletal muscles are attached to hard tissues by tendons to allow movement by transmitting tensile forces produced by the muscle fibres during contraction. To create movement, one end of the muscles must be stationary (origin) and the other end movable (insertion) (Standring, 2008). The insertion and origin positions are used to define the landmark of each muscle. The cervical musculature is composed of a complex arrangement of layered skeletal muscles that work in conjunction with each other to produce movement of the head. In addition, they provide stability in the cervical column, and help maintain posture. Muscles in the neck are arranged in symmetric pairs about the mid-sagittal plane and can be activated bilaterally to produce flexion and extension, or can be activated unilaterally to produce lateral bending and/or axial rotation. These muscles are primarily divided into the anterior and posterior groups by the location and type of movement they produce when activated bilaterally (flexion and extension) (Standring, 2008).

The sternocleidomastoid is a superficial muscle that wraps around the anterior and posterior aspect of the neck (Figure 2-20) (Standring, 2008). This muscle originates from the sternum and clavicle and runs posterolaterally to the mastoid process on the skull. Flexion and anterior head translation are produced when

activated bilaterally. Ipsilateral lateral bending and contralateral axial rotation result from unilateral activation.

The infrahyoid muscles are attached and located inferior to the hyoid bone: sternohyoid, sternothyroid, and omohyoid (Figure 2-20) (Standring, 2008). These muscles produce principal actions that contribute to the movement of the hyoid bone and thyroid cartilage to facilitate speech and swallowing, with the potential to act synergistically with other muscle to produce flexion. The sternohyoid and sternothyroid originate from the clavicle and sternum respectively and insert onto the hyoid bone. The omohyoid is separated into two bellies, linked together by an intermediate tendon. It originates from the upper border of the scapula and attaches onto the hyoid bone.

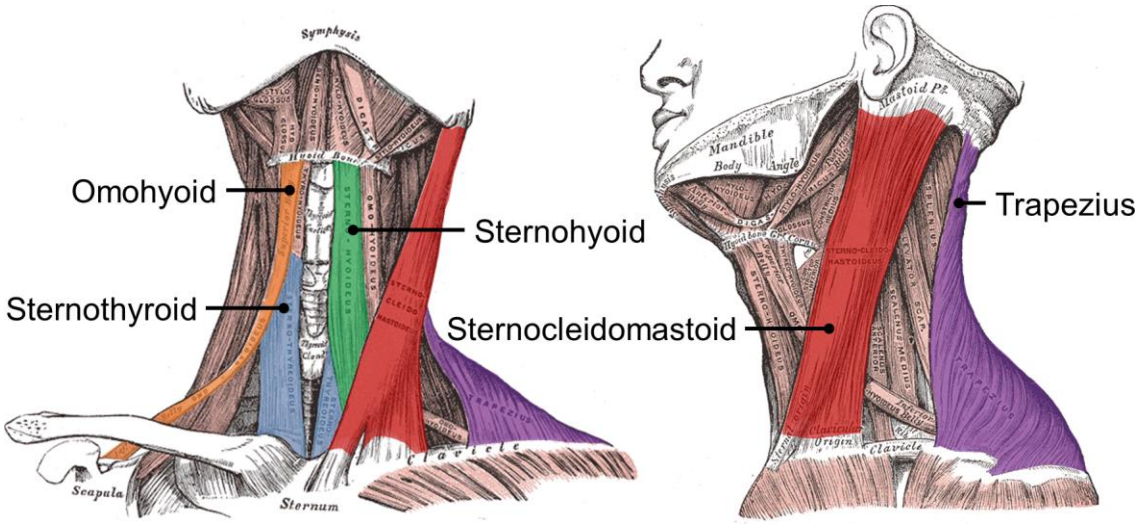

FIGURE 2-20: ANTERIOR NECK MUSCLES AND TRAPEZIUS *(Adapted from Gray, 1918)*

The prevertebral muscle group consists of the remaining anterior muscles: suboccipital (rectus capitis anterior and rectus capitis lateralis), deep anterior (longus capitis and longus colli), and lateral vertebral (scalenus anterior, scalenus medius, scalenus posterior) muscles (Figure 2-21) (Standring, 2008). The anterior suboccipital muscles both originate from the transverse process of the atlas and insert onto the occipital bone of the skull, with the rectus capitis anterior running superomedially and the rectus capitis lateralis running superiorly. The rectus capitis is responsible for atlanto-occipital anterior flexion, while the rectus capitis lateralis performs ipsilateral lateral head flexion. The longus capitis and longus colli are long narrow muscles that run superiorly adjacent to the anterior surface of the vertebral bodies of the cervical column. The longus capitis produce head flexion and originate from the transverse process of C3-C6 with attachment to the occipital bone. The longus colli arises from the transverse process of C3-T3 and attaches

onto the anterior surface of the C2-C6 vertebral bodies. Neck flexion is produced when activated bilaterally, while ipsilateral neck flexion and contralateral axial rotation during unilateral activation. Lastly, the lateral vertebral muscles are split into the scalenus anterior, medius and posterior muscles, all of which runs obliquely from the vertebral column to the first and second rib. The scalenus anterior originate from the transverse process of C3-C6 with attachment onto the first rib and produces neck ipsilateral anterolateral flexion and contralateral rotation of the neck. The scalenus medius arises from the transverse process of C1-C2 and insert onto the first rib, and produces ipsilateral anterolateral flexion of the neck. The scalenus posterior initiates ipsilateral flexion and arise from the transverse process of C4-C6 and attach onto the second rib.

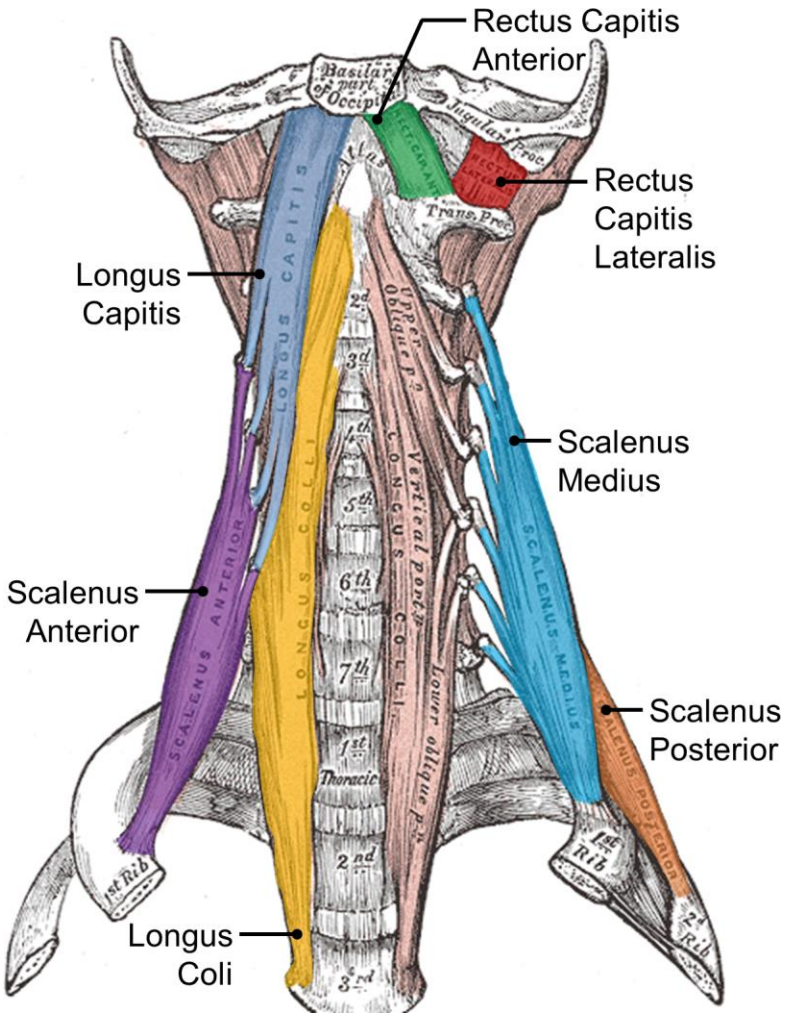

FIGURE 2-21: ANTERIOR NECK MUSCLES *(Adapted from Gray, 1918)*

The trapezius is the most superficial muscle located on the posterior neck region and along with the rhomboideus minor and levator scapulae, form the scapular group (Figure 2-22) (Standring, 2008). The trapezius originates from the external occipital protuberance of the skull, the ligamentum nuchae, and the spinous process of C7-T10 and inserts onto the clavicle and scapula in the anterior and posterior aspect respectively. The primary function is to elevate and retract the scapula, but can also aid in head extension when the shoulders are fixed. The rhomboideus minor initiates from the spinous process of C7-T1 and attaches onto the medial end of the scapula, with a primary function of scapula retraction. Lastly, the levator scapulae arise at the spinous process of C1-C4 and attach onto the superior medial end of the scapula, with the purpose of scapula elevation.

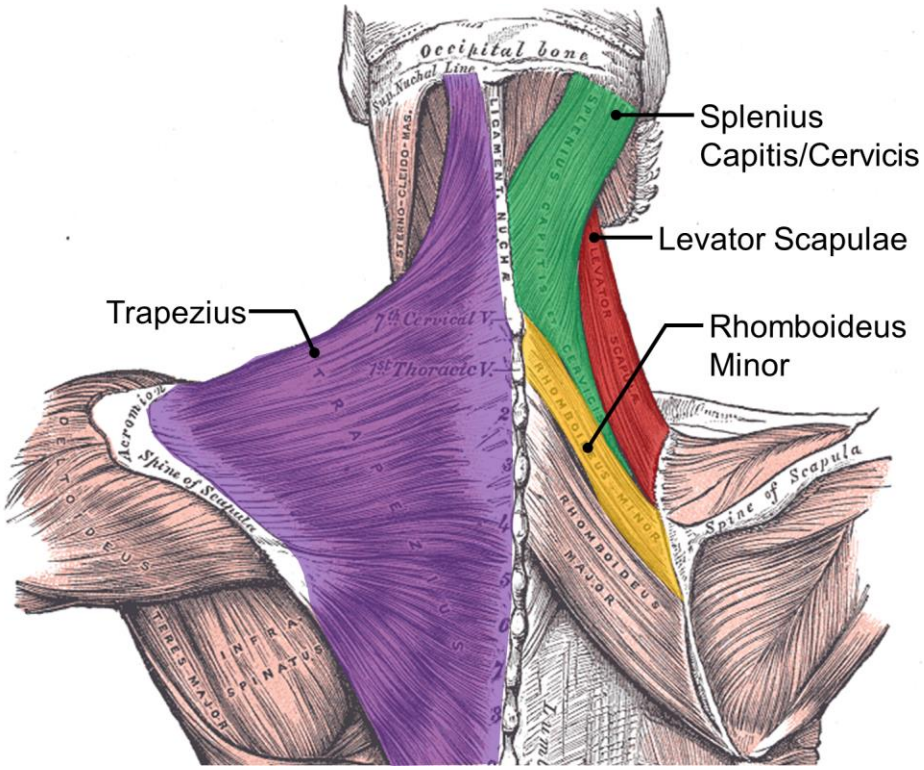

FIGURE 2-22: POSTERIOR BACK MUSCLES *(Adapted from Gray, 1918)*

The splenius capitis and cervicis are posterior muscles, which are located subjacent to the trapezius (Figure 2-22) (Standring, 2008). The splenius capitis begins at the ligamentum nuchae and the spinous process of C7-T4 and runs superolaterally to towards the mastoid process of the skull. Bilateral activation produces head extension, while unilateral activation with the contralateral sternocleidomastoid yields ipsilateral head axial rotation. The splenius cervicis is a continuation of the splenius capitis, which arise from the spinous process of T3-T6 and attaches onto the transverse process of C1-C3. Principle actions for

bilateral and unilateral activation include upper cervical spine extension and ipsilateral axial rotation respectively.

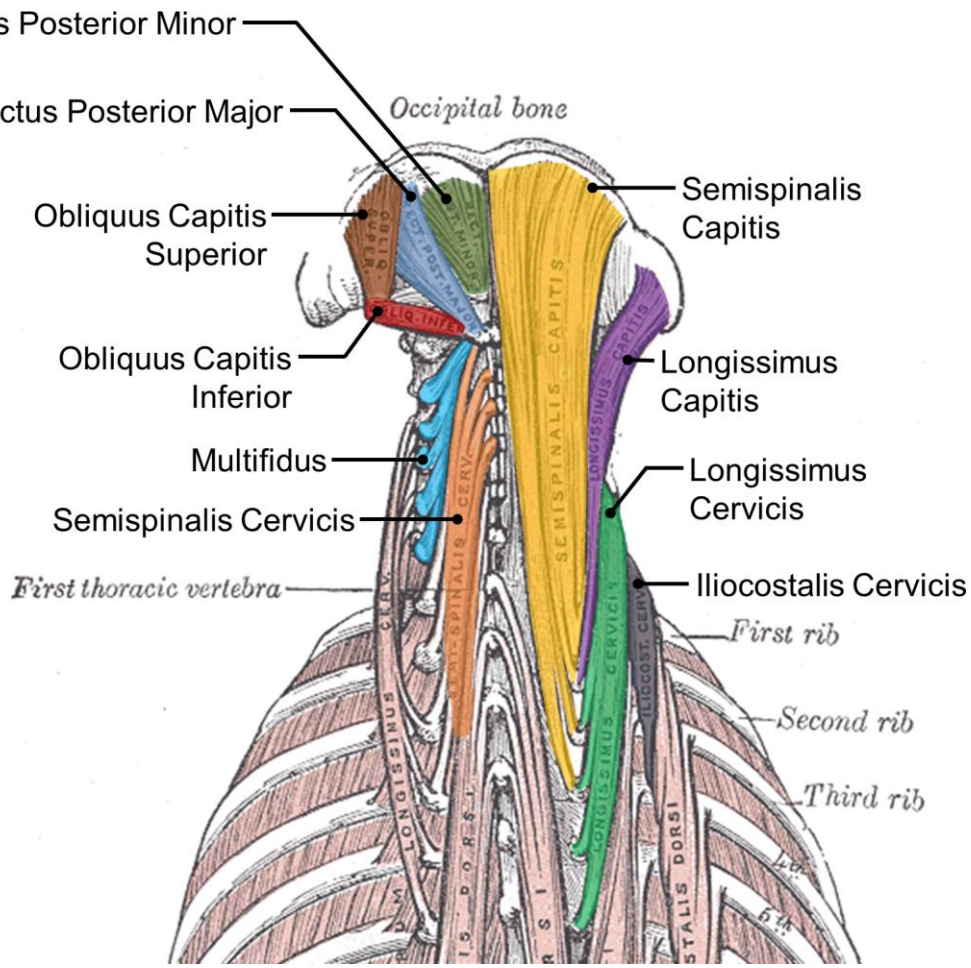

FIGURE 2-23: POSTERIOR NECK MUSCLES *(Adapted from Gray, 1918)*

The cervical erector spinae muscle group aids in cervical column extension and includes the longissimus capitis, longissimus cervicis, and iliocostalis (Figure 2-23) (Standring, 2008). The longissimus capitis originates from the transverse and articular process of T1-T5 and C4-C7 respectively and is affixed onto the mastoid process of the skull. Neck extension and ipsilateral axial rotation during bilateral and unilateral activation respectively. The longissimus cervicis initiate from the transverse process of T1-T5 and insert onto the transverse process of C2-C6. The iliocostalis arises from the third to sixth rib and inserts onto the transverse process of C4-C6. Both of these muscles produce neck extension during bilateral activation and ipsilateral lateral flexion when activated unilaterally.

The spinotranverse group consists of the multifidus, semispinalis capitis, and semispinalis cervicis (Figure 2-23) (Standring, 2008). The multifidus originates from the articular process of C4 to the sacrum and inserts superomedially onto superior vertebrae's spinous process (C2 – sacrum). This muscle's primary action includes extension and stabilization of the neck. The semispinalis capitis initiates at the transverse and articular process of C7-T7 and C4-C6 respectively and attaches onto the occipital bone. This muscle produces head extension during bilateral activation and ipsilateral head rotation during unilateral activation. The semispinalis cervicis arise from the transverse process of T1-T6 and attach onto the spinous process of C2-C5. Neck extension and ipsilateral rotation occur during bilateral and unilateral activation respectively.

The last group of the posterior neck muscles is the suboccipital group, which includes the rectus capitis minor, rectus capitis major, obliquus capitis superior and obliquus capitis inferior (Figure 2-23) (Standring, 2008). The rectus capitis minor produce head extension, and originate from the posterior arch of the atlas, inserting onto the occipital bone. The rectus capitis major arises from the spinous process of the axis, and attach onto the occipital bone. This muscle is responsible for head extension, and ipsilateral lateral flexion and rotation during bilateral and unilateral activation respectively. The obliquus capitis superior begins at the transverse process of the atlas and ends at the occipital bone. Head extension and lateral flexion are produced during bilateral and unilateral activation respectively. Lastly, the obliquus capitis inferior is initiated from the spinous process of the axis that insert onto the transverse process of the axis, and is responsible for the axial rotation of the atlas.

TABLE 2-1: NECK MUSCLE GROUPS *(Standring, 2008)*

Muscle	Group	Origin	Insertion	Function
Anterior				
Sternocleidomastoid	Anterior	Sternum and clavicle	Mastoid Process	Head flexion | Ipsilateral lateral flexion and contralateral rotation*
Sternothyroid	Infrahyoid	Posterior surface of sternum	Thyroid Cartilage	Larynx depression and head flexion
Sternohyoid	Infrahyoid	Posterior surface of sternum	Hyoid bone	Hyoid bone depression
Omohyoid Superior	Infrahyoid	Upper border, scapula	Intermediate tendon	Hyoid bone and larynx depression
Omohyoid Inferior	Infrahyoid	Intermediate tendon	Hyoid bone	Hyoid bone and larynx depression
Rectus Capitis Anterior	Suboccipital	Transverse process, C1	Occipital bone anterior surface	Head flexion, stabalize atlanto-occiptial joint
Rectus Capitis Lateral	Suboccipital	Transverse process, C1	Occipital bone jugular process	Ipsilateral lateral flexion, stabalize atlanto-occipital joint
Longus Capitis	Anterior Vertebral	Transverse process, C3-C6	Occiptial bone	Head flexion
Longus Colli	Anterior Vertebral	Transverse process, C3-T3	Anterior vertebral body, C2-C6	Neck flexion | Ipsilateral neck flexion and contralateral rotation*
Scalenus Posterior	Lateral Vertebral	Transverse process, C4-C6	Second rib	Ipsilateral lateral flexion
Scalenus Medius	Lateral Vertebral	Transverse process, C1-C2	First rib	Ipsilateral anterolateral flexion
Scalenus Anterior	Lateral Vertebral	Transverse process, C3-C6	First rib	Ipsilateral anterolateral flexion and contralateral rotation
Posterior				
Rectus Capitis Minor	Suboccipital	Posterior arch, C1	Occipital bone	Head extension
Rectus Capitis Major	Suboccipital	Spinous process, C2	Occipital bone	Head extension, lateral flexion and rotation
Obliquus Capitis Superior	Suboccipital	Transverse process, C1	Occipital bone	Head extension and lateral flexion
Obliquus Capitis Inferior	Suboccipital	Spinous process, C2	Transverse process, C1	Atlas rotation
Longissimus Capitis	Erector Spinae	Transverse process, T1-T5 | Articular process, C4-C7	Mastoid process	Neck extension | Ipsilateral rotation*
Longissimus Cervicis	Erector Spinae	Transverse process, T1-T5	Transverse process, C2-C6	Neck extension | Lateral flexion*
Iliocostalis	Erector Spinae	Rib angle, third-sixth	Transverse process, C4-C6	Neck extension | Lateral flexion*
Splenius Capitis	Erector Spinae	Ligamentum nuchae | Spinous process, C7-T4	Mastoid Process	Head extension | Ipsilateral rotation*
Splenius Cervicis	Erector Spinae	Spinous process, T3-T6	Transverse process, C1-C3	Upper neck extension | Ipsilateral rotation*
Multifidus	Spinotransverse	Articular process, C4-Sacrum	Spinous process, C2-Sacrum	Stabalize spinal column, neck extension
Semispinalis Capitis	Spinotransverse	Transverse process, C7-T7 | Articular process, C4-C6	Occipital bone	Head extension | Ipsilateral rotation*
Semispinalis Cervicis	Spinotransverse	Transverse process, T1-T6	Spinous process, C2-C5	Neck extension | Ipsilateral rotation*
Levator Scapulae	Scapular	Transverse prcoess, C1-C4	Superior medial end, Scapula	Scapula elevation
Rhomboideus Minor	Scapular	Spinous process, C7-T1	Medial end, Scapula	Scapula retraction
Trapezius	Scapular	External occipital protuberance | Ligamentum nuchae | Spinous process, C7-T10	Clavicle and scapula	Scapula elevation, retraction | Head extension

*Unilateral activation

2.2 Whiplash Associated Disorders

In 1928, (Crowe, 1928) first defined the term whiplash to describe neck injuries that occurred from acceleration-deceleration events. In 1995, the Quebec Task Force has adopted the term whiplash-associated disorders (WAD) as: "Whiplash is an acceleration-deceleration mechanism of energy transfer to the neck. It may result from rearend or side-impact motor vehicle collisions, but can also occur during diving or other mishaps. The impact may result in bony or soft-tissue injuries (whiplash injury), which in turn may lead to a variety of clinical manifestations" (Spitzer et al., 1995). Symptoms include: neck pain, neck stiffness, headache, shoulder pain, arm pain and arm numbness, paresthesia, weakness, dysphagia, visual and auditory disturbances and dizziness (Norris and Watt 1983; Barnsley et al., 1994; Spitzer et al., 1995). These symptoms are hypothesised to arise from an organic basis that involve tissue lesion in the cervical spine, when stretched beyond their physiologic range of motion or non-physiologic motions of cervical spinal segments (Curatolo et al., 2011). Injuries that result from whiplash are typically classified as AIS 1 (minor) and sometimes AIS 2 (moderate) in terms of severity. The abbreviated injury scale (AIS) is a global rating system used to classify the severity of injury for different anatomical regions (Table 2-2), developed by the Association for the Advancement of Automotive Medicine (AAAM).

TABLE 2-2: AIS RATING SYSTEM AND EXEMPLAR INJURIES FOR THE CERVICAL SPINE *(AAAM, 2005)*

AIS Rating	Injury Examples
1 (Minor)	Spinous ligament injury, acute strain with no fracture or dislocation
2 (Moderate)	Disc injury, dislocation (no cord involvement), fracture of the spinous process, transverse process, facet, lamina, pedicle (no cord involvement), nerve root contusion or laceration
3 (Serious)	Cord contusion, odontoid fracture, bilateral facet dislocation, vertebral body burst fracture (>20% loss of anterior height)
4 (Severe)	Incomplete cord syndrome
5 (Critical)	Complete cord syndrome (C4 or below), cord laceration (C4 or below)
6 (Fatal)	Complete cord syndrome (C3 or above), cord laceration (C3 or above)

A different clinical grading system (Quebec Classification of Whiplash-Associated Disorders) designed specifically for WADs was initiated by the Quebec Task Force (Spitzer et al., 1995) that includes five grades of severity (Table 2-3).

TABLE 2-3: WAD CLINICAL GRADING SYSTEM *(Spitzer et al., 1995)*

Grade	Clinical Presentation
0	No pain and physical signs
I	Neck pain, stiffness or tenderness. No physical signs
II	Neck complaint and musculoskeletal signs (decreased range of motion, tenderness)
III	Neck complaint and neurological signs
IV	Neck complaint and bone fracture or dislocation

WADs can have symptoms that are either acute (short term) or chronic (long term) which is defined as pain lasting more than 3-6 months by the European Foundation of International Association for the Study of Pain (Niv and Devor, 2007). The development of chronic symptoms from these minor injuries are related to alterations of pain processing in the central nervous systems, and could be influenced by multiple factors such as gender, impact direction, vehicle interaction etc. The most common variables that suggest slow recovery or development of chronic symptoms includes a high level of initial pain, high number of symptoms, and the female gender (Sterner and Gerdle, 2003; Schofferman et al., 2007; Carrol et al., 2008). It is estimated that half of all WAD victims continue to report symptoms one year after the initial incident (Carroll et al., 2008). The cervical spine has the highest vulnerability for AIS1 injuries to occur, in addition to the highest frequency to develop permanent medical impairment from these AIS1 injuries, and is ranked third in terms of body region for the highest risk of developing chronic symptoms from injuries in motor vehicle collisions (Gustafsson et al., 2015). Over the past four decades, advancements in vehicle safety have reduced the occurrence of AIS3+ injuries that result from motor vehicle collisions by 80%, in addition to a decrease of 76% of the disability risk that result from AIS 2+ injuries (Kullgren et al., 2002). In contrast, the disability risk from AIS1 injuries increased by 18%, and the neck was the only body region that demonstrated an increase in disability risk (14%) whereas other body region had on average a 90% reduction (Kullgreen et al., 2002).

Females have approximately double the risk in both the development of WAD and the transition to chronic symptoms when compared to males (Carlsson et al., 2010; Carstensen et al., 2012). Some difference between the male and female gender include neck circumference, neck muscle moment arms, and vertebra dimensions in size matched individuals. When compared to females, males have a greater increase in neck circumference with body weight, and have a larger neck circumference when compared to female volunteers with the same body weight (Vasavada et al., 2008). Males also have greater muscle moment arms when compare to size matched females because the neck muscles are situated further away from the cervical spine, which indicate that the neck musculature in males have greater moment generating

capabilities (Stemper et al., 2008). Females typically have a smaller cervical vertebra (vertebral width and disc-facet depth) and vertebral body dimension (vertebral body depth and width) when compared to male vertebrae, which suggests that the female vertebra would experience higher stresses (Stemper et al., 2009). The current literature has suggested that the increased risk of injury from WAD may be more dependent on morphologic differences of the cervical spine and head, rather than differences in gender (Stemper and Corner, 2016). These factors indicated that the same morphological differences that are more commonly present in females, such as neck slenderness and smaller neck circumference will also influence injury risk in the male population that posses these same morphologic factors (Stemper and Corner, 2016).

Epidemiological data has suggested that AIS1 soft tissue injury can occur in the neck after exposure to frontal, rear and lateral impact configurations, with rear impacts have the highest risk of sustaining whiplash injury followed by frontal impacts and side impacts (Kullgren et al., 2013; Watanabe et al., 2000; Hell et al., 2003; Martin et al., 2008; Cassidy et al., 2000; Berglund et al., 2002; Morris and Thomas 1996; Kullgreen et al., 2000; Jakobsson et al., 2000; Kraftt, 1998). Although rear impacts have the highest risk to sustain WAD, the total number of occurrences of injury from frontal and side impacts are often equal to or exceed the occurrence from rear impact (Table 2-4) (Berglund et al., 2003, Kullgren et al., 2013; Martin et al., 2008, Morris and Thomas, 1996; Krafft 1998, Hell et al., 2003; Otte et al., 1997; Temming and Zobel, 1998). This signifies the importance of investigating whiplash injury that involve frontal and side impacts in addition to rear impacts.

TABLE 2-4: WAD FREQUENCY IN FRONTAL, REAR, AND LATERAL IMPACT DIRECTIONS

Study	Frontal	Rear	Lateral
Martin et al., 2008	43.9%	37.7%	18.4%
Berglund et al., 2003	22.6%	38.4%	11.5%
Morris and Thomas, 1996	55%	12.6%	24.8%
Krafft, 1998	33.2%	47.9%	9.6%
Hell et al., 2003	44%	32.6%	23.4%
Otte et al., 1997	34.6%	21.2%	12.2%
Temming and Zobel, 1998	38%	16%	11.8%
Kullgren et al., 2013	37%	43%	20%
Richter et al., 2000	36%	16%	12%

Whiplash tolerance is difficult to quantify due to many crash factors (e.g. vehicle crash performance, seat and headrest design, impact severity and orientation, etc.) as well as individual differences (e.g. age, stature, etc.) that may account for the outcome of the injury. These factors are further limited by the relatively low number of cases used to generate injury tolerance curves for different crash scenarios, and

may not be fully representative of the entire population. Despite these shortcomings, the current injury tolerance data in the literature are still useful and contribute to our understanding of the human tolerance to WADs.

In frontal impact, the risk for sustaining WAD for Volvo vehicles in Sweden in the year of 1997 to 1998 was 18% for velocity changes of 0 km/h to 8 km/h, 25% for 9 km/h to 16 km/h and 30% for 17 km/h to 24 km/h (Jakobsson et al., 2000). A study on Volvo vehicles that included 24 occupants in 16 frontal impacts that suffered WAD found that most symptoms developed in crash severities >5 km/h, with higher symptom intensity arising from >10 km/h (Jakobsson et al., 2003). In the German population, Ritcher et al., 2000 identified that 10% of occupants developed WAD for crash velocities <10km/h, and 28% for crash velocities 11 km/h to 20 km/h. Cappon et al., 2004 analyzed four European databases for WAD and found a 20% risk to develop symptoms from a mean acceleration of 5 g (velocity change <20 km/h), in addition to development of WAD II (QTF) symptoms in the range of 18 km/h to 25 km/h.

Ritcher et al., (2000) identified that 42% of all WAD from rear impacts were from crash velocities of <10 km/h. Krafft et al., (2002) showed that rear impacts above 7g mean vehicle acceleration had almost 100% risk for sustaining both short term and long term WAD, while the risk was significantly lower for mean vehicle accelerations below 3g. For short term symptoms (<1 month), the injury risk was 20% for 2g mean acceleration (velocity change of 5 km/h) and 35% for 2g to 3g mean acceleration (velocity change of 5 km/h to 10 km/h), and a injury risk of >60% for 3g to 4g mean acceleration (10 km/h to 15 km/h). A separate study based on 79 real life rear end crashes where the vehicle was installed with a crash recorder demonstrated that for all vehicles, the average change of velocity was 10 km/h with an average mean acceleration of 3.5g (Kullgren et al., 2003). Additionally, the injury risk for initial symptoms was estimated to be approximately 20% for a mean acceleration of 2.5g (velocity change of 5 km/h) and 40% for 4g mean acceleration (velocity change of 10 km/h). Symptoms that persist for greater than one month had a risk of 20% for mean acceleration of 5g (velocity change of 15 km/h) and 60% for mean acceleration of 5.5g (velocity change of 17.5 km/h).

Due to a lack of data in the epidemiological literature for side impacts, estimated tolerance for WAD are currently not available. Other studies have however indicated that WAD from side impacts can develop from velocity changes of less than 10 km/h (Ritcher et al., 2000). In addition, the risk for developing WAD was approximately 20% for all side impact conditions of varying severities and doubled when the vehicle compartment intrusion exceeded 15 cm, and increased by 2.8 times when the head had impacted the interior of the vehicle (Jakobsson et al., 2000).

2.2.1 Pain Sources

There are two types of pain experienced after sustaining WAD: radicular pain and somatic pain. Radicular pain refers to pain and neurological symptoms that typically persist in the upper extremities, which arise from injury to the cervical nerve roots and dorsal root ganglia. Radicular pain is described as a sharp shooting pain that travels towards the affected upper limb and is commonly related to symptoms of paresthesia (Bogduk, 2003). Somatic pain is perceived at the source of injury when a tissue is loaded mechanically past a critical threshold, which cause high threshold (nociceptor) nerve endings to transmit pain signals along afferent fibres to the spinal cord and brain. Mechanoreceptors are low threshold afferent fibres that activate when the tissues are deformed by non-noxious stimuli for the purpose of providing proprioception. The mechanism of pain is an important physiologic response to noxious stimuli in living organisms to alert and prevent damage to tissues or to prevent further damage to already injured tissues (Costigan et al., 2009). Peripheral sensitization refers to a temporary state of lowered threshold and increased firing frequency of pain signals, which leads to a state of heightened sensitivity and decreased activation thresholds (Winkelstein 2004; Latremoliere and Woolf, 2009). This is a normal reaction due to the inflammatory response of the body that follows tissue injury to promote healing (Winkelstein, 2004). Chronic pain develops through changes to nociceptive processing in the central nervous system through a process called central sensitization that can result in permanent pain hypersensitivity or sensitization (Winkelstein, 2004; Latremoliere and Woolf, 2009; Winkelstein 2011). This can lead to a continued pain response long after the initial injury site has completely healed. For this reason, chronic pain is considered to be pathologic, as it no longer functions as a physiologic response to protect organisms against potential tissue damage (Basbaum et al., 2009; Ita et al., 2017).

Several anatomical sites in the neck have been identified as potential pain sources during whiplash injury: facet joint, spinal ligaments, intervertebral discs, nerve root, muscles, and vertebral artery (Siegmund et al., 2009). Each anatomical site have been investigated in varying levels of details, with the facet joint being the most investigated to date (Table 2-5).

TABLE 2-5: SUMMARY OF WHIPLASH INJURY LOCATIONS AND STATE OF DEVELOPMENT *(Adapted from Curatolo et al., 2011)*

Development	Facet Joint	Ligaments	Disc	Nerve Root	Muscle	Vertebral Artery
Theoretical model	Yes	Yes	Yes	Yes	Yes	Yes
Cadaver or volunteer						
Injury demonstrated	Yes	Yes	Yes	-	Yes	Yes
Animal model						
Injury produced	Yes	-	-	Yes	Yes	-
Nociception produced	Yes	-	-	-	Yes	-
Patient						
Valid diagnosis	Yes	-	-	-	-	-
Effective treatment	Yes	-	-	-	-	-

Facet Joint

The cervical facet joint is a highly innervated structure that has been identified as the most common anatomical location for neck pain (Barnsley et al., 1995; Siegmund et al., 2009). Clinical studies have demonstrated that 60% of patients with chronic neck pain experienced pain relief after double-blinded anesthetic blocks to the cervical medial branch, which indicated that the pain originated from the facet joint. Further studies also provided histologic evidence that both mechanoreceptors and nociceptors exist in the facet joint capsule (Inami et al., 2001; Ohtori et al., 2004; Kallakuri et al., 2003). Two mechanism of injury has been proposed: synovial fold (meniscus) pinching during rear impact and excessive stretching of the capsular ligament. The first mechanism was first proposed by (Ono et al., 1997; Kaneoka et al., 1997), where in a rear impact; thoracic ramping caused by seatback interactions resulted in compression of lower cervical spine. It was identified through radiographic imaging that the compressive force caused the instantaneous center of rotation of the lower cervical segment to shift upwards. This resulted in a non-physiologic motion of the lower cervical spine segment, which caused the inferior facet of superior vertebra to impact the superior facet of the inferior vertebra, and therefore hypothesized to pinch and impinge on the synovial fold. Evidence of nerve endings in the synovial fold have been discovered but the mechanism and tolerance to activate the nociceptors from compression remains unknown. This mechanism of facet joint synovial fold impingement has not been further explored by biomechanical or animal models and therefore, remains to be a speculation (Siegmund et al., 2009). The second mechanism of excessive facet joint stretching was first proposed by (Yang et al., 1997) as the shear hypothesis theory, which indicated that shear forces in the cervical spine could cause soft tissue injury. This led to a series of full body PMHS rear impact tests to examine the local facet kinematics and engineering strains of the facet joints (22% to 60%

strain) (Deng et al., 2000). Other rear impact PHMS experiments have identified excessive strains in the facet joint (28% to 40%) when compared to physiologic strains (6% to 21%), with maximum strains occurring in the lower cervical spine segments (Panjabi et al., 1998; Pearson et al., 2004). Furthermore, isolated testing of PHMS cervical spine segments has identified sub-failure strain thresholds of the capsular ligament to be between 35% to 65% (Winkelstein et al., 2000; Siegmund et al., 2001), which indicated that rear impacts may cause sub-failure of the capsular ligament. When the facet joint is distracted within the sub-failure region, micro lesions form in the CL and exhibits increased ligament laxity that can lead to acute or chronic cervical spine instability (Tominaga et al., 2006; Ivancic et al., 2008). Ligament laxity in the lower cervical spine can exhibit cervical instabilities that can cause chronic pain and has been associated with clinical symptoms of painful muscle spasms and paresthesia (Panjabi, 2006; Steilen et al., 2014). In-vivo animal models of pain has provided confirmation of nociceptive responses from excessive stretching of the facet joint (~48% strain for nociceptor activation), through nociceptor signalling and behavioural sensitivity studies (Lu et al., 2005; Lee et al., 2004; Lee et al., 2008). Interestingly, it was discovered that rodents exposed to in-vivo sub-failure loading of the CL produced behavioural sensitivity with increased duration when compared to loading that caused catastrophic failure (Lee et al., 2008). This was hypothesized to occur due to nociceptor termination from the CL rupture and suggest that an increase in pain response and pain duration may result from sub-failure injury to the CL.

To date, cervical facet joint pain is the most investigated source of WAD (Curatolo et al., 2011). The facet joint has been identified as a highly innervated structure, with histologic evidence of afferent fibres that contain mechanoreceptors and nociceptors. The facet joint shear hypothesis and excessive stretching has been successfully demonstrated in PHMS experiments but also reproduced in animal models of pain through evidence of nociceptor signalling, and behavioural sensitivity studies. Furthermore, they are the only anatomical source of neck pain that can be clinically diagnosed through anesthetic nerve blocks with an available treatment option that involves radiofrequency neurotomy of the nerve endings (Bogduk 2011; Curatolo et al., 2011).

Ligaments

The ligaments in the cervical spine may sustain acute injury in automotive impact events through either non-physiological motion of the cervical segments, or motion that exceeds physiologic limits. Minor sprains and strains are difficult to detect through current medical imaging techniques that result in challenges in clinical diagnosis. Injured ligaments may cause a pain response, lead to a potential increase in ligament laxity and can lead to chronic cervical spine instability (Siegmund et al., 2009). In addition, instability may

cause modified muscle activation response that may further lead to decreased range of motion and proprioception (Panjabi, 2006; Siegmund et al., 2009). The cervical spine ligaments have not been studied for nociceptors, however, studies in the lumbar spine have identified nociceptors, which may imply that they exist for the cervical spine ligaments, and may exhibit a pain response when injured. Injury of the cervical vertebrae ligaments is well documented in the experimental literature, and has been shown to exceeded physiological ranges of motion and physiological strains in rear, side and frontal impacts (Ito et al., 2004; Maak et al., 2007; Ivancic et al., 2005; Ivancic et al., 2004; Panjabi et al., 2004). In frontal impacts, isolated PHMS neck specimens indicated a significant increase in ligament strains when compared to physiologic strains for the interspinous and supraspinous ligament (C23, C34, C67), and ligamentum flavum (C67) at an impact severity of 4g (Panjabi et al., 2004). In addition, a significant increase in range of motion and neutral zone was observed in isolated neck specimens when subjected to 8g frontal impacts (Ivancic et al., 2005). In the rear impact condition, isolated PHMS neck specimens also indicated a significant increase in ligament strain in the anterior longitudinal ligament at the C45 segment at 3.5g impact severity (Ivancic et al., 2004). Furthermore, isolated neck specimens subjected to 5g rear impacts demonstrated a significant increase in range of motion and neutral zone for the lower cervical spine segments. For side impacts, a 6.5g impact severity demonstrated a significant increase in neutral zone and range of motion in flexion, axial rotation, and lateral bending for the lower cervical spine segments. These PHMS experiments provide evidence that the ligaments and soft tissues in the cervical spine can be injured and cause a significant increase in range of motion and laxity. The upper cervical spine contain a complex arrangement of ligaments due to the lack of an intervertebral disc between the atlas and axis. Attempts have been made to identify possible lesions in the upper cervical spine complex using MRI signal intensity changes (Kaale et al., 2005; Krakenes and Kaale, 2006), but the validity of these results remain controversial (Dullerud et al., 2010; Li et al., 2013; Vetti et al., 2010; Vetti et al., 2011). In addition, PHMS experiments in head turned rear impacts and side impacts (up to 8g severity) demonstrated injury to the lower cervical spine ligaments but not in the upper cervical spine ligaments. These studies suggest that the upper cervical spine ligamentous complex remain challenging to diagnose, and that symptoms of pain from whiplash patients may not occur in the upper cervical spine for low severity impacts, and may be the result of injury in other anatomical sites (Siegmund et al., 2009).

Intervertebral Disc

The intervertebral disc in the cervical spine is an innervated structure that has the potential to generate pain and symptoms related to WAD (Bogduk 2002). Injury to the disc may result in herniation that can cause irritation to the surrounding neural structures that can cause radicular symptoms and pain.

Disc herniation has been shown to occur in the lower cervical spine but occur more commonly in the lumbar spine (Mall et al., 2012). Several studies used MRI and observed cervical disc herniation on patients that have sustained a whiplash trauma, with herniation occurring most frequently in the lower cervical spine (Davis et al., 1991; Jonsson et al., 1994; Pettersson et al., 1997). Minor disc lesions such as annulus fibrosus tears, disc rim lesions, and endplate avulsions have been documented from post-mortem examination of motor vehicle crash victims (Taylor and Twomey, 1993; Jonsson et al., 1994). In addition, rear impact full body PHMS sled experiments (4.5g) revealed disc rim lesions (avulsion) among other ligamentous injury in all specimens using computed tomography scans and cryomicrotomy (Yoganandan et al., 2001). PHMS experiments on isolated head neck specimens identified non-physiological disc strains initiating at maximum accelerations of 6g and 3.5g for frontal and rear impacts respectively (Ito et al., 2005; Panjabi et al., 2004). Like other soft tissues in the neck, minor lesions and acute tissue strains remains challenging to diagnose due to difficulties in detecting these injuries using medical imaging techniques. There are currently no animal models of pain that have been used to investigate potential nociceptive signalling or behaviour sensitivity for intervertebral disc injuries. The literature suggests that the cervical intervertebral disc can be potentially injured during whiplash loading conditions, but whether or not excessive stretching or sub-failure of the annular fibres can cause a pain response remains inconclusive (Siegmund et al., 2009).

Nerve Root

The cervical nerve root and dorsal root ganglia may be susceptible to injury from a motor vehicle crash event that may result in radicular pain and other neurological symptoms (weakness and numbness) due to impaired local sensory processing (Siegmund et al., 2009). Two mechanism of injury have been proposed for the cervical nerve root and dorsal root ganglion: the pressure gradient theory and direct impingement. Rapid movement of the head was hypothesized to generate transient pressure gradients in the spinal canal that may cause injury to the nerve root and ganglion (Aldman, 1986). Histopathological examination on in-vivo porcine subjects that were exposed to rapid head perturbations provided evidence of cellular injury to the ganglia nerve cells (Svensson et al., 2000). Rapid motion of the neck may cause transverse compression of the cervical nerve root and ganglion from narrowing of the intervertebral foramen space and may be an injury mechanism that produces pain. Due to challenges in monitoring the impingement of the nerve root experimentally, changes in foraminal dimensions were measured as an alternative method to quantify the risk for impingement (Curatolo et al., 2011). PHMS experiments that utilized isolated head neck specimens have identified a reduction in forminal area and extensive narrowing from extension and lateral bending that suggest potential impingement of the nerve roots and dorsal root ganglia may occur from rear or side impacts (Nuckley et al., 2004; Panjabi et al., 2006; Tominaga et al., 2006; Ivancic et al., 2012). Additionally,

individuals with symptoms of spinal degeneration such as cervical stenosis and spondylosis may have an increased risk of nerve root impingement due to the narrowing of the intervertebral foramina space (Panjabi et al., 2006; Tominaga et al., 2006; Ivancic et al., 2012). Furthermore, in-vivo rodent experiments that applied mechanical loads on the cervical nerve roots demonstrated an increase in pain response, which provided evidence that direct impingement may be associated to pain (Rothman et al., 2005; Hubbard and Winkelstein, 2005; Hubbard et al., 2008). In contact sports, radicular symptoms known as burners or stingers can occur from both nerve root impingement and an alternate mechanism that involves stretching or traction of the nerve roots and brachial plexus (Levitz et al., 1997). This injury mechanism could possibly occur from vehicle side impacts loading conditions where the head is accelerated rapidly towards the shoulder, but to date has not been studied outside the context of sport injuries.

Muscles

Myofascial pain in the neck occur frequently in WAD patients (Evans, 1992). The primary mechanism of injury for the neck muscles occur after eccentric contraction during an impact event. Volunteers subjected to low speed rear impacts demonstrated in-vivo muscle strains of the sternocleidomastoid and semispinalis capitis muscles that exceeded the predicted threshold for muscle injury (Brault et al., 2000; Vasavada et al., 2007; Mcpherson et al., 1996; McCully and Faulkner, 1985). A rise in serum creatine kinase has been associated with damaged induced muscle soreness (Evans et al., 1986). A clinical study of WAD patients has identified increased levels of serum creatine kinase within 24 hours after the initial injury, but returned to baseline levels within 48 hours, while patients with persistent neck pain for more than three months demonstrated normal levels of serum creatine kinase (Scott and Sanderson, 2002). Therefore, clinical evidence has suggested that muscle injury from whiplash exposure may be associated with acute pain but the development of chronic pain from injury to the neck muscles remains inconclusive. Muscles in the cervical spine may also cause pain and other symptoms through interactions with other anatomical sites in the neck. Anatomical dissection studies have identified that the cervical multifidus muscle is directly inserted onto the facet capsule (Winkelstein et al., 2000; Anderson et al., 2005). It was hypothesised that the sudden reflex activation of these muscles may exacerbate capsular ligament stretching during rear impact events (Siegmund et al., 2008). Further biomechanical studies are required to investigate the involvement of neck muscles in both acute and chronic neck pain following impacts that results in WADs.

Vertebral Arteries

The vertebral arteries arise bilaterally from the subclavian arteries and travel superiorly along the transverse foramen starting from the C6 to C1 vertebrae before entering the foramen magnum. The vertebral artery can become elongated during an impact event and cause narrowing in the vasculature diameter due to Poisson's ratio (Nibu et al., 1997; Siegmund et al., 2009). This can induce vertebral artery lesion and cause altered blood flow patterns that are hypothesized to be associated with WAD symptoms (Seric et al., 2000; Reddy et al., 2002). PMHS testing have indicated that the vertebral artery strain exceeded the physiological elongation in side impacts, and head turned rear impacts, but not for frontal and rear impacts (Ivancic et al., 2006; Carlson et al., 2007). Although PHMS studies have identified the vertebral artery to be a potential injury location due to excessive elongation, there is insufficient evidence of acute or chronic pain development. Furthermore, there are currently no valid diagnostic test that can determine whether or not the vertebral artery is damaged after an impact event.

2.3 Experimental Studies for Boundary Conditions and Response Kinematics

2.3.1 Frontal Impact

The Naval Biodynamics Laboratory (NBDL) performed 39 in-vivo sled test on eight human male volunteers that ranged from maximum accelerations of 2g to 15g (Thunnissen et al., 1995). All potential volunteers underwent a rigorous screening process and were selected based on physical fitness. A rigid seat was fixed onto a HYGE acceleration sled and volunteers were secured with a five-point restraint system. The seat was accelerated backwards from rest to various closing velocities to simulate different frontal impact conditions. Volunteers had accelerometers and motion trackers attached to a mouthpiece, head, and T1 spinous process that were active during the perturbation event. High-speed video was also used in conjunction with the instrumentation to collect data on the volunteers (Figure 2-24). Together, detailed information such as velocity, acceleration and displacement of the head center of gravity and T1 were collected for each test run for all volunteers. To date, this is the most complete dataset of volunteer neck and head kinematics in the frontal impact configuration, which also covers the largest range of severity; most of which are not allowed today due to ethical regulations. The T1 kinematics are therefore an ideal candidate to be used to investigate potential soft tissue injury in frontal impacts.

FIGURE 2-24: NBDL VOLUNTEER KINEMATICS IN A FRONTAL IMPACT *(Adapted from Muzzy and Lustick, 1976)*

A series of low speed frontal impact experiments were performed by (Beeman et al., 2011) on five human male volunteers with anthropometrics similar to the 50th percentile male. In total, 20 tests were conducted: 10 tests with maximum acceleration severity of 2.5g (change in velocity of 4.8 km/h) and 10 tests with maximum acceleration severity of 5g (change in velocity of 9.7 km/h) utilizing a custom sled setup with a rigid seat and mounted footrest and steering column. Subjects were secured to the seat by a standard three-point seatbelt, and instructed to place their feet on the footrest and hands on the steering wheel. Markers were attached to the head and body of the volunteers to capture accelerations of the head CG and C7 vertebra during the perturbation. Although this series of experiments provided information on occupant kinematics, the acceleration severity was not high enough to cause potential tissue damage in the volunteers.

2.3.2 Rear Impact

The Japan Automobile Research Institute (JARI) conducted a series of volunteer tests to simulate rear impact loading condition (Ono et al., 1997). Twelve male volunteers were subjected to speed change of 4 km/h, 6 km/h, and 8 km/h using an inclined sled without a head restraint. The 8 km/h sled condition produced a maximum sled acceleration of 4g. T1 and head center of gravity accelerations were collected using accelerometers during the perturbation. A second set of experiments were conducted by JARI to simulate a rear impact loading condition (Ono et al., 2006). Six volunteers were subjected to a maximum impact speed of 6 km/h (4g maximum acceleration) using a horizontal sled with a rigid seat without a headrest. Two accelerometers were used to measure the accelerations of the T1 and head center of gravity during the impact event. A series of 28 rear impact sled test were performed by (Davidsson et al., 1998) on thirteen human volunteers. A bullet sled was used to strike a target sled to subject the volunteers to a velocity change of 5 km/h (3g) and 7 km/h (3.8g). A standard Volvo seat and a custom laboratory seat was mounted on the target sled. Accelerometers were mounted onto the volunteers to capture the kinematics of the head

center of gravity and the T1 vertebra. Although all three of the above-mentioned experiments provided the necessary T1 kinematics as input boundary conditions to simulate a rear impact, the maximum sled acceleration was 4g and less than 10 km/h, which is considered to be a non-injurious input.

A series of 26 rear impact test were performed by (Deng et al., 2000) using six whole body PHMS. A rigid seat that was attached onto a HYGE mini-sled was used to simulate rear impacts with velocity changes that ranged from 5 km/h to 15.5 km/h (5g to 10g maximum sled acceleration). Markers and accelerometers that were attached onto the cadaver subjects were used to track motion of the cervical spine and to measure the kinematics of the T1 and head center of gravity. This set of experiments was performed above the injurious threshold of 4g max acceleration of human volunteers to provide the necessary T1 input boundary conditions to simulate a rear impact that is severe enough to cause soft tissue injury. In addition, this boundary condition has the benefit of already being validated with the GHBMC 50^{th} percentile male and 5^{th} percentile female neck model.

2.3.3 Lateral Impact

The Naval Biodynamics Laboratory (NBDL) performed series of in-vivo sled test on nine human volunteers that ranged from maximum accelerations of 4g to 7g (Wismans et al., 1986). All potential volunteers underwent a rigorous screening process and was selected based on physical fitness. A rigid seat was fixed onto a HYGE acceleration sled and volunteers were secured with a five-point restraint system. The sled setup was similar to the series of frontal impact tests except the seat was rotated 90 degrees to allow lateral acceleration from rest, to a closing velocity of 25 km/h with different durations to simulate different lateral impact conditions (Figure 2-25). Volunteers had accelerometers and motion trackers attached to a mouthpiece, head, and T1 spinous process that were active during the perturbation event. High-speed video was also used in conjunction with the instrumentations to collect data on the volunteers (Figure 2-25). Together, detailed information such as velocity, acceleration and displacement of the head center of gravity and T1 were collected for each test run for all volunteers. To date, this is the only dataset of volunteer sled experiment in the lateral impact configuration that provide kinematics of both the T1 and head center of gravity in acceleration severities of 4g and higher. Therefore, the T1 inputs from this set of experiments are ideal boundary condition inputs to simulate soft tissue injury in a lateral impact scenario.

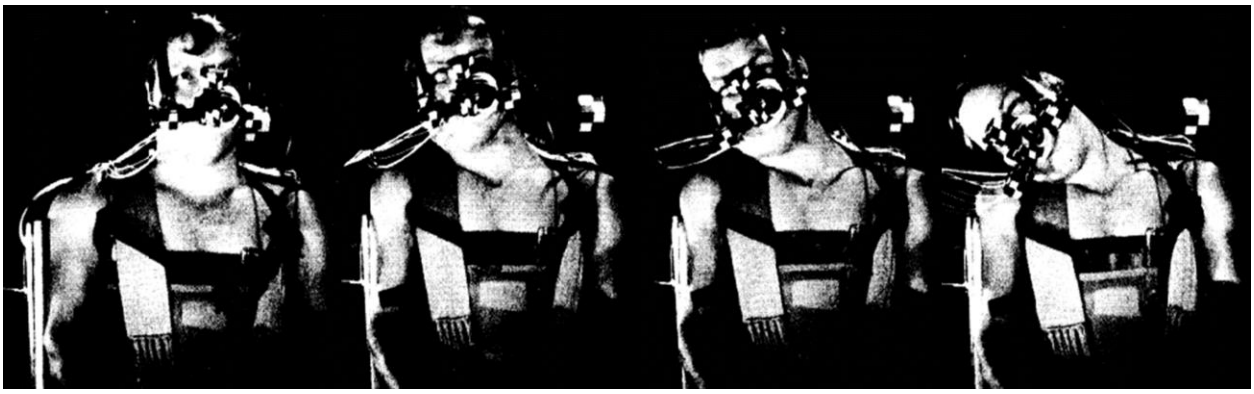

FIGURE 2-25: NBDL VOLUNTEER KINEMATICS IN A LATERAL IMPACT *(Adapted from Ewing et al., 1977)*

A series of simulated lateral impacts were conducted by the Japan Automobile Research Institute (JARI) on eight human volunteers to understand the neck response and cervical vertebral motions in the lateral direction (Ono et al., 2005). An inertia impactor was used to strike the volunteer's shoulder (400 N to 600 N) to apply loading on to the body to simulate an automobile lateral collision. Accelerometers attached to a mouthpiece and T1 were used to monitor the kinematics of the T1 and head center of gravity. The 600 N impactor resulted in a maximum torso acceleration of approximately 6g. Although this series of experiments provided experimental corridors of T1 and head center of gravity from the shoulder impactor, the impact severity was not high enough to cause injury in the volunteers. In addition, it was unknown what the equivalent resultant acceleration of the vehicle when using the shoulder impactor.

Another series of low speed lateral impact experiments were conducted by JARI on three human volunteers using a sled with a mounted rigid seat (Ejima et al., 2012). The sled was accelerated laterally from a standstill to two severities of 0.4g and 0.6g. Volunteers were secured to the rigid seat with a lap belt during the perturbation. Several instrumentations on the torso and mouthpiece was used to measure the acceleration response of the T1 and head center of gravity. The purpose of this experiment was to recreate an aggressive lane change maneuver to mimic swerving for obstacle avoidance. Therefore, the severity applied to the volunteers is very low and would not cause injury to the volunteer.

2.4 Human Body Models

Human body models (HBMs) are useful tools that allow researchers and engineers to investigate and understand mechanisms of injury in complex loading events. The ultimate goal for the development of HBMs is to design countermeasures to better protect and reduce the frequency of injury in vehicle occupants and pedestrians during a collision (Yang et al., 2018). Anthropometric test devices (ATDs) are physical

human surrogates that are designed to have similar geometric and mass properties that reflect a range of statures (Schneider et al., 1983) to represent the general adult population (e.g. 95th percentile male or large male, 50th percentile male or average male and 5th percentile female or small female). ATDs have been employed since the 1970s by the automotive industry to assess protection and safety for both occupants and pedestrians. Although ATDs can be instrumented with load cells and accelerometers, the assessment of injury can only be accomplished for global body regions due to the absence of detailed anatomical structures such as internal organs and hard tissues (Yang et al., 2018). One of the most valuable benefits of utilizing a HBM when compared to an ATD is the ability to predict local injury for any body region at the tissue level. This is crucial in discerning detailed injury locations to understand complex injury mechanisms for a given impact scenario. Furthermore, ATDs are only optimized for uni-directional loading (e.g. Hybrid III for frontal impact, BioRID II for rear impact and WorldSID for side impact); while a HBM can be used to investigate multi-directional loadings. Examples of current state-of-the art HBMs include the Global Human Body Model Consortium (GHBMC) model (Schwartz et al., 2015; Davis et al., 2016), Total HUman Model for Safety (THUMS) (Kato et al., 2018), and the Virtual Vehicle-safety Assessment (ViVA) model (Östh et al., 2017).

In order to utilize HBMs to assess injury, there are three major inputs that are required: boundary conditions to load the model, material properties with the correct constitutive law, and geometric parameters such as accurate anatomical and anthropometric detail (Figure 2-26). These three inputs will yield model response parameters such as kinematic and kinematic response that can be used to compare with injury metrics for injury prediction.

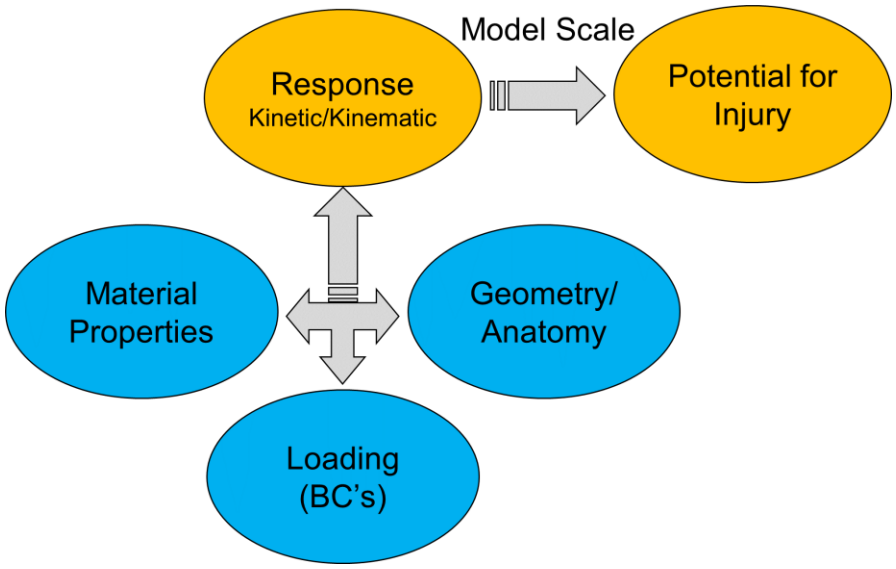

FIGURE 2-26: HBM INPUTS AND OUTPUT FOR INJURY PREDICTION *(Adapted from Cronin, 2014)*

2.4.1 Computational Human Neck Models

Numerous computational models of the cervical spine have been created by researchers since the 1970s (Yang et al., 2018). Simple spring-mass systems were used to create multi-body models of the cervical spine to allow for kinematic analysis of spinal motions. However, these multi-body models are limited in their ability to evaluate stresses and strains of neck tissues, which is critical in predicting injury at the tissue level. To address this issue, finite element models of varying levels of details have been created by various researchers globally. Early finite element models of the neck had simplified geometric details and often represented the vertebrae as simple rigid bodies, and lacked active and passive musculature due to limitations of computational resources (Kleinberger, 1993). As computational resources became more accessible, neck models included detailed geometries obtained from computed tomography (CT) and magnetic resonance imaging (MRI) scans of human subjects, along with deformable models of the vertebrae. In addition, the neck musculature was included, along with the function of muscle activation for increased biofidelity.

One of the first finite element neck models that was developed using anatomical data from MRI scans of a young 50^{th} percentile male volunteer was the Wayne State University Neck model (Yang et al., 1998). The model consisted of the C1 to T1 vertebrae and included soft tissues such as the ligaments, intervertebral disc, and muscles. The vertebrae were modelled using solid elements with a linear elastic-plastic formulation and the IVD was modelled using a linear viscoelastic material model. The ligaments were represented using tension only 1-D spring elements as well as 2-D membrane elements. The modelled contained only passive musculature and was modelled using 60 tension only spring elements.

Deng et al., 1999 developed a finite element model of the ligamentous cervical spine using 3-D anatomical data. Vertebrae, IVDs had solid elements, with the hard tissues modelled as non-deformable rigid bodies. The cervical spine ligaments were modelled using 2-D membrane elements with a linear viscoelastic formulation. The model also contained 15 pairs of active musculature, represented using contractile beam elements using the Hill muscle model.

The KTH model was developed by KTH Royal Institute of Technology, and was developed based on computed tomography scans of a 27 year old male that was scaled to represent a 50^{th} percentile male (Brolin et al., 2006). The model was composed of a rigid skull, with deformable and rigid cervical vertebrae that were separated into cortical and trabecular bone using 4-node shell and 8-node solid elements respectively. The spinal ligaments were modelled with 2-node tension only spring elements, and 4-node membrane elements and the facet cartilage were modeled using 8-node solid elements. The intervertebral discs were

composed of the annulus fibrosus (4-node membrane elements), annulus matrix (8-node solid elements), and the nucleus pulposus (8-node solid elements). The model contained 24 pairs of cervical musculature that was represented using 3-D non-linear viscoelastic elements for the passive behaviour, and embedded 1-D Hill-Type beam elements to model the active behaviour of the muscle. The model has been used to optimize muscle activation to fit experimental corridors, study muscle load distribution, and is also one of the first models that incorporate 3-D passive elements in a neck model (Brolin et al., 2006; Hedenstierna et al., 2008).

The Total HUman Model for Safety (THUMS) was created by Toyota Motor Corporation and Toyota Central R&D Labs., Inc. to investigate injuries to the human body in real-world traffic accidents and is commercially available for use. The THUMS model is representative of a 50^{th} percentile male and a 5^{th} percentile female model was later created. The cervical spine contained deformable vertebra with cortical bone modelled as 2-D shell elements, and trabecular bone modelled as 3-D solid elements. The ligaments were modelled using 2-D shell elements and the intervertebral discs were modelled using 3-D solid elements with distinct annulus fibrosus and nucleus pulpous. In addition, the spinal cord was also included, with the white matter, gray matter, and cerebral spinal fluid modelled as 3-D hexahedral solid elements, and the pia mater, dura mater and denticulate ligament modelled using 2-D shell elements (Kimpara et al., 2006). The neck muscles were represented using a hybrid muscle model that contained 3-D solid elements for the passive muscle and Hill-Type 1-D beam elements for the active muscle (Iwamoto et al., 2009). The THUMS model has received multiple enhancements over the years, with the latest version being THUMS version 6 (Kato et al., 2018). The THUMS model has been utilized to study the effects of full body bracing during an impact event, effect of gender and spinal alignments (Iwamoto et al., 2015; Kitagawa et al., 2015; Sato et al., 2016).

The University of Waterloo (UW) neck model (Panzer et al., 2011) was created based on the geometry of the neck model by (Deng et al., 1999). The model contained the skull in addition to the cervical spine and T1 vertebrae, which were modelled as deformable bodies. The cortical bone was represented using 2-D quadrilateral shell elements with elastic-plastic formulation, and the trabecular bone was modelled using 3-D hexahedral elements with an elastic-plastic formulation. The intervertebral discs composition included the nucleus pulposus and ground substance, which were represented using 3-D solid elements, while the annulus fibrosus was modelled using 2-D membrane elements. Ligaments were modelled using non-linear tension only beam elements with rate effects. Both the passive and active musculature were modelled using 1-D Hill-Type beam elements with 87 symmetrical pairs to represent the neck musculature. The UW model has been utilized to study kinematics and neck tissue response in frontal impacts of varying severities

(Panzer et al., 2011), rear impacts examining tissue response of potential pain sources (Fice et al., 2011, Cronin, 2014), in addition to rear impact in rotated head postures (Shateri and Cronin, 2014).

The VIVA mid-size female human body model was created using CT scans of a 26 year old female (height: 167cm, weight: 59kg) (Östh et al., 2016). The vertebrae were modelled using triangular shell elements for the cortical bone and tetrahedral elements for the trabecular bone, both with elastic-plastic formulations. All ligaments were represented with 2-D orthotropic quadrilateral membrane elements. The intervertebral disc was modelled using 3-D hexahedral elements for the nucleus pulposus, while the annulus fibrosus was modelled using 2-D quadrilateral membrane elements with orthotropic nonlinear elastic material property. Additionally, the facet joints were modelled using contacts with no friction between the articular cartilages. Both active and passive muscles were represented using 1-D Hill-type beam elements. The Viva model has been validated for physiological loading conditions and full body rear impacts utilizing volunteer data (Östh et al., 2016; Östh et al., 2017).

The GHBMC neck models (50^{th} percentile male and 5^{th} percentile female) were developed by the University of Waterloo, which incorporated improved modelling techniques and material properties that were used in the development of the UW neck model. Detailed comparisons of both neck response and tissue level injury in frontal, rear, and lateral impacts, for both the 50^{th} percentile male and 5^{th} percentile female comparison have not been studied to date. A detailed description of the GHBMC neck models will be provided in section 2.6.

2.5 Active Muscles

2.5.1 Numerical Implementation

Fundamentally, finite element neck models currently use the active muscle implementation based on the phenomenological Hill-Type muscle model, with differences in the implementation of the active elements in conjunction with the passive musculature and the activation strategy. In this section, the Hill-Type muscle model as implemented in the LS-DYNA finite element software will be described along with a brief description of the integration of active musculature in current neck models.

The Hill-Type muscle model is composed of a contractile element (CE) and a passive element (PE) that work collectively to represent a human skeletal muscle (Figure 2-27) (Zajac, 1989; Winters, 1995) . The CE is representative of the active contractile behaviour of the muscle, while the PE represents the passive tensile lengthening response, with the summation of the forces in these two elements that produce

the total force of the muscle. In modern HBMs, the passive behaviour of the muscles are usually represented with 3-D elements because they provide a better anatomical representation of a muscle by occupying volume in the human body. Hence, the focus of this section will be on the CE portion of the Hill-Type muscle model.

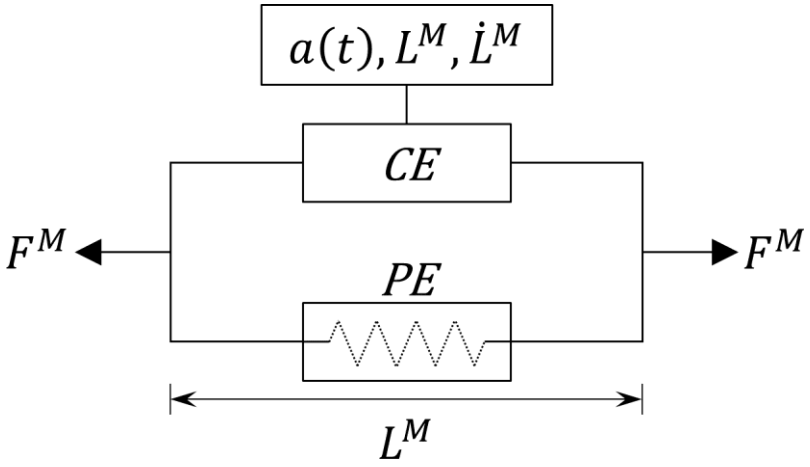

FIGURE 2-27: HILL-TYPE MUSCLE MODEL SCHEMATIC

There are two general parameters (maximum isometric stress and PCSA) and three non-linear input functions for the contractile element (activation state dynamics, force-length, force-velocity) that describe the instantaneous force generated by a muscle during contraction at any given time step.

$$F = (\sigma_{max}) \cdot (PCSA) \cdot A(t) \cdot f\left(\frac{l}{l_{orig}}\right) \cdot g(\dot{\varepsilon})$$

The maximum isometric stress represents the maximum force per unit area that a human skeletal muscle can generate. The PCSA is a physical quantity that is used to normalize the cross-sectional area of any skeletal muscle to that of an idealized muscle, such that all muscle fibres are oriented along the principal line of action. The PCSA is therefore a function of the muscle pennation angle, muscle volume, and muscle fibre length.

The normalized force-length relationship (Figure 2-28) corresponds to a force-scaling factor based on the current length of the muscle (<1= concentric contraction, 1= default resting length, >1= eccentric lengthening) (Figure 2-28). The maximum force occurs at an optimized length (L_{opt} = 1.05), which is the length that allows for the maximum number of cross-bridge formation in a muscle (Winters, 1995).

The normalized force-velocity relationship (Figure 2-28) describes a force-scaling factor based on the velocity of the muscle during contraction (negative velocity represent concentric contraction, zero velocity represent isometric contraction, and positive velocity represent eccentric contraction) (Hill, 1938). The physiologic basis for this phenomenon is related to the kinetics of cross-bridge formation (Seow, 2013). As contraction velocity increases during concentric contraction (negative velocity), the amount of time for cross-bridge formation decrease, until a maximum velocity is reached where no cross-bridges can be formed. Conversely, as contraction velocity decreases and approach isometric contraction (zero velocity) and transition into eccentric contraction (positive velocity), there will be more cross-bridge formation, hence higher force.

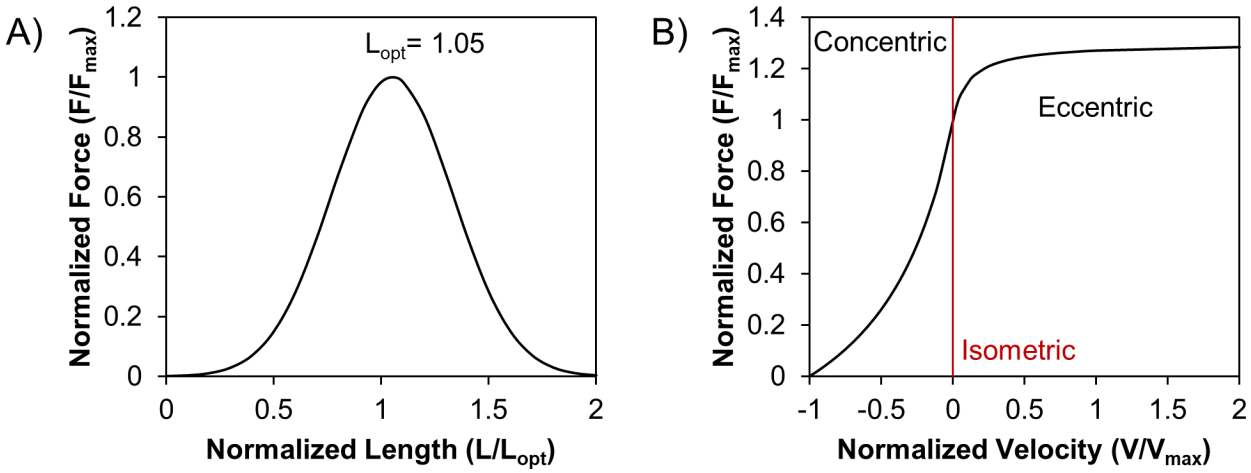

FIGURE 2-28: A) NORMALIZED FORCE-LENGTH, B) NORMALIZED FORCE-VELOCITY

The muscle activation state dynamics a(t) describe the muscle activation with respect to time and ranges from zero to one (0= not activated, 1= fully activated). There are two different methods to implement activation dynamics into a Hill-Type muscle model: pre-determined activation dynamics or closed-loop feedback control. One example of a pre-determined activation dynamics include direct input of volunteer EMG data to represent a(t) to mimic the in-vivo activation of volunteers (Iwamoto et al., 2012). A(t) can also be determined mathematically by equations of active and de-active state dynamics that describe the bio-molecular mechanism of muscle activation from neural inputs to cross-bridge kinetics and force generation (Happee et al., 1994; Winters 1995; Panzer et al., 2011) (Figure 2-29). An initial delay is introduced before the activation to represent the activation delay onset (reflex time from external stimuli to muscle activation), and the muscle remained activated for 100 ms to achieve a maximum activation of 87% (Panzer et al., 2011). The positive slope of the activation represents the active dynamics (muscle activation), and the negative slope represents the de-active dynamics (muscle deactivation). As mentioned previously,

calcium ions bond onto regulatory proteins on the thick filament (myosin) that allow for cross-bridge formation to occur. When activation begins, the process occurs quickly, but as activation continues, the dynamic process decelerates due to delayed diffusion and slower calcium ion release from the sarcoplasmic reticulum into the muscle fibre (Winters 1995). Conversely, when a muscle starts to deactivate, the rate of deactivation is decelerated as calcium ions are transferred back into the sarcoplasmic reticulum, which causes less efficient ion transfer (Winters 1995). These two phenomena describe the gradual decrease in the muscle activation and deactivation rate in the activation curve (Figure 2-29).

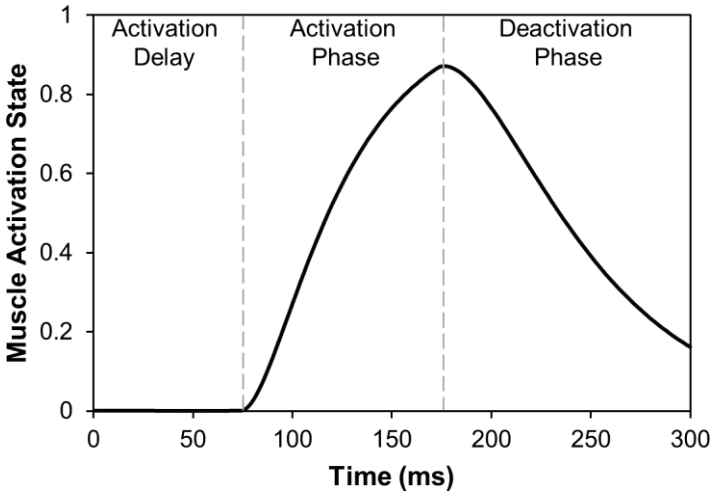

FIGURE 2-29: EXEMPLAR ACTIVATION CURVE

A(t) can be replaced with a closed loop feedback muscle controller that uses proportional-integral-derivative (PID) control to modulate the activation of the muscle based on external targets such as joint angle and reaction force (Östh et al., 2012; Kato et al., 2017).

Different muscle implementation strategies have been developed in HBMs. Although the Hill-Type muscle model can account for passive resistance, many modern HBMs represent the passive portion of the musculature as 3-D solid elements to improve the biofidelity of the model. Hybrid approaches that integrate 1-D Hill-Type muscle elements into the 3-D passive are present in the KTH model, THUMS model and GHBMC model. The KTH (Hedenstierna et al., 2008) and THUMS (Iwamoto et al., 2009) model follow a similar approach where the 1-D Hill-Type beam elements are integrated into the mesh of the 3-D passive muscles in the muscle fibre direction (Figure 2-30). The GHBMC model contains 1-D Hill-Type beam elements that are segregated into multiple segments and divided into parallel pairs. These elements are integrated into the 3-D passive muscles, where the nodes of the 1-D Hill-Type muscles are coincident with

the mesh of the 3-D passive muscles. Details of the GHBMC hybrid muscle model are covered in section 2.6.4

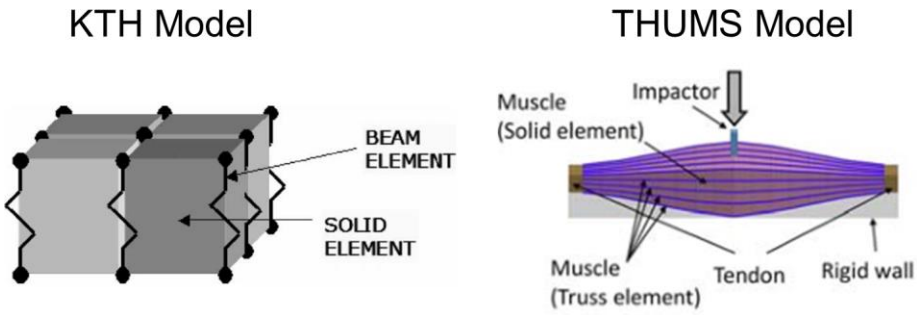

FIGURE 2-30: HYBRID MUSCLE MODELS *(Adapted from Hedenstierna et al., 2008; Yang et al., 2018)*

2.5.2 Activation Onset Time

During a motor vehicle collision, occupants experience rapid acceleration-deceleration events with typical durations of less than 300 ms. In that time frame, the effect of muscle contraction may be an important contributor to the response of the body, particularly in low severity impact scenarios. There are two typical scenarios, one where the occupant or diver is unaware of the impending impact and one where the occupant is aware of the oncoming impact. If the occupant is aware of the oncoming impact, they can pre-brace by tensing all of the neck muscles before the onset of the impact, thereby stiffening the neck and reduce head kinematics. When an occupant is unaware of the oncoming impact, the motor vehicle collision will evoke a multitude of stimulus onto the individual that will trigger the onset of muscle activity by a startle response, which is regarded as a protective response triggered by the autonomic nervous system. This delay between the external stimuli and the onset of muscle activity is called the activation onset time and is an important measure that can determine whether or not the neck muscles play a role in short duration impact events (Siegmund et al., 2002).

The muscle activation onset time is comprised of two components: the reflex delay (time for the nervous system to process the external stimuli (acoustic, tactile, etc.) to activate the motor neurons, and the electromechanical delay (time from motor neuron stimulation to the initiation of the muscle contraction for force production). These two components are measured as a combined quantity at the onset of the sled/seat perturbation during human volunteer experiments.

The muscle activation onset times are measured using electromyography (EMG) testing, which allows direct monitoring and collection of data regarding muscle activation time, and activation magnitude by

tracking the electrical impulse signal from the activation of the muscle. Two variations of this technique are used: surface EMG, or electrode (indwelling wire) EMG. Surface EMG involves attaching the electrodes directly onto the surface of the skin to track the EMG signals of the muscles subcutaneous to the skin. This method is widely used but is limited to tracking superficial muscles. Indwelling electrode EMG allows tracking of both superficial and deep muscles by inserting the electrodes directly into the belly of the muscle. Before the testing can begin, the volunteers are asked to fully activate their muscles at maximum effort, and the EMG signals are recorded. This quantity is called the maximal voluntary contraction (MVC) and is used to normalize all subsequent electrical signals that are collected during testing.

Muscle activation onset times are well documented in the experimental literature (Foust et al., 1973; Snyder et al., 1975; Szabo and Welcher, 1996; Ono et al., 1997; Magnusson et al., 1999; Brault et al., 2000; Wittek et al., 2001; Siegmund et al., 2001; Siegmund et al., 2003; Kumar et al., 2002; Blouin et al., 2003; Kumar et al., 2003; Kumar et al., 2004a; Kumar et al., 2004b; Hernandez et al., 2005). These studies reported the activation onset time from one or multiple cervical muscles as the summation of the reflex time and the electromechanical delay. Perturbation was applied to the volunteers either to the head by an applied jerk, to the torso by the means of a sled or a test vehicle, or by a loud auditory stimulus, while muscle activity was monitored using EMG.

Foust et al., (1973) performed dynamic anterior and posterior head jerks on 180 volunteers by using an electromagnet to drop a 455 g weight. Surface EMG was used to measure muscle activity on the sternocleidomastoid (flexors) in addition to the splenius capitis and semispinalis capitis (extensors). The onset time was defined as the onset of muscle activity and the beginning of head acceleration. The average onset time for the cervical extensors and flexors were 65 ms. Snyder et al., 1975 followed the same methodology as Foust et al., 1973 and measured the EMG signals of the same muscles. The average onset time for the cervical extensors and flexors were 66 ms and 77 ms respectively.

Szabo and Welcher (1996) conducted full-scale vehicle testing (change in speed of 10 km/h) with five volunteers. To make sure all occupants were unaware of the time of impact, auditory and visual cues were removed. Bilateral surface EMG was used to measure the muscle activity of the sternocleidomastoid, cervical extensors, and trapezius. The onset time was defined as the start of muscle activity with respect to bumper contact. The average activation onset time ranged from 110 ms to 125 ms, with minimal difference between left and right muscles.

Ono et al., (1997) subjected three male volunteers to simulated rear impacts of 6 km/h with a custom sled apparatus. Subjects were asked to be relaxed, while surface EMG was used to measure the activity of the sternocleidomastoid. Onset time ranged from 76 ms to 93 ms with an average of 79 ms.

Magnusson et al., (1999) performed rear impact tests on eight male volunteers using a car seat mounted on a sled. Electrode EMG was used to measure the activity of the levator scapulae, splenius capitis and semispinalis capitis, and surface EMG for the sternocleidomastoid and trapezius. Auditory and visual signals were removed from the volunteers to simulate an unaware impact. Activation onset time was measured from the sled movement onset to muscle activity. The average activation onset time for the sternocleidomastoid, levator scapulae, trapezius, splenius capitis and semispinalis capitis was 72.2 ms, 80.8 ms, 75.4 ms 148.5 ms and 160.6 ms respectively.

Brault et al., (2000) conducted low-speed rear impacts on 42 volunteers using full-scale vehicle testing for striking velocities of 4 km/h and 8km/h. Surface EMG was used to monitor the sternocleidomastoid and the cervical paraspinal muscles. Auditory and visual cues were eliminated to conduct an unexpected impact. Activation onset time was lower for the 8 km/h impact, with average times of 81 ms and 83.5 ms for the sternocleidomastoid and cervical paraspinal muscles respectively.

Wittek et al., (200l) utilized the same sled apparatus as Ono et al., 1997 to subject four male volunteers to rear impact tests of 6 km/h. Both surface and electrode EMG was used to measure the muscle activity of the sternocleidomastoid. The average onset time was 79 ms and 81 ms for the electrode and surface EMG respectively.

Siegmund et al., (2001) used a loud auditory stimulus (124 dB) to evoke a startle response on 20 volunteers. Surface EMG was used to measure the bilateral activity of the sternocleidomastoid and cervical paraspinal muscles. Average onset times were 52 ms and 59.5 ms for the sternocleidomastoid and cervical paraspinal muscles respectively.

Siegmund et al., (2003) performed rear impact tests (max acceleration of 1.5 g) on 44 volunteers using a car seat mounted on a custom linear sled setup. Half of the subjects were aware of the oncoming impact, and the other half were unaware. Surface EMG was used to measure the bilateral activity of the sternocleidomastoid and paraspinal muscles. Activation onset time differences for aware and unaware subjects were not statistically significant. The activation onset time of the sternocleidomastoid and paraspinal muscles were 71 ms and 79.5 ms respectively.

Blouin et al., (2003) subjected nine volunteers to simulated unaware rear impacts (max acceleration of 1.1g) using a car seat mounted on a custom linear sled setup. Surface EMG was used to monitor the activity of the scalenus, sternocleidomastoid, paraspinal, and trapezius muscles. The average activation onset time was 59 ms, 55 ms, 65 ms, and 72 ms for the scalenus, sternocleidomastoid, paraspinal, and trapezius muscles respectively.

Kumar et al., (2002) used a test sled to subjected seven volunteers to simulated rear impacts of varying severities (0.5g, 0.9g, 1.1g, 1.4g). Bilateral surface EMG was used to measure the muscle activity of the sternocleidomastoid, trapezius, and the splenius capitis muscles. Auditory and visual cues were removed from the volunteers to simulate an unexpected impact. Muscle onset time was defined at the onset of the sled. The activation onset time for the sternocleidomastoid ranged from 83 ms to 116 ms, while the splenius capitis ranged from 78 ms to 104.5 ms, and the trapezius had activation onset time in the range of 237 ms to 879 ms.

Kumar et al., (2003) used the same test setup as Kumar et al., (2002), and subjected 10 volunteers to simulated frontal impacts of varying severities (0.5g, 0.9g, 1.1g, 1.4g). Test procedure and muscles monitored were the same as Kumar et al., (2002). The activation onset time for the sternocleidomastoid ranged from 303.5 ms to 1535.5 ms, while the splenius capitis ranged from 188 ms to 321 ms, and the trapezius ranged from 83 ms to 98 ms.

Kumar et al., (2004a) and Kumar et al., (2004b) subjected unaware volunteers to right lateral and left lateral perturbations with a test sled following the same procedure and severity as (Kumar et al., 2002), while bilateral EMG activity was monitored. For both test cases, the splenius capitis muscle displayed activation asymmetry. The splenius capitis muscle contralateral to head movement reached >80% of its MVC, while the ipsilateral side reached <40% MVC. The authors suggested that cervical muscle response may be triggered by muscle stretch. Activation onset times for muscles contralateral to the side of the head movement were less than the ipsilateral side. For the right lateral impact, the contralateral sternocleidomastoid had activation onset time in the range of 110.7 ms to 251.3 ms, while the contralateral splenius capitis was in the range of 76.7 ms to 207.3 ms, and the contralateral trapezius was in the range of 109.7 ms to 315.3 ms. For the left lateral impact, the contralateral sternocleidomastoid had activation onset time in the range of 65.3 ms to 217 ms, while the contralateral splenius capitis was in the range of 43.3 ms to 160 ms, and the contralateral trapezius was in the range of 67.3 ms to 588 ms.

Hernandez et al., (2005) conducted simulated rear impacts (average acceleration of 0.46 g and 1.03g) on 29 volunteers using a car seat mounted to a pneumatic sled. Surface EMG was used to measure the

muscle activity of the sternocleidomastoid muscle. Onset time was defined as the start of sled acceleration. The average activation onset time was 130.7 ms for the slower sled pulse, and 99.1 ms for the faster sled pulse.

2.5.3 Physiological Cross Sectional Area

There are limited complete sets of data on cervical muscle PCSA available in the existing literature. PSCA values in HBMs are often calculated with a combination of different sets of data in the literature (e.g. muscle volumes from the visible human project used with published dissection data on muscle fibre length).

Three notable literature sources present cervical spine PCSA data on multiple muscles. Kamibayashi and Richmond (1998) reported PCSA values for 18 pairs of cervical muscles through a cadaver dissection method. Muscle mass, pennation angle and fascicle lengths were measured from 10 human cadavers (3F, 7M, age: 66-92) from which muscle PCSA was calculated. A normalization technique on fascicle lengths was used to correct the non-physiological shortening that occurs during rigour mortis to that of in-vivo humans. In general, the PCSA was smaller for the female PMHS than the male counterparts. A few limitations existed for the study: anthropometries of the subjects were not reported and possible errors from utilizing elderly donors due to muscle atrophy may not be representative of the young population. Borst et al., 2011 reported PCSA values for 34 neck muscles through unilateral (left side) dissection of a PHMS subject with similar anthropometry as a 50^{th} percentile male (age: 86, height 1.71m, weight: 75kg). Muscle mass, pennation angle and fibre length data were collected and used to calculate PCSA values. This is the most complete set of neck PCSA data that is available in the literature. However, the same limitation exists where muscle atrophy due to old age may not be representative of the young population. Knaub et al., 1998 presented cervical PCSA muscle volume geometry for 24 pairs of cervical muscle utilizing a hybrid approach, where MRI was used to obtain muscle volumes from human volunteers and pennation angle and fascicle lengths were obtained from cadaveric dissections (4 males, 2 females, age: 71-83, weight: 50-68 kg, height: 5'1" - 5'11"). Volunteers were recruited based on anthropometric requirements and included six 50^{th} percentile males, one 95^{th} percentile male, and two 5^{th} percentile females. This hybrid approach was utilized because large differences in muscle volumes were found between the young volunteers and the elderly PHBMS subjects. This is the only study that reported the neck muscle PCSA based on the 50^{th} percentile male, 95^{th} percentile male, and 5^{th} percentile female statures, which provided differences on anthropometric muscle volumes.

2.6 GHBMC Human Body Models

The GHBMC M50 HBM was developed from the geometry of a male subject (age: 26 years, height: 174.9 cm, mass: 78.6 kg, body mass index (BMI): 25.7) from computed tomography and magnetic resonance imaging techniques (Davis et al., 2016), and the GHBMC F05 human body model was developed from geometries of a 5th percentile female volunteer (age: 24 years, height: 149.9 cm, mass: 48.1 kg, BMI: 21.4) using computed tomography and magnetic resonance imaging techniques (Schwartz et al., 2015) (Figure 2-31). The development of the HBM was divided into body region models (BRM) including (head, neck, upper extremities, thorax, abdomen, lower extremities) as a collaborative effort between institutions around the world. Each body region was separately developed and validated before consolidated into the full body model. The neck BRM was developed by the Neck Center of Expertise (Neck COE) at the University of Waterloo.

The neck model contained detailed structures consisted of key anatomical components such as the ligaments, cartilage, tendon, intervertebral disc, passive and active muscles, cortical and trabecular bone (Figure 2-32). The model was assessed for biofidelity by performing extensive verification and validation cases, ranging from a single element to full neck validation against experimental human volunteer and cadaver test data. Appropriate material constitutive models were selected for each tissue in the model and validated against material data from the literature. Each tissue was integrated into a motion segment to form the LCS (six total, C23 to C7T1) which included all connective tissues (ligaments, intervertebral disc, and cartilage) and was individually validated against experimental data for flexion, extension, lateral bending, shear (anterior, posterior, lateral), axial rotation, tension and compression type loading for quasi-static and dynamic loading conditions until failure (Barker et al., 2017). The upper cervical spine (skull, C1-C2) was validated separately against flexion, extension, axial rotation and tension data from the experimental literature (Laswell et al., 2017). The following step included assembling the head with the validated lower and upper cervical spine segment (ligament, intervertebral disc, and cartilage) into the ligamentous spine and validating against axial tension, axial rotation. Furthermore, the ligamentous spine was validated against experimental frontal and rear impacts with T1 motion boundary condition, and tissue strains were compared with the experiments. The final step required the integration of all tissues into the full neck (ligamentous spine, skin, flesh, passive muscles, active muscles) and was fully validated against human volunteer experiments in frontal and lateral impacts, in addition to rear impacts (full body cadaver). The boundary condition was applied to the T1, and head kinematics was used as the metric for evaluation. A cross-correlation method was used to generate a rating that ranged from zero to one (zero being a low correlation, and one being high correlation) to assess the biofidelity of the model. The kinematic response of the model was compared to the average kinematic response of the volunteers with an objective rating

program called CORA. Three assessments (shape, size, and phase shift), in addition to a corridor rating, was used to determine a final weighted average score to rate the performance of the model (Table 2-6 and Table 2-7).

TABLE 2-6: M50 CORA SCORES

CORA	8gFRT	15gFRT	7gLAT	7gREAR
Corridor	0.478	0.498	0.656	0.822
Shape	0.918	0.954	0.885	0.730
Size	0.632	0.704	0.611	0.672
Phase	0.462	0.886	0.412	0.667
Average	0.575	0.673	0.646	0.756

TABLE 2-7: F05 CORA SCORES

CORA	8gFRT	15gFRT	7gLAT	7gREAR
Corridor	0.507	0.405	0.649	0.803
Shape	0.859	0.904	0.788	0.832
Size	0.767	0.773	0.631	0.699
Average	0.660	0.621	0.679	0.785

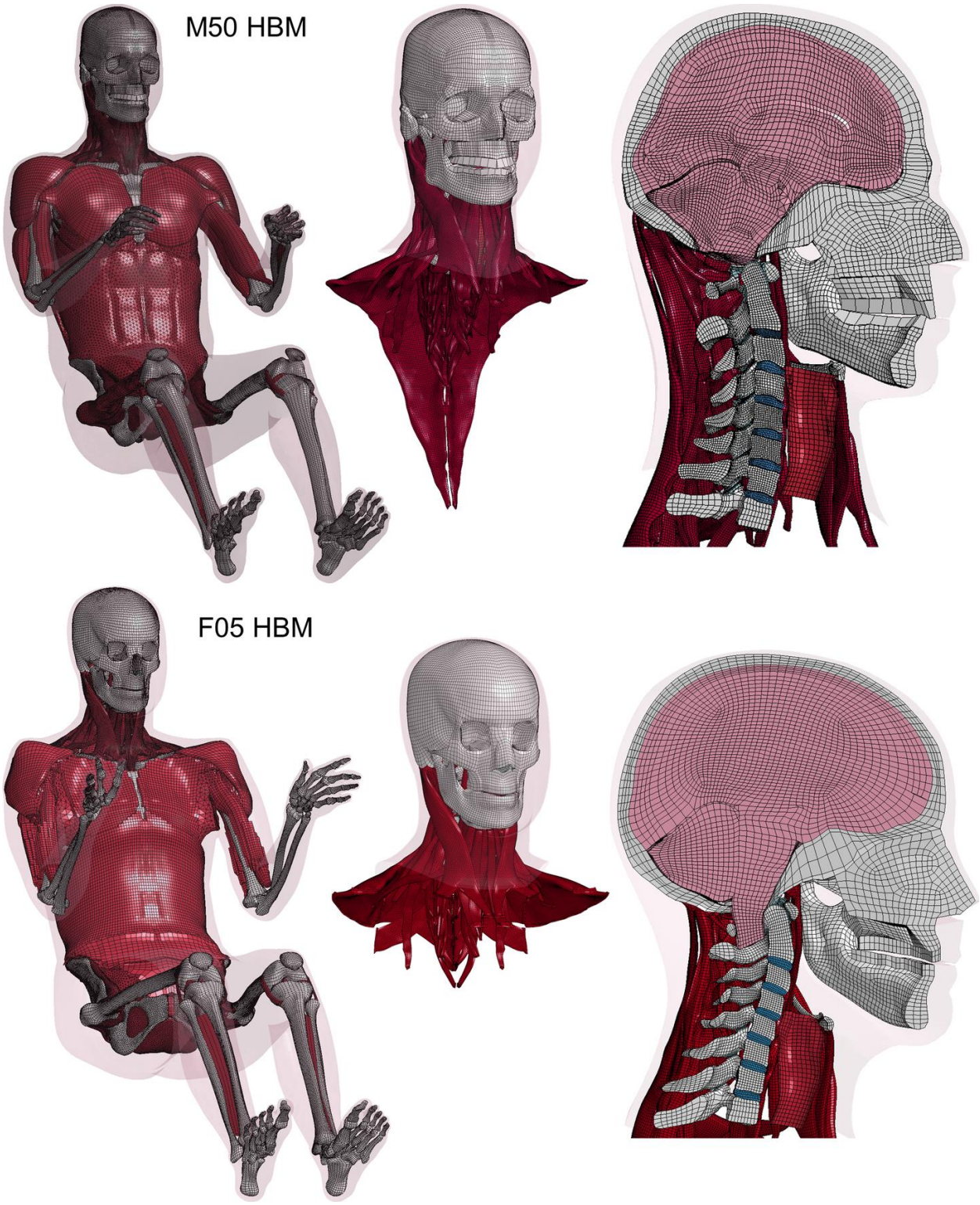

FIGURE 2-31: 50TH PERCENTILE MALE AND 5TH PERCENTILE FEMALE HBM AND EXTRACTED NECK MODEL (RELATIVE SIZE NOT-TO-SCALE)

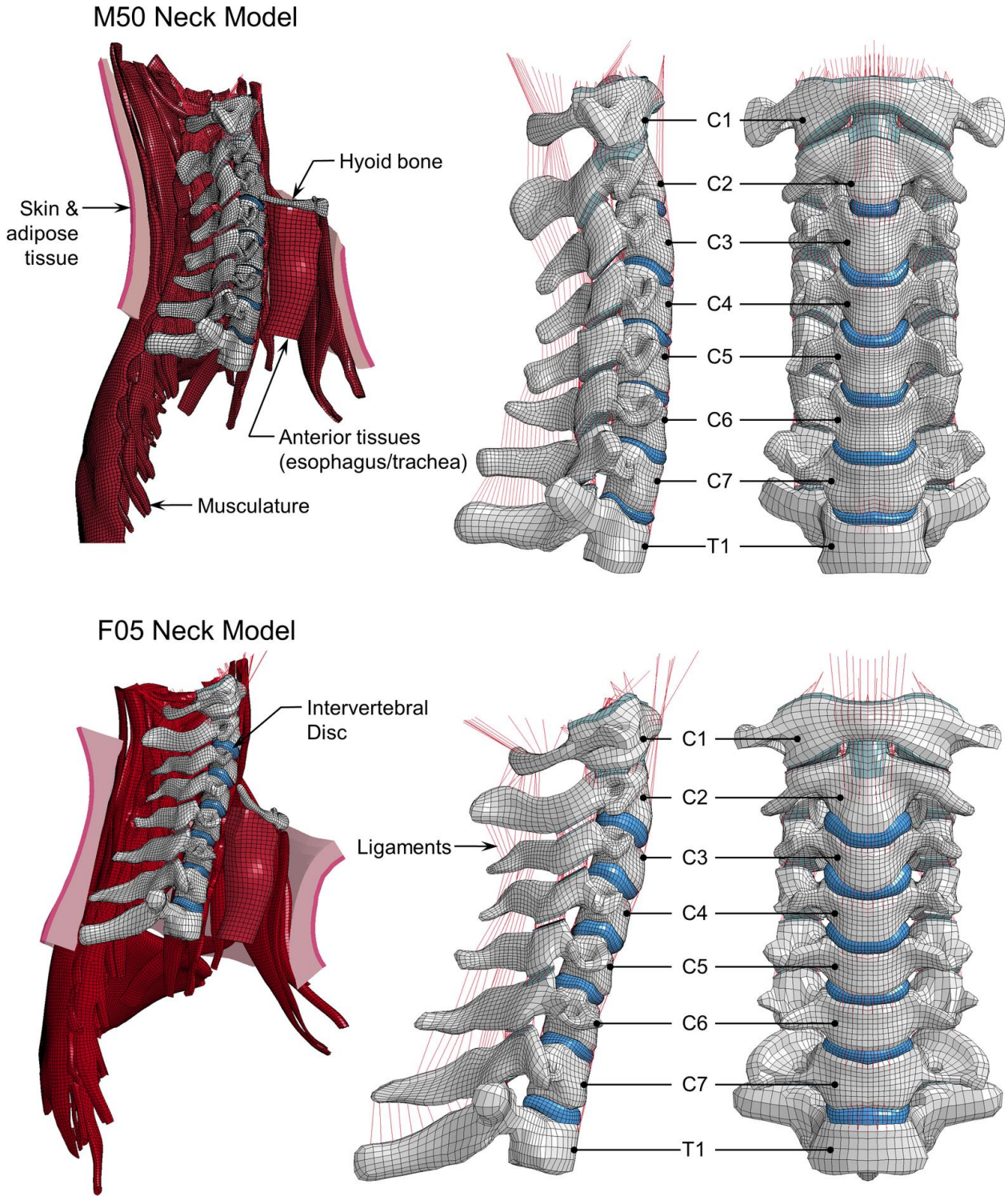

FIGURE 2-32: GHBMC M50 AND F05 NECK MODEL DETAILS

2.6.1 Hard Tissues

Hard tissues were modelled using an isotropic elastic-plastic formulation with a separate elastic and plastic bilinear response, where the end of the elastic region is defined as the yield stress of the bone (Table 2-8). Bone failure is represented by element erosion based on an ultimate plastic strain failure criterion. Cortical bone was modelled using 2-D quadrilateral shell elements, while the trabecular bone used 3-D solid hexahedral elements (Figure 2-33).

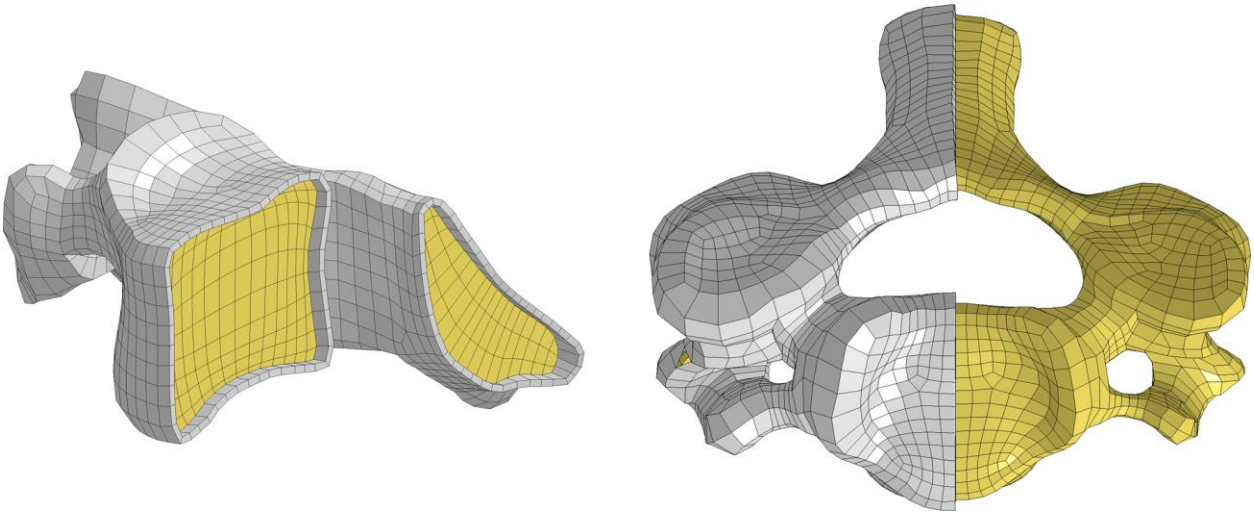

FIGURE 2-33: HARD TISSUE COMPOSITION: WHITE (CORTICAL BONE), YELLOW (TRABECULAR BONE)

The cortical bone is modelled using (*MAT_PLASTIC_KINEMATIC) isotropic elastic-plastic material model with a failure strain of 1.78% to initiate element erosion based on a plastic strain failure criterion. The trabecular bone was modelled using (*MAT_ISOTROPIC_ELASTIC_PLASTIC) solid elements with a failure strain of 9.5%.

TABLE 2-8: HARD TISSUE MATERIAL PROPERTIES

Property	Cortical	Trabecular
Density (kg/mm^3)	2.00 E-6	1.10 E-6
Elastic modulus (GPa)	18.439	0.442
Poisson's ratio	0.28	0.30
Yield stress (GPa)	0.1898	0.00283
Plastic modulus (GPa)	1.2489	0.0301
Failure strain	0.0178	0.095

2.6.2 Intervertebral Disc

The intervertebral disc is comprised of three components, the annulus lamellae, ground substance, and the nucleus pulposus (Figure 2-34). The assembly of the disc parts are attached to the cartilaginous endplates on the vertebral bodies through a tiebreak contact interface.

The annulus fibrosus was modelled as a composite material, with the fibre portion containing the annular lamellae and the matrix portion containing the ground substance. The lamellae were modelled using a non-linear anisotropic elastic material model (*MAT_FABRIC) with ten layers of concentric four node quadrilateral shell elements, with material properties from tensile testing of annulus fibres (Holzapfel et al., 2005, Ebara et al., 1996, Skaggs et al., 1994). The ten layers were divided into five pairs of lamellae and were used to represent the collagen fibre orientation from the outer layer (25º) to the inner layer (45º) in 5º increments (Figure 2-34) (Cassidy et al., 1989), with each pair having opposite fibre angles (Figure 2-34). The ground substance was represented with a compressible foam model (*MAT_HILL_FOAM) with 8-node solid hexahedral elements and shared nodes with the annulus lamellae. The tensile and compressive material behaviour was modelled from experimental data of radial properties of annulus fibrosus specimens (Fujita et al., 1997, Iatridis et al., 1998). The material response from the experiment was fitted onto an isotropic strain-energy function (Hill, 1979, Storakers, 1986) (Table 2-9), using the equation below.

$$W = \sum_{j=1}^{m} \frac{C_j}{b_j}\left[\lambda_1^{b_j} + \lambda_2^{b_j} + \lambda_3^{b_j} - 3 + \frac{1}{n}(J^{-nb_j} - 1)\right], n = 2, m = 3$$

TABLE 2-9: GROUND SUBSTANCE MATERIAL CONSTANTS

j	C	b
1	-0.895	-2
2	2.101	-1
3	0.115	4

The nucleus pulposus was modelled using an elastic fluid material model (*MAT_ELASTIC_FLUID) with 8-node solid hexahedral elements and situated within the ground substance and annulus lamellae. The bulk modulus was 1720 MPa (Yang and Kish, 1988).

A normal stress failure criterion of 10 MPa was integrated into the tie-break interface between the disc ground substance and vertebral endplate to model the injury mechanism of disc avulsion (DeWit and Cronin, 2012; Kasra et al., 2004).

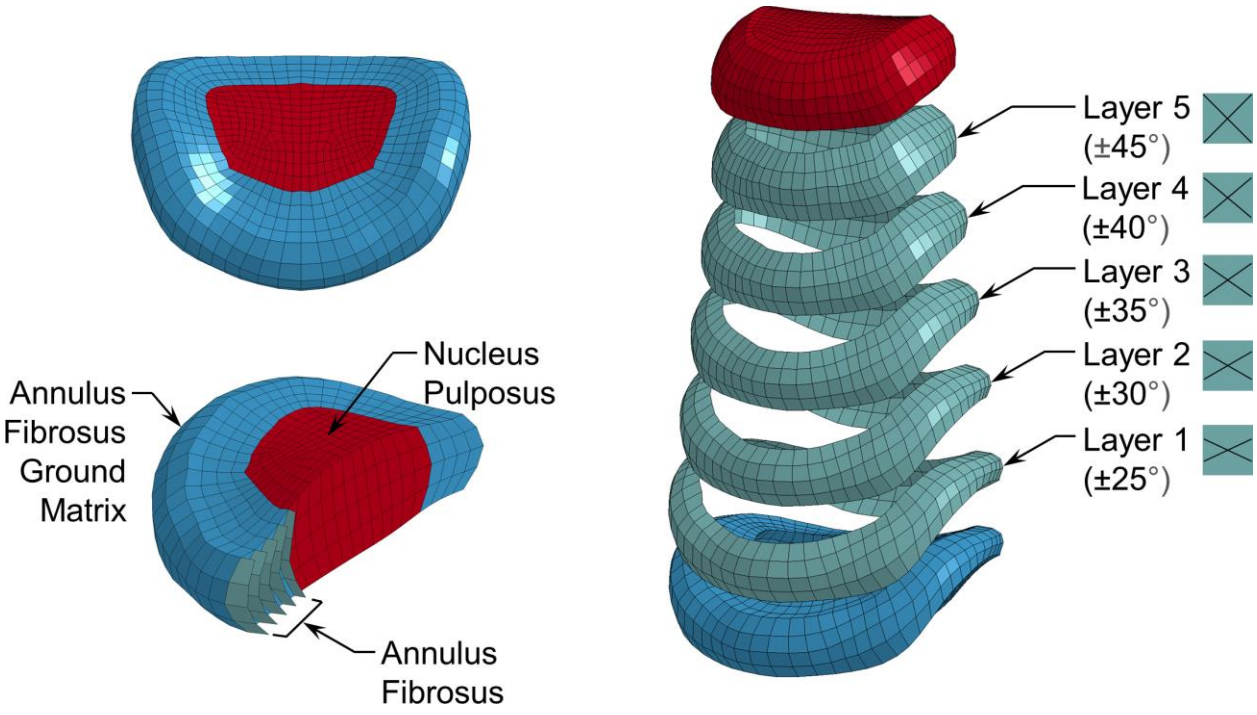

FIGURE 2-34: INTERVERTEBRAL DISC COMPOSITION

2.6.3 Ligaments

Ligaments were modelled using 1-D, two-node tension only discrete beam elements using (*MAT_ELASTIC_SPRING_DISCRETE_BEAM). The response of the ligaments was dictated by a non-linear force vs. displacement response in addition to strain rate effect scaling factors obtained from experimental testing of young cervical spine ligament specimens (Mattucci et al., 2012; Mattucci et al., 2013; Mattucci and Cronin, 2015). The ligaments are directly attached to the hard tissue and are spaced approximately 1 mm apart. In addition, progressive ligament failure was implemented to model bundles of collagen fibres in the post-traumatic region (Figure 2-35). The element would erode in a progressive manner when they reached a critical distraction value (DeWit and Cronin, 2012). The tension-only force response of the ligament was represented using the governing equation below.

$$F = F_o + Kf(\Delta L) + g(\Delta L) * h(\Delta \dot{L})$$

F_o defined the ligament pretension force (not used), $Kf(\Delta L)$ represent the quasi-static force vs displacement response curve, and $g(\Delta L)$ and $h(\Delta \dot{L})$ function was responsible for ligament strain rate effects of up to 300 s^{-1}.

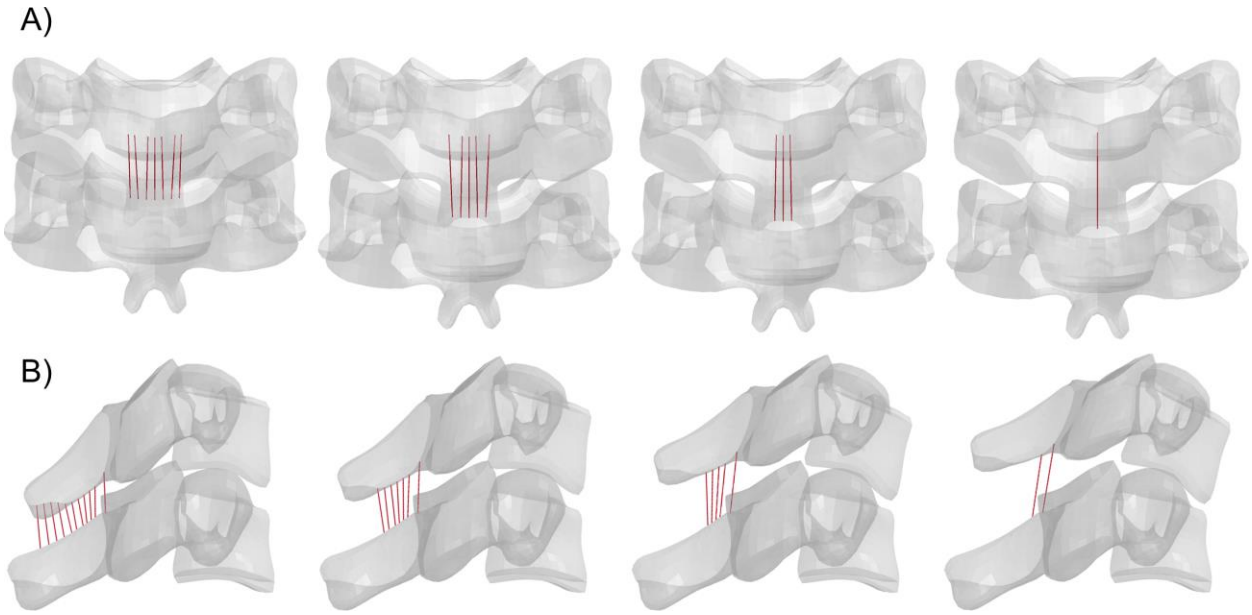

FIGURE 2-35: LIGAMENT PROGRESSIVE FAILURE, A) ALL TENSILE FAILURE, B) ISL FLEXION FAILURE

2.6.4 Musculature

The neck muscles utilized a hybrid modelling approach that involved 1-D active muscles that share nodes and are embedded in the 3-D passive muscles (Figure 2-38). The active portion of the musculature was represented with the phenomenological Hill-Type muscle model (*MAT_MUSCLE) that used 2-node contractile beam elements with no tension response. The passive portion of the musculature was represented with a viscoelastic Ogden model (*MAT_OGDEN_RUBBER) using 3-D solid hexahedral elements (Hedenstierna et al., 2008), that utilized the governing equation below. To account for strain rate effects, additional material constants were required (Table 2-10).

$$W = \sum_{i=1}^{3}\sum_{j=1}^{n}\frac{\mu_j}{\alpha_j}(\lambda^{\alpha_j} - 1) + K(J - 1 - lnJ)$$

$$j = 1, \mu = 1.33\ kPa, \alpha = 14.5$$

TABLE 2-10: PASSIVE MUSCLE STRAIN RATE MATERIAL CONSTANTS

m	G	β
1	522 kPa	1.02 s^{-1}
2	211 kPa	0.40 s^{-1}
3	375 kPa	0.65 E-01 s^{-1}
4	290 kPa	0.30 E-01 s^{-1}
5	80 kPa	1.00 E-04 s^{-1}

The contraction response of the Hill-Type muscle model is dependent on the parallel elastic (PE), the contractile element (CE) and the series elastic elements (SE). The model in the GHBMC has the CE and SE elements disabled because the passive response of the muscle and tendons are represented by the 3-D hexahedral solid elements.

Each muscle was segregated into multiple segments to represent the correct loading path of the muscle, and in some cases, the muscles were further divided into multiple parallel groups (Figure 2-36). The force that is generated in a muscle is dependent on several factors that include the max isometric stress (0.5 MPa), muscle PCSA, normalized force-length response, normalized force-velocity response, and the activation state of the muscle (Figure 2-37).

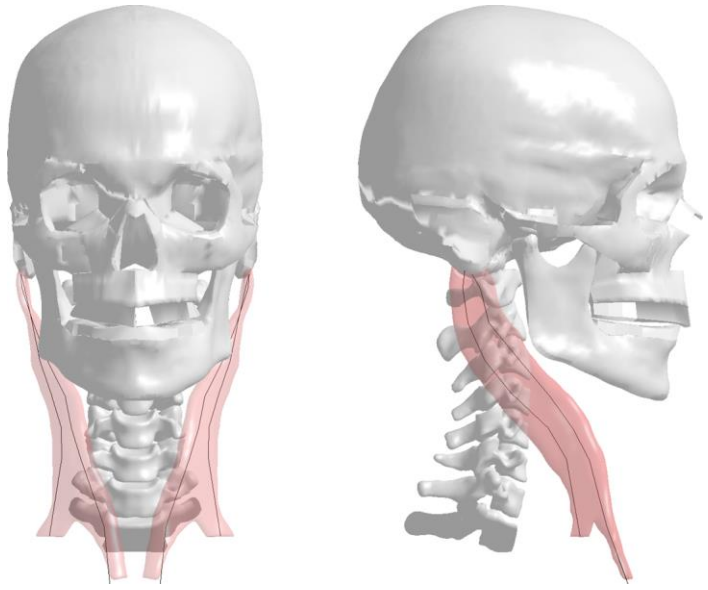

FIGURE 2-36: 1-D HILL TYPE MUSCLE ELEMENT SEGMENTATION (BLACK) IN 3-D MUSCLES (RED) FOR THE STERNOCLEIDOMASTOID

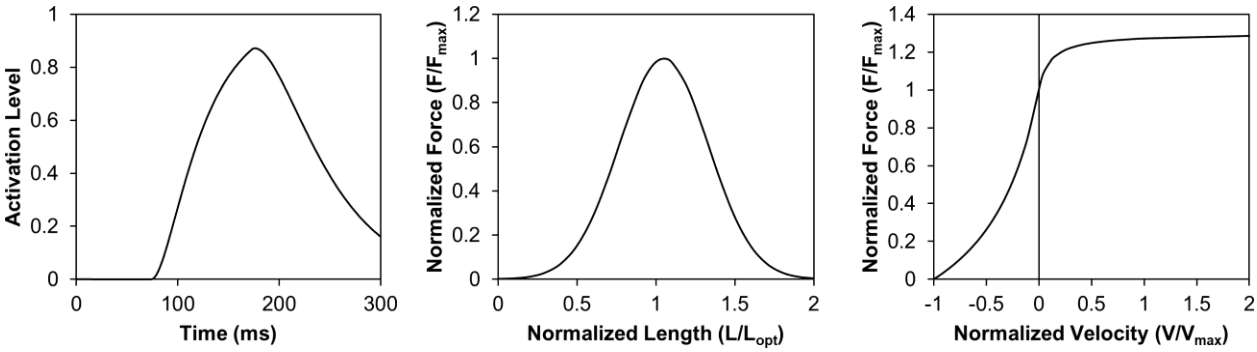

FIGURE 2-37: A) MUSCLE ACTIVATION CURVE, B) MUSCLE FORCE-LENGTH FUNCTION, C) MUSCLE FORCE-VELOCITY FUNCTION *(Panzer et al., 2011; Fice et al., 2011)*

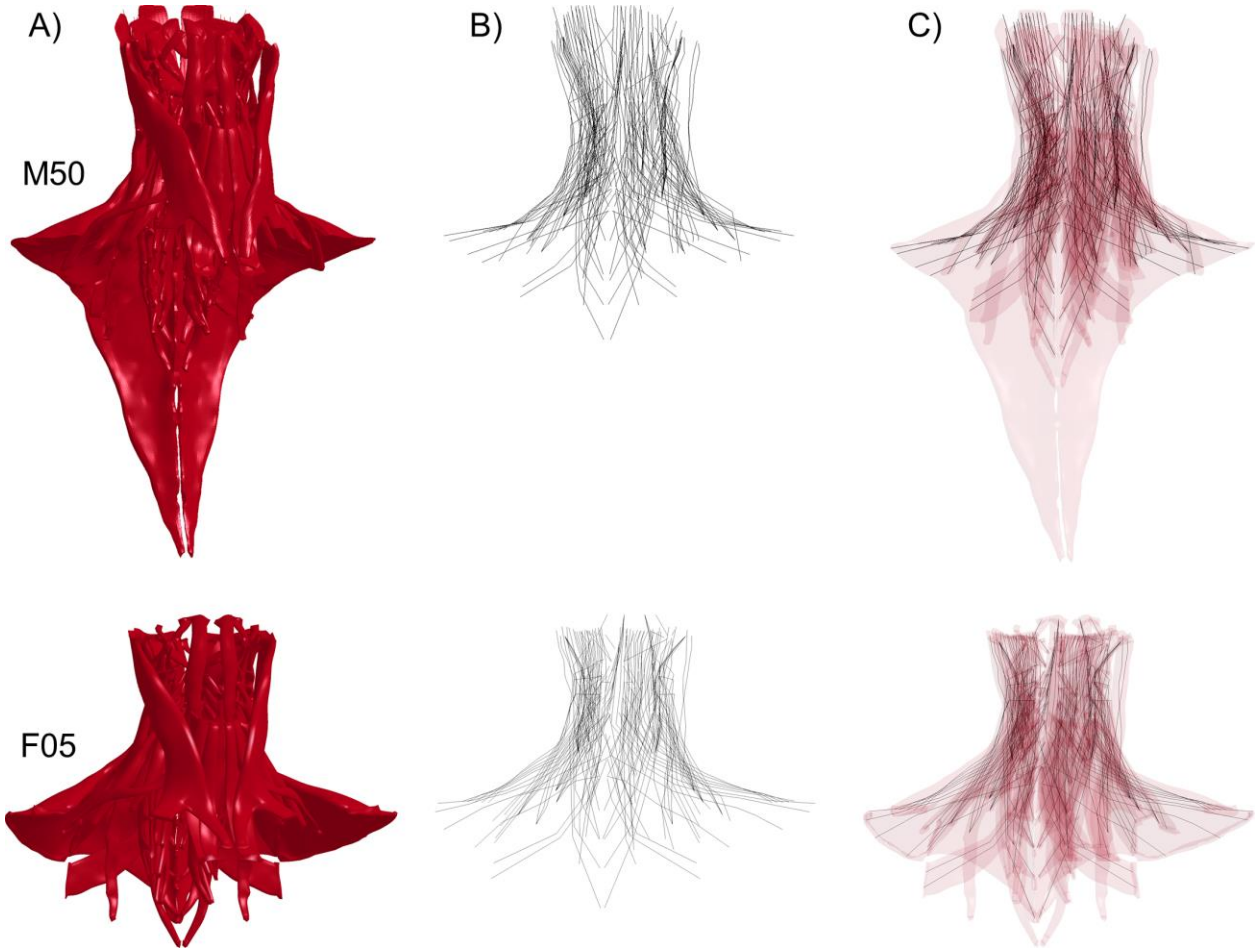

FIGURE 2-38: MUSCULATURE IMPLEMENTATION: A) 3-D PASSIVE MUSCLES, B) 2-D ACTIVE MUSCLES, C) 2-D ACTIVE MUSCLES EMBEDDED IN 3-D PASSIVE MUSCLES

In total, the neck region of the HBM contained 27 pairs of muscles. The muscles in the HBM are divided into two groups: flexors, containing all anterior cervical muscles, and extensors, containing all posterior cervical muscles (Table 2-11). Muscle activation in the baseline model is operated under the assumption that each pair of muscles in each flexor and extensor group activate synergistically with bilateral symmetry.

TABLE 2-11: MUSCLE GROUPS IN NECK REGION

Muscle	Group	M50 PCSA (mm^2)	F05 PCSA (mm^2)
Oblique Capitus Inferior	Extensor	195.0	127.9
Oblique Capitus Superior	Extensor	88.0	57.7
Iliocostalis Cervicis	Extensor	104.1	68.3
Longissimus Capitis	Extensor	98.0	64.3
Longissimus Cervicis	Extensor	148.8	97.6
Multifidus	Extensor	280.0	183.7
Semisplenius Capitus	Extensor	551.7	362.0
Semisplenius Cervicis	Extensor	306.0	200.8
Splenius Capitis	Extensor	309.2	202.9
Splenius Cervicis	Extensor	143.1	93.9
Levator Scapula	Extensor	312.0	204.7
Minor Rhomboid	Extensor	102.0	66.9
Trapezius	Extensor	1373.4	577.6
Rectus Capitus Major	Flexor	168.0	110.2
Rectus Capitus Minor	Flexor	92.0	60.4
Longus Capitis	Flexor	137.2	90.0
Longus Colli Superior	Flexor	69.0	45.3
Longus Colli Inferior	Flexor	69.0	45.3
Longus Colli Vertical	Flexor	137.1	90.0
Rectus Capitis Anterior	Flexor	80.0	52.5
Rectus Capitis Lateral	Flexor	90.0	59.0
Scalenus Anterior	Flexor	188.0	123.3
Scalenus Medius	Flexor	160.2	105.1
Scalenus Posterior	Flexor	105.0	68.9
Sternocleidomastoid	Flexor	492.0	322.8
Omohyoid	Flexor	75.0	49.2
Sternohyoid	Flexor	123.0	80.7

In addition, discrete beam elements were used to support and constrain each node of the active and passive muscles elements to the closest vertebra, and was necessary to allow the muscles to activate along the correct line of action during different modes of cervical spine movement. Without these support

elements, the muscles would form a straight loading path during contraction and intersect into the hard tissues, which is non-physiological.

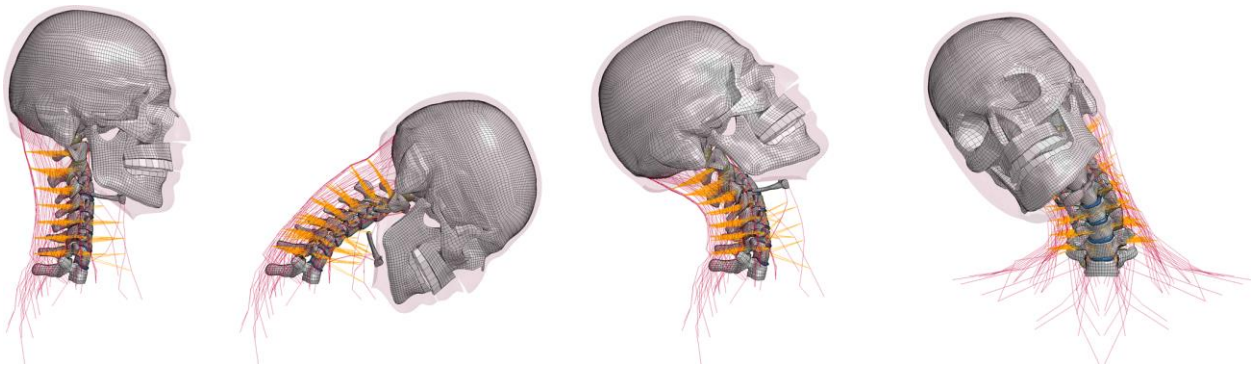

FIGURE 2-39: SUPPORT ELEMENT (ORANGE) CONNECTION TO 1-D ACTIVE MUSCLES (RED) (3-D PASSIVE MUSCLES REMOVED FOR CLARITY)

2.6.5 Scaling Factors between Male and Female

The F05 was developed after the development of the M50 HBM utilizing the same methodology. Apart from the subject-specific geometric difference from stature and gender, much of the same material properties from the M50 was used to represent the F05 HBM. Scaling was necessary to define certain material response and material parameters due to limited data for a female that exist in the current literature. Neck regional level anthropometric scaling factors were used to scale the ligament response and PCSA of the M50 HBM to represent the F05 HBM (Singh and Cronin 2017).

TABLE 2-12: NECK REGIONAL LEVEL SCALING FACTORS *(Shams et al., 2003)*

Neck Regional Level	Scale Factors
λ_x	0.81
λ_y	0.81
λ_z	0.87
λ_F (force)	0.6561
λ_d (displacement)	0.87

TABLE 2-13: EXTERIOR NECK DIMENSIONS FOR THE GHBMC 50TH PERCENTILE MALE AND 5TH PERCENTILE FEMALE HBM *(Singh and Cronin, 2017)*

Dimensions (cm)	50th Percentile Male	5th Percentile Female
Neck Length	8.98	8.75
Neck Depth mid	13.93	10.48
Neck Breadth mid	11.68	11.68
Neck Circumference mid	41.85	35.94

The ligament force-displacement response curves and failure response were scaled with respect to the factors. The muscle PCSA for the F05 model was also scaled down from the M50 model using the force-scaling factor to take into account area.

CHAPTER 3: METHODS

The objective of this study was to assess the kinematic and tissue-level response to impacts using detailed HBMs by subjecting the GHBMC 50th percentile male and GHBMC 5th percentile female HBMs to whiplash perturbations. An analysis of each loading case was first performed, utilizing the HBMs with the default parameters, that were used to establish a baseline to which other cases could be benchmarked. Next, different muscle activation strategies were investigated to observe the changes in both kinematics and tissue level responses. Lastly, an investigation on gender effects on the kinematics, tissue level response and effect of active musculature was compared between the male and female HBMs.

Two previously developed and validated finite element models from the GHBMC were used to simulate response to impact and assess the potential for injury risk: average stature male (M50 v4-5, GHBMC, Elemance, USA) and small stature female (F05 v3-1, GHBMC, Elemance, USA), representing a 50th percentile male and 5th percentile female respectively. Analysis of both models was performed using a commercial explicit finite element solver (LSTC, LS-DYNA, version R7.1.2).

Whiplash associated disorders have been primarily associated with rear impacts, but epidemiological data have suggested that acute soft tissue injury can also occur during frontal and side impacts. Therefore, three boundary conditions (frontal, rear, lateral) were identified for analysis to represent the three common modalities of neck loading during a whiplash event: flexion, extension, and lateral bending with coupled axial rotation. Analysis of the male occupant HBM was completed first to establish the methodology before analysis was performed on the female occupant HBM.

In summary, the study plan would consist of applying different muscle activation strategies to the 50th percentile male and 5th percentile female HBMs for frontal, rear, and lateral impact loading. Head kinematics and the assessment for the potential of soft tissue injury were compared between impact directions and gender (Figure 3-1). A detailed test matrix will be presented later in the chapter (Table 3-7).

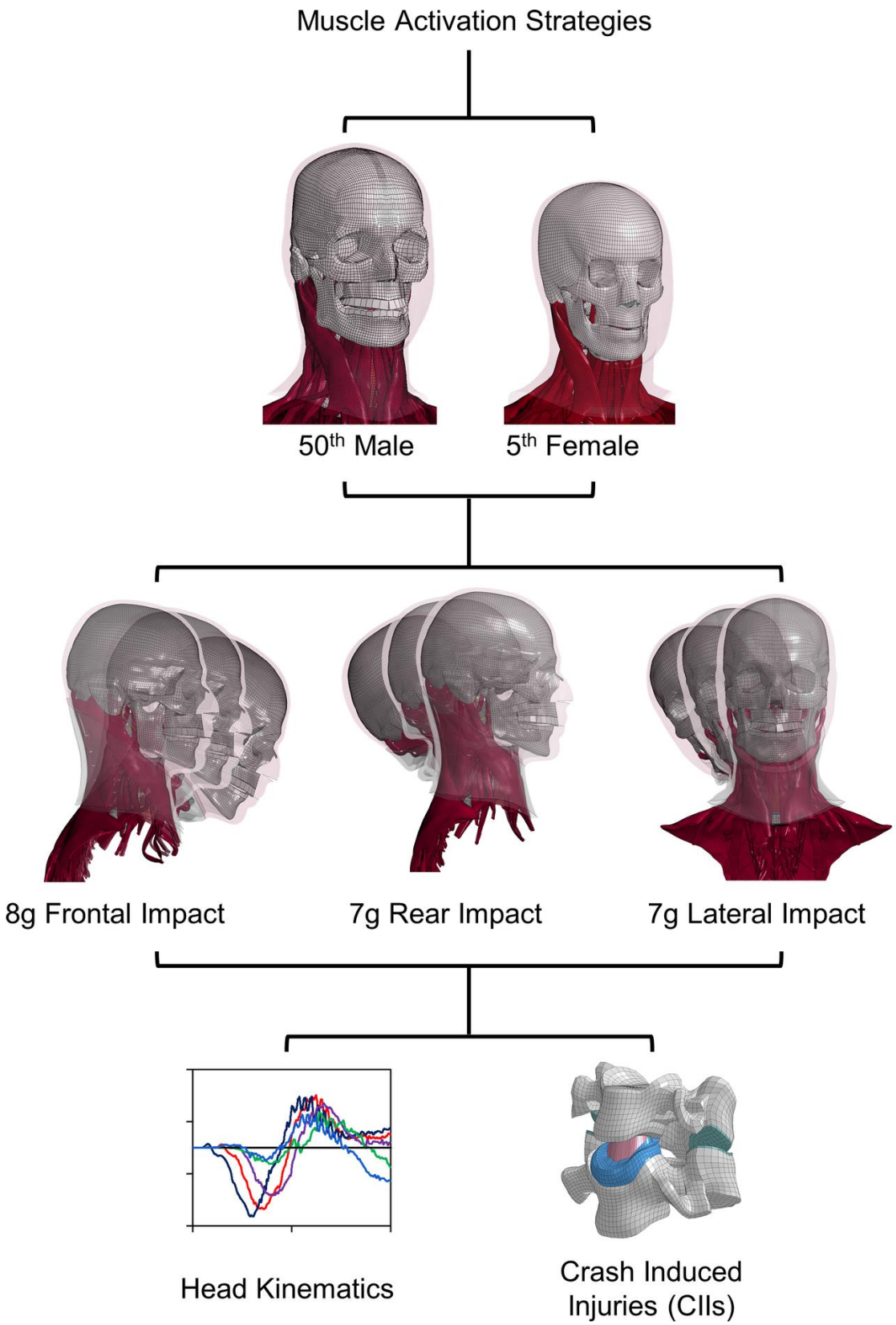

FIGURE 3-1: OVERVIEW OF MODEL BOUNDARY CONDITIONS AND LOAD CASES

3.1 FE Model Boundary Conditions for Impact Scenarios

To reproduce vehicle impact scenarios on the neck model, motion boundary conditions were prescribed to the T1 vertebra to simulate inertial loading to the head and neck complex (Figure 3-2). The sled/crash pulse could not be used directly for the T1 input due to the sequence of the events during a crash, where the seat begins to move first, followed by the T1 and finally the head (Figure 3-3). Instead, experimental data that reported T1 kinematics in addition to sled pulse and head kinematics were used. The boundary condition was applied to the T1 vertebra, which accelerated the model from a standstill to simulate a frontal, rear and lateral impact. Previous studies utilized the same methodology of applying boundary conditions to the T1 to investigate the response of the neck (Panzer et al., 2011; Fice et al., 2011; Cronin, 2014; Östh et al., 2017).

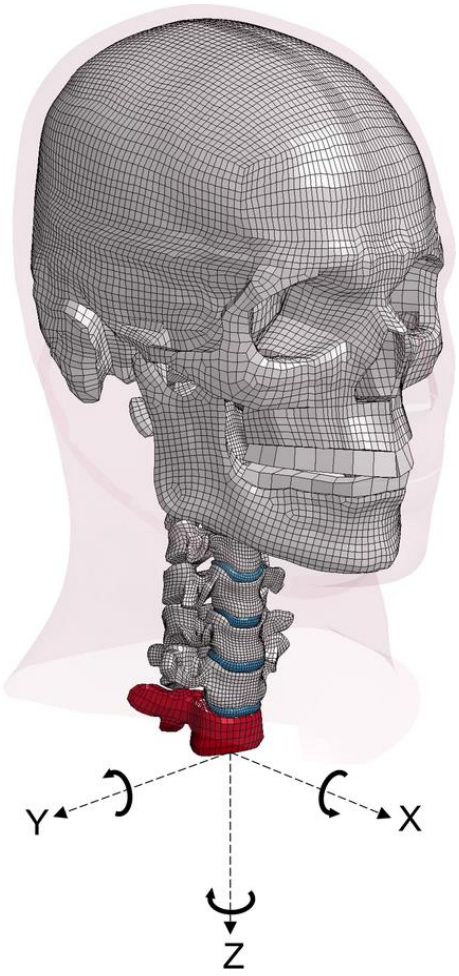

FIGURE 3-2: COORDINATE SYSTEM OF MODEL, T1 HIGHLIGHTED IN RED

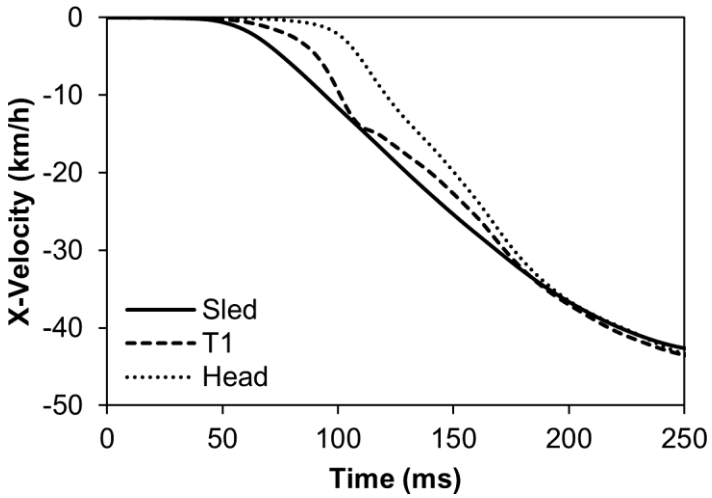

FIGURE 3-3: EXEMPLAR SEQUENCE OF EVENTS FOR AN 8G FRONTAL IMPACT (X-VELOCITY): SLED, T1 VERTEBRA AND HEAD

3.1.1 8g Frontal Impact Boundary Condition

The reported T1 kinematics from frontal impact (8g maximum acceleration, NBLD) volunteer tests (Thunnissen et al., 1995) were used as boundary conditions for the frontal impact analysis. The boundary condition inputs were selected based on multiple tests of similar maximum sled acceleration pulse of approximately 8g (Table 3-1) and had an average maximum sled velocity of 44.7 km/h. The T1 kinematics from each test was used to create an average response curve that was used as the prescribed boundary condition.

TABLE 3-1: NBDL FRONTAL IMPACT TESTS

Test No.	Max Sled G's
1587	8.1
1588	8.2
1590	8.2
1592	8.2
1593	8.2
1594	8.3
1595	8.2
1596	8.3
1597	7.9
1649	8.1

The T1 was constrained from movement in the Y-axis and Z-axis, and rotation about the X-axis and Z-axis. The T1 boundary condition included a horizontal and a sagittal rotation component. A velocity pulse was applied to the T1 in the posterior (–X direction) along with a rotational velocity about the –Y-axis to simulate the frontal impact (Figure 3-4). The total simulation time was 250 ms.

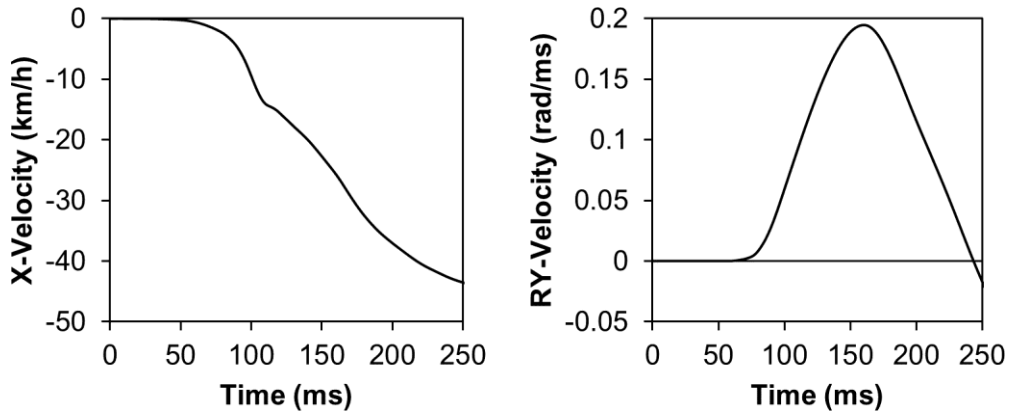

FIGURE 3-4: T1 INPUT BOUNDARY CONDITION FOR THE 8G FRONTAL IMPACT CONDITION

3.1.2 7g Rear Impact Boundary Condition

The rear impact (7g max acceleration) boundary conditions from a set of PMHS test data (Deng, 1999) were used to perform the rear impact analysis, following the methodology of Fice et al., (2011). In addition, the kinematics of the T1 and head center of gravity were reported. Medium severity impacts (~7g maximum acceleration) were considered, to apply sufficient loading in the neck to observe acute soft tissue injury. This set of PHMS data were used because lower acceleration pulses such as those used in human volunteer testing would not be severe enough to generate soft tissue injury. Conversely, PHMS tests with a higher severity acceleration pulse may cause catastrophic failure of the hard and soft tissues in the neck and therefore were not considered. The boundary condition inputs had a maximum sled acceleration pulse of approximately 7g and a peak velocity of 13 km/h.

The T1 was constrained from movement in the Y-axis, and rotation about the X-axis and Z-axis. The T1 boundary condition included a horizontal and vertical component in addition to the sagittal rotation component. An acceleration was applied in both the anterior (X direction) and superior (–Z direction), along with a rotational acceleration about the Y-axis to simulate the rear impact (Figure 3-5). The total simulation time was 235 ms.

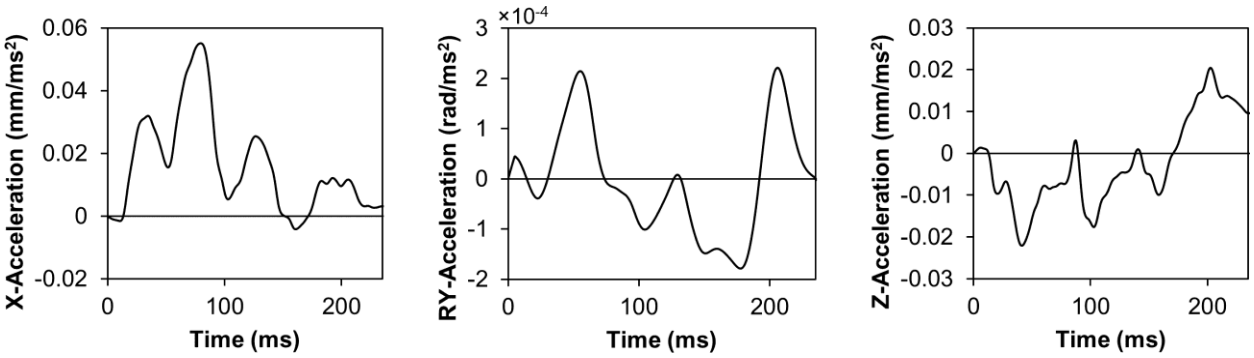

FIGURE 3-5: T1 INPUT BOUNDARY CONDITION FOR THE 7G REAR IMPACT CONDITION

3.1.3 7g Lateral Impact Boundary Condition

The lateral (7g maximum acceleration) pulses from the NBDL volunteer tests (Wisman et al., 1986) were used as boundary conditions for the lateral impact analysis. The kinematics of the sled, T1, and the head center of gravity was recorded in multiple axes for each test run to capture the complex motion during a lateral impact. The boundary condition inputs were also selected based on multiple tests of similar maximum sled acceleration pulse of approximately 7g (Table 3-2) and had an average maximum sled velocity of 23.2 km/h. The T1 kinematics from each test was used to create an average response curve and was used as the prescribed boundary condition.

TABLE 3-2: NBDL LATERAL IMPACT TESTS

Test No.	Max Sled G's
1451	7.0
1452	7.0
1453	7.0
1454	7.0
1474	7.2
1475	7.0
1478	7.2
1699	7.2
1700	7.2
1701	7.2
1702	7.1
1703	7.1
1705	7.1
1706	7.2
1707	7.2
1708	7.0
1709	7.1
1722	7.1

The T1 was constrained from movement in the Y-axis and Z-axis, and rotation about the X-axis and Z-axis. The T1 boundary condition included a lateral and a frontal plane rotational component. A velocity pulse was applied to the T1 in the lateral (–Y direction) along with a rotational velocity about the X-axis to simulate the lateral impact (Figure 3-6). The total simulation time was 250 ms.

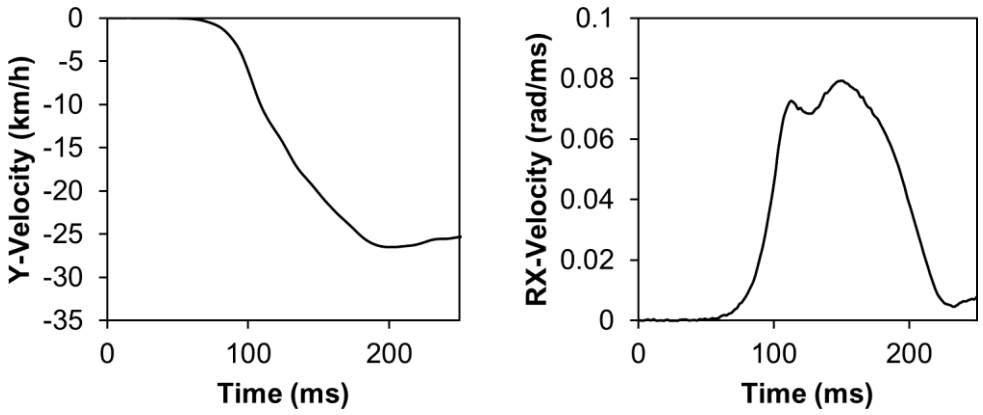

FIGURE 3-6: T1 INPUT BOUNDARY CONDITION FOR THE 7G LATERAL IMPACT CONDITION

3.2 Active Muscle Parameters

3.2.1 Default Parameters

The neck model for both the 50th percentile male and 5th percentile female contained 27 pairs of muscles. The active behaviour of the musculature was modelled with Hill-Type one-dimensional beam elements, while the passive behaviour of the musculature was modelled using three-dimensional viscoelastic elements. The force generated by the phenomenological Hill-Type muscle model is dependent on the peak isometric stress of the muscle, muscle PCSA, force-velocity response, force-length response, and the activation dynamics. For the purpose of this thesis, the effects of activation dynamics of the muscle and the muscle PCSA on head kinematics and potential for injury were investigated.

The activation dynamics of the Hill-Type muscle elements in the model are described by an activation curve based on active state dynamics and neural excitation (Happee et al., 1994, Panzer et al., 2011). The activation curve is a normalized mathematical representation of the muscle activation state (0= not activated, 1= fully activated) that is described with respect to time. The default curve can be decomposed into three time-sequenced regions: activation delay, activation phase, and deactivation phase (Figure 3-7).

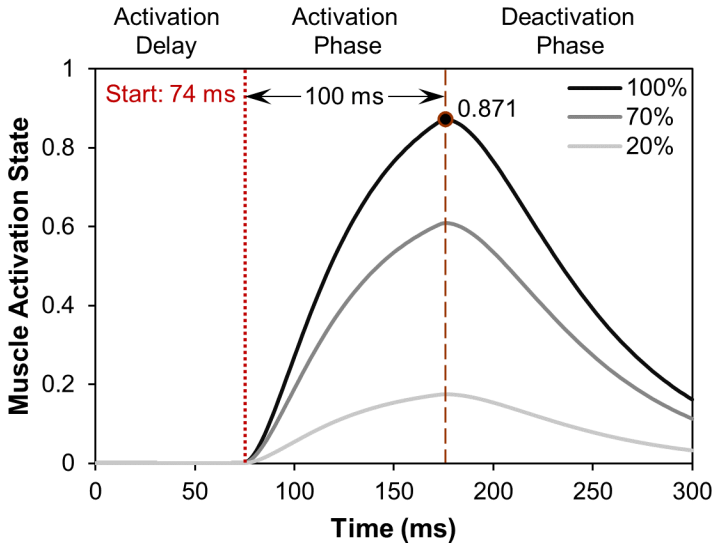

FIGURE 3-7: MUSCLE ACTIVATION CURVE (STARTLE RESPONSE) | DEMONSTRATING ACTIVATION SCALING (100%, 70%, 20%) AND THREE REGIONS (ACTIVATION DELAY, ACTIVATION PHASE, AND DEACTIVATION PHASE)

The first region represents the activation delay, which results from the muscle activation onset time for a startle reflex (delay in time between sensory inputs from external stimuli and muscle activation). The second region accounts for the dynamic bio molecular mechanisms of muscle activation, where the muscle reaches a state of peak activation. The third region represents the deactivation phase, where the muscle transitions from a state of maximum activation to a state of no activation. Different levels of the muscle activation state can be achieved by scaling the magnitude of the activation curve, where the maximum value (100% activation) is defined at 0.871. In addition, the phase of the activation curve can be shifted forward or backward in time to reflect different reflex delays.

The PCSA is an effective area that is directly proportional to the maximum force a single muscle can generate (Table 2-11). Individual neck muscles in HBMs have defined PCSA values from the literature (Knaub et al., 1998).

The muscles in the HBM are divided into two groups: flexors, containing all anterior cervical muscles, and extensors, containing all posterior cervical muscles. The flexor and extensor groups were identified as a limitation of the model when investigating lateral impact conditions because independent activation of left and right muscle groups was not possible, and was addressed in section 3.2.2 below. The baseline muscle activation is operated under the assumption that all muscles are activated synergistically, but the flexors and extensors groups can be activated at different levels by scaling the activation curve (Panzer et al., 2011; Fice et al., 2012). In the baseline model, the activation onset time and PCSA do not change, while

the activation level for flexors and extensors groups are scaled to different ratios to simulate a startle response for different impact directions (Table 3-3).

TABLE 3-3: BASELINE MUSCLE ACTIVATION SCHEMES *(Panzer et al., 2011; Fice et al., 2011)*

Impact Direction	Activation Onset	Flexor Activation	Extensor Activation	PCSA
Frontal	74 ms	100%	100%	default
Lateral	74 ms	100%	100%	default
Rear	74 ms	100%	70%	default

To investigate the effects of active musculature on injury prediction, three areas of focus were identified: muscle activation scheme, cervical muscle activation onset time, and muscle PCSA. These parameters were recognized as major contributors to the global and local kinematic of the head and neck in addition to the tissue-level response. A literature review of neck muscle PCSA and activation onset time was first conducted to understand the range of values that are viable to use in the muscle model. Next, due to the wide spectrum of available data found in the literature, an upper and lower bound value for both parameters were identified. A combination of these three parameters was used to create activation schemes to investigate the influence of neck muscle activation on head kinematics and tissue level response during dynamic neck loading.

3.2.2 Quadrant Activation Implementation

The default activation strategy in the neck models contained two groups of muscles: extensors and flexors and assumed each group activated synergistically with bilateral symmetry. A quadrant-based activation strategy (four groups of muscles) was proposed to allow independent unilateral activation of flexors and extensors muscles (Figure 3-8), which was identified as a need for lateral impact and omni-directional loading. The implementation involved a separate definition for the left and right cervical muscle in addition to flexors and extensors. The quadrant strategy could be used for future studies such as frontal, rear, and lateral oblique impacts or parametric studies for an optimized model response to match volunteer kinematic corridors.

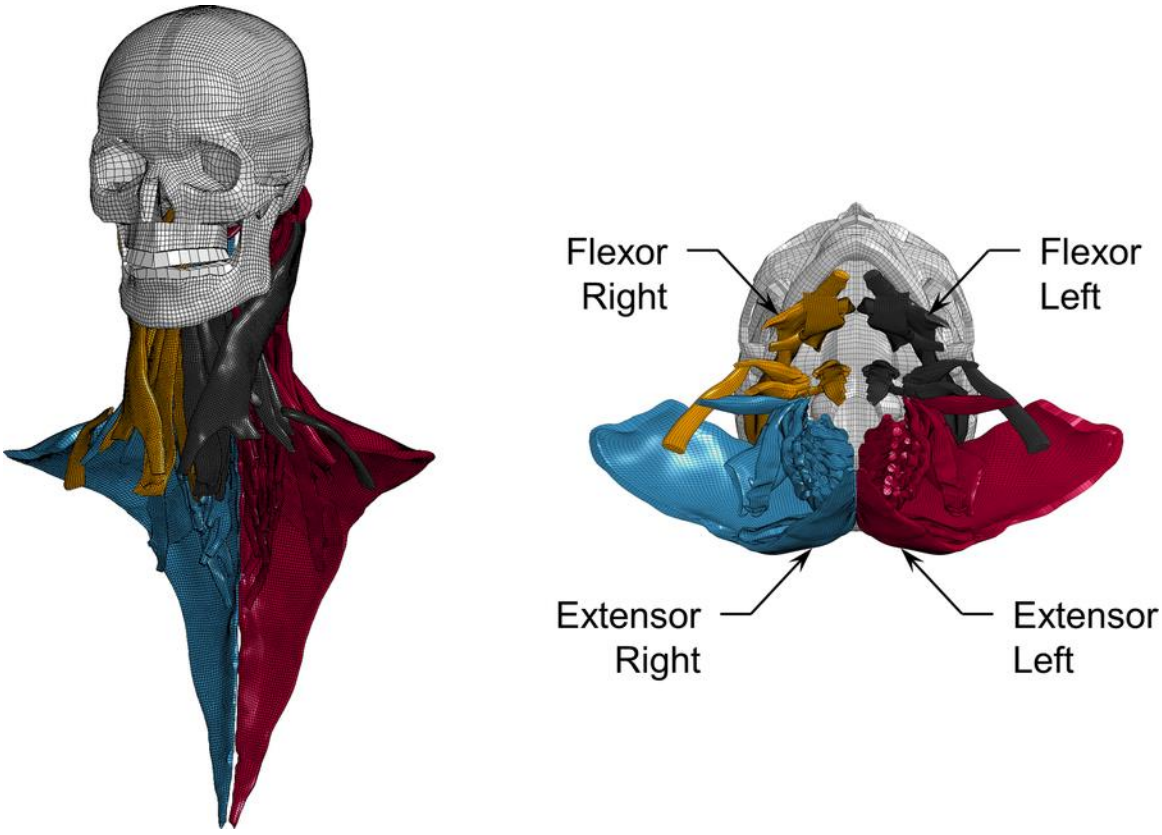

FIGURE 3-8: VISUAL REPRESENTATION OF THE QUADRANT MUSCLE GROUPS

3.2.3 Neutral Position Activation Strategy

Panzer et al., (2011) and Fice et al., (2011) previously developed the baseline activation strategy for frontal (extensor: 100%, flexor: 100%) and rear impacts (extensors: 100%, flexor: 70%) using normalized EMG data from volunteers (Siegmund et al., 2003). This activation strategy was designed to represent an unaware occupant undergoing involuntary reflex activation of their neck muscle. However, this baseline activation strategy resulted in the head undergoing considerable extension motion during activation. To address this issue, a new activation strategy was developed based on the human startle reflex response to minimize head motion during startle activation.

When the neck muscles were activated in absence of any T1 motion boundary conditions, the compressive forces generated in the cervical column rotated the head posteriorly into extension, which indicated an extensor bias. This resulted in 31 degrees of extension, and 64.9 mm posterior translation of the head for baseline frontal and lateral activation strategy and 23 degrees of extension and 50 mm posterior translation of the head for the rear activation strategy. Physiologically, humans have more posterior muscles than anterior muscles in the neck, allowing greater force generation for extension motion. Muscle force

generation is proportional to the PCSAs in the neck, with the current model having a distribution of 70% extensors and 30% flexors. Several experimental studies have identified that the maximum force and moment generation capability of cervical extensors is greater than that of flexor muscles (Vasavada et al., 2001; Lavallee et al., 2013; Fice et al., 2014).

The human startle response is an involuntary reflex that can occur when a sudden and/or intense, acoustic, visual or tactile stimuli is elicited onto an individual., This protective reflex evokes a rapid motor response to the body and is primarily a flexion response, to tense and position the body into the "ready position", in anticipation for a fight or flight event. (Koch, 1998; Yeomans et al., 2002). To address this issue, a new activation scheme was developed based on the human startle response.

A parametric study was conducted on both the 50th percentile male and 5th percentile female HBM to find an activation scheme that reduced global head rotation with the goal of minimized head movement to mimic an in-vivo startle response. To perform the parametric study, the flexors were also maintained at 100% activation while the extensor activation was varied (Figure 3-9).

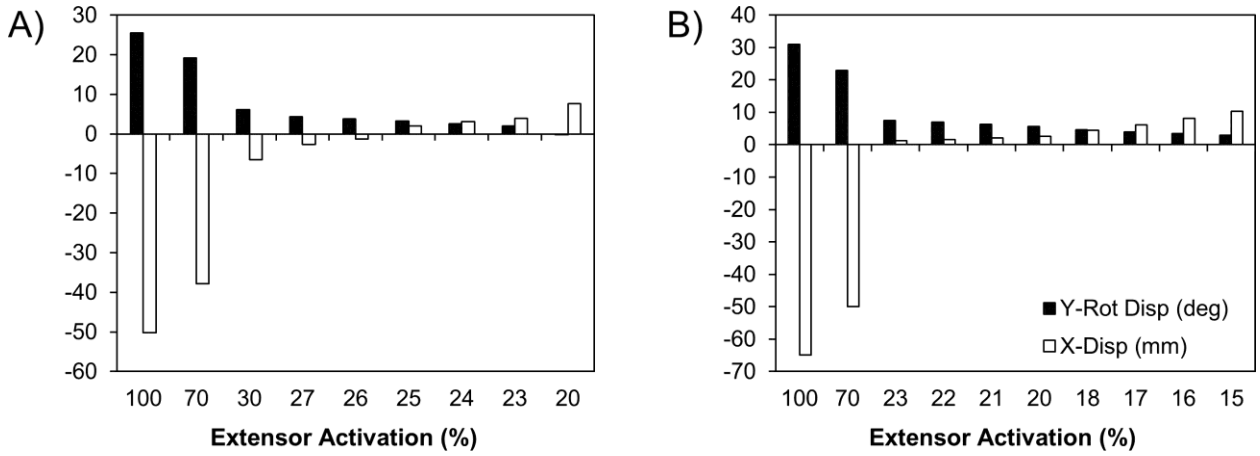

FIGURE 3-9: A) 50TH PERCENTILE MALE, B) 5TH PERCENTILE FEMALE | RESULTS FROM PARAMETRIC STUDY, POSITIVE ROTATION IS EXTENSION, POSITIVE TRANSLATION IS ANTERIOR DISPLACEMENT

The optimization target to minimize head movement and maintain a neutral head posture, resulted in an activation ratio for extensors and flexors of approximately 1:5 (extensors: 20%, flexors: 100%) for the 50th percentile male and 1:4 (extensors: 25%, flexors: 100%) for the 5th percentile female. For the 50th percentile male, the neutral activation strategy reduced the head CG Y-rotation extension angle to 5.7 degrees, and X-translation to 2.6 mm. The 5th percentile female with the optimized activation ratio reduced the head CG Y-rotation angle to 3.2 degrees, and X-translation to 2 mm (**FIGURE** 3-10). The neutral

activation strategy with the default activation onset time and PCSA was evaluated with both the M50 and F05 HBM to compare kinematics and injury response to the previously defined activation strategy.

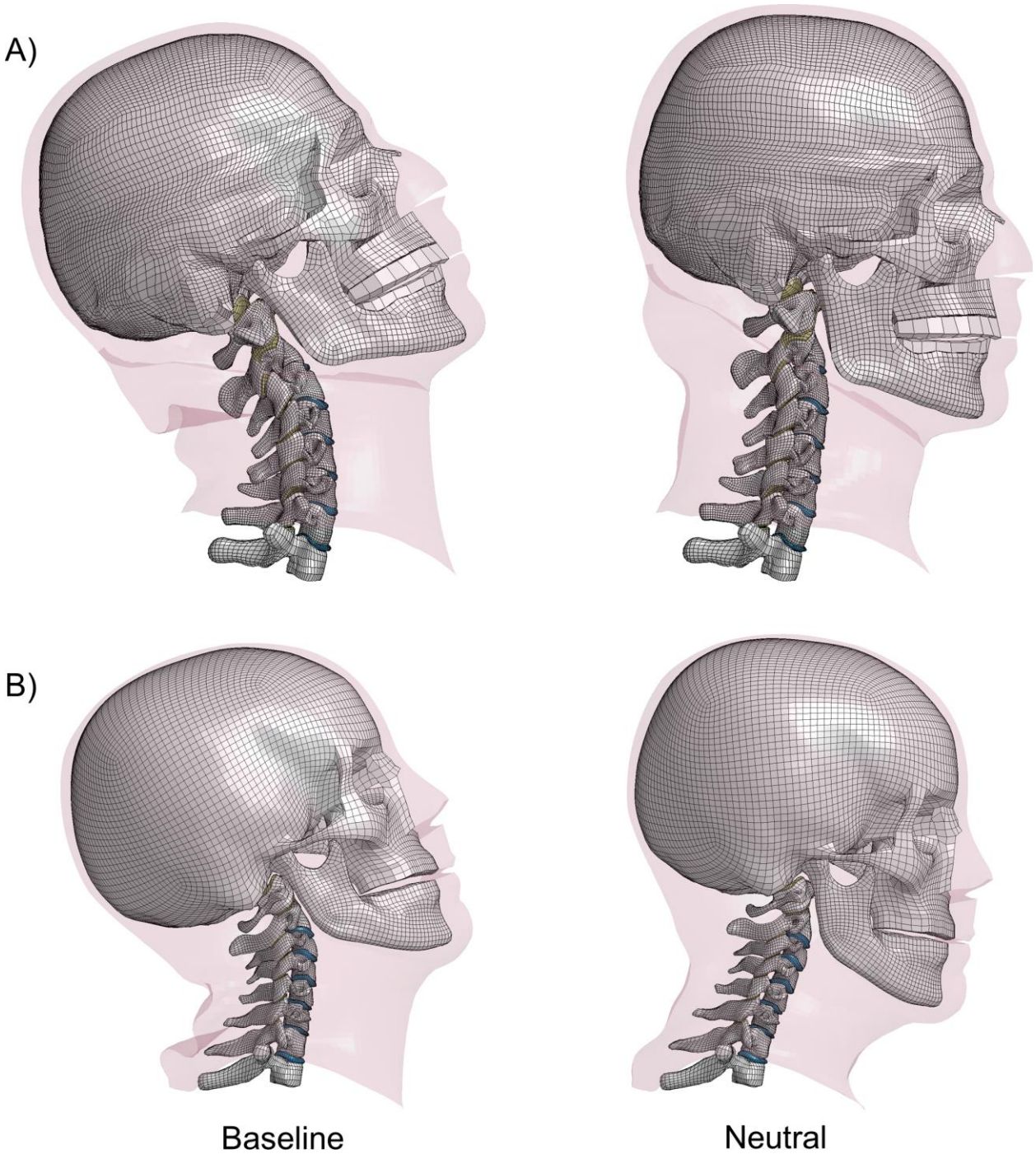

FIGURE 3-10: A) 50TH PERCENTILE MALE, B) 5TH PERCENTILE FEMALE, ILLUSTRATING BASELINE ACTIVATION AND NEUTRAL ACTIVATION

3.2.4 Lateral Impact Activation Sensitivity Study

The literature has reported that the muscle contralateral to the head movement undergoes eccentric contraction (i.e. lengthening) during a side impact while demonstrating increased activation (Kumar et al., 2004a, Kumar et al., 2004b). This was a preliminary study to identify strategies for lateral muscle activation. A parametric test was performed using both 50^{th} percentile male and 5^{th} percentile female models on the 7g lateral impact case to study the sensitivity of head kinematics and tissue level response due to flexor and extensor bilateral asymmetry. Flexors and extensors contralateral to the direction of head movement were maintained at 100% activation while the flexors and extensors ipsilateral to the direction of impact was decreased from 100% to 25% in 25% decrements (Table 3-4). The initial activation strategy used for this study was based on the neutral strategy, where the extensor to flexor activation ratio was kept constant at 1:5 for the M50 and 1:4 for the F05 model.

TABLE 3-4: 7G LATERAL QUADRANT SENSITIVITY STUDY PLAN

Case	Ipsilateral Activation (%)	Contralateral Activation (%)
1	100	100
2	75	100
3	50	100
4	25	100

3.2.5 Activation Onset Time

To determine an upper and lower range of activation onset times that are reported in the literature, an average value and standard deviation were calculated from the fastest onset time that was measured in the experiment, by either muscle group, velocity change, or acceleration. An average activation time of 78 ms with 15.8 ms standard deviation was calculated from 15 literature sources (Table 3-5). The average value of 78 ms was in good agreement with the default activation time of 74 ms in the GHBMC model. The standard deviation of 15.8 ms was approximately ±20% of the average time with a lower bound of 62.2 ms and upper bound of 93.8 ms. Therefore, an activation onset time of 60 ms and 90 ms was selected to represent the upper and lower bound to create the muscle activation strategies.

TABLE 3-5: SUMMARY OF NECK MUSCLE ACTIVATION ONSET TIME (STARTLE / UNAWARE ONLY)

Literature	Muscle	Onset Time (ms)	Perturbation Type
Foust et al., 1973	Neck Flexors	64.9	Rear head jerk
Snyder et al., 1975	Neck Extensors	66.0	Frontal head jerk
Szabo and Welcher, 1996	Sternocleidomastoid	110.0	Rear impact
Ono et al., 1997	Sternocleidomastoid	79.0	Rear impact
Magnusson et al., 1999	Sternocleidomastoid	72.2	Rear impact
Brault et al., 2000	Sternocleidomastoid	81.0	Rear impact
Wittek et al., 2001	Sternocleidomastoid	79.0	Rear impact
Siegmund et al., 2001	Sternocleidomastoid	52.0	Acoustic startle
Siegmund et al., 2003	Sternocleidomastoid	72.0	Rear impact
Kumar et al., 2002	Sternocleidomastoid	83.3	Rear impact
Blouin et al., 2003	Sternocleidomastoid	55.0	Rear impact
Kumar et al., 2003	Trapezius	82.9	Frontal impact
Kumar et al., 2004a	Splenius Capitis L	76.7	Right Lateral impact
Kumar et al., 2004b	Splenius Capitis R	97.5	Left Lateral impact
Hernandez et al., 2005	Sternocleidomastoid	99.1	Rear impact
Average (sd)		**78 (15.8)**	

3.2.6 Muscle PCSA

Knaub et al., (1998) observed that the muscle volumes in the neck of 50th percentile male volunteers were on average 64% greater than volumes obtained from cadaveric dissections, with differences as large as 128%. Furthermore, it was found that the 95th percentile male subject had on average 72% greater muscle volume when compared to the 50th percentile male subject, while the 5th percentile female subjects had muscle volumes that were on average 77% smaller than the 50th percentile male subjects. The mathematical formula to calculate PCSA is presented below:

$$PCSA = \frac{Muscle\ Volume * \cos(\ Pennation\ angle\ (\theta))}{Fiber\ length}$$

Since the fibre length and pennation angles used to calculate the respective PCSAs were reported as average values from all cadaver subjects, with the assumption that the fibre length and pennation angle is representative of in vivo humans, an increase or decrease to muscle volume is directly proportional to the resultant PCSA.

The upper and lower bound values for the PCSA that were used to create the muscle activation strategies were based on the muscle volume quantitative data presented by Knaub et al., (1998). The upper and lower boundaries of ±30% of the baseline PCSA in the GHBMC model was selected to be a reasonable

representation for 50th percentile male subjects that does not exceed the 95th percentile male or underscore the muscle volumes of the 5th percentile female subjects. Only the PCSA of the active muscles elements were scaled, while the volume of the 3-D passive tissues remained unchanged. Although scaling all the cervical musculature by the same percentage may not be physiological, this was a first estimation to study the effects of muscle forces on dynamic neck response.

3.3 Active Muscle Study Plan

3.3.1 Muscle Activation Schemes

Activation schemes were formed by a combination of the activation strategy, muscle activation onset time and muscle PCSA. Activation strategy refers to the grouping of the muscles in the neck (e.g. baseline scheme: 2 groups – extensors, flexors), and activation ratio (e.g. 100% flexor and 100% extensor activation) (Table 3-6). The first activation scheme was the baseline configuration of the model with the baseline active muscle parameters and baseline muscle activation strategy. The second scheme was the upper bound configuration and utilized the neutral activation strategy with a combination of the lower bound onset time and upper bound PCSA. The third scheme was the neutral configuration and utilized the neutral activation scheme with the baseline activation onset time and baseline muscle PCSA. The fourth scheme was the lower bound configuration and utilized the neutral activation scheme with a combination of the upper bound onset time and lower bound muscle PCSA. The fifth scheme was the activation off scheme with the active muscles turned off (i.e. passive muscles only). The baseline and activation off scheme was important because they establish a baseline configuration of the model, as well as a boundary where no muscle activation was present; with the latter representing a cadaveric response. The neutral activation scheme was important to evaluate the effect of the neutral activation strategy based on a startle response. The upper bound and lower bound activation schemes defined a state of high and low activation to represent the range of muscle activation effectiveness in the HBMs.

TABLE 3-6: SUMMARY OF ACTIVATION SCHEMES

Scheme	Strategy	Onset Time	PCSA
1. Baseline	Baseline	74 ms	Baseline
2. Upper Bound	Neutral	60 ms	Upper (+30%)
3. Neutral	Neutral	74 ms	Baseline
4. Lower Bound	Neutral	90 ms	Lower (-30%)
5. Activation Off	-	-	-

3.3.2 Simulation Matrix for Impact Studies

The proposed activation schemes will be applied to the HBM muscle model for each impact case (8g frontal, 7g rear, and 7g lateral). In addition, the quadrant sensitivity study will be applied to the HBM only for the 7g lateral impact condition (Table 3-4). The study will be conducted on both the 50th percentile male and 5th percentile female HBM for a total of 38 simulation runs (Table 3-7).

TABLE 3-7: TEST MATRIX FOR 50TH PERCENTILE MALE AND 5TH PERCENTILE FEMALE HBMS

	Scheme	Onset Time (ms)			PCSA			Activation Strategy			
		60	74	90	-30%	±0%	+30%	Off	Baseline	Neutral	Quad
8g FRT	**1**		✓			✓			✓		
	2			✓	✓					✓	
	3		✓			✓				✓	
	4	✓					✓			✓	
	5		-			-		✓			
7g REAR	**1**		✓			✓			✓		
	2			✓	✓					✓	
	3		✓			✓				✓	
	4	✓					✓			✓	
	5		-			-		✓			
7g LAT	**1**		✓			✓			✓		
	2			✓	✓					✓	
	3		✓			✓				✓	
	4	✓					✓			✓	
	5		-			-		✓			
	Quad (x4)		✓			✓				✓	✓

3.4 Head Kinematics

Head kinematics were used as metrics to compare the effect of the different activation schemes and were evaluated at the head center of gravity following the SAE coordinate system (Figure 3-11). The kinematic responses from the model were compared to corridors created from the volunteer and cadaver experiments that were used as the input boundary condition to evaluate the neutral activation scheme. The

head kinematics included X-acceleration (AX), Y-acceleration (AY), Z-acceleration (AZ), X-rotational acceleration (RAX), Y-rotational acceleration (RAY), Z-rotational acceleration (RAZ), X-rotational displacement (RDX), Y-rotational displacement (RDY), and Z-rotational displacement (RDZ) (Table 3-8). For the frontal and rear impact scenarios, AX, AZ, RAY, and RDY were the primary metrics used to compare head kinematics. For impacts where the head does not remain in the sagittal plane such as the lateral impact scenario, AX, AY, AZ, RAX, RAY, RAZ, RDX, and RDY were used to compare the head kinematics. All accelerations were filtered with an SAE 180 Hz filter. To evaluate the differences in the muscle activation schemes within an impact direction, the timing and magnitude of the key kinematics metrics will be evaluated and compared.

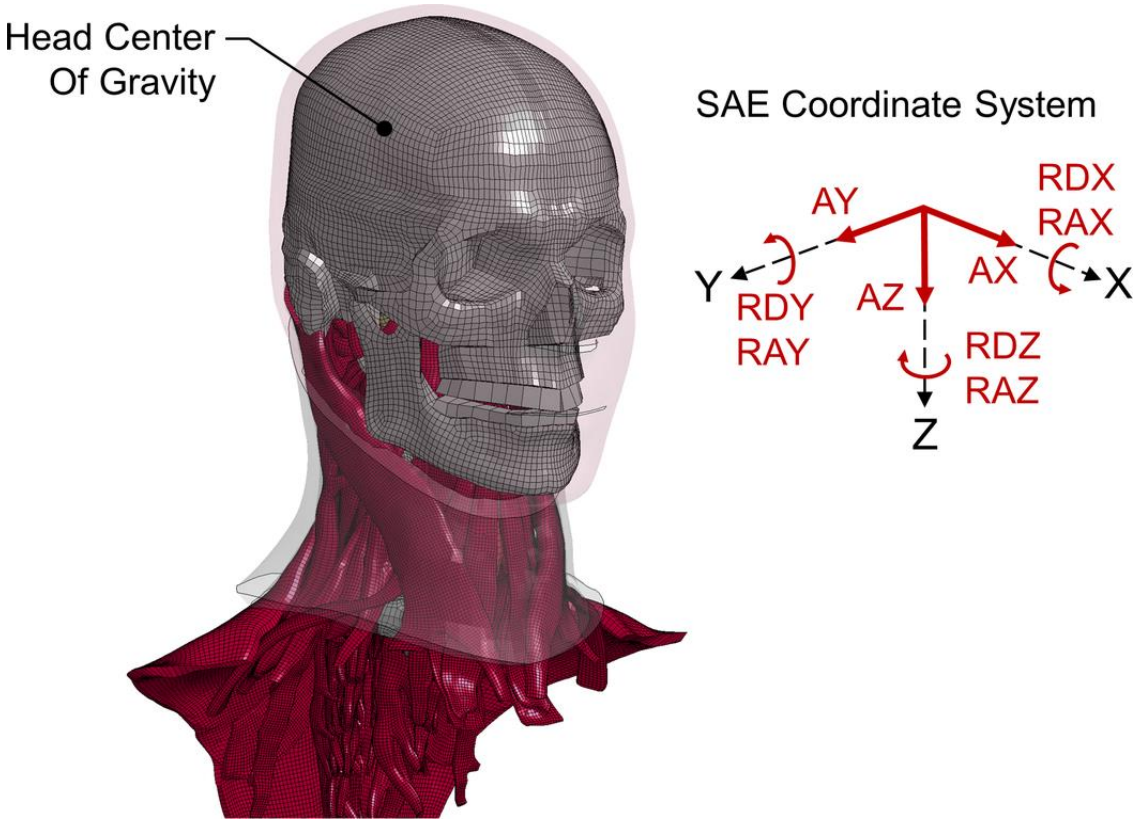

FIGURE 3-11: HEAD KINEMATICS COORDINATE SYSTEM

TABLE 3-8: HEAD KINEMATICS ABBREVIATION

Head CG Kinematics	X	Y	Z
Linear Acceleration	AX	AY	AZ
Rotational Acceleration	RAX	RAY	RAZ
Rotational Displacement	RDX	RDY	RDZ

3.5 Soft Tissue Injury Assessment in HBM

The tissues in the neck that are associated with soft tissue injury during MVC were assessed for the potential of injury risk. The tissues that were investigated included the lower cervical spine ligaments, transverse compression of the nerve roots, and disc avulsion. Spinal cord injuries were not considered due to the lack of a spinal cord model in the HBM. In addition, hard tissue failure was not expected for the range of impact severities and loading condition, therefore eliminating the risk of spinal cord injuries resulting from hard tissue interactions. Injury to the neck muscles was not quantified because the threshold for muscle injury from stretching or excessive activation is lacking in the literature. The potential for disc injury is assessed through the avulsion criterion that is implemented in the model. Disc annular failure was not investigated because the literature suggests that annular damage is less common than avulsion failures, in addition to a lack of data on annular fibres in the literature.

3.5.1 Ligament Distraction

Injury risk to the lower cervical spine ligaments was quantified by tracking the change in distance of origin and insertion points of the beam elements that represented the ligaments in the model (Figure 3-12).

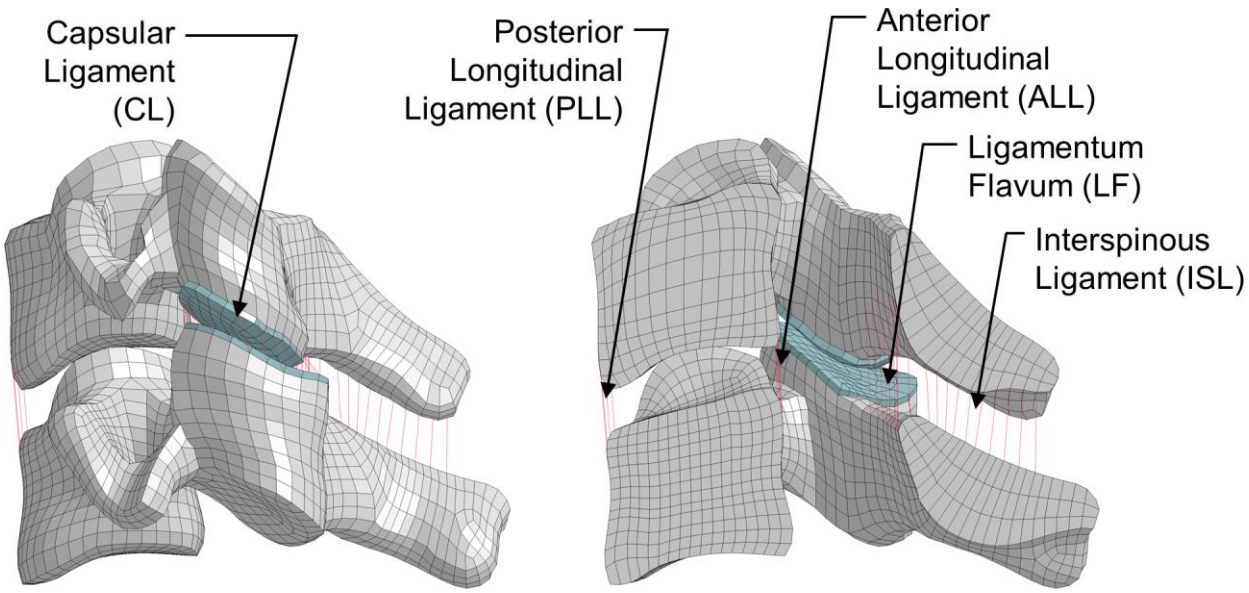

FIGURE 3-12: LOWER CERVICAL SPINE LIGAMENTS

Strains were calculated by dividing the ligament distraction value by the corresponding neutral lengths reported in the literature (Panjabi et al., 2004; Winkelstein et al., 2000).

$$Strain\ (\%) = \frac{\Delta L}{L_{neutral}} \times 100$$

This was necessary because the initial length of the ligament in the HBM was not modelled to be representative of the human body due to nodal and positioning constraints. Ligaments in the cervical spine are composed of different layers and insert over an area on the hard tissue. Therefore, it was important to utilize neutral lengths reported in the literature to compare the predicted ligament response with previous reported strains values. Each ligament had an implemented displacement-based failure criterion to predict ligament rupture during neck loading (Mattucci et al., 2012). Unfortunately, catastrophic failure of the ligament does not always occur during whiplash injury, but rather, the ligaments are distracted beyond the physiological range of motion, within the traumatic region. When ligaments are loaded to this region, small bundles of collagen fibres begin to stretch and fail and may induce pain, decrease ligament stiffness and introducing excess ligament laxity. Increased laxity and decreased stiffness may cause an increased range of motion in the neck and lead to cervical spine instabilities.

In order to predict the potential for injury, it was necessary to define the threshold for the different ligament response regions. Ligament data from Mattucci et al., (2012) was used to define a threshold for the linear region, traumatic region, post-traumatic region, and rupture (Figure 3-13). These values were used as metrics to quantify ligament distractions and relate them to the potential for injury during impact scenarios (Table 3-9, Table 3-10).

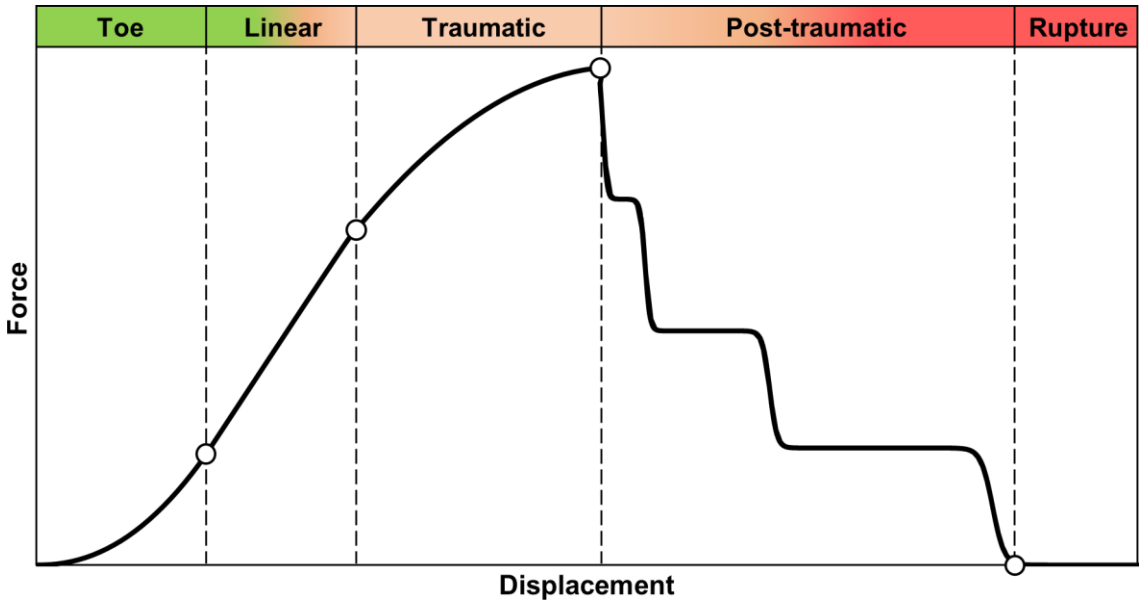

FIGURE 3-13: EXEMPLAR FORCE VS. DISPLACEMENT CURVE FOR A LIGAMENT, ILLUSTRATING THE DIFFERENT RESPONSE REGIONS

TABLE 3-9: M50 LIGAMENT DEFINITIONS (mm)

Ligament	Distance	C23	C34	C45	C56	C67
ALL	Failure length	3.9	3.9	3.4	3.4	4.4
	Subfailure length	2.7	2.7	2.4	2.4	3.0
	Linear length	1.5	1.5	1.4	1.4	1.8
	Neutral length	13.3	14.5	13.5	11.6	13.5
PLL	Failure length	3.2	3.2	2.7	2.7	2.7
	Subfailure length	1.8	1.8	1.5	1.5	1.5
	Linear length	1.1	1.1	0.8	0.8	1.0
	Neutral length	12.2	12.1	11.9	11.4	11.6
CL	Failure length	3.9	3.9	4.8	4.8	5.0
	Subfailure length	2.1	2.1	2.6	2.6	2.7
	Linear length	1.2	1.2	1.4	1.4	1.6
	Neutral length	5.3	5.3	5.3	5.3	5.3
LF	Failure length	4.4	4.4	5.4	5.4	7.3
	Subfailure length	3.7	3.7	4.5	4.5	6.2
	Linear length	2.9	2.9	3.4	3.4	5.8
	Neutral length	7.6	6.4	7.2	7.1	7.1
ISL	Failure length	6.1	6.1	6.6	6.6	7.3
	Subfailure length	3.8	3.8	4.1	4.1	4.6
	Linear length	2.6	2.6	2.3	2.3	3.8
	Neutral length	13.2	10.4	11.4	13.7	11.3

TABLE 3-10: F05 LIGAMENT DEFINITIONS (mm)

Ligament	Distance	C23	C34	C45	C56	C67
ALL	Failure length	3.4	3.4	3.0	3.0	3.8
	Subfailure length	2.4	2.4	2.1	2.1	2.6
	Linear length	1.3	1.3	1.2	1.2	1.6
	Neutral length	11.6	12.6	11.7	10.1	11.7
PLL	Failure length	2.8	2.8	2.3	2.3	2.3
	Subfailure length	1.5	1.5	1.3	1.3	1.3
	Linear length	1.0	1.0	0.7	0.7	0.9
	Neutral length	10.6	10.5	10.4	9.9	10.1
CL	Failure length	3.4	3.4	4.1	4.1	4.3
	Subfailure length	1.9	1.9	2.3	2.3	2.4
	Linear length	1.0	1.0	1.2	1.2	1.4
	Neutral length	4.6	4.6	4.6	4.6	4.6
LF	Failure length	3.8	3.8	4.7	4.7	6.4
	Subfailure length	3.2	3.2	3.9	3.9	5.4
	Linear length	2.5	2.5	3.0	3.0	5.0
	Neutral length	6.6	5.6	6.3	6.2	6.2
ISL	Failure length	5.3	5.3	5.7	5.7	7.3
	Subfailure length	3.3	3.3	3.6	3.6	4.6
	Linear length	2.3	2.3	2.0	2.0	3.8
	Neutral length	11.5	9.0	9.9	11.9	11.3

3.5.2 Transverse Nerve Root Complex Compression

To predict the potential for transverse compression of the nerve roots, the intervertebral foramen space (IVF) height and width reduction were tracked during impact, following the methodology of Panjabi et al., (2006) (Figure 3-14). The height was measured from the middle medial zone of the IVF between adjacent vertebrae, and width was measured from the anterior medial zone of the superior vertebra to the posterior medial zone of the inferior vertebra. A threshold value (Table 3-11) was calculated by subtracting the IVF neutral height and width of the HBMs from measured experimental width and height of the nerve root (Table 3-12) of the dorsal root ganglion and ventral root complex (Alleyne et al., 1998). These threshold values were then used to evaluate whether or not the nerve root were at risk of transverse compression during neck loading in different impact directions.

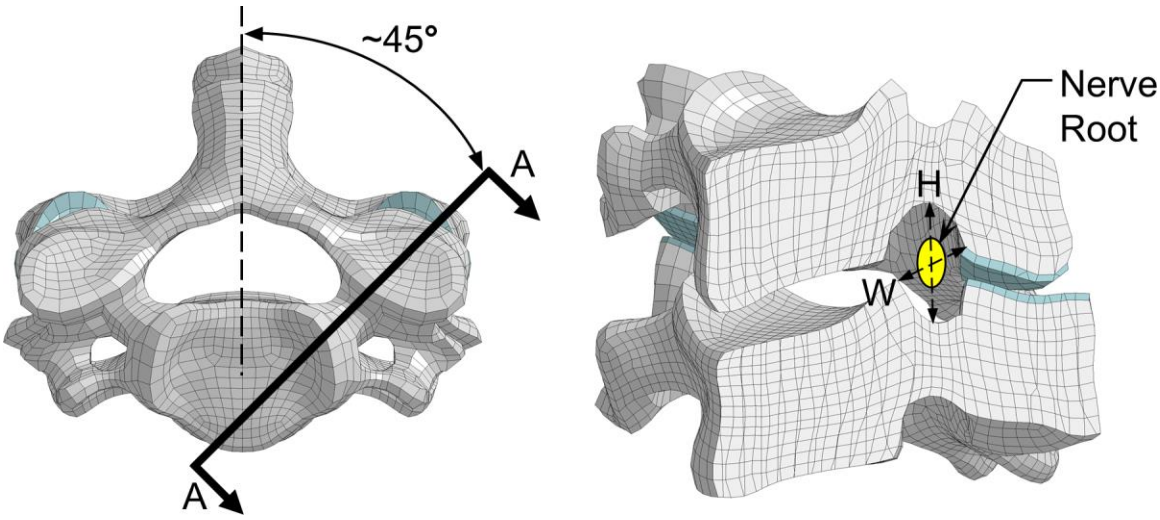

FIGURE 3-14: INTERVERTEBRAL FORAMEN SPACE HEIGHT AND WIDTH DEFINITION

TABLE 3-11: EXPERIMENTAL NERVE ROOT DIMENSIONS (mm)

Cervical Level	Root Height	Root Width
C23	5.3	3.8
C34	5.1	3.4
C45	5.8	3.8
C56	6.6	4.4
C67	7.3	5.7

TABLE 3-12: IVF HEIGHT AND WIDTH REDUCTION THRESHOLD (mm)

Cervical Level	Male Height	Male Width	Female Height	Female Width
C23	7.7	5.0	3.0	3.2
C34	5.3	5.0	2.3	4.1
C45	5.7	5.8	2.7	3.6
C56	4.8	4.3	2.2	3.5
C67	2.5	1.1	2.1	1.9

CHAPTER 4: RESULTS

4.1 Average Stature Male (M50) Neck Model Results

4.1.1 8g Frontal Impact Head Kinematics and Neck Tissue Response

In a frontal impact with the neutral activation scheme, the neck underwent shear deformation, corresponding to head x-translation (50 ms), followed by flexion (100 ms). The flexion response resulted in forward rotation of the head until the maximum flexion angle was reached (190 ms), before returning to the initial position (Figure 4-1).

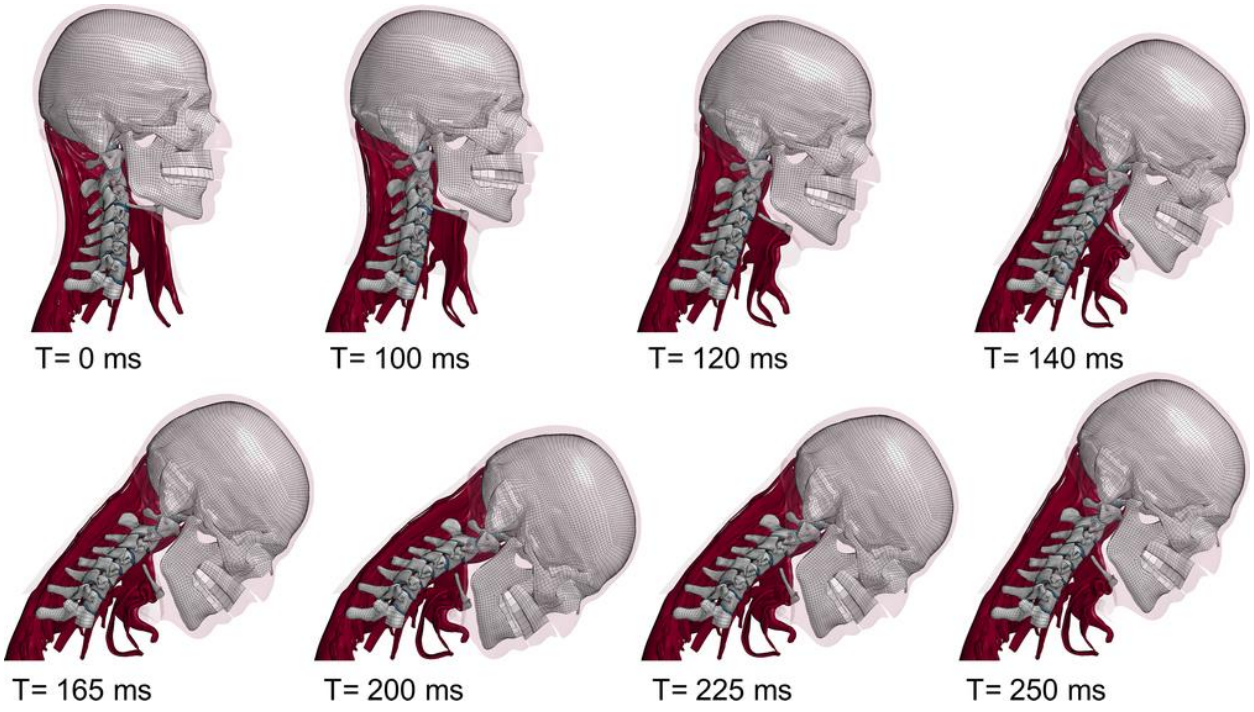

FIGURE 4-1: M50 8G FRONTAL IMPACT KINEMATIC SEQUENCE (NEUTRAL ACTIVATION SCHEME)

In a frontal impact, the head motion occurred within the sagittal plane and the primary head CG kinematic metrics were the X-acceleration Y-rotation flexion angle. When the head reached maximum flexion, the baseline activation scheme yielded 24.5˚, while the neutral and activation-off schemes yielded 64.6˚ and 78.6˚ respectively. The baseline activation scheme had a lower flexion response when compared to the average NBDL volunteer response corridors (68˚), and was outside the experimental response

corridor (Figure 4-2). The baseline activation scheme reached maximum flexion approximately 50 ms sooner when compared to the average volunteer response. The model with the neutral activation scheme resulted in a flexion response with a similar magnitude when compared to the volunteer response. In addition, the flexion response curve was within the experimental corridor during the flexion phase.

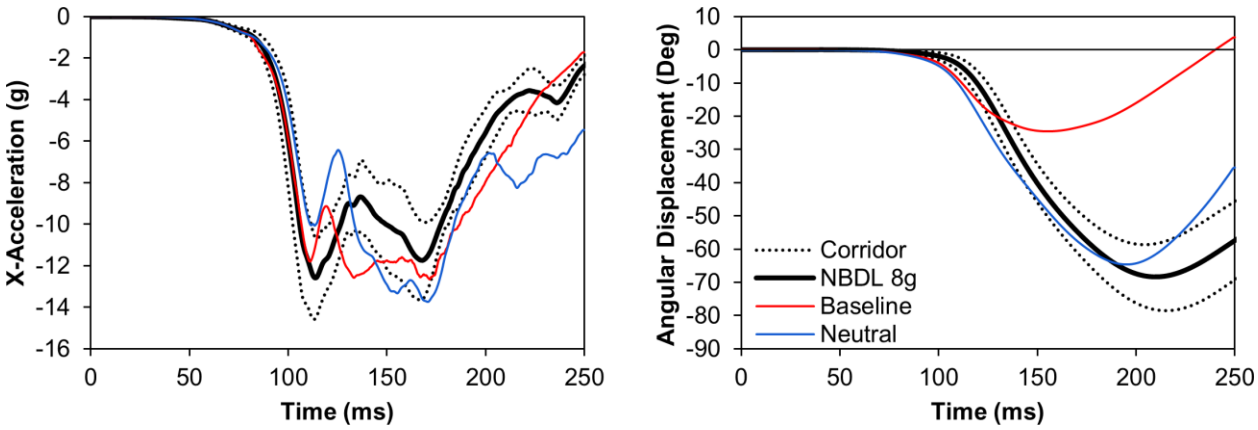

FIGURE 4-2: M50 8G FRONTAL IMPACT HEAD CG: X-ACCELERATION AND Y-ROTATION FLEXION ANGLE VS. NBDL CORRIDORS

When compared to the baseline activation scheme, the neutral activation scheme resulted in a maximum flexion angle increase of 163% while the activation-off scheme increased by 221% (Figure 4-3). The lower bound activation scheme yielded 71.7˚ (+11%), and upper bound 58.6˚ (-9%) when compared to the neutral activation scheme. Head x-acceleration generally occurred earlier with higher levels of muscle activation compared to the activation off scheme. Peak head rotation for the baseline activation scheme was reached at approximately 150 ms, while the other schemes occurred later at approximately 200 ms.

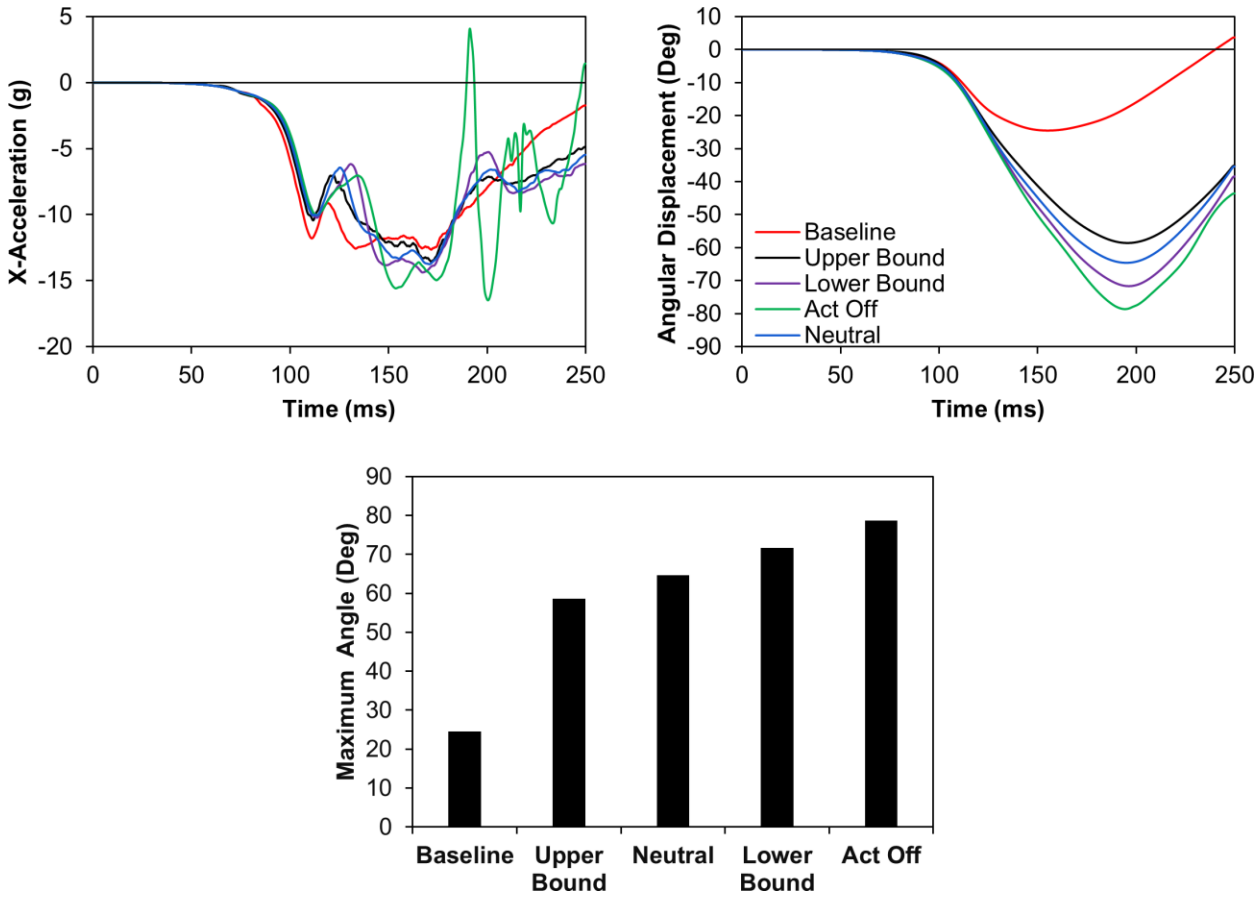

FIGURE 4-3: M50 8G FRONTAL IMPACT HEAD CG: X-ACCELERATION, Y-ROTATION FLEXION ANGLE, MAXIMUM Y-ROTATION ANGLE

During a frontal impact, the ligaments along the posterior aspect of the neck are responsible for limiting flexion and had the highest predicted injury risk based on ligament distraction (Figure 4-4). The CL and ISL are the ligaments with the greatest predicted injury risk for a frontal impact. In general, tissue strains increased with decreased muscle activation levels. Strains increased from the upper levels (C23) towards the lower levels (C67) for all ligaments except the CL, which peaked at the mid-cervical spine level (C45). None of the ligaments was fully ruptured from the 8g frontal impact (Figure 4-6).

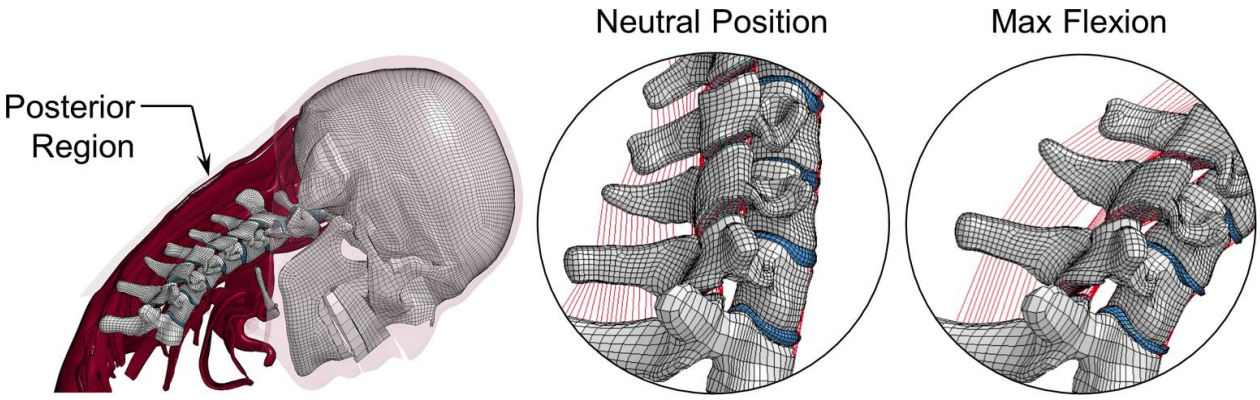

FIGURE 4-4: POSTERIOR LIGAMENTS LOADED IN TENSION

The CL did not enter the post-traumatic region regardless of the activation strategy (Figure 4-5). The C45 level had the largest CL strains, with all activation schemes within the traumatic region except the baseline activation scheme. The CL demonstrated strains in the traumatic region for the neutral and lower level activation schemes at the C56 level. The neutral activation scheme prevented the ligament distraction from exceeding the linear region at the C34 level.

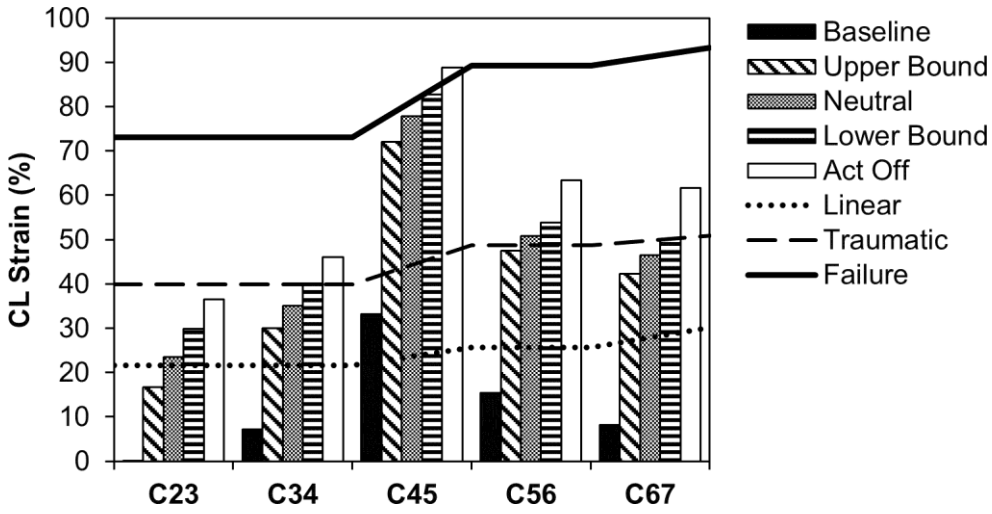

FIGURE 4-5: M50 8G FRONTAL IMPACT CL STRAIN

The PLL and LF strains were within the linear and toe regions for all activation schemes. The only exception was the PLL, which entered the traumatic region for the activation-off scheme at the C67 level. Both the PLL and LF had higher strains toward the lower cervical spine segments and with lower activation levels.

The ISL was the only ligament that had distractions in the post-traumatic region during an 8g frontal impact (Figure 4-7). The ISL demonstrated general trends of increased strain with both decreasing segment levels and decreased activation level. Ligament strains entered the post-traumatic region at the C67 level for all activation levels lower than the neutral activation scheme. The C45 and C56 levels had had ISL distractions within the traumatic region for all activation schemes except for the baseline activation scheme. The neutral and upper bound activation scheme prevented the ISL from entering the traumatic region at the C23 and C34 levels respectively.

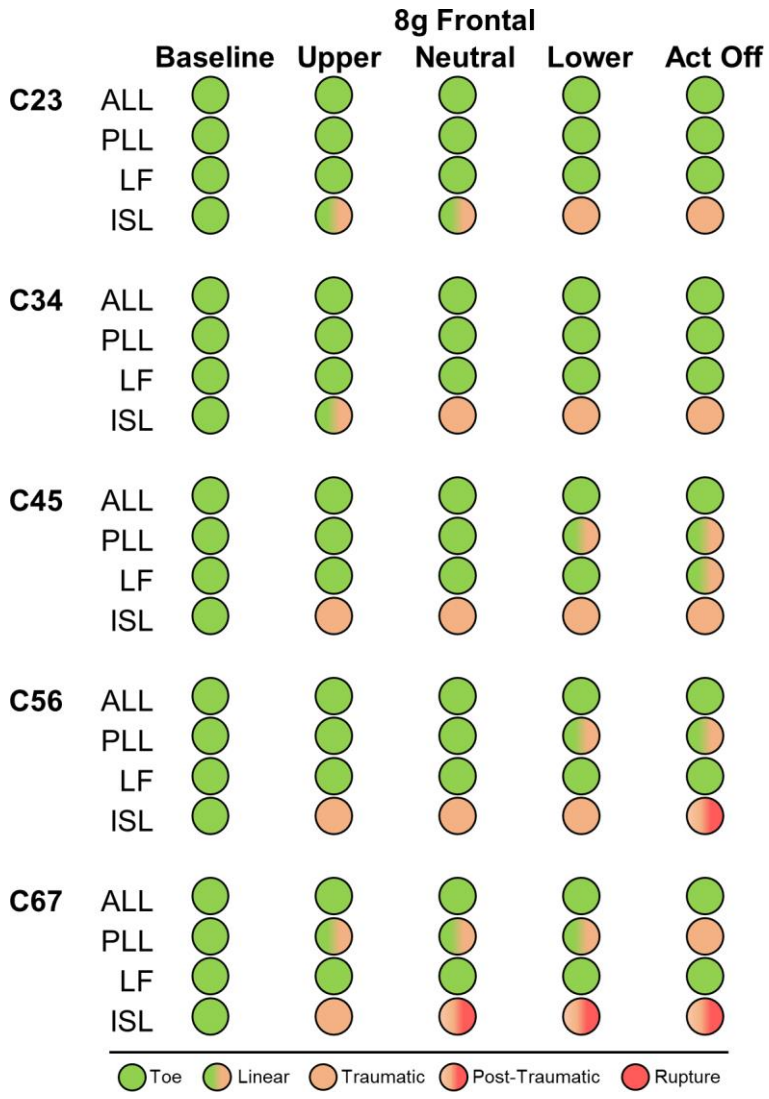

FIGURE 4-6: M50 8G FRONTAL IMPACT LIGAMENT INJURY RISK SUMMARY

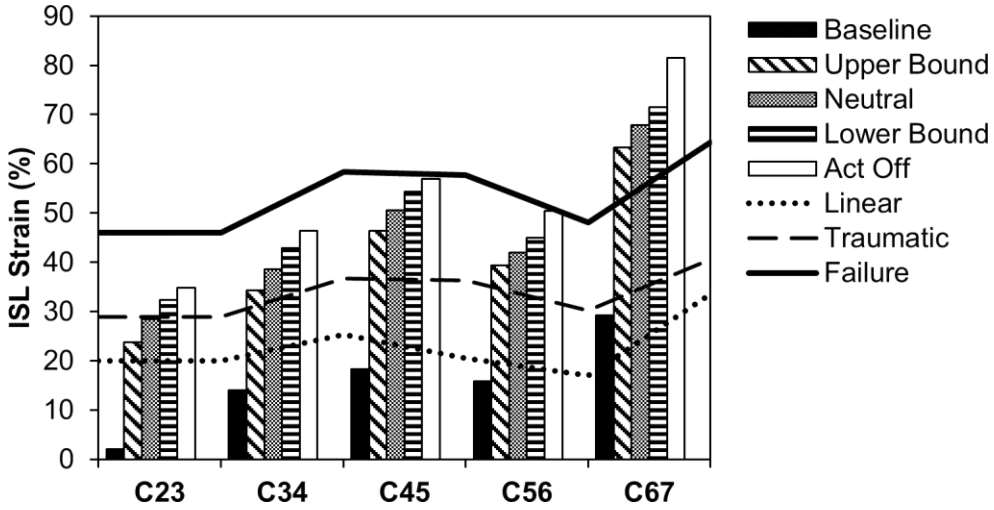

FIGURE 4-7: M50 8G FRONTAL IMPACT ISL STRAIN

The IVF height and width reduction did not reach the impingement threshold for all activation schemes and levels (Figure 4-8). IVF height reduction was generally below 1 mm for all segments, with the strongest activation scheme yielding the largest height reduction. IVF width reduction for all segment levels was negligible with the exception of the C23 segment, which had a reduction of approximately 2 mm.

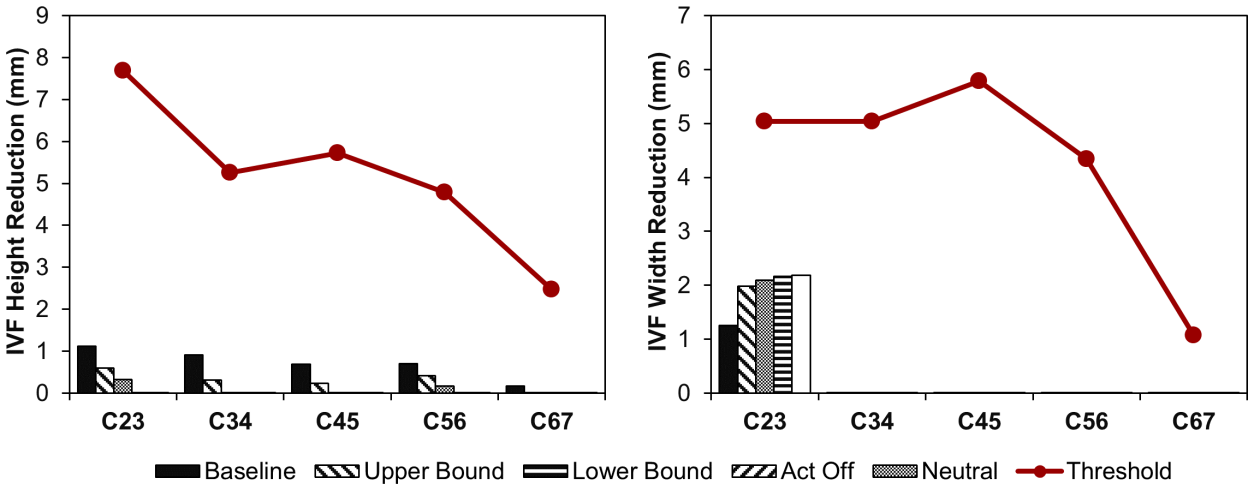

FIGURE 4-8: M50 8G FRONTAL IMPACT IVF HEIGHT AND WIDTH REDUCTION

4.1.2 7g Rear Impact Head Kinematics and Neck Tissue Response

In the rear impact condition with the neutral activation scheme, the neck underwent flexion in the upper cervical spine and extension in the lower cervical spine (30 ms) which corresponded to head retraction before eventually reaching full extension motion (60 ms). The extension response resulted in a rearward rotation of the head until maximum head extension (170 ms) before returning forward to the initial position (Figure 4-9).

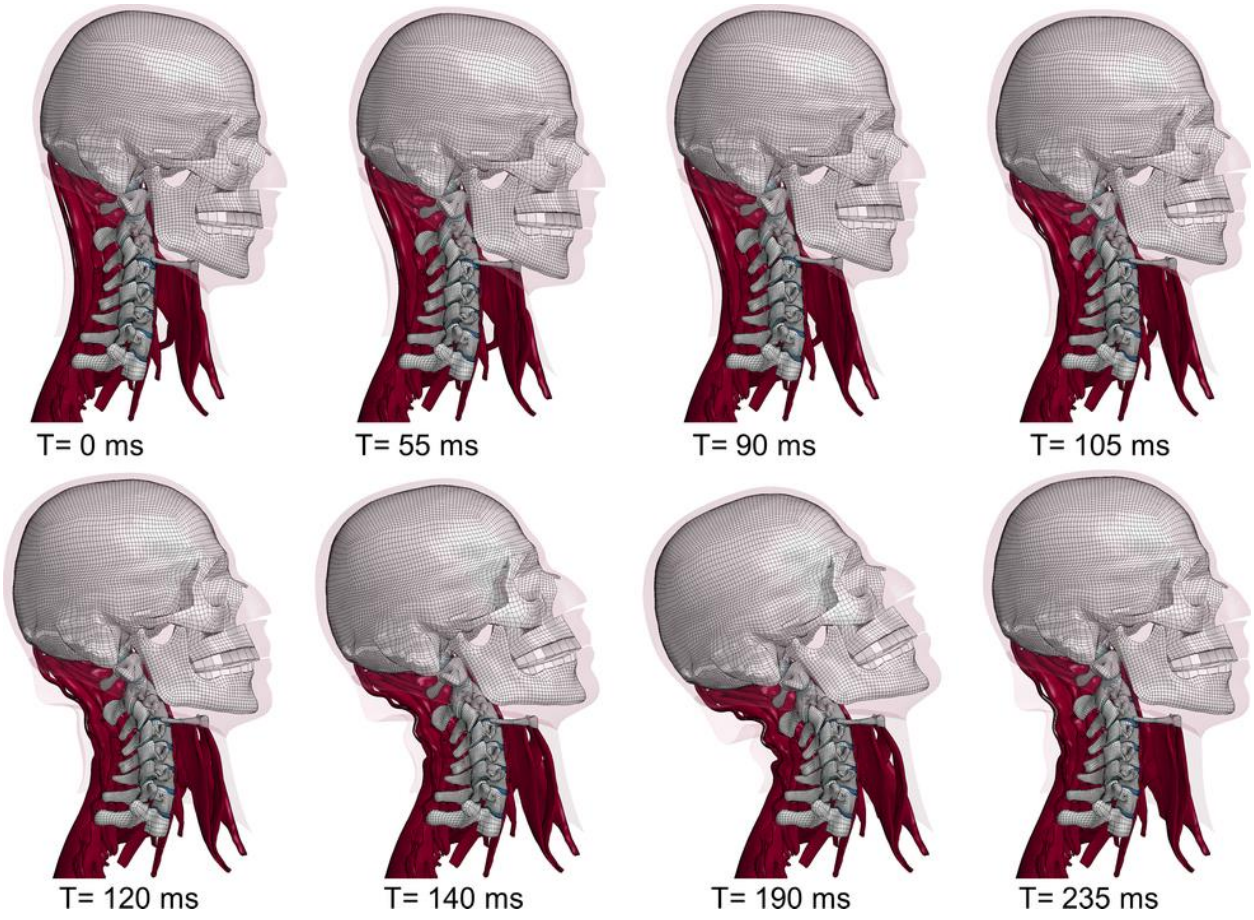

FIGURE 4-9: M50 7G REAR IMPACT KINEMATIC SEQUENCE (NEUTRAL ACTIVATION SCHEME)

The head motion in a rear impact occurred within the sagittal plane and the primary head CG kinematic metrics were the X-acceleration and Y-rotation extension angle. When the head reached maximum extension, the baseline activation scheme yielded 56.8˚, while the neutral and activation-off schemes yielded 50.7˚ and 52.2˚ respectively. The baseline activation scheme increased the extension response of the neck when compared to the activation-off scheme but was within the lower bounds of the experimental PMHS corridor (Figure 4-10).

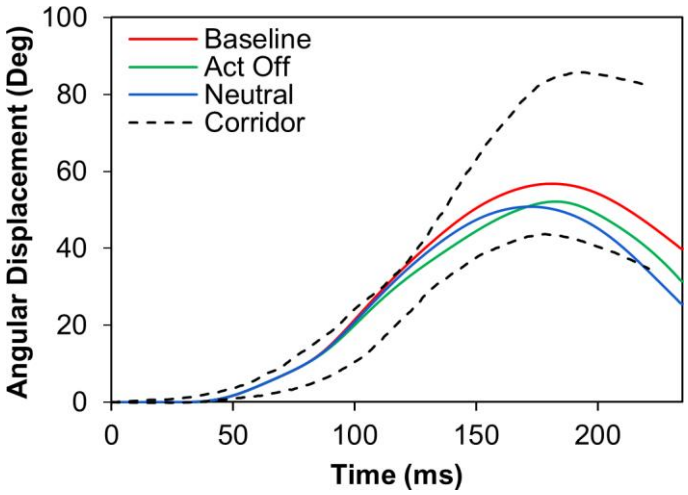

FIGURE 4-10: M50 7G REAR IMPACT HEAD CG Y-ROTATION EXTENSION ANGLE VS. DENG 1999

When compared to the baseline activation scheme, the neutral activation scheme resulted in a maximum head extension decrease of 12% while the activation-off scheme was decreased by 8%. The neutral activation scheme reduced the maximum head extension angle when compared to the activation-off scheme (-3%) (Figure 4-11). The lower bound activation scheme yielded 52.2˚ (+3%), and upper bound 49.3˚ (-3%) when compared to the neutral activation scheme. Peak head rotation was reached at approximately 180 ms for the baseline activation scheme and was reduced with higher levels of muscle activation (170 ms for the lower bound activation scheme).

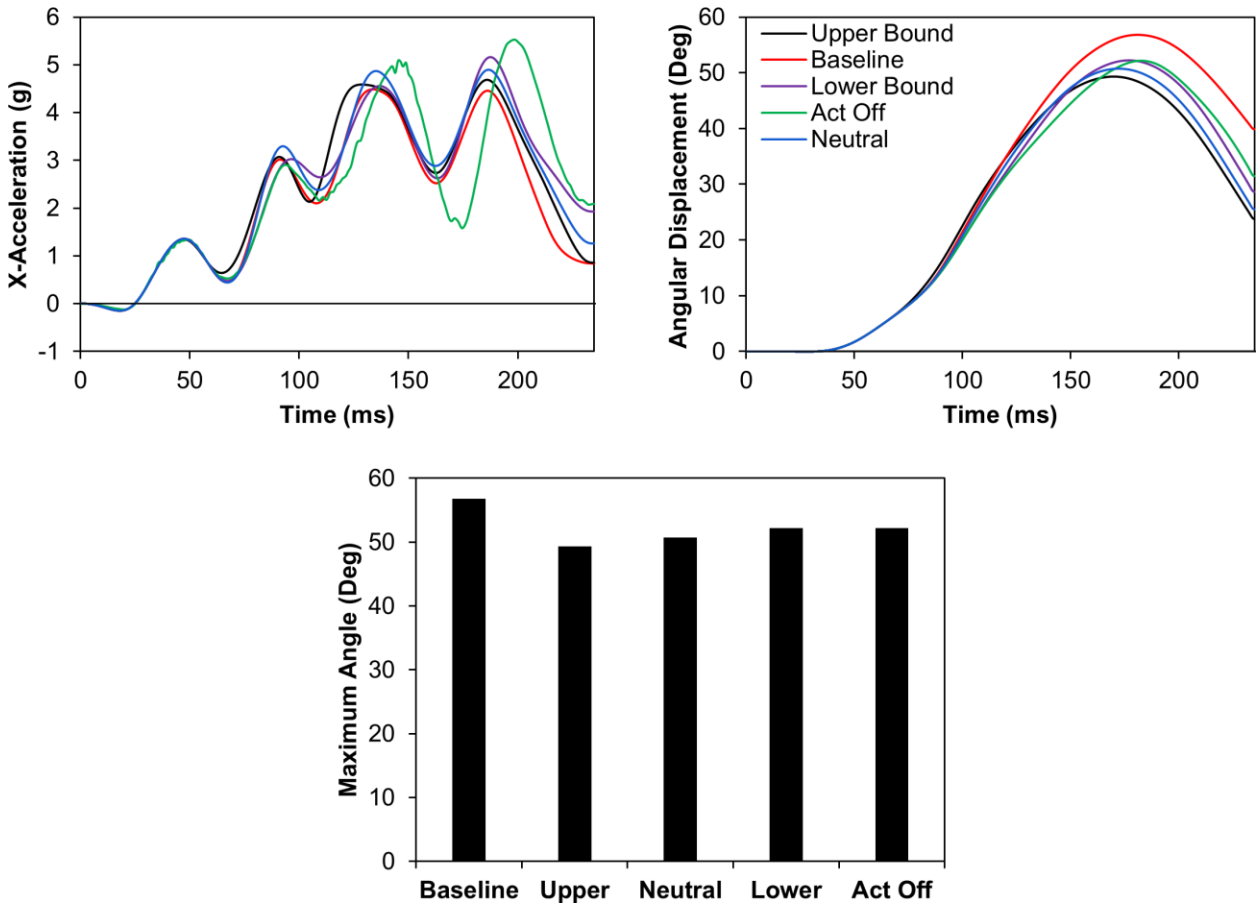

FIGURE 4-11: M50 7G REAR IMPACT HEAD CG: X-ACCELERATION, Y-ROTATION EXTENSION ANGLE, MAXIMUM Y-ROTATIONAL ANGLE

In a rear impact, the ligaments around the facet joint and anterior aspect of the neck are responsible for limiting the extension motion of the neck and had the highest predicted injury risk based on ligament distraction (Figure 4-12). The ALL and CL demonstrated the greatest strains during a rear impact. Overall, tissue strains decreased with higher levels of muscle activation, with the peak strains occurring in the upper segments (C23 and C34) for both the ALL and the CL.

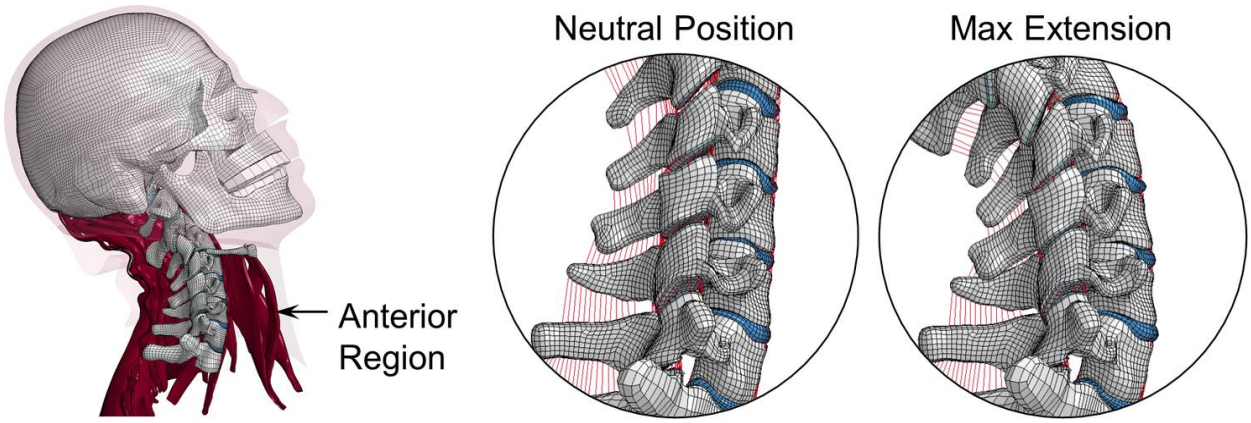

FIGURE 4-12: ANTERIOR LIGAMENTS LOADED IN TENSION

In general, the model predicted a low potential for ligament injury during a 7g rear impact scheme (Figure 4-14), although the ALL and CL had higher distractions compared to the remaining posterior ligaments (ISL, LF, PLL). Ligament distractions were in the toe region for all activation schemes and segment levels. The CL demonstrated the largest strain in the C23 segment (Figure 4-13). The model predicted that all lower cervical spine ligaments were not at risk of injury after subjected to the applied 7g rear impact pulse.

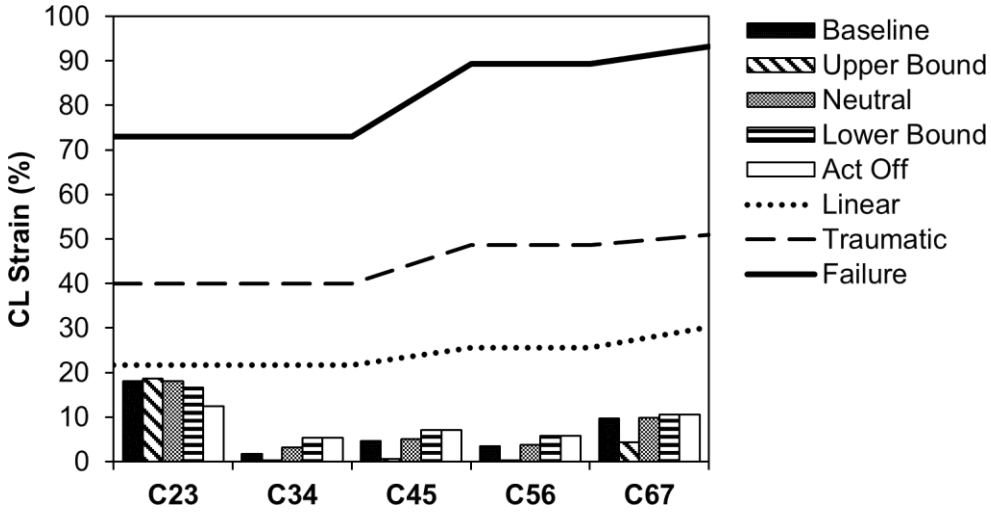

FIGURE 4-13: M50 7G REAR IMPACT CL STRAIN

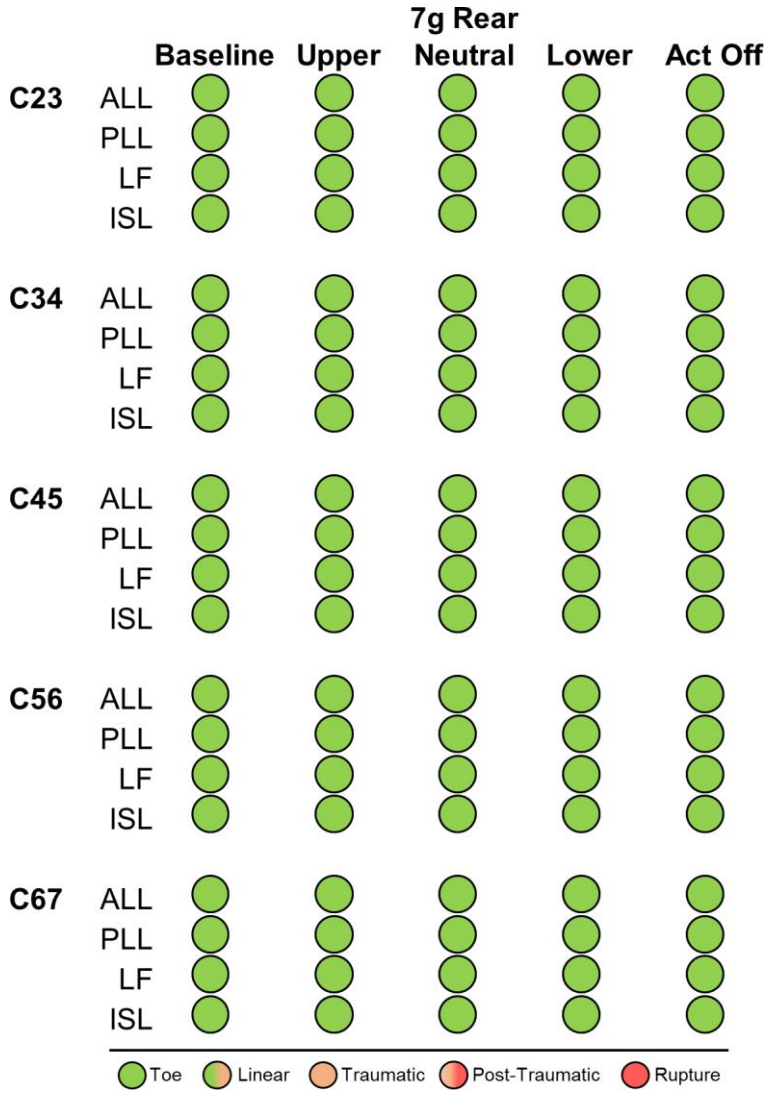

FIGURE 4-14: M50 7G REAR IMPACT LIGAMENT INJURY RISK SUMMARY

The IVF height and width reduction did not reach the impingement threshold for all activation schemes and levels (Figure 4-15). IVF height reduction was generally below 2 mm with general trends of decreased height reduction towards the lower segments and increased height reduction with higher level activation schemes. The IVF width reduction for all segment levels was below 1 mm with the exception of the C34 level, which had a reduction of approximately 2 mm. The C67 segment was at the highest risk of impingement due to the reduced threshold at that level.

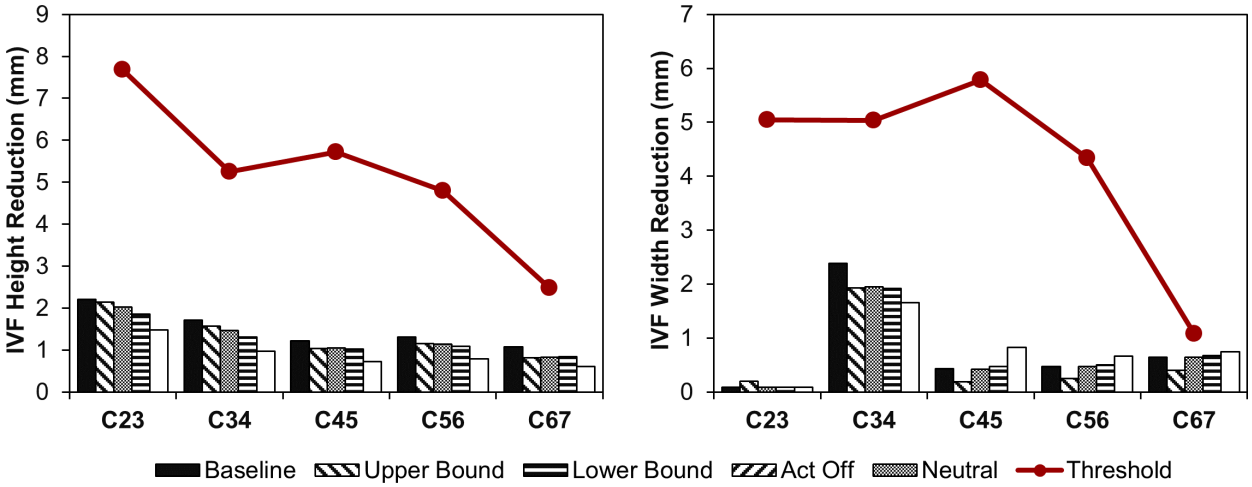

FIGURE 4-15: M50 7G REAR IMPACT IVF HEIGHT AND WIDTH REDUCTION

4.1.3 7g Lateral Impact Head Kinematics and Neck Tissue Response

In lateral impact, the neck underwent a coupled motion of lateral flexion and axial rotation along with extension or flexion, depending on the muscle activation strategy. The neutral activation scheme resulted in a combination of lateral flexion and axial rotation response (60 ms) with combined neck flexion (100 ms) before reaching maximum head lateral and axial angle (170 ms) and returning in the contralateral direction toward the initial position (Figure 4-16).

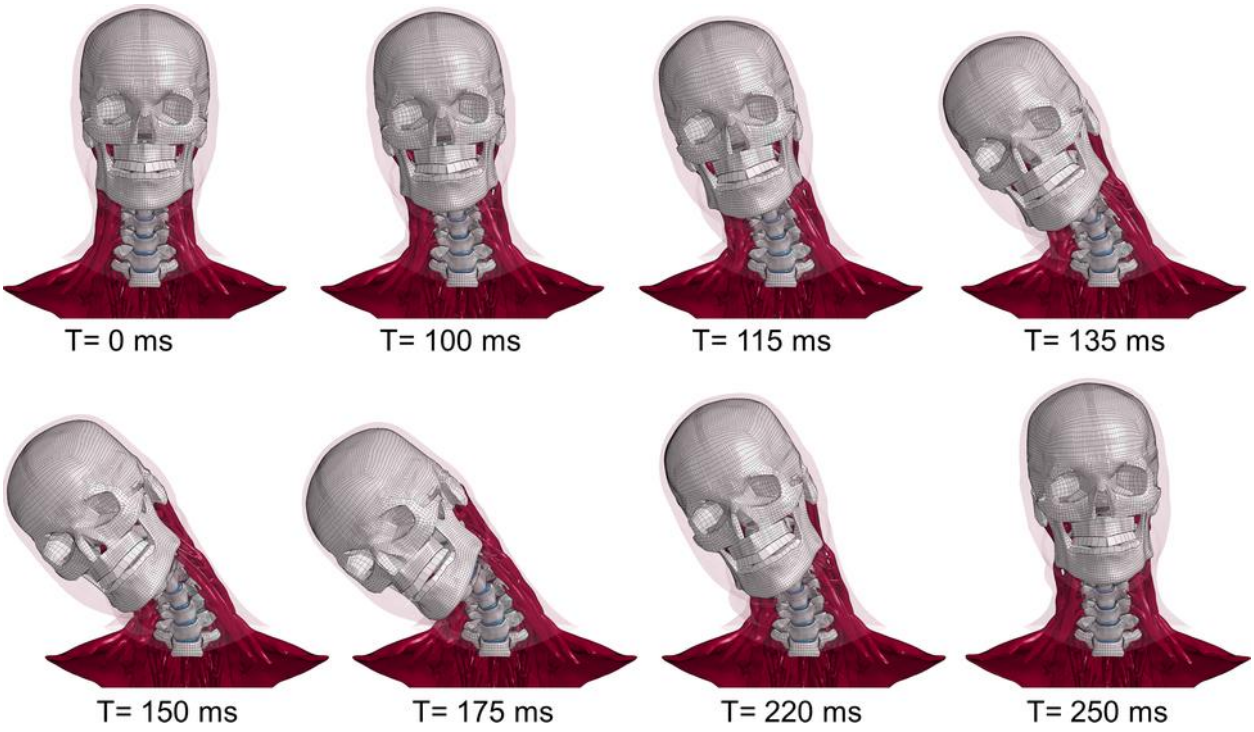

FIGURE 4-16: M50 7G LATERAL IMPACT KINEMATIC SEQUENCE (NEUTRAL ACTIVATION SCHEME)

Due to the complex motion of the neck and head complex in a lateral impact, the head CG kinematic metrics such as Y-acceleration and angle (X-rotation lateral flexion, Y-rotation sagittal angle, Z-rotation axial rotation) were investigated. When the head reached maximum lateral flexion, the baseline activation scheme yielded 33.8˚, while the neutral and activation-off schemes yielded 45.5˚ and 58.6˚ respectively. The baseline activation scheme had a lower maximum lateral flexion response when compared to the NBDL volunteer response corridors, with the loading phase of the curve demonstrating a lower magnitude (Figure 4-17). The neutral activation scheme improved the response of the model to match closely with the average volunteer response magnitude. In addition, the flexion response of the neutral activation scheme was within the experimental corridor, throughout the entire loading phase of the impact. The maximum head lateral flexion angle with the neutral activation scheme compared favourably to the average experimental

maximum head lateral flexion angle of 48˚. The sagittal head motion for both the baseline activation scheme and the neutral activation scheme had opposite directions and were mostly outside the experimental corridor. Both the neutral activation scheme and volunteer response resulted in head flexion while the baseline activation scheme resulted in head extension. The average volunteer axial rotation was above 50˚, while the model with the default and neutral had a stiffer response and yielded below 20˚. The model with the neutral activation scheme produced head rotational displacements that were closer to the average volunteer response in all three directions.

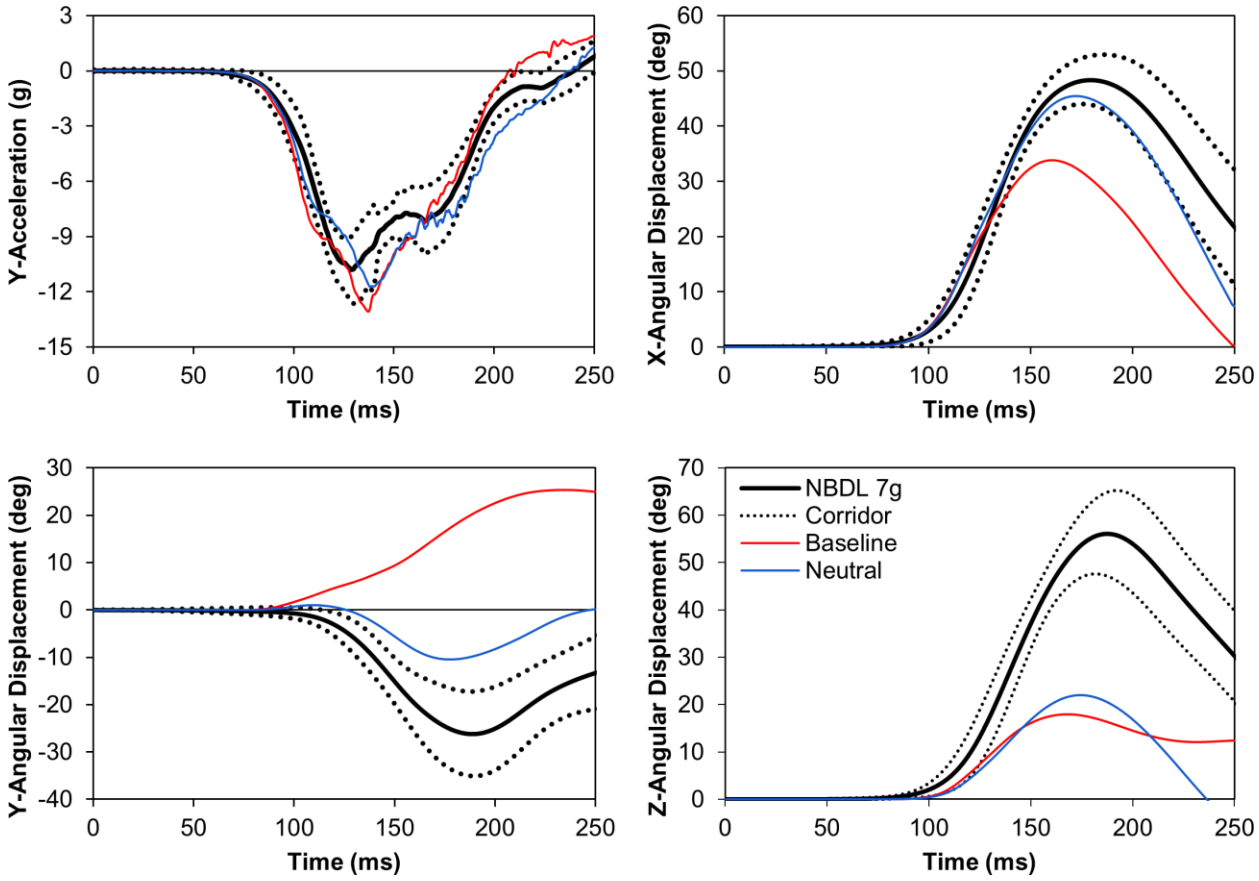

FIGURE 4-17: M50 7G LATERAL IMPACT HEAD CG: Y-ACCELERATION, X-ROTATION LATERAL FLEXION, Y-ROTATION SAGITTAL ANGLE, Z-ROTATION AXIAL ROTATION VS. NBDL RESPONSE

When compared to the baseline activation scheme, the neutral activation scheme resulted in a maximum lateral flexion increase of 26% while the activation-off scheme had an increase of 73%. The upper bound activation scheme yielded 37.5˚ (-18%), and lower bound 52.2˚ (+15%) when compared to the neutral activation scheme. The onset of head y-acceleration occurred earlier and had a larger magnitude with increased levels of activation. In general, peak head rotation (sagittal, axial, and lateral) increased and

occurred later with decreased muscle activation level. All schemes resulted in head flexion except the baseline activation scheme, which resulted in head extension (Figure 4-18). In general, activation schemes were more sensitive to head lateral flexion than head flexion and axial rotation.

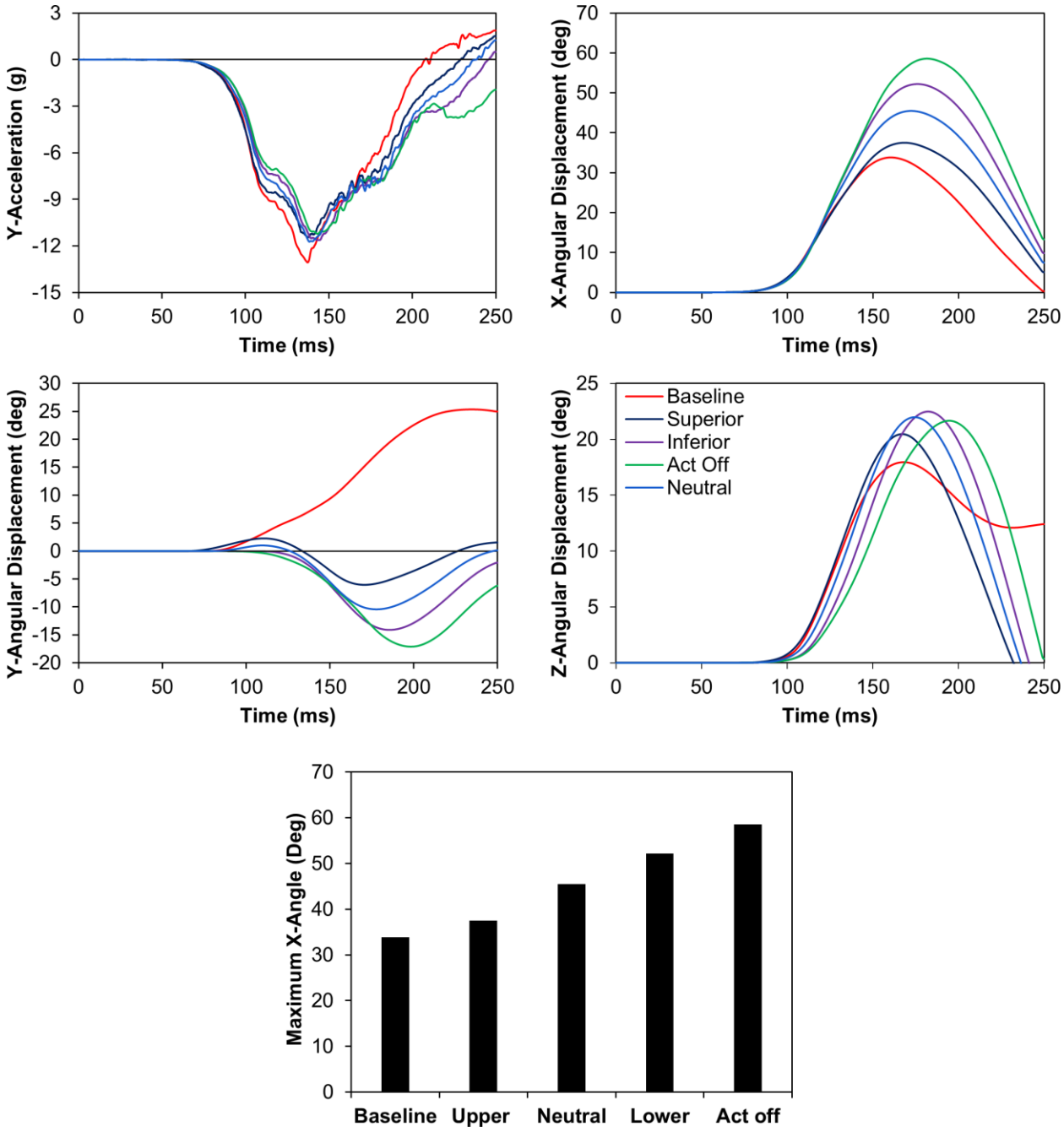

FIGURE 4-18: M50 7G LATERAL IMPACT HEAD CG: Y-ACCELERATION, X-ROTATION LATERAL FLEXION, Y-ROTATION SAGITTAL ANGLE AND Z-ROTATION AXIAL ROTATION. MAXIMUM X-ANGLE

During a side impact, the ligaments located along the lateral aspect of the cervical spine are responsible for limiting lateral flexion of the neck. The ligaments that are located contralateral to the direction of the impact are in tension and had the highest predicted injury risk based on ligament distraction, while the ligaments located on the ipsilateral side was in compression (Figure 4-19). A very small amount of bone failure was predicted based on hard tissue plastic strain, at the C6 and C7 vertebrae ipsilateral facet surface. In general, tissue strains increased with a decrease to the muscle activation level, with the C34 and C45 levels demonstrating the largest strains (Figure 4-21). All other spinal ligaments are located along the neutral axis of bending during lateral flexion of the neck and demonstrated low distractions that were within the linear and toe regions.

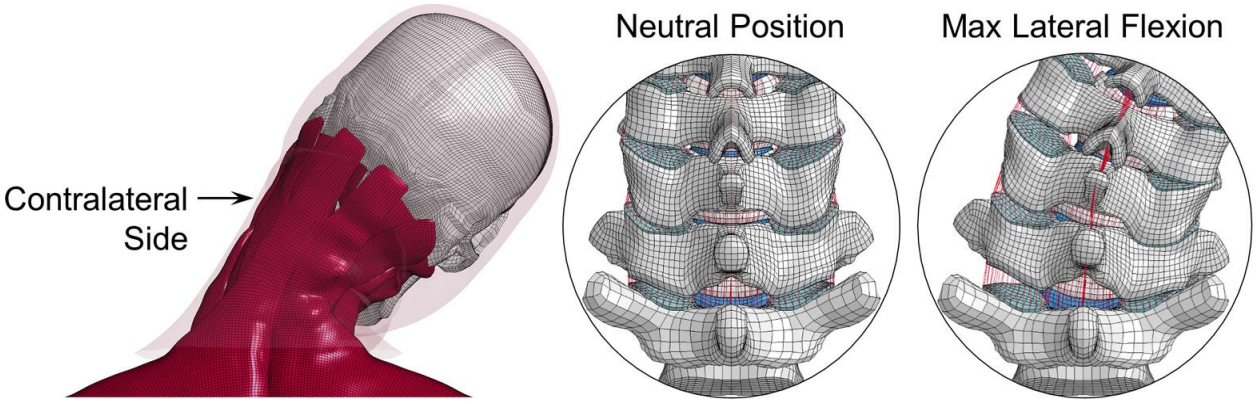

FIGURE 4-19: CONTRALATERAL LIGAMENTS LOADED IN TENSION

The CL has the highest risk of injury (Figure 4-20) during a lateral crash with a general trend of increased distraction with lower activation level. The CL did not rupture but demonstrated distractions in the post-traumatic region for different segments, which depended on the muscle activation strategy.

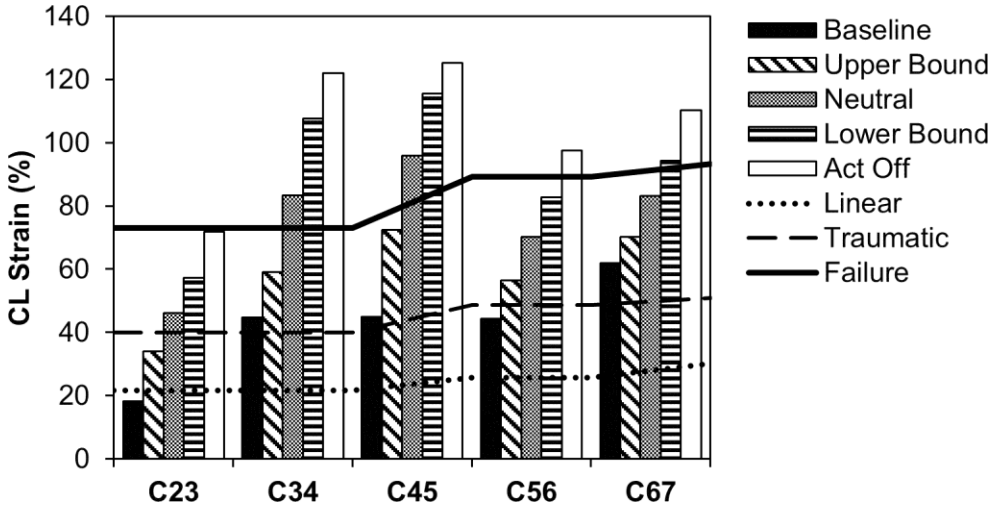

FIGURE 4-20: M50 7G LATERAL IMPACT CL STRAIN

The CL distraction was in the post-traumatic region of the ligament force-displacement curves at the C34 and C45 segments for the neutral and lower activation schemes. The CL in the remaining segments were distracted into the sub-traumatic region in all schemes. Higher activation schemes relative to the neutral activation scheme demonstrated distractions within the sub-traumatic and linear regions. The lower bound activation scheme resulted in CL distractions in the post-traumatic region for the C67, in addition to the C34 and C45. The activation-off scheme had distractions within the post-traumatic region for all cervical levels except for the C23, which was within the sub-traumatic region. The upper bound activation scheme prevented the CL distractions at the C34 and C45 from entering the post-traumatic region. The baseline activation scheme produced the stiffest response of the neck and resulted in only the C34 level to enter the sub-traumatic region, with the remaining levels within the toe and linear region. The middle cervical spine levels displayed the highest risk in sustaining distractions within the post-traumatic region during a lateral impact.

The PLL had distractions, which entered the linear region for the act off scheme at the C23, C45 and C56 segment levels. All other levels and activation schemes were within the toe region. Similarly, the ISL entered the linear region at the C45 segment level starting from the neutral activation scheme. All other ISL at all segments and activation schemes were within the toe region. The LF and ALL were all within the toe region for all activation schemes and segment.

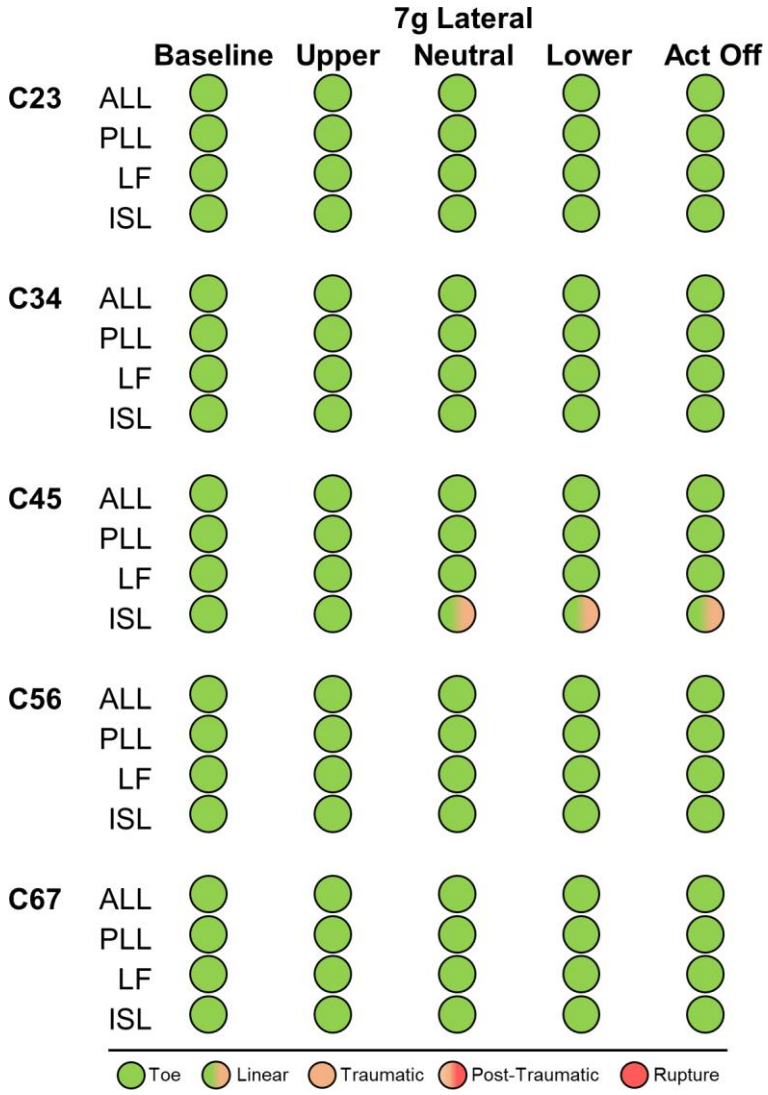

FIGURE 4-21: M50 7G LATERAL IMPACT LIGAMENT INJURY RISK SUMMARY

The IVF located on the ipsilateral side of impact had the greatest risk for nerve impingement due to reductions in IVF height and width. In contrast, the contralateral side demonstrated an increase in IVF height and width, therefore was not at risk for nerve impingement. The C67 level reached the height reduction threshold of impingement for all activation schemes. The IVF had a general trend of lowered height reduction with decreased activation levels (Figure 4-22). The maximum height reduction was within three millimetres for all segments regardless of the activation scheme. Reduction in IVF width did not exceed the threshold at any segment level or activation scheme (Figure 4-22). The C34 level had the greatest reduction in width when compared to the other levels that generally remained below 2 mm. The width reduction for all segments generally increased with lower muscle activation levels. For a 7g lateral impact,

the C67 level demonstrated the highest risk for nerve root impingement due to the IVF height reduction, while the C34 level demonstrated the largest reduction in IVF width.

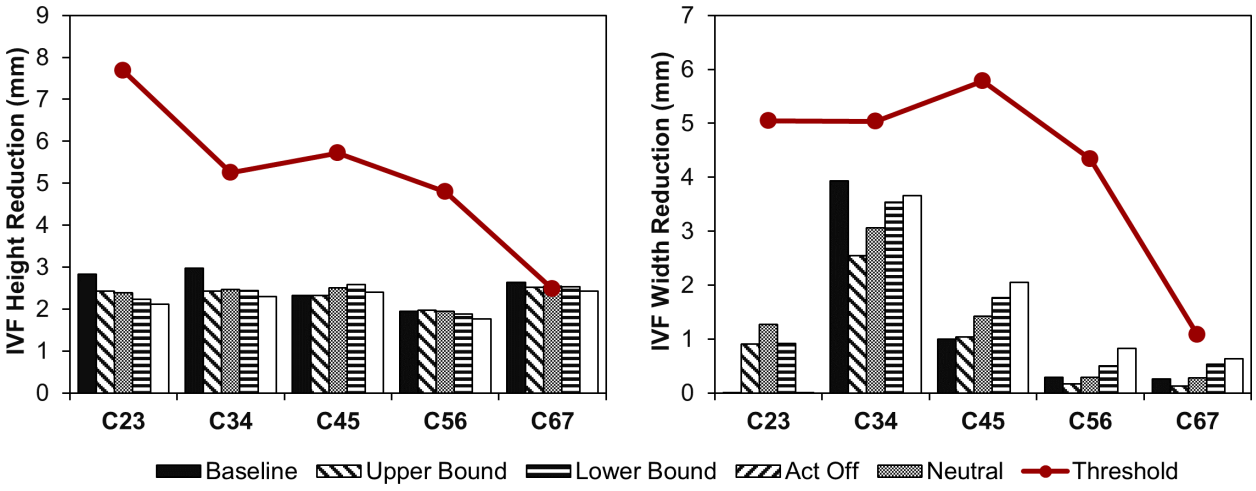

FIGURE 4-22: M50 7G REAR IMPACT IVF HEIGHT AND WIDTH REDUCTION

Quadrant Muscle Activation Investigation for Lateral Impact

The effect of muscle activation on the ipsilateral neck muscles for a 7g lateral impact was investigated. The neutral activation scheme was used as the baseline, where the extensors and flexors were activated at a ratio of 1:5, respectively. The activation levels of the muscles on the contralateral side remained constant while the activation levels on the ipsilateral side were varied by 25% decrements while the 1:5 extensors to flexors activation ratio was maintained.

The lateral acceleration of the head was insensitive to lowered levels of muscle activation on the ipsilateral side of impact (Figure 4-23). Overall, a decrease of activation on the ipsilateral side resulted in a decrease of lateral flexion, an increase in head forward flexion, and an increase in axial rotation (Figure 4-23).

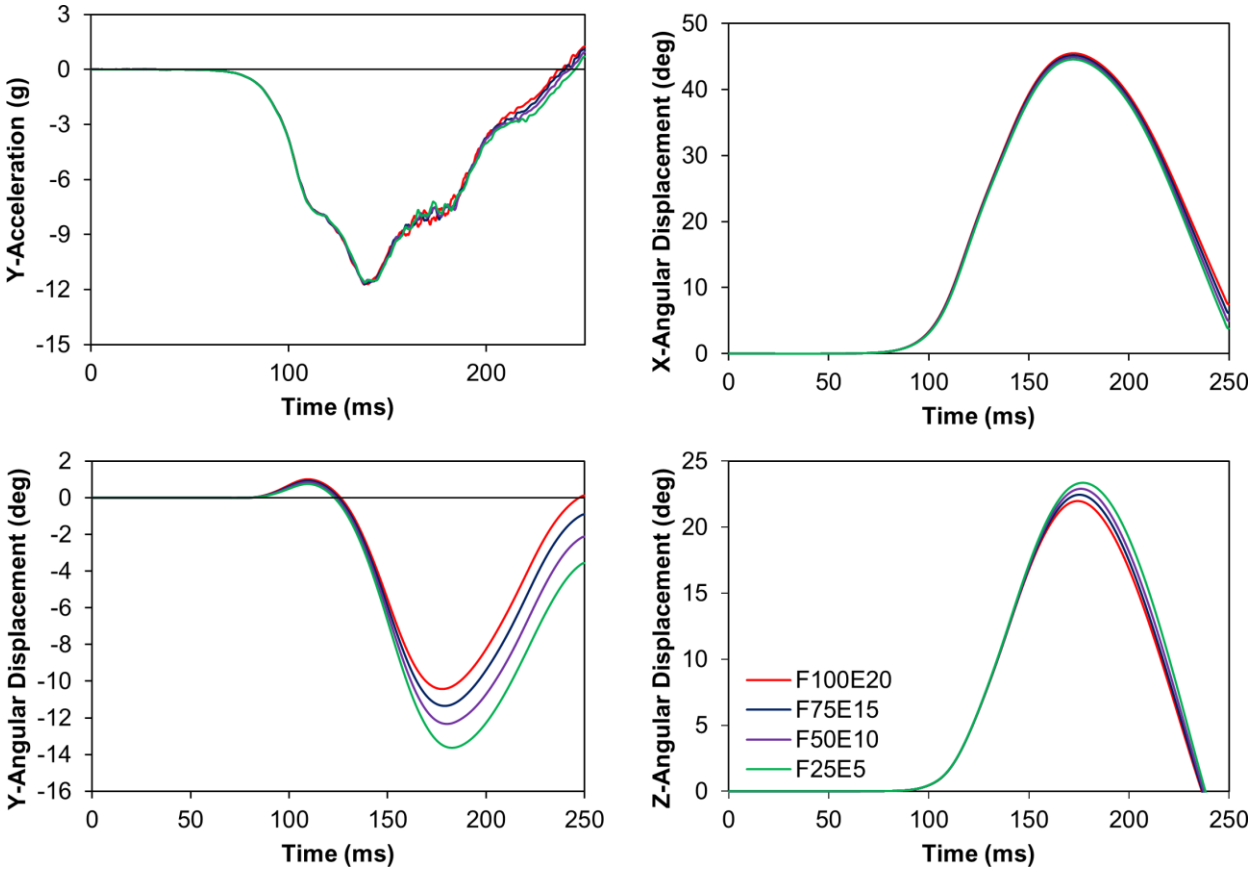

FIGURE 4-23: M50 7G LATERAL IMPACT QUADRANT SCHEME HEAD CG: Y-ACCELERATION, X-ROTATION LATERAL FLEXION, Y-ROTATION SAGITTAL ANGLE AND Z-ROTATION AXIAL ROTATION

In general, the ligament strains increased when the ipsilateral activation level was decreased but did not change the injury potential (Figure 4-24). Both the IVF height and width were reduced with decreasing ipsilateral activation, with the maximum reduction at the C23 segment (Figure 4-25). The lowered activation level of the ipsilateral muscles did not affect the potential for nerve root compression.

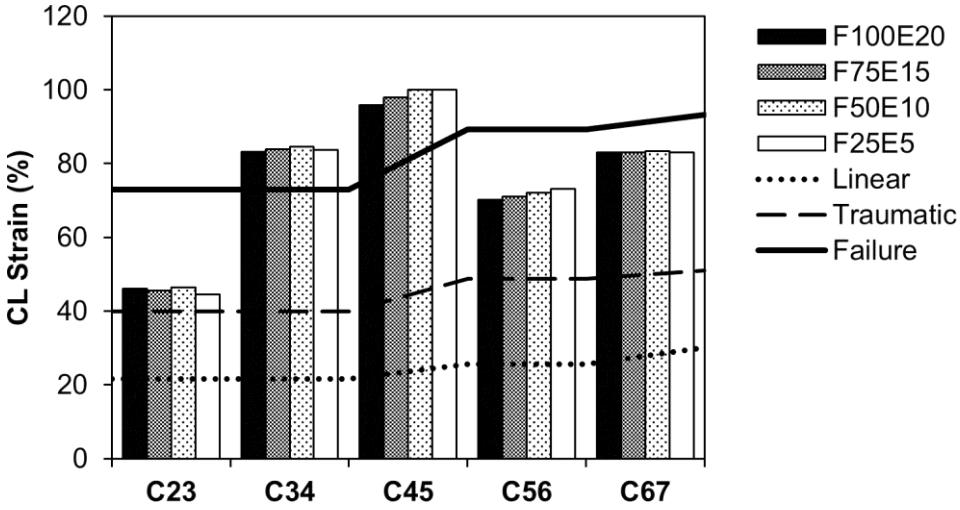

FIGURE 4-24: CL STRAIN QUADRANT SCHEME STUDY

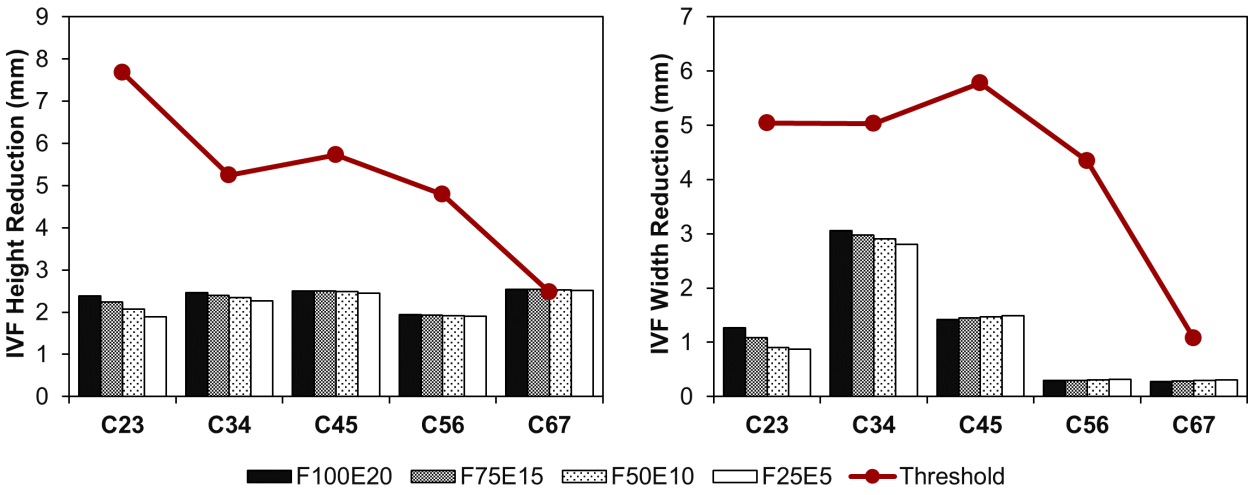

FIGURE 4-25: IVF HEIGHT AND WIDTH REDUCTION, QUADRANT SCHEME STUDY

4.2 Small Stature Female (F05) Neck Model Results

4.2.1 8g Frontal Head Kinematics and Neck Tissue Response

In a frontal impact with the neutral activation scheme, the neck underwent shear deformation, corresponding to head x-translation (40 ms), followed by flexion (90 ms). The flexion response resulted in forward rotation of the head until the maximum flexion angle was reached (175 ms), before returning to the initial position (Figure 4-26).

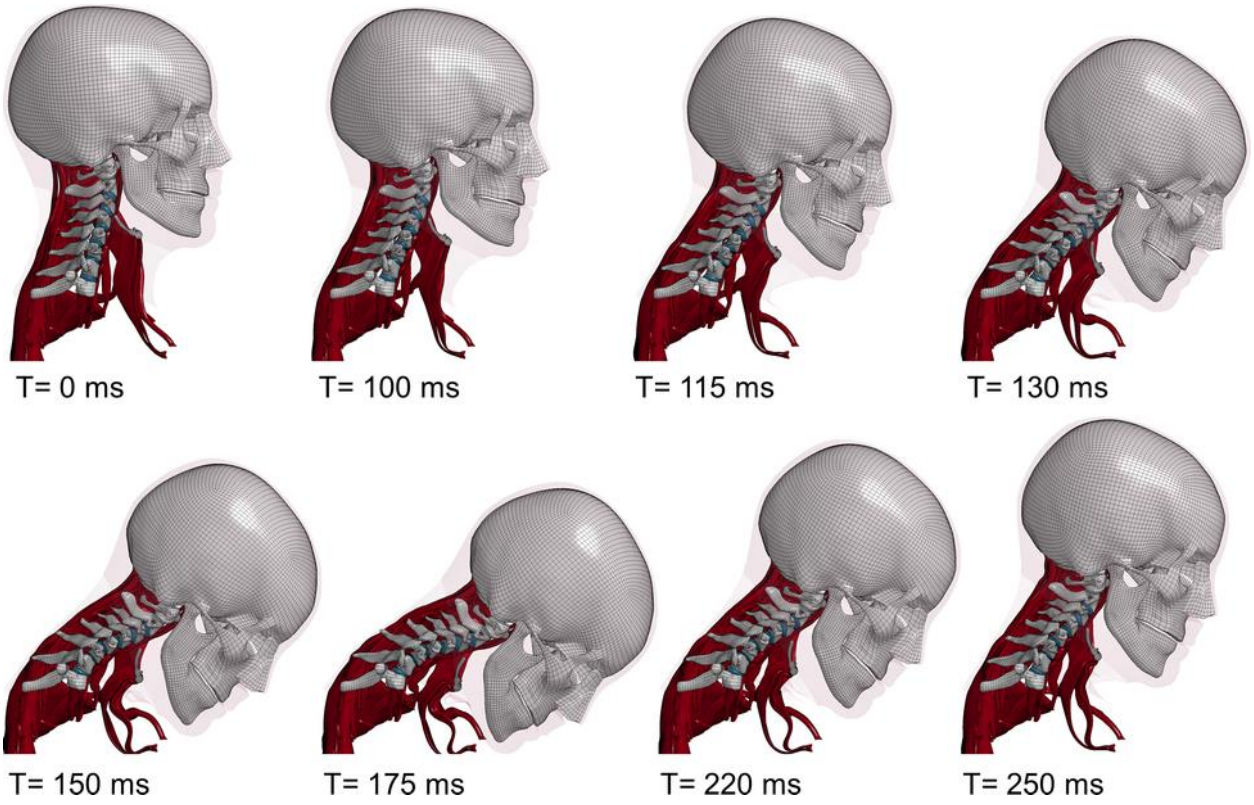

FIGURE 4-26: F05 8G FRONTAL IMPACT KINEMATIC SEQUENCE (NEUTRAL ACTIVATION SCHEME)

The primary neck motion during a frontal impact occurred within the sagittal plane and the primary head CG kinematic metrics included the X-acceleration and Y-rotation flexion angle were investigated. The maximum head flexion angle for the baseline activation scheme resulted in 45.4˚ of rotation, while the neutral and activation-off scheme demonstrated 64.4˚ and 70˚ of head flexion respectively. The baseline activation scheme demonstrated a stiffer flexion response when compared to the NBDL volunteer response

corridors, with most of the curve outside the corridor. In addition, both magnitude and onset were lower when compared to the NBDL response corridors. The neutral activation scheme resulted in a flexion response that matched closer to the volunteer response with most of the curve within the experimental corridor (Figure 4-27). The NBDL response corridors were not scaled to be stature-matched to the 5th percentile female.

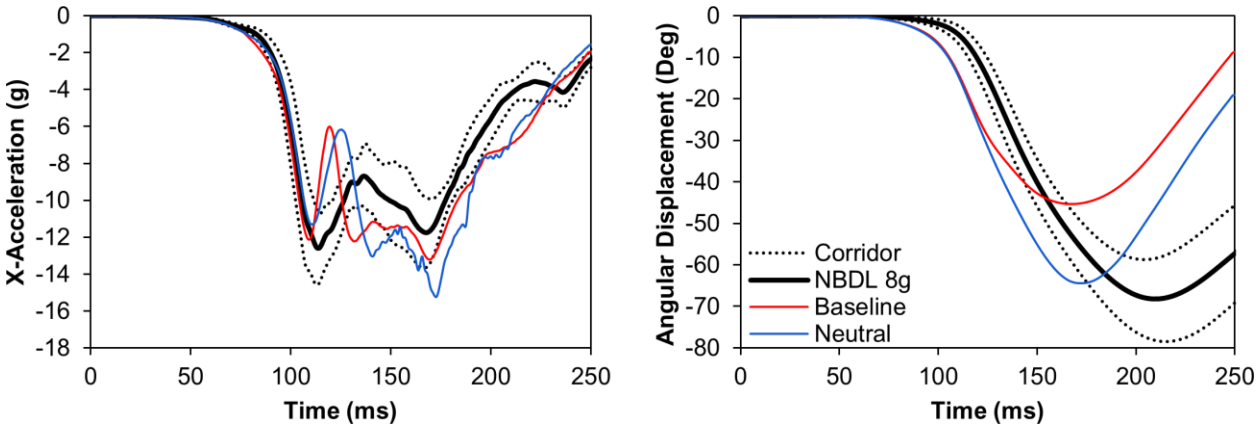

FIGURE 4-27: F05 8G FRONTAL IMPACT HEAD CG: X-ACCELERATION AND Y-ROTATION FLEXION ANGLE

The peak head flexion angle increased with lower activation schemes. Accelerations traces were similar, with higher muscle activation demonstrating lower peaks and earlier occurrence in time. When compared to the baseline activation scheme, the neutral activation scheme resulted in a maximum head rotation increase of 42% while the activation-off scheme increased by 54%. Maximum head flexion angle for the upper bound activation scheme yielded 60.9˚ (-5.5%), and lower bound 67.2˚ (+4.4%) when compared to the neutral activation scheme (Figure 4-28).

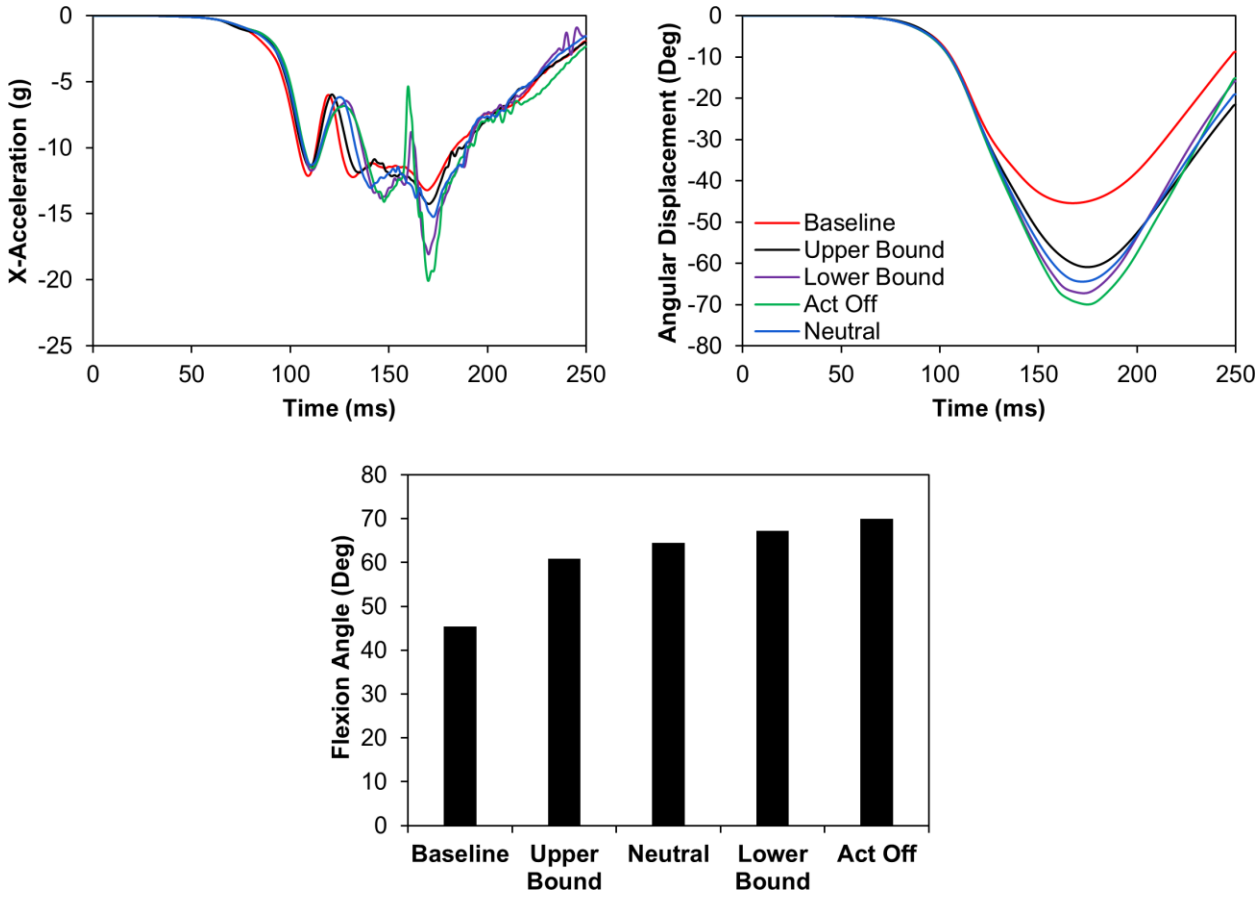

FIGURE 4-28: F05 8G FRONTAL IMPACT HEAD CG: X-ACCELERATION AND Y-ROTATION FLEXION ANGLE, MAXIMUM Y-ROTATION ANGLE

The posterior ligaments in the neck were loaded in tension during a frontal impact in the neck have the highest predicted injury risk based on ligament distraction because they are loaded in tension during a frontal impact. The ISL was the only ligament that entered the post-traumatic region in the C67 segment for all activation schemes. Ligaments that sustained sub-traumatic damage include the PLL, CL, and the LF. In general, ligament strain increased with a lower muscle activation level, and strains increased towards the lower cervical spine segments (Figure 4-30).

The CL at the C23, C34 and C45 segment levels had strains that were in the linear region of the ligament response curve (Figure 4-29). Stronger activation schemes reduced the strains to within the toe region. In the C56 and C67 segments, the CL was distracted past the linear region and entered the traumatic region. For the C56 segment, failure occurred only with the activation-off scheme. The C67 segment was within the traumatic region, for all the activation schemes.

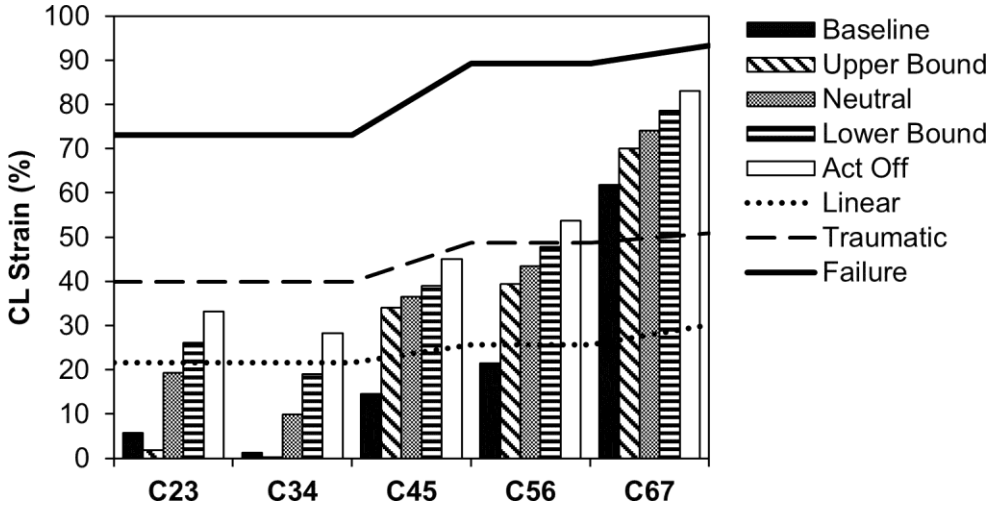

FIGURE 4-29: F05 8G FRONTAL IMPACT CL STRAIN

The PLL sustained sub-traumatic damage starting at the lower bound activation scheme at the C67 level, and for the activation-off scheme in the C56 segment. The neutral activation scheme had the C23, C56 and C67 segments that were in the linear region of the ligament load curve. In general, the lower cervical segments sustained higher strains when compared to the upper segments. The LF followed the same trend as the PLL, with increased strains towards the lower cervical segments, and increasing strain with decreased activation level. The LF was in the traumatic region for the activation-off scheme for both the C56 and C67 segment levels. The ISL was in the traumatic region for the activation-off scheme at the C45 segment, and for lower activation schemes relative to the upper bound activation scheme for the C56 segment. The C67 segment had ligament failure for all muscle activations schemes.

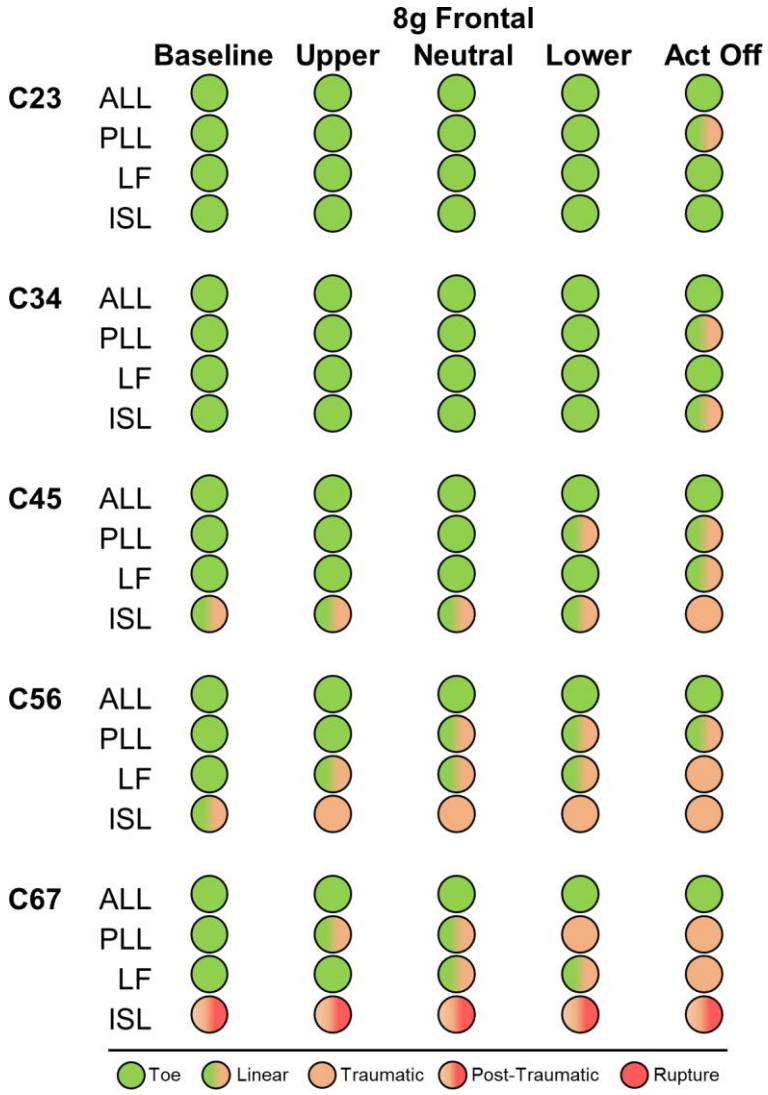

FIGURE 4-30: F05 8G FRONTAL IMPACT LIGAMENT INJURY RISK SUMMARY

The IVF height and width reduction did not reach the impingement threshold for any activation schemes and for any segment levels (Figure 4-31). The IVF had a height reduction that was below 1.2 mm for all segments, with a general trend of increased height reduction with the highest level of muscle activation. The IVF width had negligible reductions for all segment levels for the 8g frontal impact.

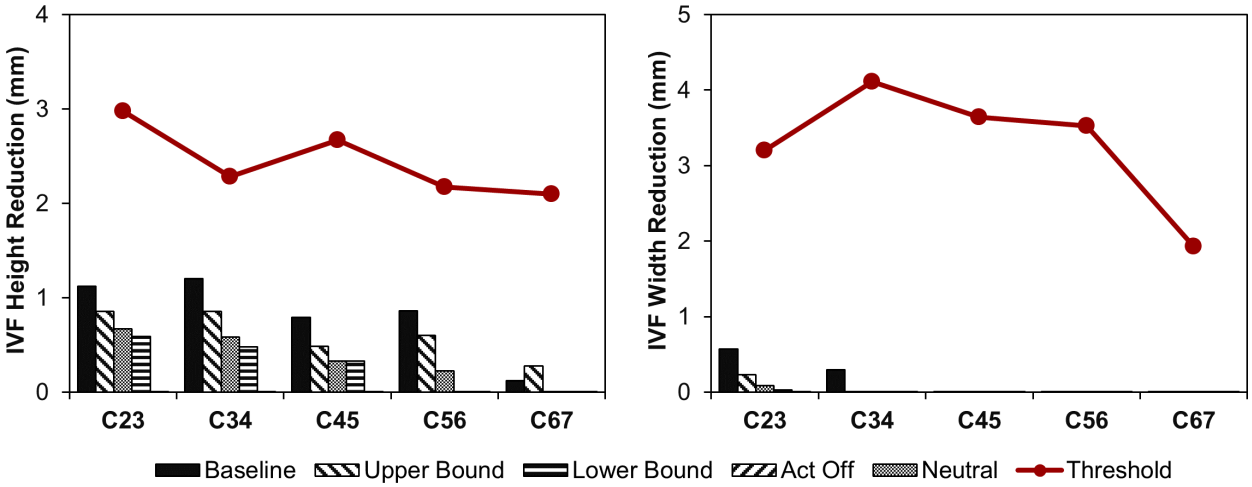

FIGURE 4-31: F05 8G FRONTAL IMPACT IVF HEIGHT AND WIDTH REDUCTION

4.2.2 7g Rear Impact Head Kinematics and Neck Tissue Response

In the rear impact condition with the neutral activation scheme, the neck underwent flexion in the upper cervical spine and extension in the lower cervical spine (30 ms) which corresponded to head retraction before eventually reaching full extension motion (55 ms). The extension response resulted in a rearward rotation of the head until maximum head extension (170 ms) before returning forward to the initial position (Figure 4-32).

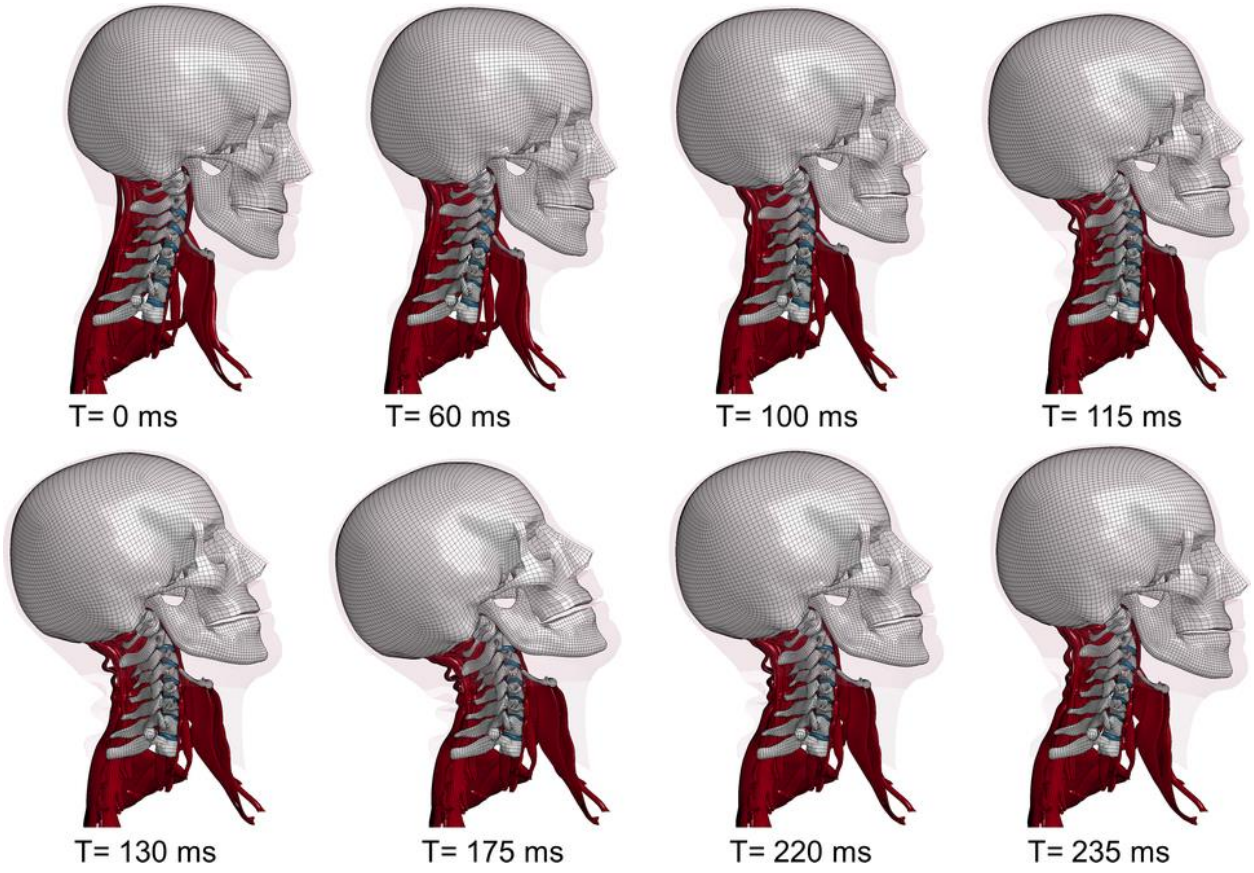

FIGURE 4-32: F05 7G REAR IMPACT KINEMATIC SEQUENCE (NEUTRAL ACTIVATION SCHEME)

The primary neck motion in a rear impact occurred within the sagittal plane, and therefore the primary head CG kinematic metrics include the X-acceleration and Y-rotation extension angle was investigated. The F05 model reached a maximum extension angle of 55.7˚ for the baseline activation scheme, while the neutral and activation-off scheme reached 52.2˚ and 55.1˚ respectively. The neutral activation scheme decreased head extension angle by 6.3% while the activation-off scheme decreased head extension angle

by 1.2%. The baseline activation scheme exacerbated the extension response of the neck when compared to the activation-off scheme but was within the PHMS experimental corridor (Figure 4-33). The neutral activation scheme was able to reduce head extension by reducing the extensor bias that existed in the baseline activation scheme.

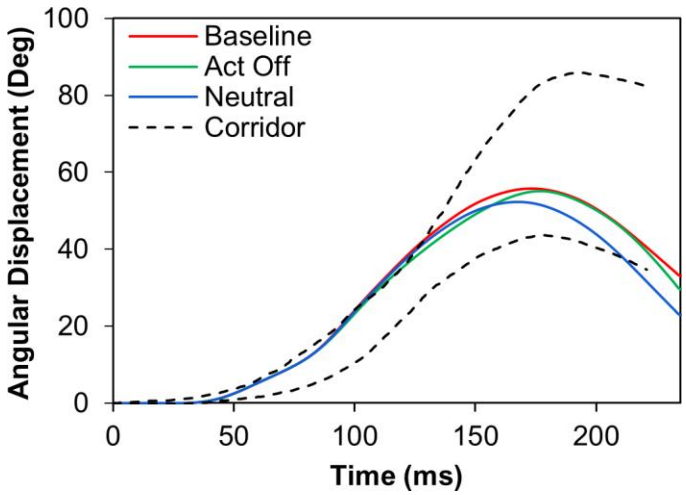

FIGURE 4-33: F05 7G REAR IMPACT HEAD CG Y-ROTATION EXTENSION RESPONSE VS. DENG 1999

The head X-acceleration trace for all schemes was similar. The activation schemes with lower levels of activation had a positive phase shift in time and greater peaks due to the reduced stiffness of the neck musculature. In general, higher levels of muscle activation reduced head extension angle and the resulting maximum extension occurred earlier in time. When compared to the neutral activation scheme, the lower bound activation scheme yielded a head extension angle of 53.9˚ (+3.2%), while the upper bound activation scheme yielded 50.6˚ (-3.1%) (Figure 4-34).

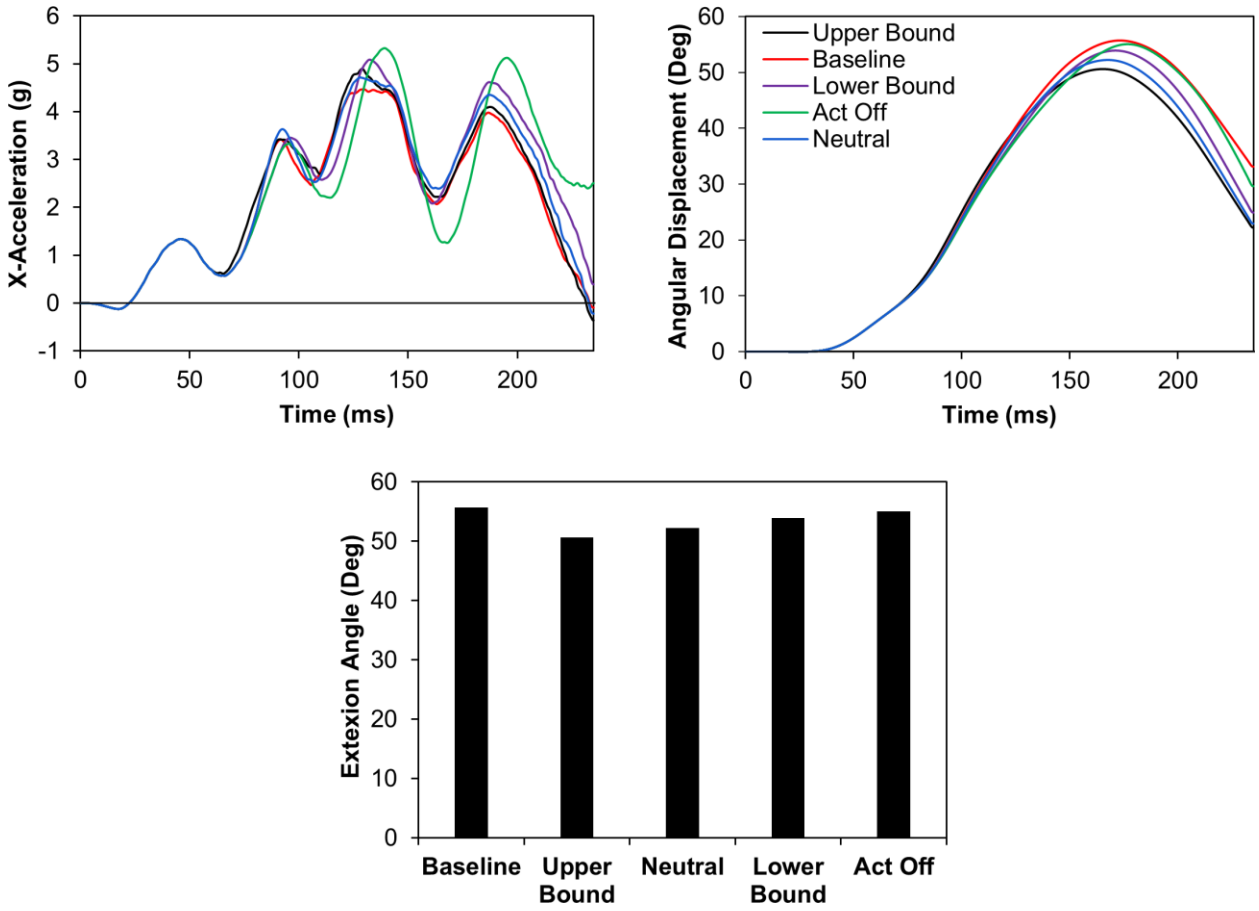

FIGURE 4-34: F05 7G REAR IMPACT HEAD CG: X-ACCELERATION AND Y-ROTATION EXTENSION ANGLE. MAXIMUM Y-ROTATION ANGLE

In a rear impact, the ligaments in the anterior region of the neck are loaded in tension to resist extension and had the highest predicted injury risk based on ligament distraction. Tissue level strains generally increased with a decrease in the muscle activation level and reached peak strains at the lower cervical levels (Figure 4-36). All ligaments in the model were within the toe region of the ligament response curves except for the activation-off scheme where the CL entered the linear region (Figure 4-35).

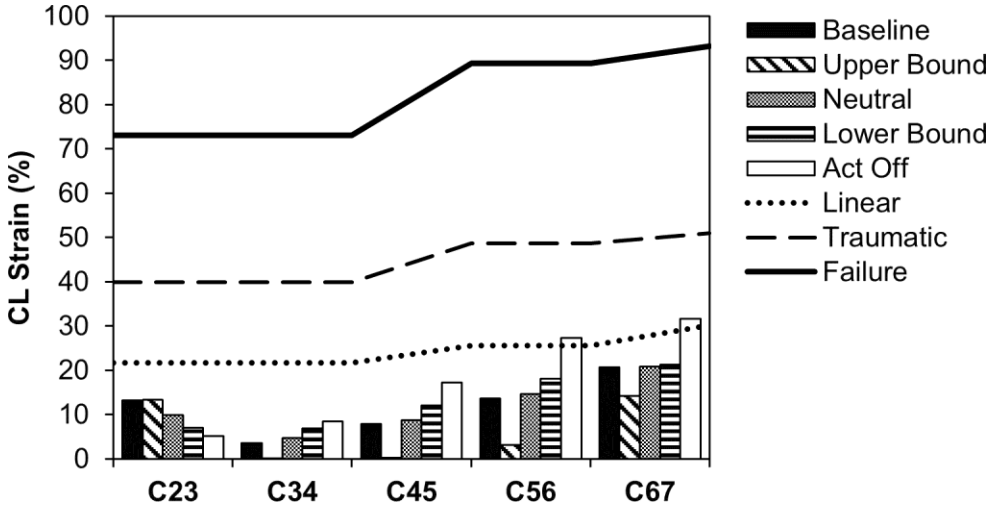

FIGURE 4-35: F05 7G IMPACT CL STRAINS

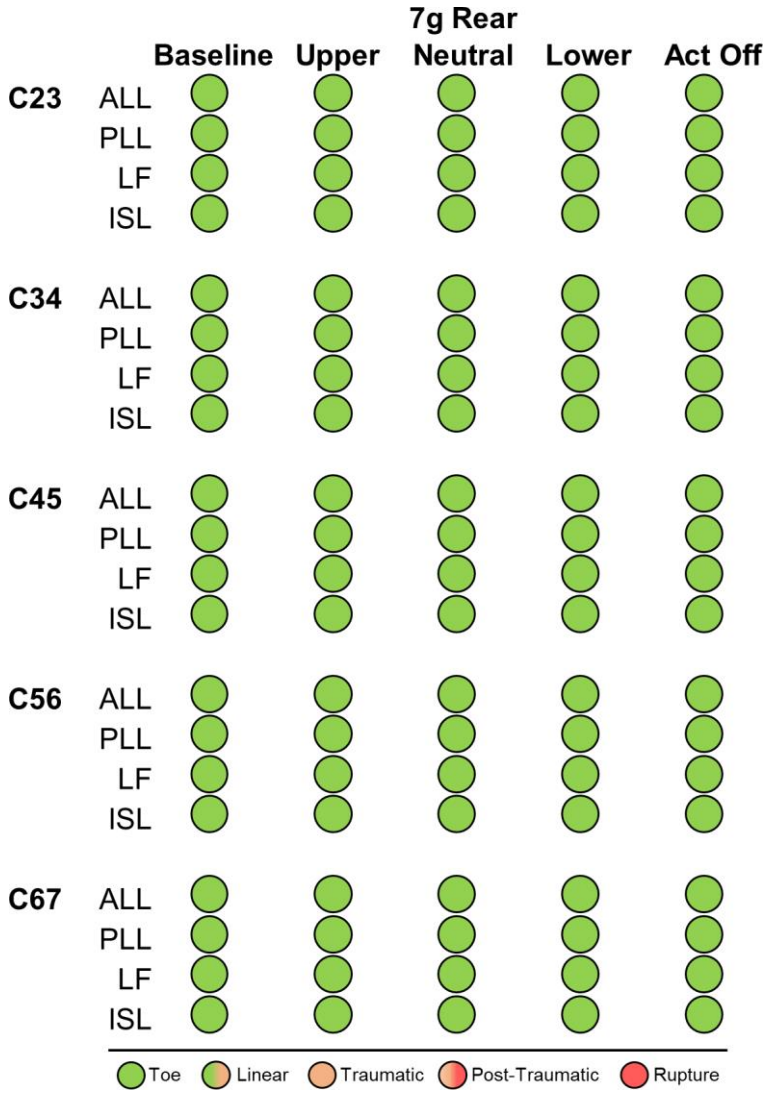

FIGURE 4-36: F05 7G REAR IMPACT LIGAMENT INJURY RISK SUMMARY

Reduction in the IVF height and width did not exceed the threshold for any activation schemes at all segment levels (Figure 4-37). The IVF height reduction decreased with lower levels of activation levels. The IVF width reduction decreased at the C23 and C34 levels but height reduction increased for the C45 and lower levels. In general, the height and width reduction were below two millimetres for activations schemes and levels.

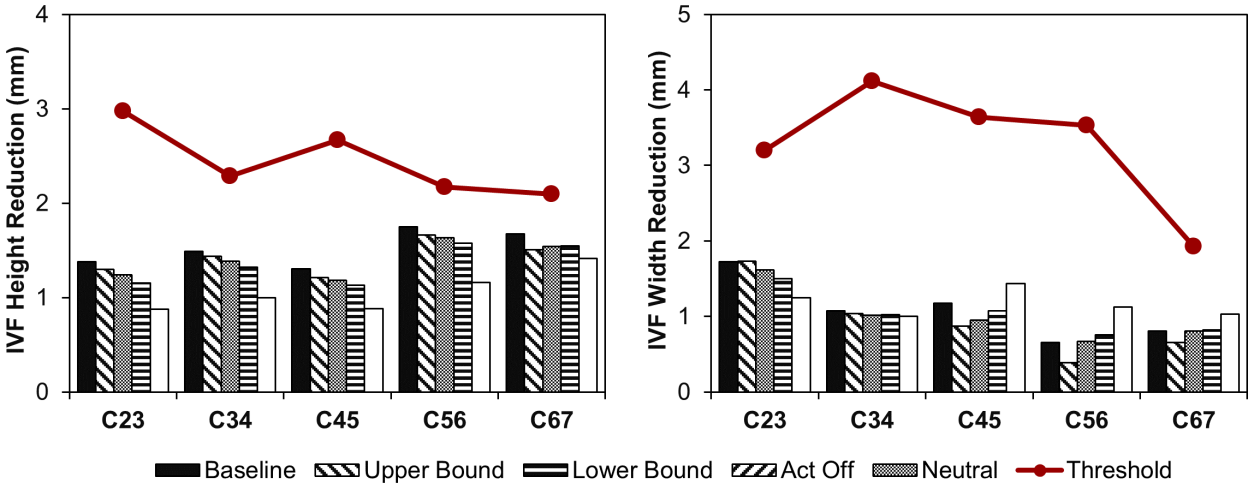

FIGURE 4-37: F05 7G REAR IMPACT IVF HEIGHT AND WIDTH REDUCTION

4.2.3 7g Lateral Impact Head Kinematics and Neck Tissue Response

The lateral impact with the neutral activation scheme resulted in a combination of neck lateral flexion and axial rotation response (65 ms) with combined neck flexion (100 ms) before reaching maximum head lateral and axial angle (155 ms) and returning in the contralateral direction toward the initial position (Figure 4-38).

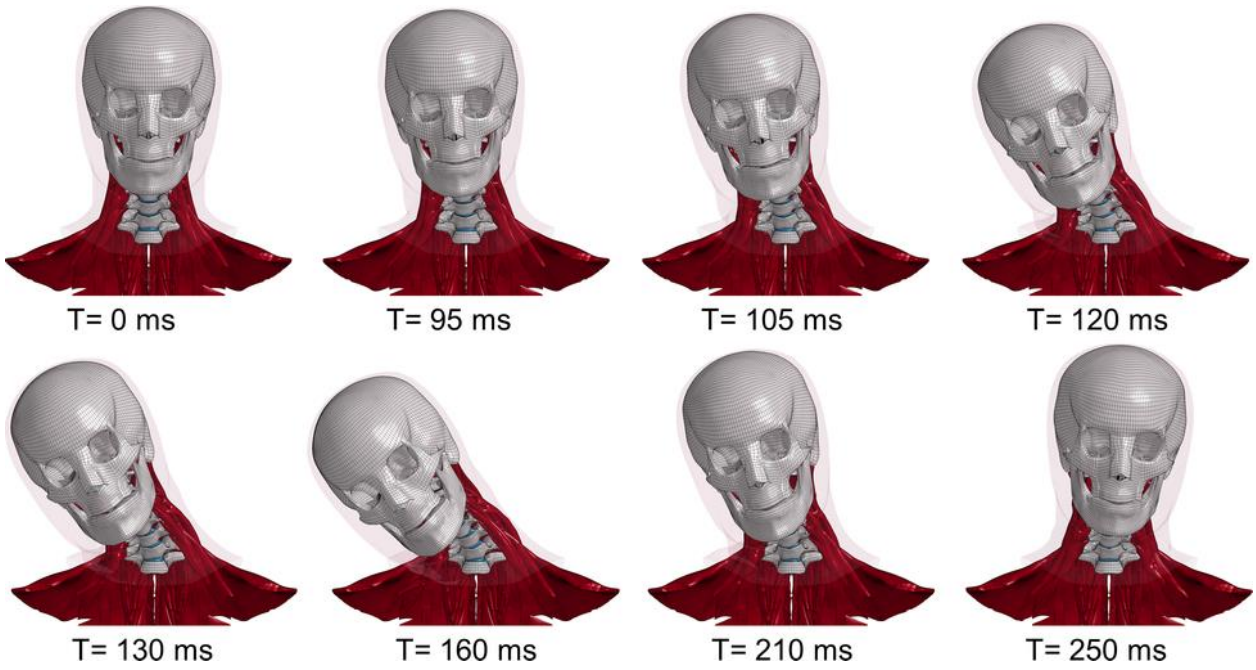

FIGURE 4-38: F05 7G LATERAL IMPACT KINEMATIC SEQUENCE (NEUTRAL ACTIVATION SCHEME)

The neck response to a side impact is complex and occurs in multiple planes of motion. The F05 head returned past the initial neutral position in the contralateral direction of impact at the end of the simulation (Figure 4-38). Head CG kinematic metrics such as Y-acceleration and angle (X-rotation lateral flexion, Y-rotation sagittal angle, and Z-rotation axial rotation) was investigated.

Head acceleration of the baseline and neutral activation scheme were similar in shape. The baseline activation scheme displayed an earlier onset of head y-acceleration when compared to the neutral activation scheme. The baseline activation scheme had a maximum lateral flexion angle of 29.8˚, while the neutral and act off scheme reached 36.4˚ and 44.9˚ respectively. Both the baseline and neutral activation scheme demonstrated lower head lateral flexion angle than the NBDL volunteer response corridors (Figure 4-39). The neutral activation scheme resulted in head flexion, while the baseline activation scheme resulted in

head extension. The model demonstrated lower axial rotation when compared to the NBDL response. The F05 model was not within the volunteer corridors for all three axes of rotation.

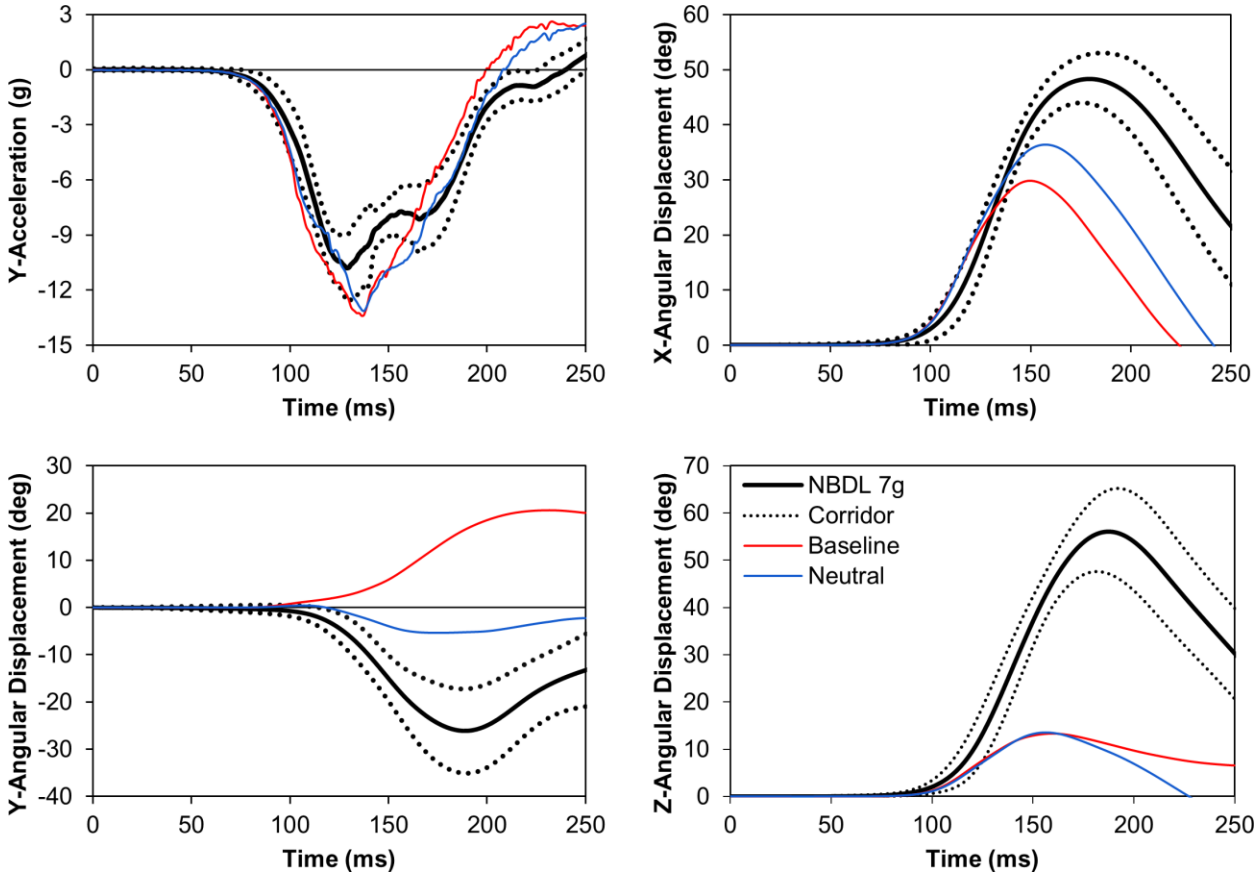

FIGURE 4-39: F05 7G LATERAL IMPACT HEAD CG: Y-ACCELERATION, X-ROTATION LATERAL FLEXION, Y-ROTATION SAGITTAL ANGLE AND Z-ROTATION AXIAL ROTATION VS NBDL RESPONSE

In general, the peak head rotation (lateral, sagittal, and axial) increased and occurred later with lower muscle activation levels (Figure 4-40). The head y-acceleration shape and magnitude were similar between activation schemes. The higher activation schemes resulted in an earlier occurrence of head movement than lower activation schemes. The upper bound activation scheme resulted in a maximum head lateral flexion angle of 31.7˚ (-13%) while the lower bound activation scheme resulted in 40.8˚ (+12.1%) when compared to the neutral activation scheme. All activation schemes resulted in head flexion except the baseline activation scheme. In general, activation schemes were more sensitive to head lateral flexion than head flexion and axial rotation.

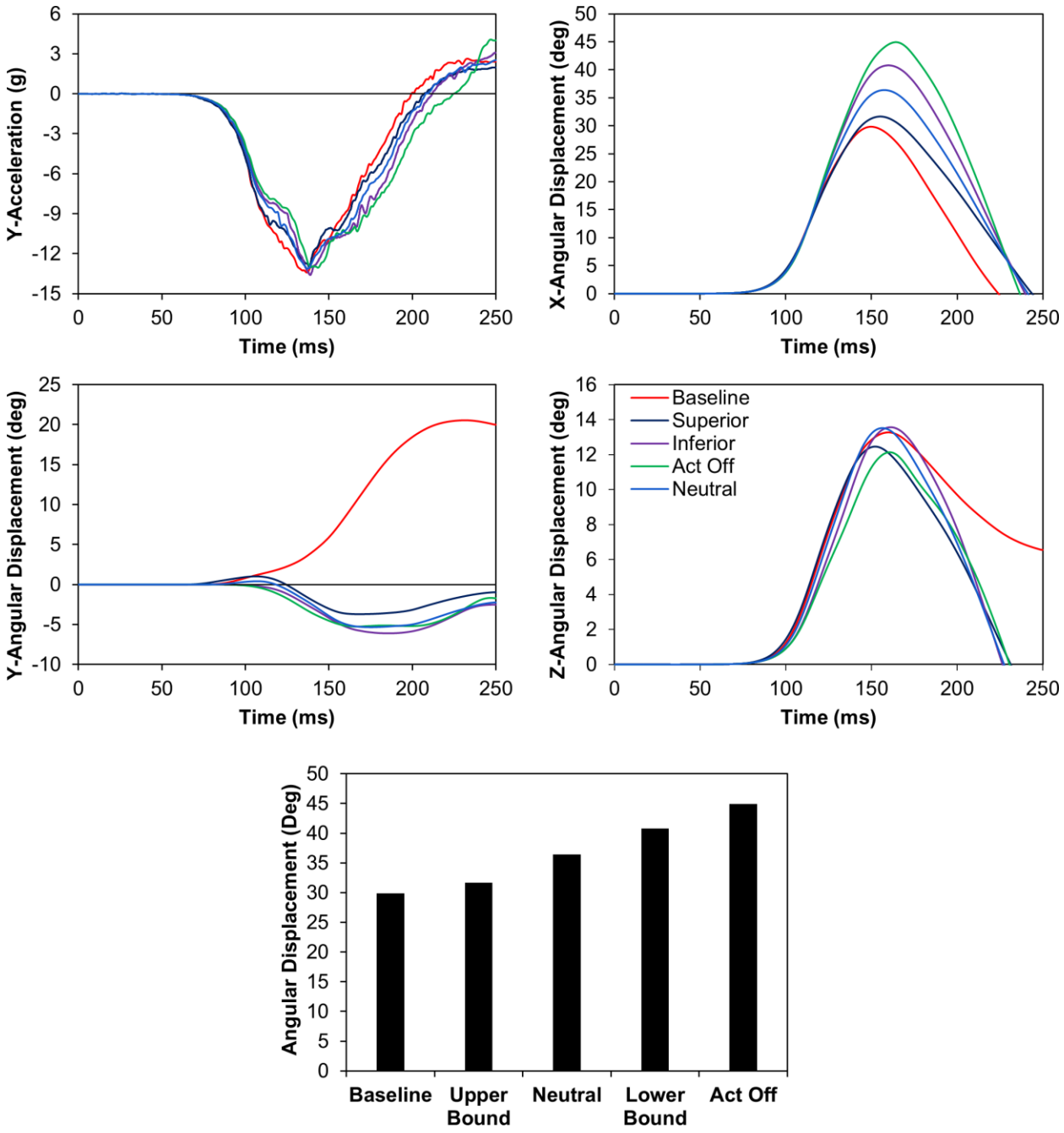

FIGURE 4-40: F05 7G LATERAL IMPACT HEAD CG: Y-ACCELERATION, X-ROTATION LATERAL FLEXION, Y-ROTATION SAGITTAL ANGLE, Z-ROTATION AXIAL ROTATION, MAXIMUM X-ROTATION ANGLE

Ligaments along the lateral aspect of the neck had the highest predicted injury risk based on ligament distraction. All ligaments except for the contralateral CL demonstrated low distractions that were within the toe region (Figure 4-42). A very small amount of bone failure was predicted based on hard tissue plastic

strain, at the C6 and C7 vertebrae ipsilateral facet surface. The tissues strains had a general trend to increase with lower activation levels, with lower cervical segment levels demonstrating larger strains.

The CL had the highest risk of injury during a lateral crash with a general trend of increased distraction with lower activations schemes and lower segment levels (Figure 4-41). The CL distractions entered the post-traumatic region at the C56 for the lower bound and act off schemes and the C67 levels for the neutral and lower activations schemes. The CL distraction entered the traumatic region at the C34 and C45 levels starting from the neutral and lower activation schemes. Both the C56 and C67 levels had CL distractions that were in the traumatic region regardless of the activation scheme. The upper bound activation scheme prevented the CL distraction from entering the traumatic region at the C34 and C45 levels.

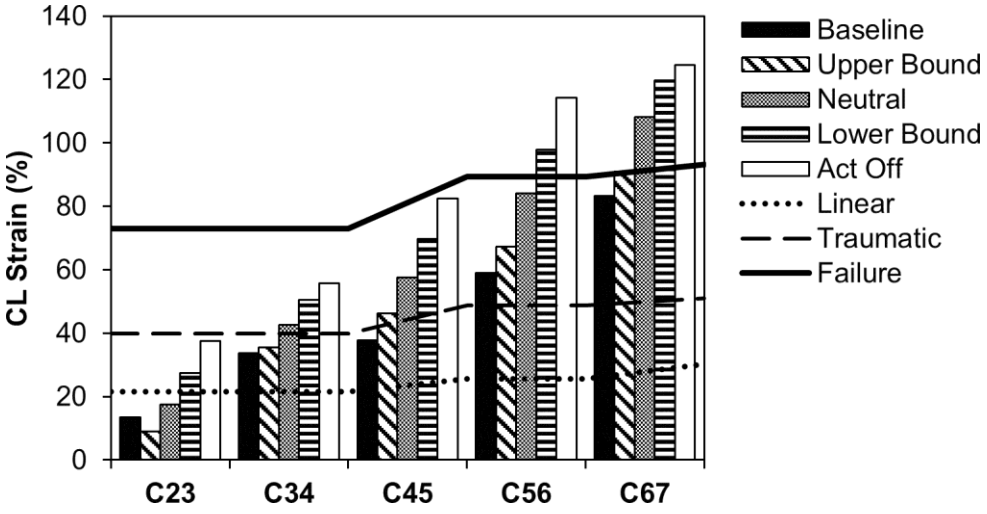

FIGURE 4-41: F05 7G LATERAL IMPACT CL STRAINS

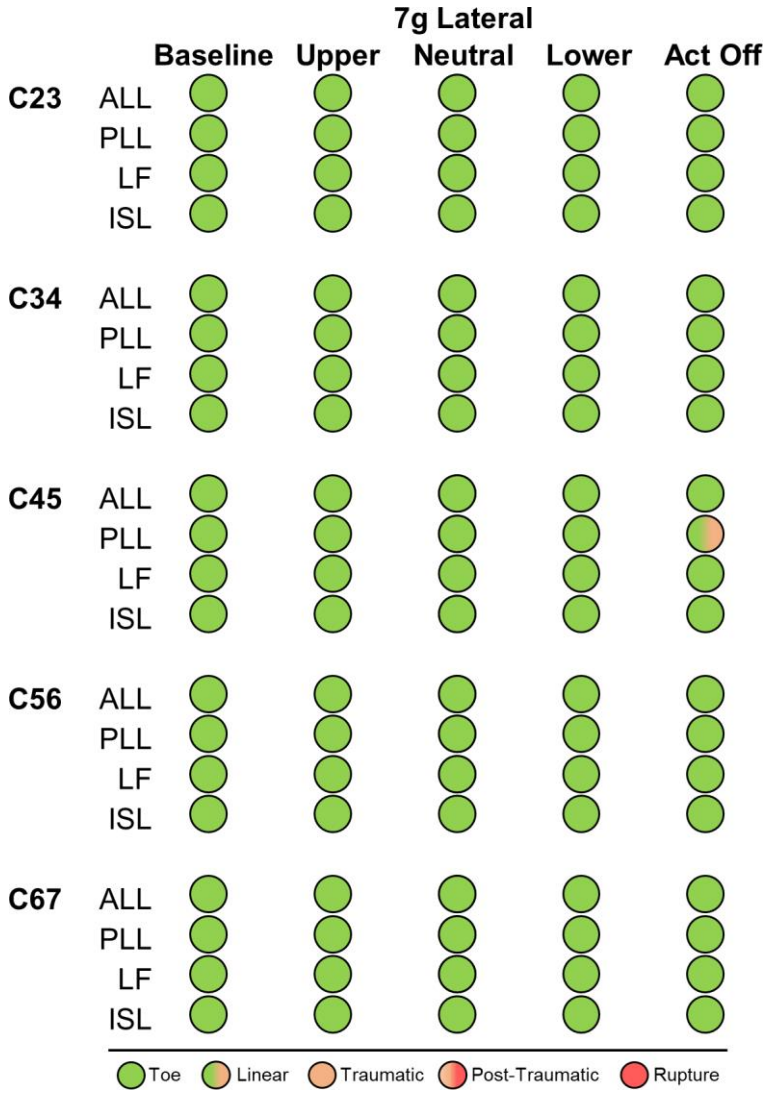

FIGURE 4-42: F05 7G LATERAL IMPACT LIGAMENT INJURY RISK SUMMARY

The IVF located on the ipsilateral side of impact had the greatest risk for nerve impingement due to reductions in IVF height and width (Figure 4-43). In contrast, the contralateral side demonstrated an increase in IVF height and width, therefore was not at risk for nerve impingement. The C67 reached the impingement threshold for all activation schemes when considering the height reduction. The IVF width reduction reached the threshold for the lower bound and activation-off scheme. In general, height reduction was below 2.5 mm and varied among segment levels but had an overall trend of decreasing with lower activation schemes. The IVF width reduction was decreased at the C23 and C34 levels with lower activation schemes but increased starting at the C45 and lower levels with lower activation schemes. Width reductions were generally consistent and were below 2.5 mm of reduction.

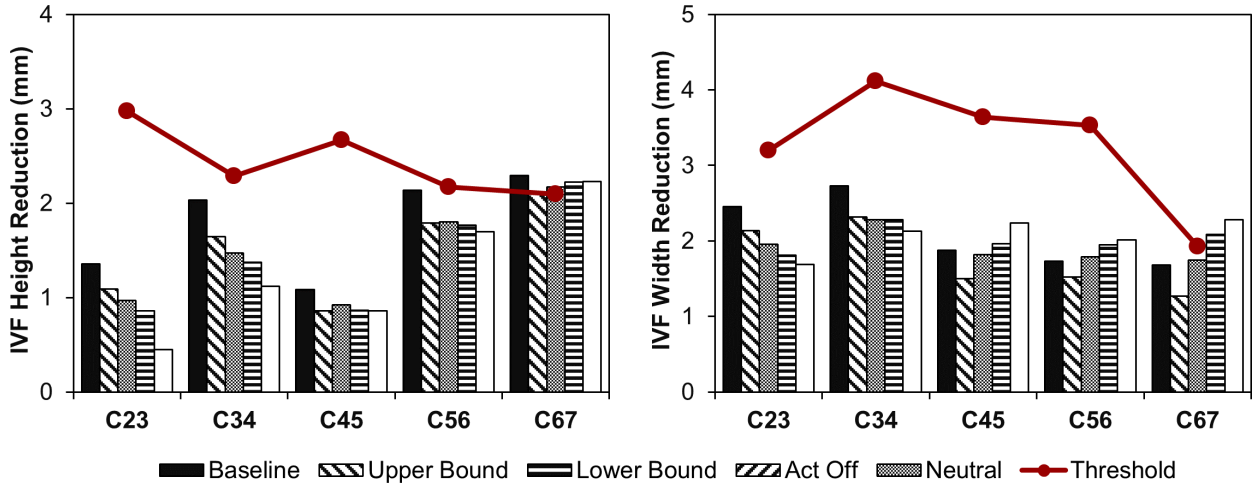

FIGURE 4-43: F05 7G LATERAL IMPACT IVF HEIGHT AND WIDTH REDUCTION

Quadrant Muscle Activation Investigation for Lateral Impact

The lateral acceleration, lateral flexion angle and axial rotation of the head were insensitive to lower ipsilateral muscle activation levels (Figure 4-44). The greatest effect was observed on the head sagittal angle, which increased with lowered ipsilateral muscle activation.

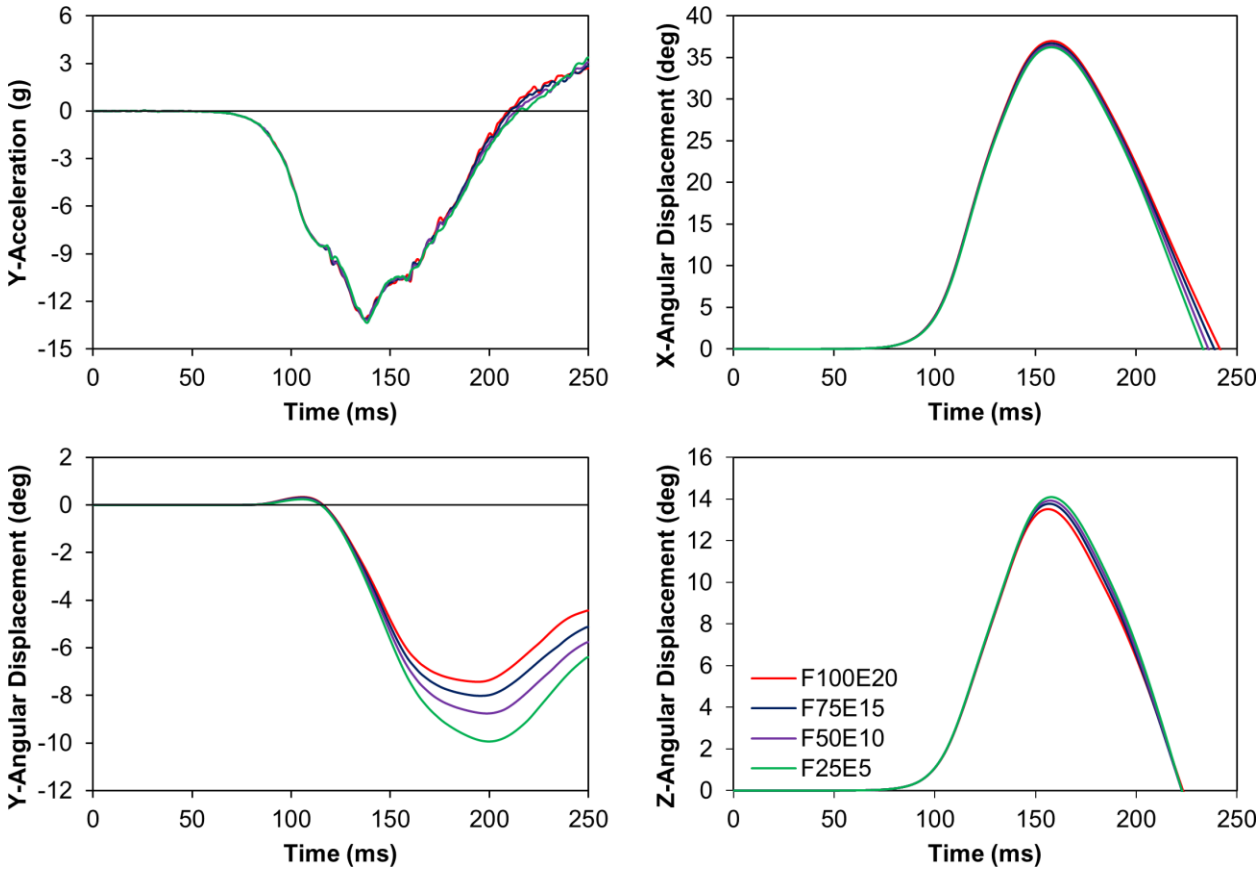

FIGURE 4-44: F05 7G LATERAL IMPACT QUAD SCHEME HEAD CG Y-ACCELERATION, X-ROTATION LATERAL FLEXION, Y-ROTATION SAGITTAL ANGLE AND Z-ROTATION AXIAL ROTATION

In general, ligaments strains increased with decreased ipsilateral activation in all segment levels except the C67 level (Figure 4-45). The activation level on the ipsilateral side did not affect the potential for injury for all ligaments. Both the IVF height and width reduction were reduced with decreased ipsilateral activation (Figure 4-46). The C67 level remained above the impingement threshold regardless of the ipsilateral activation level.

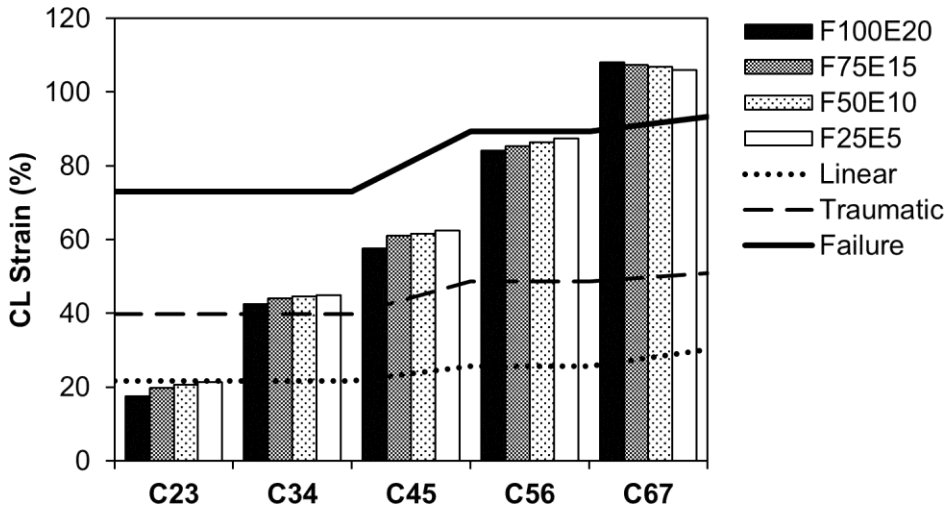

FIGURE 4-45: F05 7G LATERAL IMPACT QUADRANT SCHEME CL STRAIN

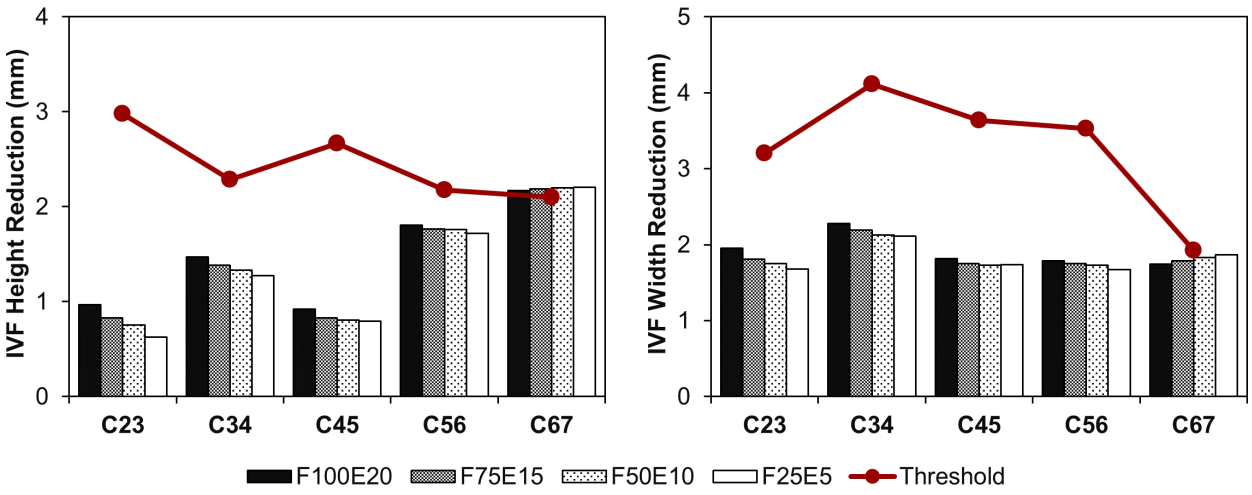

FIGURE 4-46: F05 7G LATERAL IMPACT QUADRANT SCHEME IVF HEIGHT AND WIDTH REDUCTION

CHAPTER 5: DISCUSSION

5.1 Open-Loop Neutral Muscle Activation Scheme Assessed using the M50 Neck Model

An improved open-loop muscle activation scheme was proposed in this study to provide a single activation strategy for the impact cases investigated. Open-loop control utilizes a pre-determined muscle activation curve with a specific activation onset time, maximum activation, and activation shape. The shape of the activation curve was preserved from previous studies (Panzer et al., 2011; Fice et al., 2011), while the onset time and activation levels were varied. Previously, the muscles of the neck were classified as flexors or extensors, and all muscles in each group received the same activation strategy. This was acknowledged to be an oversimplification for the complex muscle activation in the neck (Panzer et al., 2011; Fice et al., 2011), but provided a starting point for introducing muscle activation applied to frontal and rear impact. In the current study, the muscle groups were further discretized into quadrants to enable varying left-right activation levels for lateral impacts. The quadrant scheme was not used in the frontal or rear impact condition because motion occurred within the sagittal plane; however, the quadrant scheme was used to investigate unilateral muscle activation schemes for the lateral impact condition. The current model has four groups of muscles (flexor left, flexor right, extensor left, extensor right) that are activated synergistically at the start of an impact. Although the activation scheme is a simplification of muscle activation in-vivo, this approach can allow HBMs to estimate the muscle activation without the use of a closed-loop muscle activation scheme. The muscle activation scheme in an early version of the M50 model, described as the baseline muscle activation scheme, was applied for both frontal impacts (extensors: 100%, flexors: 100%, activation onset time: 74ms) (Panzer et al., 2011), and rear impacts (extensors: 70%, flexors: 100%, activation onset time: 74ms) (Fice et al., 2011) with the activation curve defined in Panzer et al., (2011). The baseline activation scheme was identified as a limitation due to the higher PCSA in the extensors when compared to the flexors, which caused the head to move into extension when the muscles were activated with no external load was present. It should be noted that all muscle activation schemes are somewhat model specific, owing to the stiffness of the surrounding tissues, cervical spine, and numerical aspects such finite element mesh size.

A closed-loop muscle activation scheme utilizes PID controllers to modulate muscle activation using external targets such as global head angle and joint reaction force. The activation of each muscle or muscle groups can therefore be individually varied and adjusted during the crash scenario with the feedback from

the external targets, and can potentially provide a more biofidelic representation of the neuromuscular response when compared to open-loop muscle control. Closed-loop muscle control has been implemented into HBMs (Östh et al., 2012; Kato et al., 2017), however there is currently no general consensus regarding the controller parameter values that are used in the implementation. The open loop control scheme was therefore pursued in the current study to investigate the fundamental effects of muscle activation on impact response and can serve as a baseline for future studies that will include a closed loop control scheme.

A new muscle activation scheme was developed for the current study, described as the neutral activation scheme that achieved two goals: addressing the extensor bias of the baseline activation scheme in the model, and providing one simple activation scheme that could be applied to all impact scenarios. The neutral activation scheme was developed with the target of minimizing head movement in flexion or extension, to maintain the head in a neutral posture when the muscles were activated with no externally applied loads (i.e. the T1 was held stationary). Previous studies have proposed 100% activation for the flexors (Panzer et al., 2011) because flexor activation was not sensitive to head forward rotation, while in a rear impact condition, the flexors were maintained at 100% due to the large contribution in constraining neck extension (Fice et al., 2011). The contribution of flexors and extensors in the lateral loading conditions are currently unclear, therefore future studies should investigate different activation ratios of the extensors and flexor muscles in response to rear and lateral impact conditions. In the current study, the flexors were assumed to activate at 100% while the activation level of the extensor was varied to achieve the optimization target of minimizing changes in both the Frankfort plane angle (i.e. line of sight) and head x-translational displacement from the initial head neutral position. The optimized result indicated an extensor to flexor ratio of 1:5 (extensors: 20%, flexors: 100%) was required to meet the optimization target. When the muscles were activated using the neutral activation scheme, the neck shortened due to the compressive force of the active muscles, and caused an increase in cervical lordosis but the head rotation and x-displacement was minimized. The M50 model includes a PCSA distribution of 70% extensors and 30% flexors, that would suggest an activation ratio of extensors to flexors of approximately 1:2.3, which was different from the 1:5 ratio from the optimization study. The large difference in the activation ratio was due to variations in muscle moment arms between the extensor and flexor muscles in the M50 model. EMG studies have demonstrated that the flexor and extensor muscle in the neck are co-contracted in unaware subjects that were subjected to low speed rear impact perturbations, and was hypothesized that this co-activation served to increase neck stiffness, therefore protecting the neck (Siegmund et al., 2003). It should be noted that the proposed neutral activation scheme was developed independent of the impact cases, hence the activation parameters were not tuned to fit the experimental responses. When applied to various impact conditions, the overall performance of the neutral activation scheme showed positive improvements to the head kinematic response

for all three impact directions compared to the baseline activation scheme, for both the M50 and F05 models.

In the 8g frontal impact condition, the baseline activation scheme over-constrained the neck flexion of the M50 model due to over-activation of the extensors (100% activation), which resulted in lowered head forward rotational displacement when compared to the average volunteer response (64% lower). The reduction of the extensor activation from 100% to 20% in the neutral activation scheme demonstrated a large improvement in the head forward rotation response of the model when compared to the average volunteer response (5.4% lower). The lower level of extensor activation reduced the neck flexion constraint of the baseline activation scheme and allowed for increased forward head rotation. The neutral activation scheme was considered to be more biofidelic due to the improvement in model response, compared to the volunteer response.

The neutral activation scheme was challenging to assess in the 7g rear impact condition because there was no volunteer response for high severity rear impact in the literature. Volunteer response data only exist for rear impacts with a severity limit of 4g maximum acceleration, which was found to not be relevant to injury risk for humans (Davidsson et al., 1996; Ono et al 1997; Ono et al 2006). Considering the model response in the current study, the 7g rear impact condition with the baseline activation scheme resulted in greater head rotational displacement when compared to the activation off scheme, which may be considered an unphysical response of the model when considering the muscles were activated. The increase in extension angle with the baseline activation scheme should not be expected when compared to the activation off scheme with the M50 model, and was due to the fully activated extensor muscles that exacerbated the head rearward rotation. The increase in head rotation angle with the baseline activation scheme was contrary to previous results (Fice et al., 2011), where the global head rotation angle was reduced with muscle activation when compared to muscle activation, and can be attributed to differences in the muscle origin and attachment points between the two different models. The neutral activation scheme reduced the head rotational displacement when compared to the activation off scheme which resulted in a better physical response compared to the baseline activation scheme. Although the head response of the M50 model was within the experimental corridor from Deng et al., (2000), these were PHMS responses and therefore did not enable a direct comparison with the current study, which included muscle activation. Future studies should investigate low severity rear impacts in order to directly compare the effect of muscle activation of the HBMs with the volunteer head kinematic response.

The 7g lateral impact condition with the baseline activation scheme demonstrated lower head lateral rotational displacement when compared to the average volunteer response (30% lower), and was attributed

to the neck moving into extension which correspondingly limits lateral flexion and axial rotation of the neck (facet joint contact in neck extension limits axial rotation); whereas neck flexion would increase lateral flexion and axial rotation. The average volunteer sagittal neck response was in flexion which indicated that the baseline activation scheme over-activated the extensor muscles in the M50 model. The neutral activation scheme addressed the over-activated extensor muscles, which resulted in neck flexion in the M50 model and correspondingly, increased the head lateral rotational displacement when compared to the baseline activation scheme. Therefore, the neutral scheme demonstrated positive improvements to the head lateral rotational displacement of the M50 model when compared to the average volunteer response (5.8% lower).

A parametric study was performed on both M50 and F05 models with the intention of improving the neck response of the models with the neutral activation scheme as a starting point. The activation level of the flexor and extensor muscles on the ipsilateral side was decreased in 25% decrements, which resulted in greater activation in the contralateral flexor and extensor groups, as evident in the experimental literature (Kumar et al., 2004a; Kumar et al., 2004b). The results of this study did not demonstrate a high sensitivity to improving the model response when comparing the neutral activation scheme to the reduced ipsilateral scheme (ipsilateral extensor: 5% activation, ipsilateral flexor: 25% activation,) for head lateral rotation (both model: 2% lower) and head axial rotation (M50: 6.3% higher, F05: 4.3% higher) because the activation of the contralateral muscles was maintained at 100% and was responsible for restricting lateral motion of the head to the ipsilateral side. The largest effect of decreasing the activation on the ipsilateral side was the increased head forward rotation angle for both models (M50: 33.8% higher, F05: 30.8% higher), which was attributed to the overall reduction of the extensor muscle activation on the ipsilateral side (from 20% to 5% activation). Future studies should be conducted on lower severity side impact scenarios to investigate the sensitivity of head lateral flexion response to decreased ipsilateral neck muscle activation.

The default activation onset time for both the M50 and F05 models was set at 74 ms, as proposed by Panzer et al., (2011) and Fice et al., (2011), and was in good agreement with the literature (Table 3-5), as 74 ms was within the reported literature range of 55 ms to 110 ms, and was comparable to the calculated average of the experimental literature of 78 ms. The upper and lower bound values for the activation onset time were based on the calculated standard deviation of the onset times in the literature, which was approximately ±20% of the average time. The upper and lower bounds used in this study were 90 ms and 60 ms respectively, which was a reasonable assumption because it was both within the range of onset times reported in the literature and was scaled to approximately represent one standard deviation of the baseline activation onset time of 74 ms, as calculated from the activation onset time range found in the literature.

The baseline neck PCSA in the M50 model was based on experimental measurements on 50th percentile male volunteers presented by Knaub et al., (1998), while the F05 PCSA values were scaled down from the M50 PCSA using neck regional dimension scaling factors (Shams et al., 2003). The upper and lower bound values of the PCSA (±30%) were used to represent the variation of muscle PCSA in the population and was calculated based on the muscle volume differences between the 50th percentile male, 5th percentile female and 95th percentile male volunteers. The 95th percentile male had on average 72% greater muscle volume than a 50th percentile male, while the 5th percentile female had on average 77% smaller muscle volume than the 50th percentile male subjects. The upper and lower bound scaling value of ±30% was selected to be within the volumetric difference between the 5th percentile female and 95th percentile male. The same PCSA scaling factor of (±30%) was applied to the F05 model, and was a reasonable assumption to ensure that the upper bound PCSA would not exceed the volumetric difference between the 5th percentile female and 50th percentile male volunteers.

The upper bound and lower bound activation scheme was created based on the neutral activation scheme to represent the upper and lower bound of PCSA and activation onset time to reflect the variation in the population. The lower bound activation scheme combined the low PCSA (-30%) and high activation onset time (90 ms) to represent the lower bracket of the population with lower and slower muscle activation. Conversely, the upper bound activation scheme combined the high PCSA (+30%) and low activation onset time (60 ms) to represent the upper bracket of the population with higher and faster muscle activation levels. Overall, both M50 and F05 models demonstrated low variations in head rotational displacement (<20%) when compared to the default PCSA and activation onset time. The M50 model demonstrated the lowest sensitivity to the variation of PCSA and activation onset time for the 7g rear impact condition (lower bound: +3%, upper bound: -3%), which indicated that variations in muscle activation force and activation onset time would result in the least difference for the head kinematic response. The flexors are the dominant muscles that restrict neck extension when activated, and the initially lower PCSA of the flexors received less scaling when compared to the extensors and hence, the head rotation response would be less sensitive. Conversely, the 7g lateral impact condition demonstrated the largest change in head lateral rotational displacement (lower bound: +15%, upper bound: -18%), which would indicate that variations in the population will more likely affect the head kinematics in a lateral impact scenario. The high sensitivity can be explained by the scaling of the extensor, which affected the sagittal plane motion of the model, hence higher neck flexion resulted in higher lateral neck flexion and the opposite for neck extension. The 8g frontal impact condition had head forward rotational displacement sensitivity between the 7g rear and 7g lateral impact condition (lower bound: +11%, upper bound: -9%). The frontal impact was more sensitive than the rear impact condition because scaling the extensors had a larger effect on the kinematic outcome

because of the higher PCSA magnitude of the extensors when compared to the flexor, and thus was more effective at limiting neck flexion. Another interesting finding was that although the extensor and flexor PCSAs were scaled equally, the resultant moment produced by the extensors and flexors did not scale linearly, due to differences in muscle moment arms, which could explain the higher sensitivity in the frontal and lateral impact case; both of which are extensor dependent. The F05 model demonstrated the same trends as the M50 model, however the sensitivity was generally the same or lower for all impact directions, attributed to the initially lower baseline muscle PCSA, which could suggest that smaller statures have lower sensitivity to musculature assessed by variations in kinematics response.

5.2 Evaluation of Soft Tissue Injury Risk

The potential for injury risk of the ligaments in the cervical spine was evaluated by quantifying the maximum ligament distraction and converting to strain for each ligament during the impact. The maximum distraction of each ligament was then compared to experimental ligament force-displacement curves, which were taken from a study by Mattucci et al., (2012). The ligament force-displacement curve has a characteristic sigmoidal shape (Mattucci and Cronin 2015) that was divided into five distinct response regions: toe region, linear region, traumatic region, post-traumatic region, rupture region (Figure 3-13). Ligament distractions from the model and transitional displacements in the ligament force-displacement curve were converted to strains using the neutral lengths of the ligament from the literature (Table 3-9, Table 3-10). The transitional strain between each region were used as thresholds to determine the injury risk of the ligament. If the ligament strain was within the toe region or linear region, the ligament was determined to be within the physiological loading range, where there was a low risk of injury. A high risk of injury was therefore categorized if the predicted ligament strain exceeded the linear region threshold, therefore moving beyond the physiological range. At the end of the linear region, the ligament stiffness transition from constant stiffness to a state of decreasing stiffness and is referred to as the traumatic region. The traumatic region represents the accumulation of damage within the ligament (Yoganandan et al., 2001; Yoganandan et al., 1988), where microdamage at the ligament fiber level may occur, while damage cannot be observed macroscopically (Nordin and Frankel, 2001). Within the traumatic region, a pain response is likely to be present, along with potential joint instability due to decreased ligament stiffness, although the ligament remains grossly intact (Cronin, 2014). Past the traumatic region is the post-traumatic region, where bundles of collagen fibers begin to rupture in a progressive manner, until the ligament is fully transected and can no longer support any load (DeWit and Cronin, 2012). There are currently no directly measured pain thresholds available for cervical spine ligaments in humans. It is therefore challenging to predict a pain response using FE models because there is no quantifiable injury metric such as strain, in relation to

potential pain response for humans. The association of ligament distraction and pain has been explored in the context of sub-traumatic injuries in the CL using animal models (Lu et al., 2005; Lee et al 2004; Lee et al 2008), specifically the study conducted by Lu et al., (2005), which monitored afferent nerve signals during CL ligament elongation. In-vivo caprine models demonstrated a low firing threshold beginning at 10% strain, that reached saturation at 38.8% strain, and a high strain threshold at 46% strain. The low strain threshold (10% to 38.8%) was hypothesized to be the activation of mechanoreceptors, while the high strain threshold beginning at 46% was hypothesized to be the threshold for nociceptor activation. A direct comparison of the caprine strain threshold for mechanoreceptor and nociceptor activation was made with the CL force-displacement response curve in the M50 model (Figure 5-1). It was acknowledged that distinct biological and anatomical differences exist between humans and animals, however the relationship of pain thresholds and ligament strain in this context can be used to provide an estimated interpretation on otherwise non-obtainable thresholds for in-vivo humans. The low threshold strain threshold (10% to 38.8%) corresponded to the toe and linear response region of the ligament, which indicate that mechanoreceptors are active within the physiological range of motion for the CL. The nociceptor activation threshold of 46% strain corresponded to the end of the linear region, before the transition into the traumatic region. Pain is a physiologic response that activates to protect the body from injury or to prevent further injury. The pain threshold at the end of the linear region is a reasonable assumption because nociceptors activate before injury occurs (Costigan et al., 2009). The end of the linear response region may therefore be attributed to the pain threshold by utilizing the ligament response curve. Therefore, the current method of quantifying the injury risk based on the traumatic region of the ligament force-displacement curve is a reasonable assumption for the onset of injury and pain response.

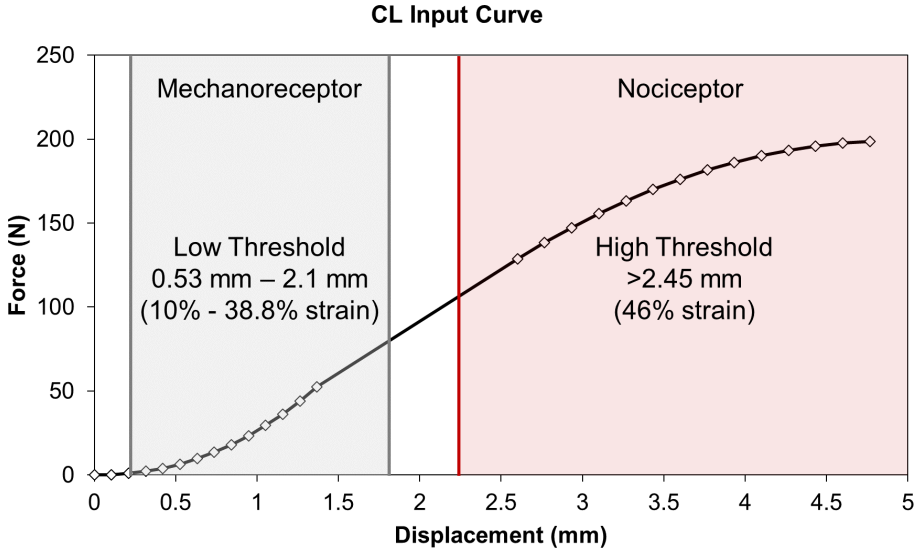

FIGURE 5-1: ESTIMATED CL PAIN THRESHOLD USING CAPRINE MODEL OF PAIN (LU ET AL., 2005)

The injury risk for transverse compression of the nerve root and ganglia was quantified by monitoring the maximum reduction of the IVF height and width at the foraminal medial zone. The IVF height and width dimension that was monitored in the M50 and F05 models for each cervical vertebral level was based on the methodology used in PHMS experiments that investigated spinal nerve injury through hard tissue compression (Panjabi et al., 2006; Tominaga et al., 2006; Ivancic et al., 2012). The method used in the current study and previous PHMS experiments only accounted for nerve root compression based on hard tissue relative motion and did not include potential interactions with the soft tissues found within the IVF. In the current study, an injury threshold was calculated for each spinal nerve (C3 to C7) that corresponded to the IVF from the C23 to C67 vertebral segment by subtracting the IVF height and width of the M50 and F05 models (in the neutral posture) to the height and width of the dorsal root ganglion and ventral root complex, as measured in the experimental literature (Alleyne et al., 1996). If the maximum IVF height or width reduction in the M50 or F05 model exceeded the threshold, a risk of spinal nerve injury was possible (Panjabi et al., 2006; Tominaga et al., 2006; Ivancic et al., 2012). The injury threshold for impingement is therefore sensitive to the IVF height and width of the cervical spine in the neutral position. In the above-mentioned PHMS studies, the neutral IVF height and width measurements were based on experimental averages from other sources of literature (Table 5-1). In general, the neutral IVF height and width dimensions used in the experimental studies were lower when compared to the neutral IVF height and width that was measured in the M50 and F05 models. The resulting thresholds that were calculated based on the IVF morphology of the M50 and F05 models were greater than the thresholds proposed in the literature (Table 5-2). At this time, there are no available data on the dorsal root ganglion and ventral root complex dimensions with respect to stature or gender. Therefore, for the current study, the M50 model had higher calculated threshold values when compared the F05 model due to the reduced neutral IVF height and width dimensions, due to the smaller stature of the F05 model.

TABLE 5-1: IVF HEIGHT AND WIDTH DIMENSIONS OF THE M50 AND F05 MODELS COMPARED WITH THE EXPERIMENTAL LITERATURE

Dimension (mm)	C23	C34	C45	C56	C67
IVF Height					
Literature	9.1	8.3	8.8	9.0	9.1
M50	13.0	10.4	11.5	11.4	9.8
F05	8.28	7.39	8.47	8.77	9.4
IVF Width					
Literature	6.2	5.5	5.8	5.9	6.0
M50	8.8	8.4	9.6	8.7	6.8
F05	7.0	7.5	7.4	7.9	7.6

TABLE 5-2: IVF HEIGHT AND WIDTH THRESHOLD BASED ON THE M50 AND F05 MODEL, COMPARED WITH THE EXPERIMENTAL LITERATURE

Threshold (mm)	C23	C34	C45	C56	C67
IVF Height					
Literature	3.8	3.2	3.0	2.4	1.8
M50	7.7	5.3	5.7	4.8	2.5
F05	3.0	2.3	2.7	2.2	2.1
IVF Width					
Literature	2.4	2.1	2.0	1.5	0.3
M50	5.0	5.0	5.8	4.3	1.1
F05	3.2	4.1	3.6	3.5	1.9

5.3 Frontal Impact Response and Potential for Injury Risk

5.3.1 M50 Injury Risk

In the 8g frontal impact condition with the neutral muscle activation scheme, hard tissue failure and disc avulsion injuries were not predicted by the model, in agreement with the NBDL test data where no such injuries were reported. The intervertebral foramen height and width reduction were negligible and therefore a low injury risk to the nerve roots was predicted, and was similar to experimental measurements of IVF dimensions, where flexion caused the foraminal area to increase (Muhle et al., 2001; Kitagawa et al., 2004). The model predicted larger strains for ligaments that were located along the posterior region of the neck (PLL, LF, ISL) and lower strains for the ALL, as expected. The model predicted the highest potential injury risk to the ISL, where post-traumatic failure was predicted at the C67 level. The anterior portion of the CL demonstrated high strains in the C45 and C56 levels, where the ligament distractions were in the traumatic region of the ligament response curve. These CL strains were much higher when compared to PHMS experiments (although the highest strain was located at the posterior aspect of the facet joint) was not observed in the experimental literature where linear strains of the CL were measured (Panjabi et al., 2004). One reason for the observed high strains in the CL during the frontal impact condition can be due to the non-physiologic gap that is between the facet cartilages of the model. During neck flexion, the gap between the facet cartilage surfaces would first need to close before contact occurs. The additional relative motion of the superior vertebra to the inferior vertebra (increased anterior shear), in order to close the gap resulted in the increased strain in the posterior region of the CL, compared to the experimental literature (Figure 5-2).

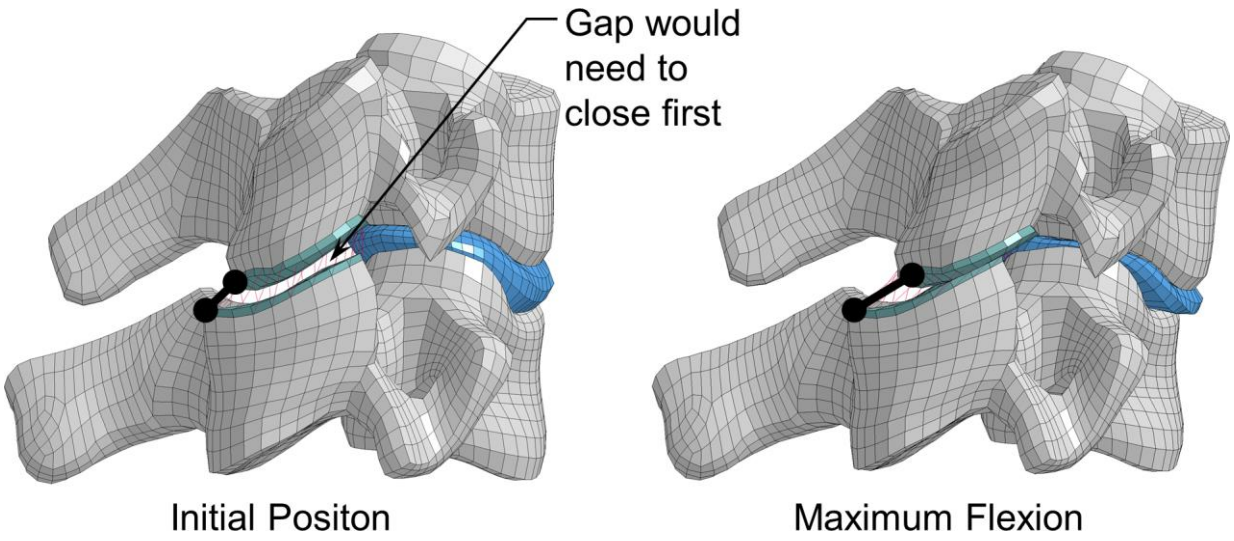

FIGURE 5-2: FACET JOINT GAP CAUSING INCREASED CL STRAIN IN FLEXION

5.3.2 F05 Injury Risk

The F05 model did not predict disc avulsion failure or hard tissue fracture for the 8g frontal impact condition with the neutral activation scheme, in agreement with the NBDL test data where no such injuries were reported. The intervertebral height and width reduction were minimal and therefore, a low risk of impingement of the spinal nerve was predicted. The ligaments that are located in the posterior region of the neck sustained the highest strains when compared to the anterior ligaments because the posterior ligaments such as the ISL are primarily responsible for restricting the flexion motion of the neck. Thus, the ISL sustained the largest strain during the frontal impact, with the C56 and C67 vertebral levels being the most likely to be injured due to strains entering the traumatic and post-traumatic regions of the ligament response curve. The post-traumatic response of the C67 ISL may be due to the boundary condition that is applied directly to the T1, causing higher strains in tissues in the vicinity of the applied boundary condition. The effect of the boundary conditions could be investigated in the future using a full HBM integrated with a restraint system and sled environment. The CL sustained the largest strains in the posterior region of the facet joint. Although no failure (post-traumatic) occurred, traumatic failure of the CL was predicted for the C67 vertebral levels. The high strains observed in the CL may be attributed to the gap between the cartilage in the facet joints, for the same reasons in the M50 model. Another contributing factor to the high strains could be due to the boundary condition that was applied directly to the T1, causing stress concentrations in the connective tissue in the lower vertebral levels.

5.3.3 Comparison of Injury Risk between M50 and F05

In general, both the M50 and F05 models demonstrated similar kinematic responses that were comparable to the volunteer experiment, in addition to similar tissue-level responses. Although the literature has suggested that females are more susceptible to injury than males, the differences in injury risk observed for the frontal impact condition was minimal. One distinct difference was the faster initiation of the F05 head forward rotation and acceleration, which could be due to the smaller stature of the female (shorter neck and smaller head mass). A shorter neck would cause the head to move sooner, and a lower head mass would result in an earlier onset of movement for the same T1 acceleration profile. The total head rotation between the M50 and F05 model was roughly the same (<0.5% difference), which indicated that the smaller stature of the F05 model and the reduced ligament properties and PCSA resulted in a similar kinematic outcome. Both the M50 and F05 models predicted the ISL to have the greatest injury risk in the frontal impact condition. Traumatic failure was predicted in the ISL for the C34 or lower vertebral levels in the M50 model, while the F05 model predicted traumatic failure starting at the C56 and lower levels. The increase in injury severity for the M50 model at the C34 and C45 ISL resulted from greater flexion in those vertebral levels and could be due to a combination of the increased head mass and the greater neck length of the M50 The IVF height and width reductions were negligible in both M50 and F05 model which indicated that nerve root and ganglion injuries from transverse compression are unlikely to occur from a frontal impact condition and an overall low risk for injury from an 8g frontal impact was observed. This was reasonable as the publications of the NBDL experiments did not document any volunteers that experienced injuries or symptoms of pain despite being subjected to a frontal impact of up to 15g maximum acceleration.

5.4 Rear Impact Response and Potential for Injury Risk

5.4.1 M50 Injury Risk

The M50 model with the neutral activation scheme in the 7g rear impact loading condition did not predict bone failure or disc avulsion injuries. The IVF height and width reductions were greater than the frontal impact condition but did not reach the impingement threshold. PHMS experiments that investigated the potential for nerve compression for a rear impact indicated that the C56 and C67 vertebral levels were at the greatest risk for impingement from the IVF width reduction (Panjabi et al., 2006). The maximum width reduction of the M50 model (C56: 0.4 mm, C67: 0.65mm) was lower than the measured PHMS width reductions from Panjabi et al., (2006) (C56: 1.7 mm, C67: 1.2mm). The higher impingement values

observed from the PHMS experiment were attributed to the lack of muscle activation, and reduced passive stiffness from using an osteoligamentous whole cervical spine, instead of a whole cadaveric neck. The ALL and CL are the primary ligaments that limit the extension and shear motion in the neck (Yoganandan et al., 2001; Ivancic et al., 2004; Pearson et al., 2004). The model predicted the largest strains in the ALL and CL but did not indicate potential for injury since the strains were all within the toe region of the ligament response curve. In the experimental literature, the ALL and CL are commonly associated with damage through strain measurements during PHMS whiplash experiments (Deng 2000; Ivancic 2004; Pearson et al 2004). Simulated rear impacts were undertaken with PMHS using similar maximum accelerations as used in the current study and indicated that the CL was at risk for injury due to large strains of 20% to 60%, which is in the range of sub-catastrophic failure (traumatic region) (Winkelstein et al., 2000; Siegmund et al., 2001). For the M50 model in the current study, the CL strain was within the toe-region of the ligament response curve at all vertebral levels, which was much lower than the strain calculated from the rear impact PHMS experiments. There are two possible reasons for the low CL strain in the model, the facet joint gap and the numerical ligament implementation. The facet joint gap that is present between each facet joint was larger than reported in the literature (Womack et al., 2008) and was attributed to differences in cartilage thickness and shape. The larger facet joint gap could reduce the observed ligament strains because the joint gap first decreases in rear impact loading, effectively shortening the ligament, and relative sliding to increase ligament distraction only occurs after the facet joint gap is closed. Modeling the correct facet joint gap is an important consideration in rear impacts because both extension and posterior shear will occur and can influence the CL strain. If the facet joint gap was smaller, the cartilage would contact sooner and initiate sliding sooner, which would increase the CL strain in rear impact scenarios. The low CL strains can also be attributed to the 1-D tension only element ligament implementation in the model. The 1-D elements are unable to capture transverse shear, as the elements are free to rotate about the nodal connections. One example where the strains are under-predicted is during sliding of the facet joint, where the joint is sliding but strains are not captured because the 1-D elements will simply pivot about their respective nodal connections, without any increase in linear strain. This concept was demonstrated experimentally when linear strain measurement resulted in three times less strain when compared to using a 3-D strain field measurement of a ligament under distraction (Holsgrove et al., 2016). Another disadvantage of using 1-D tension only elements is the inability to model contacts and interactions with the surrounding hard tissues. The 1-D tension only elements will always form a straight path between the nodal connections and do not wrap around the surface of the hard tissue during joint distraction, which can lead to an under-prediction of ligament strains. These two factors are known limitations that exist in the M50 neck model and therefore, the prediction of the CL strains are likely to be underestimated.

5.4.2 F05 Injury Risk

Hard tissue failure and disc avulsion failure did not occur for the F05 model in the 7g rear impact condition with the neutral activation scheme. In general, the IVF height and width reduction increased towards the lower vertebral levels, although the impingement threshold was not exceeded. On the contrary, the C56 and C67 vertebral levels were identified to have the highest risk for impingement (Panjabi et al., 2006). When comparing the F05 IVF width reduction to PHMS experiments, the F05 model (C56: 0.67 mm, C67: 0.8 mm) was lower than the measured PHMS width reductions from Panjabi et al., (2006) (C56: 1.7 mm, C67: 1.2mm), and can be attributed to lowered tissue stiffness from using an osteoligamentous cervical spine specimen and a lack of muscle activation. The ALL and CL experienced the largest strains when compared to the other ligaments. However, the predicted strains were all within the toe region of the ligament response curve, which indicated that no injury would occur from a 7g rear impact. As mentioned above, this result must be taken with caution because the current implementation of the CL and simplified facet cartilage may cause under prediction of the CL strains. One important difference between the F05 and M50 model was the planar facet cartilage profile of the F05 model (Figure 5-3), compared to the curved facet cartilage of the M50, which implicated a larger facet joint gap in the F05 model (Table 5-3).

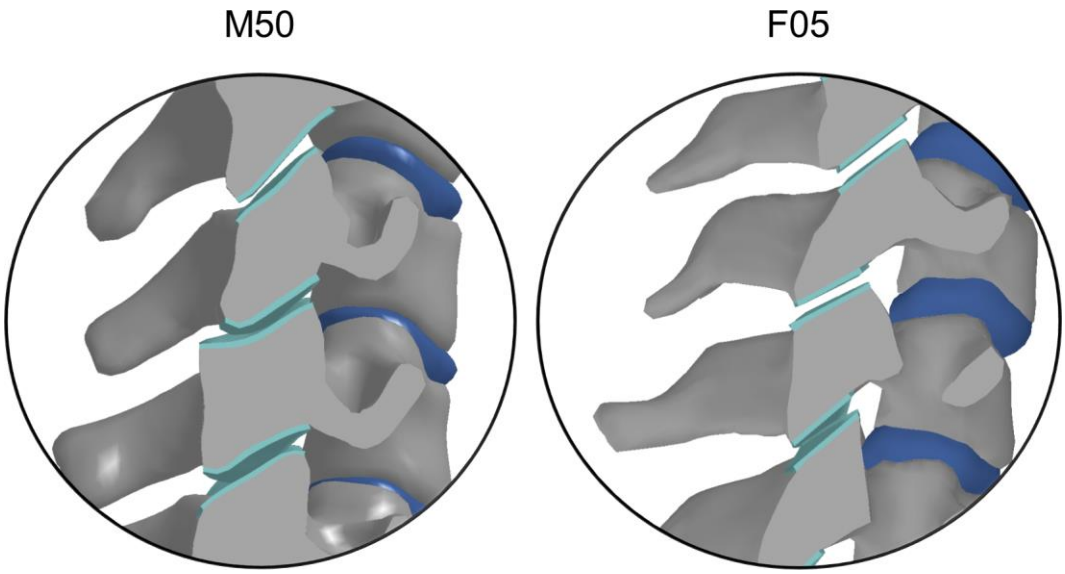

FIGURE 5-3: FACET JOINT CARTILAGE PROFILE FOR M50 (CURVED) AND F05 (PLANAR) MODEL

TABLE 5-3: FACET JOINT GAP (mm) FOR THE M50 AND F05 MODEL

Model	C23	C34	C45	C56	C67
M50	1.1	0.8	0.9	0.9	0.8
F05	1.0	1.3	1.1	1.3	1.0

5.4.3 Comparison of Injury Risk between M50 and F05

In general, the F05 model had higher levels and quicker onset of head acceleration, and greater head rotation when compared to the M50 model in a 7g rear impact, which is consistent with the experimental literature in rear impacts (Sato et al., 2014; Carlsson et al., 2008; Carlsson et al., 2012). In contrast to the epidemiological literature, which indicated females having a greater risk of injury, the F05 model predicted similar tissue-level response to the M50 model and did not predict injury risk based on the ligament distractions and IVF space reduction. Both M50 and F05 model predicted ALL distractions that were within the toe region, which did not indicate a high risk of injury. Rear impact PHMS experiments observed damage to the ALL following maximum accelerations (4.5 g to 8g), with large strains of up to 29% in the lower vertebral levels, compared to the low strains (<10%) predicted by both the M50 and F05 models. The difference in the predicted injury risk between the current study and the PHMS experiment can be attributed to the lack of active musculature and lowered passive tissue stiffness from using an osteoligamentous specimen. For the reasons mentioned above, the findings from this study suggest that, in the rear impact condition, the current ligament implementation using 1-D tension only element was not able to accurately predict the CL strains and therefore the potential for injury risk. An alternative method where injury risk could be inferred from facet joint kinematics (shear and compression of the superior facet with respect to the bottom facet using a local coordinate system (Figure 5-4) was used to compare the M50 and F05 models, following the methodology of Ivancic et al., (2004).

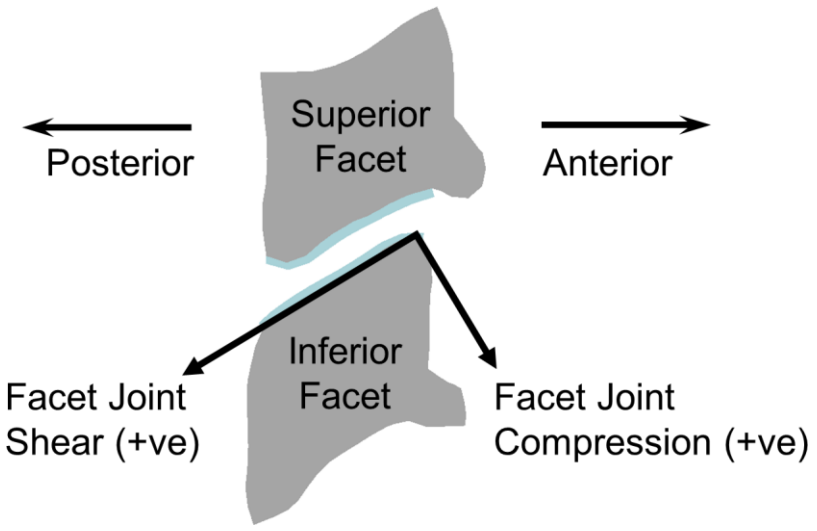

FIGURE 5-4: LOCAL COORDINATE SYSTEM ON THE INFERIOR FACET

The local facet kinematics of the mid and lower cervical vertebral levels demonstrated greater facet joint shear in the F05 model when compared to the M50 model, while the opposite was true when comparing facet joint compression (Figure 5-5). The present results indicated a negative correlation between the facet joint shear and facet joint compression. The opposite correlation between facet posterior shear and facet compression was however observed in the PHMS experiments performed by Ivancic et al., (2004), which could be due to differences in facet joint gap morphology between the M50 and F05 models with the PHMS specimens, and the lack of active musculature. The initial observation of increased facet joint shear with decreased facet joint compression may be related to the cartilage gap, which suggest that lower facet joint compression may result in higher posterior shear displacement in the facet joint in dynamic events. If the facet joint gaps were decreased, the facet contact would initiate sooner and result in increased posterior translation, hence the greater facet joint shear. In general, the facet joint shear for both the M50 and F05 model was within the lower range of maximum distraction measured in the rear impact PMHS experiments (Ivancic et al., 2004) (2.3 mm to 5.4 mm) with a maximum acceleration of 6.5g and 8g.

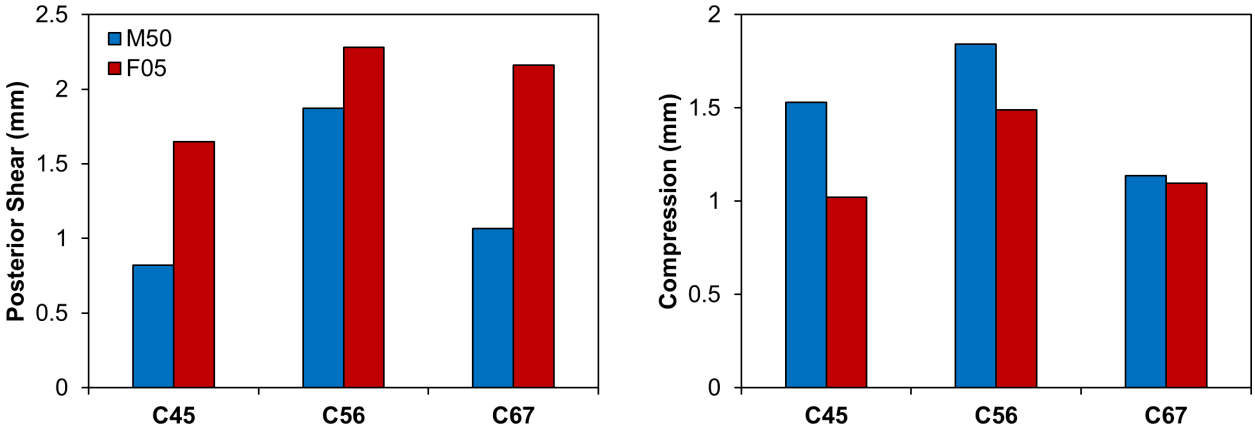

FIGURE 5-5: FACET JOINT LOCAL KINEMATICS: POSTERIOR SHEAR AND COMPRESSION FOR REAR IMPACT LOADING (DISPLACEMENT OF TOP FACET WITH RESPECT TO THE FIXED LOCAL COORDINATE SYSTEM ATTACHED TO THE BOTTOM FACET)

PHMS experiments have indicated a high risk of ganglia impingement in the lower cervical spine from rear impacts (Panjabi et al., 2006; Tominaga et al., 2006; Ivancic et al 2011). The M50 and F05 models; however, did not exceed the impingement threshold in the rear impact case considered, but had higher distractions compared to the frontal impact condition. It should be noted that the risk of impingement is highly dependent on the height and width of the intervertebral foramen when the neck is in the neutral position. The values that were used in the above-mentioned studies used IVF dimensions that were obtained from averages of multiple literature sources, which was less when compared to the IVF dimensions used in the current study that were based on the IVF height and width of the M50 and F05 model in the neutral

position. The smaller IVF dimensions used in the experiments would therefore predict a higher likelihood of injury due to the smaller thresholds.

Epidemiological data has suggested that rear impacts in the range of 6g to 7g mean acceleration (12g to 14g maximum acceleration) will result in acute WAD symptoms, and have a high risk of >80% to develop long term symptoms (Krafft et al., 2002). The 7g maximum acceleration used in this study, which corresponds to approximately 3.5g mean acceleration suggests a 40% risk to develop acute WAD symptoms, and a low <10% to develop chronic symptoms (Krafft et al., 2002). Volunteer rear impact experiments have been performed up to 4g maximum acceleration (2g mean acceleration) (Krafft et al., 2002) without any reports of injuries from the volunteers (Davidsson et al., 1996; Ono et al 1997; Ono et al 2006). The injury risk from the above epidemiological study suggests that the 7g maximum acceleration pulse used in this study is located in the transitional zone of an injury risk curve between no WAD injury and WAD injury certainty. Future work should investigate a spectrum of severities ranging from low to high in order to determine tissue level injury thresholds in more detail.

5.5 Lateral Impact Response and Potential for Injury Risk

5.5.1 M50 Injury Risk

The M50 model did not predict disc avulsion injuries but did predict high stresses in the hard tissues in the 7g lateral impact condition with the neutral activation scheme. A very small amount (<1% by volume) of bone failure was predicted to occur at the vertebrae C6 and C7 vertebrae on the ipsilateral facet surface. Although the hard tissue strain exceeded the threshold strain for fracture, the areas of failure were very localized due to bone to bone contact and variations in the vertebral geometry and was not attributed to a large-scale fracture. All ligaments in the lower cervical spine except the CL demonstrated low strains and a low injury risk was predicted because the other cervical spine ligaments are anatomically oriented along the neutral axis of the cervical spine during the lateral bending motion. The CL had the highest lateral eccentricity because it is situated furthest away from the neutral axis of bending, which will cause it to have the highest strains. The ipsilateral facet joint underwent compression while the contralateral facet separated during lateral bending and resulted in high strains in the CL. All vertebral levels had CL distractions in the traumatic region except for the C34 and C45 vertebral level, which were in the post-traumatic region. This indicates that all vertebral levels in the cervical spine are at risk for contralateral CL injury especially the C34 and C45 levels. The facet joint gap in the M50 model may attribute to increased ipsilateral facet compression, which would increase the facet joint separation on the contralateral side. If the facet joint gap

was decreased, then the model would predict lower CL strains due to the lowered contralateral facet separation, and would imply that the current model may be over-predicting the injury on the contralateral CLs. Future studies should investigate the effect of the facet joint gap on the risk of contralateral CL injury. Transverse compression of the nerve root and ganglion were highest in the lateral loading condition relative to frontal and rear impact, with the ipsilateral IVF demonstrating the largest reductions in foraminal height and width. The IVF height reduction was consistently greater than 2 mm, which was larger when compared to extension motion of the neck (Panjabi et al., 2006). Nerve root impingement was predicted to occur at the C67 level as the IVF height reduction exceeded the proposed impingement threshold. Injury to the nerve roots and ganglion through transverse compression are commonly present in contact sport athletes after exposure to lateral neck flexion, or combine lateral flexion with neck extension (Levitz et al., 1997), which imply that pure lateral loading or sagittal loading with a lateral component can greatly increase the risk for nerve root and ganglion injury.

5.5.2 F05 Injury Risk

The F05 model did not predict disc avulsion injuries but did predict high stress in the hard tissue at the C6 and C7 vertebrae for the 7g lateral impact condition with the neutral activation scheme. A very small amount (<1% by volume) of bone failure was predicted on the ipsilateral facets surface of the C6 and C7 vertebrae (Figure). Although the hard tissue strain exceeded the threshold strain for fracture, the areas of failure was very localized due to bone to bone contact and variations in the vertebral geometry and was not attributed to a large-scale fracture. Bone failure in the F05 model is predicted which may not be attributed to a real fracture. The predicted bone failures were due to high contact forces between the ipsilateral articular processes during lateral bending of the neck. The CL is most likely to sustain damage in a lateral impact condition, due to the lateral positioning with respect to the neutral axis of lateral bending. The contralateral CL had the highest strains due to facet separation, while the ipsilateral facet experienced facet compression. In general, CL strains increased towards the lower cervical spine vertebral levels. The model demonstrated strains that were in the traumatic region for the C34 to C56 vertebral level, while the C67 was in the post-traumatic region. Therefore, the risk for CL injury increased towards the lower vertebral levels. The risk of nerve impingement by transverse compression was greatest in the lateral loading condition when compared to the frontal or rear condition. The IVF height and width reduction exceeded 2 mm in some vertebral levels, with the lower levels having the highest risk for impingement. The IVF height reduction at the C67 exceeded the estimated impingement threshold, while the IVF width reduction was approaching the impingement threshold. These IVF reductions were greater than reported reduction values for PHMS experiments in rear impacts, which suggest the risk for impingement increases when lateral

bending or axial rotation of the neck is present during an impact. Therefore, the predicted high strains in the CL and large reduction in the IVF height indicate that for a lateral impact condition, a high risk for ligamentous and nerve root injury in the neck will occur, especially in the lower vertebral levels.

5.5.3 Comparison of Injury Risk between M50 and F05

The F05 model demonstrated a faster onset and higher head CG acceleration and rotational displacement when compared to the M50 model. Although higher accelerations were observed in the F05 model, the rotational displacements (lateral flexion, flexion, axial rotation) were consistently less in the F05 compared to the M50 model because the facet surface on the F05 model was planar, while the M50 facet surface had a curved profile (Figure 5-3). The planar surface of the facet-contacting surface was not physiological and limited the axial rotation between each vertebra, which translated to less lateral neck flexion in the F05 model (Figure 5-6). Another contributor to the lower head rotational displacements in the F05 model could be due to the shorter neck length and smaller head mass of the F05 model. Both M50 and F05 models predicted a high injury risk potential for the CL. The F05 had a general trend of increasing CL strains towards the lower vertebral levels with predicted post-traumatic failure at C67, while the M50 model post-traumatic failure in the C34 and C45 vertebral levels. This reason for the difference in the CL injury location was attributed to the different facet surface profile, initial position, and geometric differences that ultimately caused higher axial rotation in the mid vertebral levels in M50 compared to the F05 model. Both the CL injury and injury location observed in both models were in good agreement with PHMS experiments, where an increase in the range of motion and the neutral zone was observed from the C45 to C67, which indicating damage to the lower vertebral levels starting at a 6.5g maximum acceleration side impact (Maak et al 2007). Furthermore, lateral impact PHMS experiments documented partial or complete rupture of the contralateral CL in the lower vertebral levels after the specimens were subjected to maximum accelerations of 2g to 8g (Hartwig et al., 2004; Panjabi et al., 2005). Both models predicted higher reductions in IVF height and width reductions when compared to the frontal and rear-loading conditions, and predicted a high risk of impingement of the nerve roots at the C67 level, as the impingement threshold was exceeded. These results indicate that ligamentous and nerve root injury risk are higher for the 7g maximum acceleration side impact case considered in this study, relative to similar severity in frontal and rear impact. The results of this study indicated a high risk for injury in the CL and nerve root structures in the lower vertebral levels, however the NBDL experiment did not report any injuries to the volunteers for the 7g maximum acceleration scenario. The current available NBDL human response data for lateral impacts exist for a range of severities (4g to 7g maximum accelerations), which could indicate that 7g maximum acceleration is the tolerance for injury in humans subjected to lateral impact scenarios. Future

studies should investigate a range of lateral impact severity to explore the injury tolerance for this loading scenario.

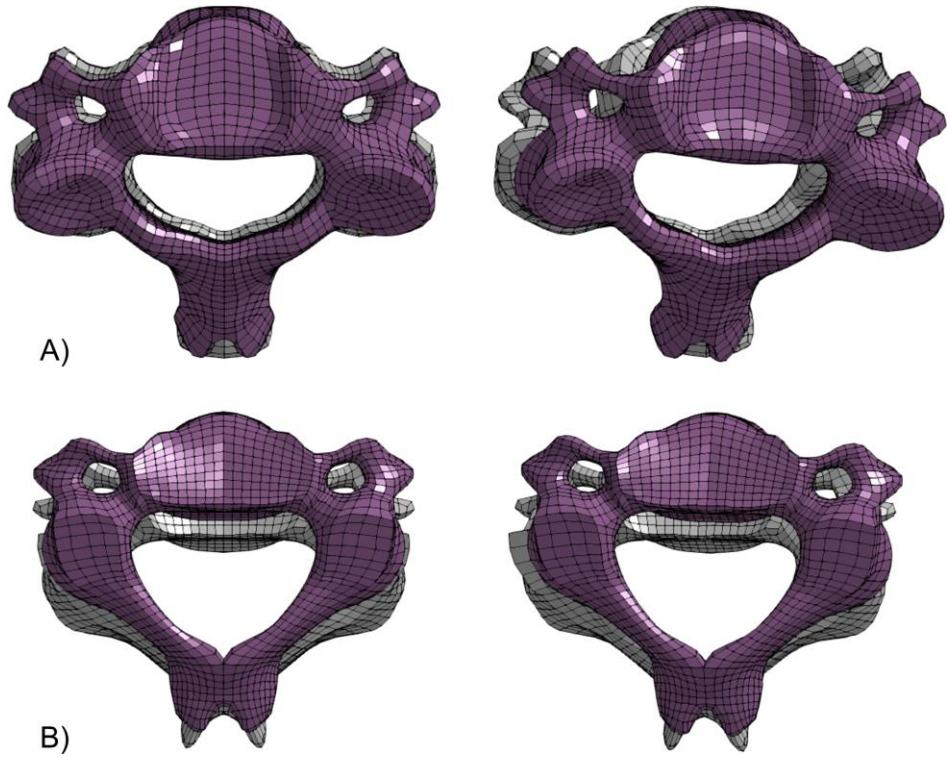

FIGURE 5-6: COMPARISON OF THE MAXIMUM AXIAL ROTATION IN THE C34 SEGMENT (SUPERIOR VIEW): A) M50 MODEL, B) F05 MODEL

5.6 Discussion & Limitations

Muscle activation is a complex phenomenon that is an important consideration when modeling impact events using HBMs, and can be dependent on the activation onset time and the PCSA of individuals. In the current study, the upper and lower bounds for activation onset time and muscle PCSA were identified through the literature and combined into two activation schemes, which served to bracket the upper the lower bounds to represent the variability in muscle PCSA and muscle activation onset time that may exist in the population. A high PCSA and faster onset time was used to represent the upper bound of muscle activation in the population, while a low PCSA and slower onset time was used to represent the lower bound. These changes were applied to the neutral activation scheme as a starting point to investigate whether or not these two parameters can alter the kinematic and tissue level response of the models. Overall, the upper bound activation scheme demonstrated a faster onset and lower magnitude of head displacement, while the lower bound activation scheme demonstrated a slower onset and higher magnitude of the head

displacement. A similar trend was observed in the tissue level response when compared to the neutral activation scheme, where the upper bound activation scheme resulted in lower injury risk and the lower bound activation scheme demonstrated higher injury risk. The lateral impact condition was the most sensitive to changes in head lateral rotation with the upper and lower bound activation schemes, compared to the frontal and rear impact, which indicated that changes to the sagittal position of the neck (induced by the active muscles) had a high sensitivity to alter the lateral neck flexion outcome. The head rotational response in the sagittal plane (frontal and rear impact condition) had sensitivities that were directly related to magnitude of the extensor and flexor PCSA, in addition to non-linear scaling of extension and flexion muscle moments in the M50 and F05 models.

A few limitations existed for the 5th percentile female model. The NBDL response corridors from the frontal and lateral impact were created only from male volunteers with larger statures when compared to a small sized female. In the current study, the volunteer T1 input boundary condition, which was measured from the larger stature male volunteers was not scaled to account for the smaller stature of the F05 model. There are several reasons why the T1 input conditions were not scaled. Firstly, the sled perturbation would not change regardless of the volunteer or PHMS used in respective study. For the rear impact PHMS experiment, a rigid seat was used and thus would eliminate or minimize any torso interaction in the anterior-posterior direction due to the absence of seat back deformation in a standard foam seat. Both the frontal and lateral impact experiments performed by the NBDL had the volunteers tightly secured onto the rigid seat with a five-point harness to prevent movement of the torso during the sled acceleration. Therefore, due to the motion of the torso being limited by both the rigid seats and the use of a five-point harness, the experimental T1 inputs were not scaled down to match the F05 stature. Another limitation of this study is the simplified muscle activation in the model. The muscles in the current model all activate at the same time using a predetermined activation curve. An open loop control strategy may not fully represent the neuromuscular activation of the neck muscle in real-life scenarios, but provided acceptable results in this study.

The current study utilized two neck models representing an average stature male and small stature female. The same boundary condition for each impact direction was applied directly to the T1 vertebra, therefore subjecting both models to the same perturbation, and eliminating all external interactions such as seat back interactions. In general, the F05 model had an earlier onset of head kinematics when compared to the M50 model for all impact directions, although the difference in head rotational displacements in the frontal and rear loading conditions were similar. In the frontal impact condition, the maximum head rotation angle of the F05 was similar to the M50 (<0.5% difference) whereas in the rear impact condition, the F05

had 2% increased head rotation angle when compared to the M50 model. The similarities in head rotational displacement were attributed to the shorter neck length, lower head mass and reduced neck circumference of the F05, offsetting the reduced PCSA of the F05 model and generally smaller dimensions compared to the M50. When compared to the M50, a shorter neck and smaller head mass would theoretically decrease the head rotational displacement, when the applied boundary condition was the same. A smaller neck circumference is generally associated with a lower neck stiffness, and lower muscle PCSA, which would reduce both bending stiffness and muscle force generation, resulting in greater head rotational displacements. Therefore, the decrease of head rotational displacement from the shorter neck and lower head mass of the F05 would be offset by the increase in head rotational due to the smaller circumference of the F05 neck. The F05 model was not a scaled down version of the M50 model, but was based on the geometry of a 5^{th} percentile female volunteer. Thus, the F05 model was not only smaller than the M50 model but had different dimensions such as smaller neck length and circumference (Schneider et al., 1983), and different vertebral geometry (Klinich et al., 2004; Singh and Cronin, 2017).The similarities in head kinematics response between the M50 and F05 models indicate that the effect of stature and local neck tissue dimensions are confounding factors in the current study for the frontal and rear impact direction. In addition, it was acknowledged that pain and injury tolerances between genders may be different and this was not considered because the differences in injury and pain threshold between male and female are not currently understood.

The lateral impact condition demonstrated large difference in the F05 head rotational displacement (the lateral flexion angle, axial rotation angle, and forward flexion angle were 20%, 49%, and 38% lower), respectively, compared to the M50 model. The large difference in head rotation was due in part to the planar surface of the facet cartilage surface on the F05 model that limited the axial rotation range of motion in lateral bending. Although the F05 model had lower head displacements than the M50 model in the lateral loading condition, traumatic CL injury was still predicted for the C34 to C67 vertebral level, while the M50 model sustained traumatic injury to all vertebral levels (C23 to C67). The epidemiological literature has indicated that females have approximately twice the risk to sustain whiplash injuries when compared to males (Carlsson et al., 2010; Carstensen et al., 2012). In the frontal and rear impact directions, there were no observed differences in injury risk based on ligament distractions and transverse compression of the nerve roots. For the rear impact condition, both models did not predict injury at the tissue level using both distractions and changes in neural foraminal dimensions, which was likely due to the current implementation of the CL, and the larger facet joint gap that resulted in the under-prediction of CL injury. Interestingly, when the local facet kinematics are compared between the M50 and F05 models, the F05 model demonstrated larger facet joint shear distraction, which can potentially translate to a higher injury

risk. The opposite was true when comparing the local facet joint compression, which may indicate that lower values of facet joint compression may result in higher facet joint shear in the models, and highlights the importance of implementing the correct facet cartilage geometry to accurately predict tissue level injury. Previous studies had investigated the risk of injury to the upper cervical spine ligaments (Fice and Cronin, 2012) and indicated a high injury risk in frontal and rear impacts starting at approximately 12g and 15g maximum acceleration respectively. The impact severities considered in this current study were well below the reported injury threshold for the upper cervical spine ligaments, and therefore was not investigated.

The current M50 and F05 models do not include the spinal cord and nerve roots structures, hence the deformation of the nerve roots cannot be monitored directly. An alternative method that quantifies the change in dimension (height and width) of the intervertebral foramen space, following the same methodology as previous experiments was used in this study. The prediction of transverse compression of the nerve roots is conservative in the model due to a lack of anatomical detail of the nerve roots and associated structures within the intervertebral foramen space. The nerve roots are surrounded by various tissues such as epidural fat, and foraminal ligaments (Daniels et al., 1986; Kraan et al., 2011; Shi et al., 2015; Lohman et al., 2015). These structures which were not accounted for in the current study can cause the impingement of the nerve roots to occur at a lower threshold when accounting for these tissues and therefore, difficult to comment on whether or not injury will occur. The results from the model, however, do indicate a larger decrease in foraminal dimensions for the lateral loading condition, compared to the frontal and rear loading where the head moves within the sagittal plane. PHMS and in-vivo studies demonstrated neural foraminal area reductions during neck extension, axial rotation, ipsilateral bending, and ipsilateral bending with combined extension (Nuckley et al., 2002; Muhle et al., 2001). This may infer that impacts such as head turned or oblique impacts may be associated with a higher risk of injury to the nerve roots due to the combine axial rotation and lateral bending of the cervical vertebrae. Conversely, neck flexion was the only loading path that resulted in an increase of the neural foraminal area, which indicated a low risk for sustaining nerve root compression in a frontal impact. Future studies should compare the foraminal dimensional changes in oblique and lateral impacts, as well as include the nerve root structures in the model to accurately assess injury in the nerve roots and associated structures.

5.7 Recommendations & Future Work

The muscle activation strategies investigated in this study were simplified representations of neuromuscular activation in humans. Specifically, the muscle activation was based on an open-loop control strategy, where the muscle activation dynamics are pre-determined for each muscle, prior to the impact.

However, the proposed neutral activation scheme provided kinematics comparable to human volunteer tests in frontal and lateral impact cases. Future studies should investigate the effect of muscle activation based on closed-loop feedback control on kinematics and tissue level injury. The facet joints in both the M50 and F05 neck models had a larger gap than what has been reported in the literature (Womack et al., 2008). The resulting gap between the facet surfaces led to abnormal CL strains in the frontal and rear impact cases. Future work should accurately model the correct thickness and surface profile of the facet cartilage, as this could greatly affect the tissue level response of the model, but not necessarily the global kinematic response. The current ligament implementation in both models utilized a tension only 1-D element approach, which cannot accurately represent transverse shear of the ligament and does not account for strains due to hard tissue contacts during motion (i.e. anatomically, a ligament will deform around the hard tissue instead of forming a straight path). Therefore, the 1-D element approach of modelling ligaments can lead to under-prediction of ligament strains during impact scenarios. Future improvements should explore the implementation of solid or membrane type elements to represent the cervical spine ligaments for increased biofidelity. The boundary conditions used in the current study are applied directly to the T1 vertebra which does not consider torso interactions with the seatback. Seatback interaction is important in rear impacts and should be addressed in future studies using full body simulations. The neural structures such as the spinal cord and nerve roots and ganglia are not present in the model. Therefore, the current study used changes in the IVF height and width dimensions as surrogate measurements to infer neural impingement. These structures are an important consideration when investigating neural injuries for complex scenarios such as oblique or head turned impacts, and should be implemented in future versions of the GHBMC HBMs. Lastly, the current study was focused on a single impact severity for each impact direction. Future work should investigate a range of impact severities that range from low to high severities, in order to determine tissue level injury thresholds in each direction of loading.

CHAPTER 6: CONCLUSION

The neutral activation scheme was developed for the M50 model (extensor: 20% activation, flexor: 100% activation) and F05 model (extensor: 25% activation, flexor: 100% activation) that demonstrated positive improvements to the head kinematics of the models for the frontal, rear and lateral impact scenarios, compared to the baseline activation scheme. The activation of the extensor and flexor muscles were not tuned to fit the experimental response, but were developed independent of each impact cases to minimize changes in the head line of sight and anterior-posterior translation without a T1 boundary condition.

The variations in PCSA and activation onset time had the highest sensitivity to the head rotational displacements in the lateral impact direction. Increased neck flexion caused by decreased extensor activation resulted in higher axial rotation between all vertebral levels and was attributed to increased lateral neck flexion.

The 8g frontal impact condition demonstrated the highest injury risk to the ISL and CL for both M50 and F05 models. The high CL strains were attributed to the facet joint gap, which increased the predicted strains in the model through coupled shear and tension distractions, and led to an overestimation of the predicted CL injury risk.

Both M50 and F05 models did not predict injury for the 7g rear impact condition, although this impact severity is associated with the onset of injury. The low injury risk prediction by the model was attributed to the large facet joint gap, relative to reported values, and the numerical implementation of the CL, which under-predicted ligament distraction. The F05 model demonstrated larger facet joint shear distraction compared to the M50 model, inferring a greater injury risk. Conversely, the F05 model demonstrated lower facet joint compression compared to the M50 model, which indicated that the local facet joint shear and compression were negatively correlated and highlighted the need for implementing an anatomically accurate facet joint gap.

The F05 had a general trend of faster onset of head acceleration and rotation compared to the M50 for all impact directions. The head kinematic and tissue level injury responses were similar between the M50 and F05 models, attributed to confounding factors between stature and local neck tissue dimensions. The effect of a decreased neck length and head mass of the F05 model was offset with the lower passive tissue stiffness and muscle contraction force.

A low risk of transverse compression of the nerve root and ganglia was predicted for both M50 and F05 models in the frontal and rear impact conditions, but was high for the lateral impact condition due to higher IVF width and height reductions. The model results suggest that impacts with a lateral bending or axial rotation component will likely result in a greater risk of nerve root impingement compared to sagittal plane impacts.

The 7g lateral impact condition resulted in lower head rotational displacement of the F05 compared to the M50 model, which was attributed to the non-physiological planar facet profile of the F05 vertebrae. A planar facet profile demonstrated decreased range of motion in axial rotation that correspondingly limited lateral bending. In addition, the CL was most vulnerable to injury in the lateral impact condition for both models. The male model demonstrated post-traumatic failure at the mid vertebral levels (C34 and C45) while the F05 demonstrated post-traumatic failure in the lower vertebral level (C67), due to the reduced axial rotation at all vertebral levels.

REFERENCES

Aldman, B. (1986). An analytical approach to the impact biomechanics of head and neck injury. In *Proceedings of the 39th American Association for Automotive Medicine Conference; October 6-8, 1986, Montreal, QC* (pp. 439–461).

Alleyne, C. H. J., Cawley, C. M., Barrow, D. L., & Bonner, G. D. (1998). Microsurgical anatomy of the dorsal cervical nerve roots and the cervical dorsal root ganglion/ventral root complexes. *Surgical Neurology*, *50*(3), 213–218. https://doi.org/10.1016/s0090-3019(97)00315-7

Anderson, J. S., Hsu, A. W., & Vasavada, A. N. (2005). Morphology, architecture, and biomechanics of human cervical multifidus. *Spine*, *30*(4), E86-91. https://doi.org/10.1097/01.brs.0000153700.97830.02

Barker, J. B., Cronin, D. S., & Nightingale, R. W. (2017). Lower Cervical Spine Motion Segment Computational Model Validation: Kinematic and Kinetic Response for Quasi-Static and Dynamic Loading. *Journal of Biomechanical Engineering*, *139*(6), 061009. https://doi.org/10.1115/1.4036464

Barnsley, L., Lord, S. M., Wallis, B. J., & Bogduk, N. (1995). The prevalence of chronic cervical zygapophysial joint pain after whiplash. *Spine*, *20*(1), 20–25; discussion 26. https://doi.org/10.1097/00007632-199501000-00004

Barnsley, L., Lord, S., & Bogduk, N. (1994). Whiplash injury. *Pain*, *58*(3), 283–307. https://doi.org/10.1016/0304-3959(94)90123-6

Basbaum, A. I., Bautista, D. M., Scherrer, G., & Julius, D. (2009). Cellular and molecular mechanisms of pain. *Cell*, *139*(2), 267–284. https://doi.org/10.1016/j.cell.2009.09.028

Beeman, S. M., Kemper, A. R., Madigan, M. L., Franck, C. T., & Loftus, S. C. (2012). Occupant kinematics in low-speed frontal sled tests: Human volunteers, Hybrid III ATD, and PMHS. *Accident Analysis & Prevention*, *47*, 128–139. https://doi.org/https://doi.org/10.1016/j.aap.2012.01.016

Berglund, A., Alfredsson, L., Jensen, I., Bodin, L., & Nygren, A. (2003). Occupant- and crash-related factors associated with the risk of whiplash injury. *Annals of Epidemiology*, *13*(1), 66–72. https://doi.org/10.1016/s1047-2797(02)00252-1

Blouin, J.-S., Descarreaux, M., Bélanger-Gravel, A., Simoneau, M., & Teasdale, N. (2003). Attenuation of human neck muscle activity following repeated imposed trunk-forward linear acceleration. *Experimental Brain Research*, *150*(4), 458–464. https://doi.org/10.1007/s00221-003-1466-9

Bogduk, N. (2003). The anatomy and pathophysiology of neck pain. *Physical Medicine and Rehabilitation Clinics of North America*, *14*(3), 455–472, v. https://doi.org/10.1016/s1047-9651(03)00041-x

Bogduk, N. (2011). On cervical zygapophysial joint pain after whiplash. *Spine*, *36*(25 Suppl), S194-9. https://doi.org/10.1097/BRS.0b013e3182387f1d

Bogduk, N. (2002). Innervation and Pain Patterns of the Cervical Spine. In R. Grant (Ed.), *Physical therapy of the cervical and thoracic spine* (3rd ed, pp. 61–72). New York: Churchill Livingstone.

Bogduk, N., & Mercer, S. (2000). Biomechanics of the cervical spine. I: Normal kinematics. *Clinical Biomechanics*, *15*(9), 633–648. https://doi.org/10.1016/S0268-0033(00)00034-6

Borst, J., Forbes, P. A., Happee, R., & Veeger, D. H. E. J. (2011). Muscle parameters for musculoskeletal modelling of the human neck. *Clinical Biomechanics (Bristol, Avon)*, *26*(4), 343–351. https://doi.org/10.1016/j.clinbiomech.2010.11.019

Brault, J. R., Siegmund, G. P., & Wheeler, J. B. (2000). Cervical muscle response during whiplash: Evidence of a lengthening muscle contraction. *Clinical Biomechanics*, *15*(6), 426–435. https://doi.org/10.1016/S0268-0033(99)00097-2

Brolin, K., Halldin, P., & Leijonhufvud, I. (2005). The effect of muscle activation on neck response. *Traffic Injury Prevention*, *6*(1), 67–76. https://doi.org/10.1080/15389580590903203

Cappon, H., van Ratingen, M., Wismans, J., Automotive, T. N. O., Hell, W., Lang, D., & Svensson, M. (2003). Whiplash injuries, not only a problem in rear-end impact. In *ESV Conference, Nagoya, Japan* (pp. 1–9).

Carlson, E. J., Tominaga, Y., Ivancic, P. C., & Panjabi, M. M. (2007). Dynamic vertebral artery elongation during frontal and side impacts. *The Spine Journal*, *7*(2), 222–228. https://doi.org/10.1016/j.spinee.2006.07.003

Carlsson, A., Siegmund, G. P., Linder, A., & Svensson, M. Y. (2012). Motion of the Head and Neck of Female and Male Volunteers in Rear Impact Car-to-Car Impacts. *Traffic Injury Prevention*, *13*(4), 378–387. https://doi.org/10.1080/15389588.2012.659362

Carroll, L. J., Holm, L. W., Hogg-Johnson, S., Côté, P., Cassidy, J. D., Haldeman, S., … Guzman, J. (2008, April). Course and Prognostic Factors for Neck Pain in Whiplash-Associated Disorders (WAD): Results of the Bone and Joint Decade 2000-2010 Task Force on Neck Pain and Its Associated Disorders. *European Spine Journal*. https://doi.org/10.1007/s00586-008-0628-7

Carstensen, T. B. W., Frostholm, L., Oernboel, E., Kongsted, A., Kasch, H., Jensen, T. S., & Fink, P. (2012). Are there gender differences in coping with neck pain following acute whiplash trauma? A 12-month follow-up study. *European Journal of Pain (London, England)*, *16*(1), 49–60. https://doi.org/10.1016/j.ejpain.2011.06.002

Cassidy, J. D., Carroll, L. J., Cote, P., Lemstra, M., Berglund, A., & Nygren, A. (2000). Effect of eliminating compensation for pain and suffering on the outcome of insurance claims for whiplash injury. *The New England Journal of Medicine*, *342*(16), 1179–1186. https://doi.org/10.1056/NEJM200004203421606

Cassidy, J. J., Hiltner, A., & Baer, E. (1989). Hierarchical structure of the intervertebral disc. *Connective Tissue Research*, *23*(1), 75–88. https://doi.org/10.3109/03008208909103905

Costigan, M., Scholz, J., & Woolf, C. J. (2009). Neuropathic pain: a maladaptive response of the nervous system to damage. *Annual Review of Neuroscience*, *32*, 1–32. https://doi.org/10.1146/annurev.neuro.051508.135531

Cronin, D. S. (2014). Finite element modeling of potential cervical spine pain sources in neutral position low speed rear impact. *Journal of the Mechanical Behavior of Biomedical Materials*, *33*(1), 55–66. https://doi.org/10.1016/j.jmbbm.2013.01.006

Crowe, H. (1964). A New Diagnostic Sign in Neck Injuries. *California Medicine*, *100*(1), 12–13.

Curatolo, M., Bogduk, N., Ivancic, P. C., McLean, S. A., Siegmund, G. P., & Winkelstein, B. A. (2011). The role of tissue damage in whiplash-associated disorders: discussion paper 1. *Spine*, *36*(25 Suppl), S309-15. https://doi.org/10.1097/BRS.0b013e318238842a

Daniels, D. L., Hyde, J. S., Kneeland, J. B., Jesmanowicz, A., Froncisz, W., Grist, T. M., … Haughton, V. M. (1986). The cervical nerves and foramina: local-coil MR imaging. *AJNR. American Journal of Neuroradiology*, *7*(1), 129–133.

Davidsson, J., Deutscher, C., Hell, W., Linder, A., Lövsund, P., & Svensson, M. Y. (1998). Human volunteer kinematics in rear-end sled collisions. In *IRCOBI Conference 1998*.

Davis, M. L., Koya, B., Schap, J. M., & Gayzik, F. S. (2016). Development and Full Body Validation of a 5th Percentile Female Finite Element Model. In *60TH Stapp Car Crash Conference*. The Stapp Association. https://doi.org/https://doi.org/10.4271/2016-22-0015

Davis, S. J., Teresi, L. M., Bradley, W. G. J., Ziemba, M. A., & Bloze, A. E. (1991). Cervical spine hyperextension injuries: MR findings. *Radiology*, *180*(1), 245–251. https://doi.org/10.1148/radiology.180.1.2052703

Deng, B. (1999). *Kinematics of human cadaver cervical spine during low speed rear end impacts.* PhD Thesis, Wayne State University.

Deng, B., Begeman, P. C., Yang, K. H., Tashman, S., & King, A. I. (2000). Kinematics of Human Cadaver Cervical Spine During Low Speed Rear-End Impacts. In *44th Stapp Car Crash Conference (2000)*. The Stapp Association. https://doi.org/https://doi.org/10.4271/2000-01-SC13

Deng, Y.-C., Li, X., & Liu, Y. (1999). Modeling of the Human Cervical Spine Using Finite Element Techniques. In *International Congress & Exposition*. SAE International. https://doi.org/https://doi.org/10.4271/1999-01-1310

DeWit, J. A., & Cronin, D. S. (2012). Cervical spine segment finite element model for traumatic injury prediction. *Journal of the Mechanical Behavior of Biomedical Materials*, *10*, 138–150. https://doi.org/10.1016/j.jmbbm.2012.02.015

Dullerud, R., Gjertsen, O., & Server, A. (2010). Magnetic resonance imaging of ligaments and membranes in the craniocervical junction in whiplash-associated injury and in healthy control subjects. *Acta Radiologica (Stockholm, Sweden : 1987)*, *51*(2), 207–212. https://doi.org/10.3109/02841850903321617

Ebara, S., Iatridis, J. C., Setton, L. A., Foster, R. J., Mow, V. C., & Weidenbaum, M. (1996). Tensile properties of nondegenerate human lumbar anulus fibrosus. *Spine*, *21*(4), 452–461. https://doi.org/10.1097/00007632-199602150-00009

Ejima, S., Ito, D., Satou, F., Mikami, K., Ono, K., Kaneoka, K., & Shiina, I. (2012). Effects of pre-impact swerving/steering on physical motion of the volunteer in the low-speed side-impact sled test. In *IRCOBI Conference 2012*.

Evans, R. W. (1992). Some observations on whiplash injuries. *Neurologic Clinics*, *10*(4), 975–997. https://doi.org/10.1016/S0733-8619(18)30191-9

Evans, W. J., Meredith, C. N., Cannon, J. G., Dinarello, C. A., Frontera, W. R., Hughes, V. A., … Knuttgen, H. G. (1986). Metabolic changes following eccentric exercise in trained and untrained men. *Journal of Applied Physiology (Bethesda, Md. : 1985)*, *61*(5), 1864–1868. https://doi.org/10.1152/jappl.1986.61.5.1864

Ewing, C. L., Thomas, D. J., Lustik, L., Muzzy, W. H., Willems, G. C., & Majewski, P. (1977). Dynamic Response of the Human Head and Neck to +Gy Impact Acceleration. In *21st Stapp Car Crash Conference*. SAE International. https://doi.org/https://doi.org/10.4271/770928

Fice, J. B., & Cronin, D. S. (2012). Investigation of whiplash injuries in the upper cervical spine using a detailed neck model. *Journal of Biomechanics*, *45*(6), 1098–1102. https://doi.org/10.1016/j.jbiomech.2012.01.016

Fice, J. B., Cronin, D. S., & Panzer, M. B. (2011). Cervical spine model to predict capsular ligament response in rear impact. *Annals of Biomedical Engineering*, *39*(8), 2152–2162. https://doi.org/10.1007/s10439-011-0315-4

Fice, J. B., Siegmund, G. P., & Blouin, J. S. (2014). Prediction of three dimensional maximum isometric neck strength. *Annals of Biomedical Engineering*, *42*(9), 1846–1852. https://doi.org/10.1007/s10439-014-1046-0

Foust, D. R., Chaffin, D. B., Snyder, R. G., & Baum, J. K. (1973). Cervical Range of Motion and Dynamic Response and Strength of Cervical Muscles. In *17th Stapp Car Crash Conference*. SAE International. https://doi.org/https://doi.org/10.4271/730975

Freeman, M. D., Croft, A. C., Rossignol, A. M., Weaver, D. S., & Reiser, M. (1999). A review and methodologic critique of the literature refuting whiplash syndrome. *Spine*, *24*(1), 86–96. https://doi.org/10.1097/00007632-199901010-00022

Fujita, Y., Duncan, N. A., & Lotz, J. C. (1997). Radial tensile properties of the lumbar annulus fibrosus are site and degeneration dependent. *Journal of Orthopaedic Research : Official Publication of the Orthopaedic Research Society*, *15*(6), 814–819. https://doi.org/10.1002/jor.1100150605

Gennarelli, T. A., & Wodzin, E. (2006). AIS 2005: a contemporary injury scale. *Injury*, *37*(12), 1083–1091. https://doi.org/10.1016/j.injury.2006.07.009

Gray, H. (1918). *Anatomy of the Human Body* (20th ed.). Philadelphia: Lea & Febiger 1918; Bartleby.com, 2000.

Gustafsson, M., Stigson, H., Krafft, M., & Kullgren, A. (2015). Risk of permanent medical impairment (RPMI) in car crashes correlated to age and gender. *Traffic Injury Prevention*, *16*(4), 353–361. https://doi.org/10.1080/15389588.2014.940459

Happee, R. (1994). Inverse dynamic optimization including muscular dynamics, a new simulation method applied to goal directed movements. *Journal of Biomechanics*, *27*(7), 953–960. https://doi.org/10.1016/0021-9290(94)90267-4

Hartwig, E., Kettler, A., Schultheiss, M., Kinzl, L., Claes, L., & Wilke, H.-J. (2004). In vitro low-speed side collisions cause injury to the lower cervical spine but do not damage alar ligaments. *European Spine Journal*, *13*(7), 590–597. https://doi.org/10.1007/s00586-003-0624-x

Hedenstierna, S., & Halldin, P. (2008). How does a three-dimensional continuum muscle model affect the kinematics and muscle strains of a finite element neck model compared to a discrete muscle model in rear-end, frontal, and lateral impacts. *Spine*, *33*(8), E236-45. https://doi.org/10.1097/BRS.0b013e31816b8812

Hell, W., Höpfl, F., Langwieder, K., & Lang, D. (2003). Cervical spine distortion injuries in various car collision directions and injury incidence of different car types in rear-end collisions. In *IRCOBI Conference 2003*.

Hernández, I. A., Fyfe, K. R., Heo, G., & Major, P. W. (2006). The role of sternocleidomastoid muscle in simulated low velocity rear-end impacts. *European Spine Journal*, *15*(6), 876–885. https://doi.org/10.1007/s00586-005-0956-9

Hill, A. V. (1938). The heat of shortening and the dynamic constants of muscle. *Proceedings of the Royal Society of London. Series B - Biological Sciences*, *126*(843), 136–195. https://doi.org/10.1098/rspb.1938.0050

Hill, R. (1979). Aspects of Invariance in Solid Mechanics. In C.-S. Yih (Ed.) (Vol. 18, pp. 1–75). Elsevier. https://doi.org/https://doi.org/10.1016/S0065-2156(08)70264-3

Holm, L. W., Carroll, L. J., Cassidy, J. D., Hogg-Johnson, S., Cote, P., Guzman, J., … Haldeman, S. (2008). The burden and determinants of neck pain in whiplash-associated disorders after traffic collisions: results of the Bone and Joint Decade 2000-2010 Task Force on Neck Pain and Its Associated Disorders. *Spine*, *33*(4 Suppl), S52-9. https://doi.org/10.1097/BRS.0b013e3181643ece

Holsgrove, T. P., Jaumard, N. V, Zhu, N., Stiansen, N. S., Welch, W. C., & Winkelstein, B. A. (2016). Upper Cervical Spine Loading Simulating a Dynamic Low-Speed Collision Significantly Increases the Risk of Pain Compared to Quasi-Static Loading With Equivalent Neck Kinematics. *Journal of Biomechanical Engineering*, *138*(12). https://doi.org/10.1115/1.4034707

Holzapfel, G. A., Schulze-Bauer, C. A. J., Feigl, G., & Regitnig, P. (2005). Single lamellar mechanics of the human lumbar anulus fibrosus. *Biomechanics and Modeling in Mechanobiology*, *3*(3), 125–140. https://doi.org/10.1007/s10237-004-0053-8

Hubbard, R. D., Quinn, K. P., Martinez, J. J., & Winkelstein, B. A. (2008). The role of graded nerve root compression on axonal damage, neuropeptide changes, and pain-related behaviors. *52nd Stapp Car Crash Conference*, *52*, 33–58.

Hubbard, R. D., & Winkelstein, B. A. (2005). Transient cervical nerve root compression in the rat induces bilateral forepaw allodynia and spinal glial activation: mechanical factors in painful neck injuries. *Spine*, *30*(17), 1924—1932. https://doi.org/10.1097/01.brs.0000176239.72928.00

Iatridis, J. C., Setton, L. A., Foster, R. J., Rawlins, B. A., Weidenbaum, M., & Mow, V. C. (1998). Degeneration affects the anisotropic and nonlinear behaviors of human anulus fibrosus in compression. *Journal of Biomechanics*, *31*(6), 535–544. https://doi.org/10.1016/s0021-9290(98)00046-3

Inami, S., Shiga, T., Tsujino, A., Yabuki, T., Okado, N., & Ochiai, N. (2001). Immunohistochemical demonstration of nerve fibers in the synovial fold of the human cervical facet joint. *Journal of Orthopaedic Research : Official Publication of the Orthopaedic Research Society*, *19*(4), 593–596. https://doi.org/10.1016/S0736-0266(00)00048-6

Ita, M. E., Zhang, S., Holsgrove, T. P., Kartha, S., & Winkelstein, B. A. (2017). The Physiological Basis of Cervical Facet-Mediated Persistent Pain: Basic Science and Clinical Challenges. *The Journal of Orthopaedic and Sports Physical Therapy*, *47*(7), 450–461. https://doi.org/10.2519/jospt.2017.7255

Ito, S., Ivancic, P. C., Pearson, A. M., Tominaga, Y., Gimenez, S. E., Rubin, W., & Panjabi, M. M. (2005). Cervical intervertebral disc injury during simulated frontal impact. *European Spine Journal*, *14*(4), 356–365. https://doi.org/10.1007/s00586-004-0783-4

Ito, S., Ivancic, P. C., Panjabi, M. M., & Cunningham, B. W. (2004). Soft tissue injury threshold during simulated whiplash: a biomechanical investigation. *Spine*, *29*(9), 979–987. https://doi.org/10.1097/00007632-200405010-00006

Ivancic, P. C., Panjabi, M. M., Ito, S., Cripton, P. A., & Wang, J. L. (2005). Biofidelic whole cervical spine model with muscle force replication for whiplash simulation. *European Spine Journal*, *14*(4), 346–355. https://doi.org/10.1007/s00586-004-0758-5

Ivancic, P. C., Pearson, A. M., Panjabi, M. M., & Ito, S. (2004). Injury of the anterior longitudinal ligament during whiplash simulation. *European Spine Journal*, *13*(1), 61–68. https://doi.org/10.1007/s00586-003-0590-3

Ivancic, P. C. (2012). Cervical neural space narrowing during simulated rear crashes with anti-whiplash systems. *European Spine Journal*, *21*(5), 879–886. https://doi.org/10.1007/s00586-012-2159-5

Ivancic, P. C., Ito, S., Tominaga, Y., Carlson, E. J., Rubin, W., & Panjabi, M. M. (2006). Effect of rotated head posture on dynamic vertebral artery elongation during simulated rear impact. *Clinical Biomechanics*, *21*(3), 213–220. https://doi.org/10.1016/j.clinbiomech.2005.10.011

Ivancic, P. C., Ito, S., Tominaga, Y., Rubin, W., Coe, M. P., Ndu, A. B., … Panjabi, M. M. (2008). Whiplash causes increased laxity of cervical capsular ligament. *Clinical Biomechanics*, *23*(2), 159–165. https://doi.org/10.1016/j.clinbiomech.2007.09.003

Iwamoto, M., Nakahira, Y., & Kimpara, H. (2015). Development and Validation of the Total HUman Model for Safety (THUMS) Toward Further Understanding of Occupant Injury Mechanisms in Precrash and During Crash. *Traffic Injury Prevention*, *16 Suppl 1*, S36-48. https://doi.org/10.1080/15389588.2015.1015000

Iwamoto, M., Nakahira, Y., Kimpara, H., & Sugiyama, T. (2009). Development of a Human FE Model with 3-D Geometry of Muscles and Lateral Impact Analysis for the Arm with Muscle Activity. In *Digital Human Modeling for Design and Engineering Conference and Exhibition*. SAE International. https://doi.org/https://doi.org/10.4271/2009-01-2266

Iwamoto, M., Nakahira, Y., Kimpara, H., Sugiyama, T., & Min, K. (2012). Development of a Human Body Finite Element Model with Multiple Muscles and their Controller for Estimating Occupant Motions and Impact Responses in Frontal Crash Situations. In *56th Stapp Car Crash Conference*. The Stapp Association. https://doi.org/https://doi.org/10.4271/2012-22-0006

Jakobsson, L., Lundell, B., Norin, H., & Isaksson-Hellman, I. (2000). WHIPS--Volvo's Whiplash Protection Study. *Accident; Analysis and Prevention*, *32*(2), 307–319. https://doi.org/10.1016/s0001-4575(99)00107-4

Jakobsson, L., Norin, H., & Isaksson-Hellman, I. (2000). Parameters influencing the risk of AIS1 neck injuries in frontal and side impacts. In *IRCOBI Conference 2000*.

Jaumard, N. V, Welch, W. C., & Winkelstein, B. A. (2011). Spinal facet joint biomechanics and mechanotransduction in normal, injury and degenerative conditions. *Journal of Biomechanical Engineering*, *133*(7), 71010. https://doi.org/10.1115/1.4004493

Jonsson, H. J., Bring, G., Rauschning, W., & Sahlstedt, B. (1991). Hidden cervical spine injuries in traffic accident victims with skull fractures. *Journal of Spinal Disorders*, *4*(3), 251–263. https://doi.org/10.1097/00002517-199109000-00001

Kaale, B. R., Krakenes, J., Albrektsen, G., & Wester, K. (2005). Whiplash-associated disorders impairment rating: neck disability index score according to severity of MRI findings of ligaments and membranes in the upper cervical spine. *Journal of Neurotrauma*, *22*(4), 466–475.

Kallakuri, S., Singh, A., Chen, C., & Cavanaugh, J. M. (2004). Demonstration of substance P, calcitonin gene-related peptide, and protein gene product 9.5 containing nerve fibers in human cervical facet joint capsules. *Spine*, *29*(11), 1182–1186. https://doi.org/10.1097/00007632-200406010-00005

Kamibayashi, L. K., & Richmond, F. J. (1998). Morphometry of human neck muscles. *Spine*, *23*(12), 1314–1323. https://doi.org/10.1097/00007632-199806150-00005

Kaneoka, K., Ono, K., Inami, S., & Hayashi, K. (1999). Motion analysis of cervical vertebrae during whiplash loading. *Spine*, *24*(8), 763–769; discussion 770. https://doi.org/10.1097/00007632-199904150-00006

Kato, D., Nakahira, Y., Atsumi, N., & Iwamoto, M. (2018). Development of human-body model THUMS version 6 containing muscle controllers and application to injury analysis in frontal collision after brake deceleration. In *IRCOBI Conference 2018*.

Kimpara, H., Nakahira, Y., Iwamoto, M., Miki, K., Ichihara, K., Kawano, S., & Taguchi, T. (2006). Investigation of Anteroposterior Head-Neck Responses during Severe Frontal Impacts Using a Brain-Spinal Cord Complex FE Model. In *50th Stapp Car Crash Conference*. The Stapp Association. https://doi.org/https://doi.org/10.4271/2006-22-0019

Kitagawa, T., Fujiwara, A., Kobayashi, N., Saiki, K., Tamai, K., & Saotome, K. (2004). Morphologic changes in the cervical neural foramen due to flexion and extension: in vivo imaging study. *Spine*, *29*(24), 2821–2825. https://doi.org/10.1097/01.brs.0000147741.11273.1c

Kitagawa, Y., Yamada, K., Motojima, H., & Yasuki, T. (2015). Consideration on gender difference of whiplash associated disorder in low speed rear impact. In *IRCOBI Conference 2015*.

Kleinberger, M. (1993). Application of Finite Element Techniques to the Study of Cervical Spine Mechanics. In *Stapp Car Crash Conference*. SAE International. https://doi.org/https://doi.org/10.4271/933131

Klinich, K. D., Ebert, S. M., Van Ee, C. A., Flannagan, C. A. C., Prasad, M., Reed, M. P., & Schneider, L. W. (2004). Cervical Spine Geometry in the Automotive Seated Posture: Variations with Age, Stature, and Gender. In *48th Stapp Car Crash Conference*. The Stapp Association. https://doi.org/https://doi.org/10.4271/2004-22-0014

Knaub, K., Van Ee, C., Cheng, C., Poon, B., Spritzer, C., & Myers, B. S. (1999). *Measurement of Human Neck Muscle Volume Geometry and Physiologic Cross-Sectional Area in 5th, 50th, and 95th Percentile Subjects Using Cadaveric Dissection and MRI*. *National Highway Traffic Safety Administration (NHTSA-98-3588-34)*.

Koch, M. (1999). The neurobiology of startle. *Progress in Neurobiology*, *59*(2), 107–128. https://doi.org/10.1016/s0301-0082(98)00098-7

Kraan, G. A., Smit, T. H., & Hoogland, P. V. J. M. (2011). Extraforaminal ligaments of the cervical spinal nerves in humans. *The Spine Journal : Official Journal of the North American Spine Society*, *11*(12), 1128–1134. https://doi.org/10.1016/j.spinee.2011.10.025

Krafft, M. (1998). A comparison of short-and long-term consequences of AIS 1 neck injuries, in rear impacts. In *IRCOBI Conference 1998*.

Krafft, M., Kullgren, A., Ydenius, A., & Tingvall, C. (2002). Influence of Crash Pulse Characteristics on Whiplash Associated Disorders in Rear Impacts--Crash Recording in Real Life Crashes. *Traffic Injury Prevention*, *3*(2), 141–149. https://doi.org/10.1080/15389580212001

Krakenes, J., & Kaale, B. R. (2006). Magnetic resonance imaging assessment of craniovertebral ligaments and membranes after whiplash trauma. *Spine*, *31*(24), 2820–2826. https://doi.org/10.1097/01.brs.0000245871.15696.1f

Kullgren, A., Krafft, M., Nygren, A., & Tingvall, C. (2000). Neck injuries in frontal impacts: influence of crash pulse characteristics on injury risk. *Accident; Analysis and Prevention*, *32*(2), 197–205. https://doi.org/10.1016/s0001-4575(99)00096-2

Kullgren, A., Krafft, M., Tingvall, C., & Lie, A. (2003). Combining crash recorder and paired comparison technique: Injury risk functions in frontal and rear impacts with special reference to neck injuries. In *ESV Conference, Nagoya, Japan*.

Kullgren, A., Krafft, M., Ydenius, A., Lie, A., & Tingvall, C. (2002). Developments in Car Safety with Respect to Disability - Injury Distributions for Car Occupants in Cars from The 80's and 90's. In *IRCOBI Conference 2002*.

Kullgren, A., Stigson, H., & Krafft, M. (2013). Development of Whiplash Associated Disorders for Male and Female Car Occupants in Cars Launched Since the 80s in Different Impact Directions. In *IRCOBI Conference 2013*.

Kumar, S., Narayan, Y., & Amell, T. (2002). An electromyographic study of low-velocity rear-end impacts. *Spine*, *27*(10), 1044–1055. https://doi.org/10.1097/00007632-200205150-00009

Kumar, S., Ferrari, R., & Narayan, Y. (2004). Electromyographic and kinematic exploration of whiplash-type neck perturbations in left lateral collisions. *Spine*, *29*(6), 650–659. https://doi.org/10.1097/01.brs.0000115136.24824.df

Kumar, S., Ferrari, R., & Narayan, Y. (2004). Cervical muscle response to whiplash-type right lateral impacts. *Spine*, *29*(21), E479-87. https://doi.org/10.1097/01.brs.0000143171.09966.6c

Kumar, S., Narayan, Y., & Amell, T. (2003). Analysis of low velocity frontal impacts. *Clinical Biomechanics (Bristol, Avon)*, *18*(8), 694–703. https://doi.org/10.1016/s0268-0033(03)00137-2

Lasswell, T. L., Cronin, D. S., Medley, J. B., & Rasoulinejad, P. (2017). Incorporating ligament laxity in a finite element model for the upper cervical spine. *The Spine Journal : Official Journal of the North American Spine Society*, *17*(11), 1755–1764. https://doi.org/10.1016/j.spinee.2017.06.040

Latremoliere, A., & Woolf, C. J. (2009). Central sensitization: a generator of pain hypersensitivity by central neural plasticity. *The Journal of Pain : Official Journal of the American Pain Society*, *10*(9), 895–926. https://doi.org/10.1016/j.jpain.2009.06.012

Lavallee, A. V, Ching, R. P., & Nuckley, D. J. (2013). Developmental biomechanics of neck musculature. *Journal of Biomechanics*, *46*(3), 527–534. https://doi.org/10.1016/j.jbiomech.2012.09.029

Lee, K. E., Davis, M. B., & Winkelstein, B. A. (2008). Capsular ligament involvement in the development of mechanical hyperalgesia after facet joint loading: behavioral and inflammatory outcomes in a rodent model of pain. *Journal of Neurotrauma*, *25*(11), 1383–1393. https://doi.org/10.1089/neu.2008.0700

Lee, K. E., Thinnes, J. H., Gokhin, D. S., & Winkelstein, B. A. (2004). A novel rodent neck pain model of facet-mediated behavioral hypersensitivity: implications for persistent pain and whiplash injury. *Journal of Neuroscience Methods*, *137*(2), 151–159. https://doi.org/10.1016/j.jneumeth.2004.02.021

Levitz, C. L., Reilly, P. J., & Torg, J. S. (1997). The pathomechanics of chronic, recurrent cervical nerve root neurapraxia. The chronic burner syndrome. *The American Journal of Sports Medicine*, *25*(1), 73–76. https://doi.org/10.1177/036354659702500114

Li, Q., Shen, H., & Li, M. (2013). Magnetic resonance imaging signal changes of alar and transverse ligaments not correlated with whiplash-associated disorders: a meta-analysis of case-control studies. *European Spine Journal*, *22*(1), 14–20. https://doi.org/10.1007/s00586-012-2490-x

Lohman, C. M., Gilbert, K. K., Sobczak, S., Brismee, J.-M., James, C. R., Day, M., … Sizer, P. J. (2015). 2015 Young Investigator Award Winner: Cervical Nerve Root Displacement and Strain During Upper Limb Neural Tension Testing: Part 2: Role of Foraminal Ligaments in the Cervical Spine. *Spine*, *40*(11), 801–808. https://doi.org/10.1097/BRS.0000000000000687

Lord, S. M., Barnsley, L., Wallis, B. J., & Bogduk, N. (1996). Chronic cervical zygapophysial joint pain after whiplash. A placebo-controlled prevalence study. *Spine*, *21*(15), 1735–1737. https://doi.org/10.1097/00007632-199608010-00005

Lu, Y., Chen, C., Kallakuri, S., Patwardhan, A., & Cavanaugh, J. M. (2005). Neurophysiological and biomechanical characterization of goat cervical facet joint capsules. *Journal of Orthopaedic Research : Official Publication of the Orthopaedic Research Society*, *23*(4), 779–787. https://doi.org/10.1016/j.orthres.2005.01.002

Maak, T. G., Ivancic, P. C., Tominaga, Y., & Panjabi, M. M. (2007). Side impact causes multiplanar cervical spine injuries. *The Journal of Trauma*, *63*(6), 1296–1307. https://doi.org/10.1097/01.ta.0000241237.72420.51

Macpherson, P. C., Schork, M. A., & Faulkner, J. A. (1996). Contraction-induced injury to single fiber segments from fast and slow muscles of rats by single stretches. *The American Journal of Physiology*, *271*(5 Pt 1), C1438-46. https://doi.org/10.1152/ajpcell.1996.271.5.C1438

Magnusson, M. L., Pope, M. H., Hasselquist, L., Bolte, K. M., Ross, M., Goel, V. K., … Wilder, D. G. (1999). Cervical electromyographic activity during low-speed rear impact. *European Spine Journal*, *8*(2), 118–125. https://doi.org/10.1007/s005860050140

Mall, N. A., Buchowski, J., Zebala, L., Brophy, R. H., Wright, R. W., & Matava, M. J. (2012). Spine and axial skeleton injuries in the National Football League. *The American Journal of Sports Medicine*, *40*(8), 1755–1761. https://doi.org/10.1177/0363546512448355

Martin, J.-L., Perez, K., Mari-Dell'olmo, M., & Chiron, M. (2008). Whiplash risk estimation based on linked hospital-police road crash data from France and Spain. *Injury Prevention : Journal of the International Society for Child and Adolescent Injury Prevention*, *14*(3), 185–190. https://doi.org/10.1136/ip.2007.016600

Mattucci, S. F. E., & Cronin, D. S. (2015). A method to characterize average cervical spine ligament response based on raw data sets for implementation into injury biomechanics models. *Journal of the Mechanical Behavior of Biomedical Materials*, *41*, 251–260. https://doi.org/10.1016/j.jmbbm.2014.09.023

Mattucci, S. F. E., Moulton, J. A., Chandrashekar, N., & Cronin, D. S. (2012). Strain rate dependent properties of younger human cervical spine ligaments. *Journal of the Mechanical Behavior of Biomedical Materials*, *10*, 216–226. https://doi.org/10.1016/j.jmbbm.2012.02.004

Mattucci, S. F. E., Moulton, J. A., Chandrashekar, N., & Cronin, D. S. (2013). Strain rate dependent properties of human craniovertebral ligaments. *Journal of the Mechanical Behavior of Biomedical Materials*, *23*, 71–79. https://doi.org/10.1016/j.jmbbm.2013.04.005

Morris, A. P., & Thomas, P. (1996). Neck Injuries in the UK Co-operative Crash Injury Study. In *40th Stapp Car Crash Conference (1996)*. SAE International. https://doi.org/https://doi.org/10.4271/962433

Muhle, C., Resnick, D., Ahn, J. M., Sudmeyer, M., & Heller, M. (2001). In vivo changes in the neuroforaminal size at flexion-extension and axial rotation of the cervical spine in healthy persons examined using kinematic magnetic resonance imaging. *Spine*, *26*(13), E287-93. https://doi.org/10.1097/00007632-200107010-00013

Muzzy, W. H., & Lustick, L. (1976). Comparison of Kinematic Parameters Between Hybrid II Head and Neck System with Human Volunteers for -Gx Acceleration Profiles. In *20th Stapp Car Crash Conference (1976)*. SAE International. https://doi.org/https://doi.org/10.4271/760801

Nibu, K., Cholewicki, J., Panjabi, M. M., Babat, L. B., Grauer, J. N., Kothe, R., & Dvorak, J. (1997). Dynamic elongation of the vertebral artery during an in vitro whiplash simulation. *European Spine Journal*, *6*(4), 286–289. https://doi.org/10.1007/bf01322455

Niv, D., & Devor, M. (2007). Position paper of the European Federation of IASP Chapters (EFIC) on the subject of pain management. *European Journal of Pain (London, England)*, *11*(5), 487–489. https://doi.org/10.1016/j.ejpain.2007.03.005

Nordin, M., & Frankel, V. H. (2001). *Basic biomechanics of the musculoskeletal system* (3rd ed.). Philadelphia : Lippincott Williams & Wilkins.

Norris, S. H., & Watt, I. (1983). The prognosis of neck injuries resulting from rear-end vehicle collisions. *The Journal of Bone and Joint Surgery. British Volume*, *65*(5), 608–611.

Nuckley, D. J., Konodi, M. A., Raynak, G. C., Ching, R. P., & Mirza, S. K. (2002). Neural space integrity of the lower cervical spine: effect of normal range of motion. *Spine*, *27*(6), 587–595. https://doi.org/10.1097/00007632-200203150-00006

Ohtori, S., Takahashi, K., & Moriya, H. (2003). Calcitonin gene-related peptide immunoreactive DRG neurons innervating the cervical facet joints show phenotypic switch in cervical facet injury in rats. *European Spine Journal*, *12*(2), 211–215. https://doi.org/10.1007/s00586-002-0506-7

Ono, K., Ejima, S., Kaneoka, K., Fukushima, M., Yamada, S., Ujihashi, S., & Compigne, D. (2005). Biomechanical responses of head/neck/torso to lateral impact loading on shoulders of male and female volunteers. In *IRCOBI Conference 2005*.

Ono, K., Ejima, S., Suzuki, Y., Kaneoka, K., Fukushima, M., & Ujihashi, S. (2006). Prediction of neck injury risk based on the analysis of localized cervical vertebral motion of human volunteers during low-speed rear impacts. In *IRCOBI Conference 2006* (pp. 103–113).

Ono, K., Kaneoka, K., Wittek, A., & Kajzer, J. (1997). Cervical Injury Mechanism Based on the Analysis of Human Cervical Vertebral Motion and Head-Neck-Torso Kinematics During Low Speed Rear Impacts. In *41st Stapp Car Crash Conference*. SAE International. https://doi.org/https://doi.org/10.4271/973340

Osth, J., Brolin, K., & Happee, R. (2012). Active muscle response using feedback control of a finite element human arm model. *Computer Methods in Biomechanics and Biomedical Engineering*, *15*(4), 347–361. https://doi.org/10.1080/10255842.2010.535523

Osth, J., Brolin, K., Svensson, M. Y., & Linder, A. (2016). A Female Ligamentous Cervical Spine Finite Element Model Validated for Physiological Loads. *Journal of Biomechanical Engineering*, *138*(6), 61005. https://doi.org/10.1115/1.4032966

Östh, J., Mendoza-Vazquez, M., Linder, A., Svensson, M. Y., & Brolin, K. (2017). The VIVA OpenHBM finite element 50th percentile female occupant model: whole body model development and kinematic validation. In *IRCOBI Conference 2017*.

Otte, D., Pohlemann, T., & Blauth, M. (1997). Significance of soft tissue neck injuries AIS 1 in the accident scene and deformation characteristics of cars with delta-V up to 10 km/h. In *IRCOBI Conference 1997*.

Panjabi, M. M., Cholewicki, J., Nibu, K., Grauer, J., & Vahldiek, M. (1998). Capsular ligament stretches during in vitro whiplash simulations. *Journal of Spinal Disorders*, *11*(3), 227–232.

Panjabi, M. M., Oxland, T., Takata, K., Goel, V., Duranceau, J., & Krag, M. (1993). Articular facets of the human spine. Quantitative three-dimensional anatomy. *Spine*, *18*(10), 1298–1310. https://doi.org/10.1097/00007632-199308000-00009

Panjabi, M. M. (2006). A hypothesis of chronic back pain: ligament subfailure injuries lead to muscle control dysfunction. *European Spine Journal*, *15*(5), 668–676. https://doi.org/10.1007/s00586-005-0925-3

Panjabi, M. M., Ito, S., Pearson, A. M., & Ivancic, P. C. (2004). Injury mechanisms of the cervical intervertebral disc during simulated whiplash. *Spine*, *29*(11), 1217–1225. https://doi.org/10.1097/00007632-200406010-00011

Panjabi, M. M., Ivancic, P. C., Tominaga, Y., & Wang, J.-L. (2005). Intervertebral neck injury criterion for prediction of multiplanar cervical spine injury due to side impacts. *Traffic Injury Prevention*, *6*(4), 387–397. https://doi.org/10.1080/15389580500257100

Panjabi, M. M., Maak, T. G., Ivancic, P. C., & Ito, S. (2006). Dynamic intervertebral foramen narrowing during simulated rear impact. *Spine*, *31*(5), E128-34. https://doi.org/10.1097/01.brs.0000201243.81745.ba

Panjabi, M. M., Pearson, A. M., Ito, S., Ivancic, P. C., Gimenez, S. E., & Tominaga, Y. (2004). Cervical spine ligament injury during simulated frontal impact. *Spine*, *29*(21), 2395–2403. https://doi.org/10.1097/01.brs.0000143173.92241.ab

Panzer, M. B., Fice, J. B., & Cronin, D. S. (2011). Cervical spine response in frontal crash. *Medical Engineering and Physics*, *33*(9), 1147–1159. https://doi.org/10.1016/j.medengphy.2011.05.004

Pearson, A. M., Ivancic, P. C., Ito, S., & Panjabi, M. M. (2004). Facet joint kinematics and injury mechanisms during simulated whiplash. *Spine*, *29*(4), 390–397. https://doi.org/10.1097/01.BRS.0000090836.50508.F7

Pettersson, K., Hildingsson, C., Toolanen, G., Fagerlund, M., & Bjornebrink, J. (1997). Disc pathology after whiplash injury. A prospective magnetic resonance imaging and clinical investigation. *Spine*, *22*(3), 283–287; discussion 288. https://doi.org/10.1097/00007632-199702010-00010

Quinlan, K. P., Annest, J. L., Myers, B., Ryan, G., & Hill, H. (2004). Neck strains and sprains among motor vehicle occupants - United States, 2000. *Accident Analysis and Prevention*, *36*(1), 21–27. https://doi.org/10.1016/S0001-4575(02)00110-0

Reddy, M., Reddy, B., Schoggl, A., Saringer, W., & Matula, C. (2002). The complexity of trauma to the cranio-cervical junction: correlation of clinical presentation with Doppler flow velocities in the V3-segment of the vertebral arteries. *Acta Neurochirurgica*, *144*(6), 575–580; discussion 580. https://doi.org/10.1007/s007010200078

Richter, M., Otte, D., Pohlemann, T., Krettek, C., & Blauth, M. (2000). Whiplash-type neck distortion in restrained car drivers: frequency, causes and long-term results. *European Spine Journal*, *9*(2), 109–117. https://doi.org/10.1007/s005860050220

Rothman, S. M., Kreider, R. A., & Winkelstein, B. A. (2005). Spinal neuropeptide responses in persistent and transient pain following cervical nerve root injury. *Spine*, *30*(22), 2491–2496. https://doi.org/10.1097/01.brs.0000186316.38111.4b

Sato, F., Nakajima, T., Ono, K., Svensson, M., Brolin, K., & Kaneoka, K. (2014). Dynamic cervical vertebral motion of female and male volunteers and analysis of its interaction with head/neck/torso behavior during low-speed rear impact. In *IRCOBI Conference 2014*.

Sato, F., Odani, M., Miyazaki, Y., Yamazaki, K., Osth, J., & Svensson, M. (2017). Effects of whole spine alignment patterns on neck responses in rear end impact. *Traffic Injury Prevention*, *18*(2), 199–206. https://doi.org/10.1080/15389588.2016.1227072

Schmitt, K.-U., Niederer, P. F., Cronin, D. S., Morrison III, B., Muser, M. H., & Walz, F. (2019). *Trauma biomechanics: an introduction to injury biomechanics*. Springer.

Schofferman, J., Bogduk, N., & Slosar, P. (2007). Chronic whiplash and whiplash-associated disorders: an evidence-based approach. *The Journal of the American Academy of Orthopaedic Surgeons*, *15*(10), 596–606.

Schwartz, D., Guleyupoglu, B., Koya, B., Stitzel, J. D., & Gayzik, F. S. (2015). Development of a computationally efficient full human body finite element model. *Traffic Injury Prevention*, *16 Suppl 1*, S49-56. https://doi.org/10.1080/15389588.2015.1021418

Scott, S., & Sanderson, P. L. (2002). Whiplash: a biochemical study of muscle injury. *European Spine Journal*, *11*(4), 389–392. https://doi.org/10.1007/s00586-002-0410-1

Seow, C. Y. (2013). Hill's equation of muscle performance and its hidden insight on molecular mechanisms. *The Journal of General Physiology*, *142*(6), 561–573. https://doi.org/10.1085/jgp.201311107

Seric, V., Blazic-Cop, N., & Demarin, V. (2000). Haemodynamic changes in patients with whiplash injury measured by transcranial Doppler sonography (TCD). *Collegium Antropologicum*, *24*(1), 197–204.

Shams, T., Huang, T. J., Rangarajan, N., & Haffner, M. (2003). Design requirements for a fifth percentile female version of the THOR ATD. In *ESV Conference, Nagoya, Japan* (pp. 19–22).

Shateri, H., & Cronin, D. S. (2015). Out-of-Position Rear Impact Tissue-Level Investigation Using Detailed Finite Element Neck Model. *Traffic Injury Prevention*, *16*(7), 698–708. https://doi.org/10.1080/15389588.2014.1003551

Shi, B., Zheng, X., Zhang, H., Sun, C., Cao, Y., Jin, A., & Ding, Z. (2015). The morphology and clinical significance of the extraforaminal ligaments at the cervical level. *Spine*, *40*(1), E9-17. https://doi.org/10.1097/BRS.0000000000000668

Siegmund, G. P., Inglis, J. T., & Sanderson, D. J. (2001). Startle response of human neck muscles sculpted by readiness to perform ballistic head movements. *The Journal of Physiology*, *535*(Pt 1), 289–300. https://doi.org/10.1111/j.1469-7793.2001.00289.x

Siegmund, G. P., Myers, B. S., Davis, M. B., Bohnet, H. F., & Winkelstein, B. A. (2001). Mechanical evidence of cervical facet capsule injury during whiplash: a cadaveric study using combined shear, compression, and extension loading. *Spine*, *26*(19), 2095–2101. https://doi.org/10.1097/00007632-200110010-00010

Siegmund, G. P., Winkelstein, B. A., Ivancic, P. C., Svensson, M. Y., & Vasavada, A. (2009). The Anatomy and biomechanics of acute and chronic whiplash injury. *Traffic Injury Prevention*, *10*(2), 101–112. https://doi.org/10.1080/15389580802593269

Siegmund, G. P., Blouin, J.-S., Carpenter, M. G., Brault, J. R., & Inglis, J. T. (2008). Are cervical multifidus muscles active during whiplash and startle? An initial experimental study. *BMC Musculoskeletal Disorders*, *9*, 80. https://doi.org/10.1186/1471-2474-9-80

Siegmund, G. P., Brault, J. R., & Chimich, D. D. (2002). Do Cervical Muscles Play a Role in Whiplash Injury? *Journal of Whiplash & Related Disorders*, *1*(1), 23–40. https://doi.org/10.3109/J180v01n01_03

Siegmund, G. P., Sanderson, D. J., Myers, B. S., & Inglis, J. T. (2003). Rapid neck muscle adaptation alters the head kinematics of aware and unaware subjects undergoing multiple whiplash-like perturbations. *Journal of Biomechanics*, *36*(4), 473–482. https://doi.org/10.1016/s0021-9290(02)00458-x

Singh, D., & Cronin, D. S. (2017). An investigation of dimensional scaling using cervical spine motion segment finite element models. *International Journal for Numerical Methods in Biomedical Engineering*, *33*(11). https://doi.org/10.1002/cnm.2872

Skaggs, D. L., Weidenbaum, M., Iatridis, J. C., Ratcliffe, A., & Mow, V. C. (1994). Regional variation in tensile properties and biochemical composition of the human lumbar anulus fibrosus. *Spine*, *19*(12), 1310–1319. https://doi.org/10.1097/00007632-199406000-00002

Snyder, R. G., Chaffin, D. B., & Foust, D. R. (1975). *Bioengineering study of basic physical measurements related to susceptibility to cervical hyperextension-hyperflexion injury*.

Spitzer, W. O., Skovron, M. L., Salmi, L. R., Cassidy, J. D., Duranceau, J., Suissa, S., & Zeiss, E. (1995). Scientific monograph of the Quebec Task Force on Whiplash-Associated Disorders: redefining "whiplash" and its management. *Spine*, *20*(8 Suppl), 1S-73S.

Standring, S. (2008). *Gray's Anatomy - The Anatomical Basis of Clinical Practice* (40th ed.). Churchill Livingstone Elsevier.

Steilen, D., Hauser, R., Woldin, B., & Sawyer, S. (2014). Chronic neck pain: making the connection between capsular ligament laxity and cervical instability. *The Open Orthopaedics Journal*, *8*, 326–345. https://doi.org/10.2174/1874325001408010326

Stemper, B. D., & Corner, B. D. (2016). Whiplash-Associated Disorders: Occupant Kinematics and Neck Morphology. *The Journal of Orthopaedic and Sports Physical Therapy*, *46*(10), 834–844. https://doi.org/10.2519/jospt.2016.6846

Stemper, B. D., Yoganandan, N., Pintar, F. A., Maiman, D. J., Meyer, M. A., DeRosia, J., … Paskoff, G. (2008). Anatomical gender differences in cervical vertebrae of size-matched volunteers. *Spine*, *33*(2), E44-9. https://doi.org/10.1097/BRS.0b013e318160462a

Sterner, Y., & Gerdle, B. (2004). Acute and chronic whiplash disorders--a review. *Journal of Rehabilitation Medicine*, *36*(5), 193–209; quiz 210. https://doi.org/10.1080/16501970410030742

Storåkers, B. (1986). On material representation and constitutive branching in finite compressible elasticity. *Journal of the Mechanics and Physics of Solids*, *34*(2), 125–145. https://doi.org/https://doi.org/10.1016/0022-5096(86)90033-5

Svensson, M. Y., Bostrom, O., Davidsson, J., Hansson, H. A., Haland, Y., Lovsund, P., … Saljo, A. (2000). Neck injuries in car collisions--a review covering a possible injury mechanism and the development of a new rear-impact dummy. *Accident; Analysis and Prevention*, *32*(2), 167–175. https://doi.org/10.1016/s0001-4575(99)00080-9

Szabo, T. J., & Welcher, J. B. (1996). Human Subject Kinematics and Electromyographic Activity During Low Speed Rear Impacts. In *40th Stapp Car Crash Conference*. SAE International. https://doi.org/https://doi.org/10.4271/962432

Taylor, J. R., & Twomey, L. T. (1993). Acute injuries to cervical joints. An autopsy study of neck sprain. *Spine*, *18*(9), 1115–1122. https://doi.org/10.1097/00007632-199307000-00001

Temming, J., & Zobel, R. (1998). Frequency and risk of cervical spine distortion injuries in passenger car accidents: significance of human factors data. In *IRCOBI Conference 1998*.

Thunnissen, J., Wismans, J., Ewing, C. L., & Thomas, D. J. (1995). Human Volunteer Head-Neck Response in Frontal Flexion: A New Analysis. In *39th Stapp Car Crash Conference (1995)*. SAE International. https://doi.org/https://doi.org/10.4271/952721

Tominaga, Y., Maak, T. G., Ivancic, P. C., Panjabi, M. M., & Cunningham, B. W. (2006). Head-turned rear impact causing dynamic cervical intervertebral foramen narrowing: implications for ganglion and nerve root injury. *Journal of Neurosurgery. Spine*, *4*(5), 380–387. https://doi.org/10.3171/spi.2006.4.5.380

Tominaga, Y., Ndu, A. B., Coe, M. P., Valenson, A. J., Ivancic, P. C., Ito, S., … Panjabi, M. M. (2006). Neck ligament strength is decreased following whiplash trauma. *BMC Musculoskeletal Disorders*, *7*, 103. https://doi.org/10.1186/1471-2474-7-103

Vasavada, A. N., Li, S., & Delp, S. L. (2001). Three-dimensional isometric strength of neck muscles in humans. *Spine*, *26*(17), 1904–1909. https://doi.org/10.1097/00007632-200109010-00018

Vasavada, A. N., Brault, J. R., & Siegmund, G. P. (2007). Musculotendon and fascicle strains in anterior and posterior neck muscles during whiplash injury. *Spine*, *32*(7), 756–765. https://doi.org/10.1097/01.brs.0000259058.00460.69

Vasavada, A. N., Danaraj, J., & Siegmund, G. P. (2008). Head and neck anthropometry, vertebral geometry and neck strength in height-matched men and women. *Journal of Biomechanics*, *41*(1), 114–121. https://doi.org/10.1016/j.jbiomech.2007.07.007

Versteegen, G. J., Kingma, J., Meijler, W. J., & ten Duis, H. J. (1998). Neck sprain not arising from car accidents: a retrospective study covering 25 years. *European Spine Journal*, *7*(3), 201–205. https://doi.org/10.1007/s005860050056

Vetti, N., Krakenes, J., Damsgaard, E., Rorvik, J., Gilhus, N. E., & Espeland, A. (2011). Magnetic resonance imaging of the alar and transverse ligaments in acute whiplash-associated disorders 1 and 2: a cross-sectional controlled study. *Spine*, *36*(6), E434-40. https://doi.org/10.1097/BRS.0b013e3181da21a9

Vetti, N., Krakenes, J., Eide, G. E., Rorvik, J., Gilhus, N. E., & Espeland, A. (2010). Are MRI high-signal changes of alar and transverse ligaments in acute whiplash injury related to outcome? *BMC Musculoskeletal Disorders*, *11*, 260. https://doi.org/10.1186/1471-2474-11-260

Watanabe, Y., Ichikawa, H., Kayama, O., Ono, K., Kaneoka, K., & Inami, S. (2000). Influence of seat characteristics on occupant motion in low-speed rear impacts. *Accident Analysis & Prevention*, *32*(2), 243–250. https://doi.org/https://doi.org/10.1016/S0001-4575(99)00082-2

Winkelstein, B. a, Nightingale, R. W., Richardson, W. J., & Myers, B. S. (2000). The cervical facet capsule and its role in whiplash injury: a biomechanical investigation. *Spine*, *25*(10), 1238–1246. https://doi.org/10.1097/00007632-200005150-00007

Winkelstein, B. A. (2004). Mechanisms of central sensitization, neuroimmunology & injury biomechanics in persistent pain: implications for musculoskeletal disorders. *Journal of Electromyography and Kinesiology : Official Journal of the International Society of Electrophysiological Kinesiology*, *14*(1), 87–93. https://doi.org/10.1016/j.jelekin.2003.09.017

Winkelstein, B. A. (2011). How can animal models inform on the transition to chronic symptoms in whiplash? *Spine*, *36*(25 Suppl), S218-25. https://doi.org/10.1097/BRS.0b013e3182387f96

Winters, J. M. (1995). How detailed should muscle models be to understand multi-joint movement coordination? *Human Movement Science*, *14*(4), 401–442. https://doi.org/https://doi.org/10.1016/0167-9457(95)00023-6

Wismans, J., van Oorschot, H., & Woltring, H. J. (1986). Omni-Directional Human Head-Neck Response. In *30th Stapp Car Crash Conference (1986)*. SAE International. https://doi.org/https://doi.org/10.4271/861893

Wittek, A., Ono, K., Kajzer, J., Ortengren, R., & Inami, S. (2001). Analysis and comparison of reflex times and electromyograms of cervical muscles under impact loading using surface and fine-wire electroces. *IEEE Transactions on Bio-Medical Engineering*, *48*(2), 143–153. https://doi.org/10.1109/10.909635

Womack, W., Woldtvedt, D., & Puttlitz, C. M. (2008). Lower cervical spine facet cartilage thickness mapping. *Osteoarthritis and Cartilage*, *16*(9), 1018–1023. https://doi.org/10.1016/j.joca.2008.01.007

Yang, K. H., Begeman, P. C., Muser, M., Niederer, P., & Walz, F. (1997). On the Role of Cervical Facet Joints in Rear End Impact Neck Injury Mechanisms. In *SAE International Congress and Exposition*. SAE International. https://doi.org/https://doi.org/10.4271/970497

Yang, K. H., Iwamoto, M., Cronin, D. S., Singh, D., Gierczycka, D., Barker, J., & Shen, D. (2018). *Chapter 1 - Introduction, Chapter 11 - Modeling Passive and Active Muscles, Chapter 13 - Modeling the Neck for Impact Scenarios*. (K.-H. Yang, Ed.), *Basic Finite Element Method as Applied to Injury Biomechanics*. Academic Press. https://doi.org/https://doi.org/10.1016/B978-0-12-809831-8.00001-5

Yang, K. H., & Kish, V. L. (1988). Compressibility measurement of human intervertebral nucleus pulposus. *Journal of Biomechanics*, *21*(10), 865. https://doi.org/https://doi.org/10.1016/0021-9290(88)90059-0

Yang, K. H., Zhu, F., Luan, F., Zhao, L., & Begeman, P. C. (1998). Development of a Finite Element Model of the Human Neck. In *Stapp Car Crash Conference*. SAE International. https://doi.org/https://doi.org/10.4271/983157

Yeomans, J. S., Li, L., Scott, B. W., & Frankland, P. W. (2002). Tactile, acoustic and vestibular systems sum to elicit the startle reflex. *Neuroscience and Biobehavioral Reviews*, *26*(1), 1–11. https://doi.org/10.1016/s0149-7634(01)00057-4

Yoganandan, N., Cusick, J. F., Pintar, F. A., & Rao, R. D. (2001). Whiplash injury determination with conventional spine imaging and cryomicrotomy. *Spine*, *26*(22), 2443–2448. https://doi.org/10.1097/00007632-200111150-00010

Yoganandan, N., Maiman, D. J., Pintar, F., Ray, G., Myklebust, J. B., Sances, A. J., & Larson, S. J. (1988). Microtrauma in the lumbar spine: a cause of low back pain. *Neurosurgery*, *23*(2), 162–168. https://doi.org/10.1227/00006123-198808000-00006

Yoganandan, N., Kumaresan, S., & Pintar, F. A. (2001). Biomechanics of the cervical spine. Part 2. Cervical spine soft tissue responses and biomechanical modeling. *Clinical Biomechanics*, *16*(1), 1–27. https://doi.org/10.1016/S0268-0033(00)00074-7

Zajac, F. E. (1989). Muscle and tendon: properties, models, scaling, and application to biomechanics and motor control. *Critical Reviews in Biomedical Engineering*, *17*(4), 359–411.